

ELECTRON-BASED ION ACTIVATION AND CHEMOMETRIC APPROACHES  
FOR THE TANDEM MASS SPECTROMETRY OF SULFATED  
GLYCOSAMINOGLYCAN CARBOHYDRATES

by

FRANKLIN E. LEACH III

(Under the Direction of I. Jonathan Amster)

ABSTRACT

The structural characterization of sulfated glycosaminoglycan (GAG) carbohydrates poses an analytical challenge due to a high level of heterogeneity inherent to a non-template based bio-synthesis and lability of the sulfate half-ester modification. Recently, tandem mass spectrometry has provided a sensitive method for the location of sites of sulfation in these complex biomolecules as well as determination of the stereochemistry of the C-5 carbon in hexuronic acid residues. In the presented work, electron-based ion activation methods, including electron detachment dissociation (EDD) and negative electron transfer dissociation (NETD), in conjunction with a Fourier transform ion cyclotron resonance (FT-ICR) mass spectrometer have been applied to GAG glycoforms constituting all of the major sulfated classes (heparan sulfate, heparin, and chondroitin sulfates). In each case, the location of sites of sulfation are assigned and as well as hexuronic acid stereochemistry in cases where epimer pairs are available. In some epimer pairs, the application of chemometric analysis is required to distinguish the two diastereomers.

INDEX WORDS: Sulfated glycosaminoglycan, carbohydrate, Fourier transform ion cyclotron resonance mass spectrometry, electron detachment dissociation, negative electron transfer dissociation, multivariate statistics, principal component analysis

ELECTRON-BASED ION ACTIVATION AND CHEMOMETRIC APPROACHES  
FOR THE TANDEM MASS SPECTROMETRY OF SULFATED  
GLYCOSAMINOGLYCAN CARBOHYDRATES

by

FRANKLIN E. LEACH III

B.S., The Mississippi State University, 2001

A Dissertation Submitted to the Graduate Faculty of The University of Georgia in Partial

Fulfillment of the Requirements for the Degree

DOCTOR OF PHILOSOPHY

ATHENS, GEORGIA

2011

© 2011

FRANKLIN E. LEACH III

All Rights Reserved

ELECTRON-BASED ION ACTIVATION AND CHEMOMETRIC APPROACHES  
FOR THE TANDEM MASS SPECTROMETRY OF SULFATED  
GLYCOSAMINOGLYCAN CARBOHYDRATES

by

FRANKLIN E. LEACH III

Major Professor: I. Jonathan Amster

Committee: Ron Orlando  
Lance Wells

Electronic Version Approved:

Maureen Grasso  
Dean of the Graduate School  
The University of Georgia  
May 2011

## DEDICATION

To Beth, the bug squad, the franimals, and my family.

## ACKNOWLEDGEMENTS

I have in no way completed this body of work on my own. First, I would like to thank my advisor, Jon Amster, for taking a chance on a wandering soul and providing direction by introducing me to Fourier transform mass spectrometry (FTMS) and the nuances therein. Additional thanks are due to Jeremy Wolff for mentoring on various aspects of FTMS, tandem mass spectrometry, and continued collaboration and discussions. Although I am a chemist on paper, the experiments described within would not be possible without the work of proper carbohydrate chemists in the labs of Robert J. Linhardt at Rensselaer Polytechnic Institute (Tania Laremore, Mellisa Ly, and Zhongping Xiao) and Geert-Jan Boons at the Complex Carbohydrate Research Center at the University of Georgia (Sailaja Arungundram, Kanar Al-Mafraji, and Andre Venot). Thanks are especially due to Bob, Tania, and Mellisa for discussions about GAG chemistry during my tenure and hosting me for a week to gain a new perspective on what really goes on before I receive micrograms of purified sample. Last, and certainly not least, I would like to thank my family and friends for continued support regardless of where my rambling has led.

## TABLE OF CONTENTS

	Page
ACKNOWLEDGEMENTS .....	v
LIST OF TABLES .....	viii
LIST OF FIGURES .....	ix
CHAPTER	
1 Introduction and Literature Review .....	1
2 Experimental Methods .....	29
3 Evaluation of the Experimental Parameters Which Control Electron Detachment Dissociation and Their Effect on the Fragmentation Efficiency of Glycosaminoglycan Carbohydrates .....	40
4 Electron Detachment Dissociation of Synthetic Heparan Sulfate Glycosaminoglycan Oligosaccharides Varying In Degree Of Sulfation And Hexuronic Acid Stereochemistry .....	66
5 Determination of Hexuronic Acid Stereochemistry in Chondroitin Sulfate Glycosaminoglycans by Electron Detachment Dissociation .....	97
6 Electron Detachment Dissociation and Infrared Multiphoton Dissociation of Heparin Tetrasaccharides .....	131
7 Negative Electron Transfer Dissociation Fourier Transform Mass Spectrometry of Glycosaminoglycan Oligosaccharides .....	157
8 Conclusions .....	183

## APPENDICES

A	The FT-ICR Mass Analyzer.....	187
B	Comparison of Particle-in-cell Simulations with Experimentally Observed Frequency Shifts Between Ions of the Same Mass-to-charge in Fourier Transform Ion Cyclotron Resonance Mass Spectrometry .....	249
C	Analysis of Phase Dependent Frequency Shifts in Particle-in-cell Simulated Fourier Transform Mass Spectrometry Time Domain Transients by the Filter Diagonalization Method.....	272
D	Supplemental Data.....	293

## LIST OF TABLES

	Page
Table B.1: .....	255
Table C.1: .....	278
Table D.1: .....	295

## LIST OF FIGURES

	Page
Figure 1.1: .....	3
Figure 1.2: .....	4
Figure 1.3: .....	5
Figure 1.4: .....	6
Figure 1.5: .....	11
Figure 2.1: .....	33
Figure 2.2: .....	35
Figure 3.1: .....	47
Figure 3.2: .....	51
Figure 3.3: .....	53
Figure 3.4: .....	53
Figure 3.5: .....	55
Figure 3.6: .....	56
Figure 3.7: .....	58
Figure 3.8: .....	59
Figure 4.1: .....	75
Figure 4.2: .....	76
Figure 4.3: .....	78
Figure 4.4: .....	80

Figure 4.5: .....	81
Figure 4.6: .....	83
Figure 4.7: .....	86
Figure 4.8: .....	88
Figure 5.1: .....	106
Figure 5.2: .....	108
Figure 5.3: .....	110
Figure 5.4: .....	111
Figure 5.5: .....	113
Figure 5.6: .....	114
Figure 5.7: .....	115
Figure 5.8: .....	116
Figure 5.9: .....	117
Figure 5.10: .....	118
Figure 5.11: .....	120
Figure 5.12: .....	122
Figure 6.1: .....	139
Figure 6.2: .....	142
Figure 6.3: .....	143
Figure 6.4: .....	145
Figure 6.5: .....	146
Figure 6.6: .....	147
Figure 6.7: .....	149

Figure 6.8: .....	150
Figure 7.1: .....	167
Figure 7.2: .....	168
Figure 7.3: .....	169
Figure 7.4: .....	171
Figure 7.5: .....	172
Figure 7.6: .....	174
Figure 7.7: .....	175
Figure 7.8: .....	176
Figure A.1: .....	191
Figure A.2: .....	194
Figure A.3: .....	196
Figure A.4: .....	197
Figure A.5: .....	201
Figure A.6: .....	203
Figure A.7: .....	204
Figure A.8: .....	206
Figure A.9: .....	207
Figure A.10: .....	209
Figure A.11: .....	210
Figure A.12: .....	211
Figure A.13: .....	212
Figure A.14: .....	213

Figure A.15: .....	214
Figure A.16: .....	216
Figure A.17: .....	217
Figure A.18: .....	218
Figure A.19: .....	221
Figure A.20: .....	224
Figure A.21: .....	225
Figure A.22: .....	228
Figure A.23: .....	229
Figure A.24: .....	230
Figure A.25: .....	231
Figure B.1: .....	257
Figure B.2: .....	258
Figure B.3: .....	260
Figure B.4: .....	262
Figure B.5: .....	264
Figure C.1: .....	280
Figure C.2: .....	281
Figure C.3: .....	283
Figure C.4: .....	284
Figure C.5: .....	285
Figure C.6: .....	286

## **CHAPTER 1**

### **INTRODUCTION AND LITERATURE REVIEW**

The work presented in this dissertation further extends electron-based ion activation to structurally characterize glycosaminoglycan carbohydrates varying in sulfation and hexuronic acid stereochemistry. Glycosaminoglycans (GAGs) are sulfated carbohydrates present in organisms ranging from bacteria to humans [1] that participate in many important biological processes including the regulation of biochemical pathways and disease progression [2-9]. GAGs are linear biomolecules that are typically associated with a core protein as proteoglycans, but complexity arises based on a series non-template based enzymatic modifications including sulfation, N-modification of the amino sugar, and stereochemical modification of the hexuronic acid [10].

The relationship between variability in sulfation and epimerization and cellular function [11, 12] has led to increased interest in the characterization of domain structure [13] and sulfation patterns [14]. The most notable of these domains is the five-residue heparin sequence for binding to antithrombin [4, 15]. The binding motif consists of eight sulfate groups specifically distributed along the pentasaccharide, of which the tri-sulfated disaccharide (IdoA2S-GlcNS6S) is a key element in protein recognition [16]. Additional variation of domain structure has been observed based upon organism age [17] as well as specificity to organ-type [18]. To fully understand these patterns and variations, there has been increased interest in the full characterization of structure-function relationships, generally known as glycomics [19].

The associated GAG chains can be categorized based upon constituent hexose residues, glycosidic linkage between hexoses, extent of O- or N-sulfation and N-acetylation, and hexuronic acid stereochemistry into specific glycoform classes i.e. chondroitin sulfate, heparan sulfate, hyaluronan, etc. displayed in Figure 1.1.



location of a modification within a saccharide ring. Although GAGs vary in stereochemical features, such as linkage position and hexuronic acid constituents, between glycoform classes, they consist of a conserved backbone, and modifications such as sulfation or acetylation can be treated as perturbations to a defined mass shown in Figure 1.2.

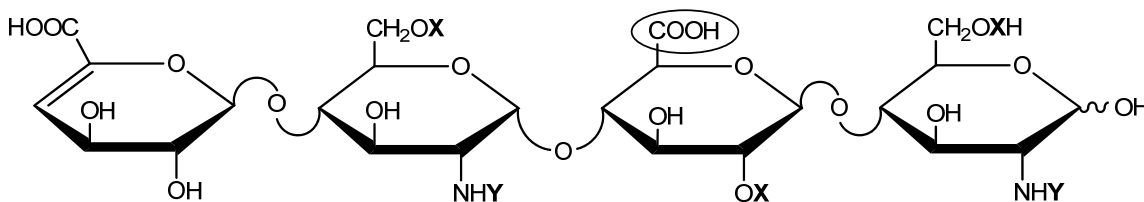


**Figure 1.2** The hexose rings linked by glycosidic bond linkages form a conserved backbone structure for all GAG chains. Sites of variable substitution are X: H or SO<sub>3</sub>H and Y: H, Ac, or SO<sub>3</sub>H. Additionally the hexuronic acid stereochemistry can vary between glucuronic acid shown by the circled carboxyl group which is pointed upward or iduronic acid where the carboxyl would be pointed downward, but this subtle difference does not induce a change in mass.

A mass measurement by Fourier transform ion cyclotron resonance mass spectrometry (FT-ICR MS) provides an accurate mass and isotopic resolution, which combined can be used to determine the oligomer length. Tandem mass spectrometry is then used to sequence the oligomer, locating a modification to a saccharide ring by glycosidic bond cleavage and to a subsistent ring position by cleavage of bonds across the hexose ring. The nomenclature utilized to assign these cleavages is shown in Figure 1.3.

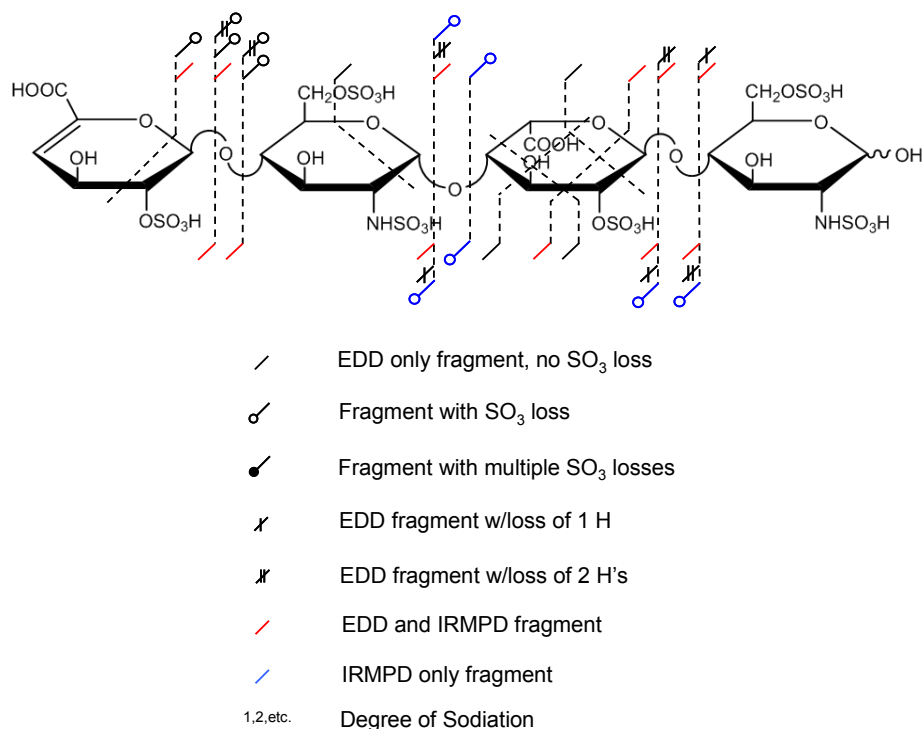


**Figure 1.3** Modification of the Domon-Costello nomenclature for carbohydrate hexoses to represent fragmentation products observed in electron-based ion activation.

Tandem mass spectrometry of sulfated GAGs presents an analytical challenge because the labile sulfate group is readily lost from the GAG during low-energy or threshold-type dissociation techniques, hampering efforts to locate this modification. The specific type of ion activation further sub-classifies threshold methods. The first type is collisional induced dissociation (CID) where ions undergo slow heating during collisions with an inert gas, typically argon, and dissociate given sufficient collision energy. The second type is infrared multiphoton dissociation (IRMPD) where absorption of multiple infrared photons eventually exceeds a dissociation energy threshold [31]. Both types of activation result in the cleavage of the most labile bond first. In the application to

sulfated GAGs, this bond is the sulfate half-ester. Minimal activation of a protonated sulfate is required to initiate a hydrogen rearrangement that results in the neutral loss of  $\text{SO}_3$ . To minimize the loss of sulfate groups, the sulfate should be ionized or paired with a metal counter-ion, e.g.  $\text{Na}^+$ , as shown in Figure 1.4.

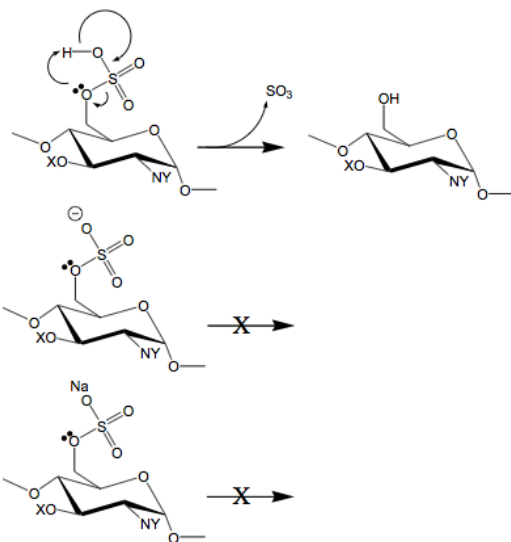


**Figure 1.4** The presence of protonated sulfate groups during the activation of GAG precursor ions for MS/MS readily leads to the loss of  $\text{SO}_3$  through a hydrogen rearrangement mechanism. This pathway is shunted by ionizing the sulfate or pairing with a counterion. Figure adapted from Zaia [32].

#### *Threshold Ion Activation*

Threshold activation techniques have been utilized to sequence GAG oligosaccharides ranging from dp2-dp10 (degree of polymerization) in ion trap mass spectrometers as well as FTMS instruments. The majority of this work has focused on the characterization of chondroitin glycoforms, which contain either 4-O or 6-O sulfated

hexosamine residues in combination with variations in hexuronic acid stereochemistry, e.g. CS-A is 4-O-sulfated and contains glucuronic acid, CS-B (aka dermatan sulfate, DS) contains 4-O-sulfated hexosamine and iduronic acid, and CS-C contains 6-O-sulfated galactosamine residues in conjunction with glucuronic acid. This comparatively low level of disaccharide variation results in a defined repeat unit. Chondroitin glycoforms have largely been examined in the context of binary mixtures to either differentiate the extent of 4- or 6-O sulfation or glucuronic or iduronic acid content [33-37]. For each stereochemical possibility the intensities of diagnostic ions have been shown to be indicative, but these methods require the generation of a new binary mixture curve for each possibility. More recently, IRMPD has been utilized to activate DS oligomers ranging from dp4-10 and varying in charge state and sodiation, but without hexuronic acid differentiation [38].

To a lesser extent, heparan sulfate and heparin have been examined by collisional activation. Due to the large number of combinatorial possibilities and purification required to obtain sufficient material, only a few systems have been studied in detail. A systematic study of the fragmentation mechanism in heparan sulfate (HS) disaccharides has been conducted [39, 40]. This approach was later extended to a study the effect of sulfation position in a heparin octasaccharide on binding to the CCL2 protein [41]. Although this work extended the oligomer length examined, the method relied on reduction to disaccharides and not direct tandem mass spectrometric interrogation of the intact octasaccharide. Direct MS<sup>n</sup> of highly sulfated heparin-like GAGs has been performed up to the pentasaccharide [30] and hexasaccharide [29] length in ion trap mass

spectrometers. Glycosidic bond and limited cross-ring cleavage was observed. The addition of  $\text{Ca}^{2+}$  was shown to induce minimal cross-ring cleavage [30].

Although appropriate precursor ion selection can reduce or eliminate sulfate loss in GAGs, recent progress has been demonstrated for direct chemical modification prior to tandem mass spectrometry [42]. Prior to separation or mass spectrometric analysis, the hydroxyl groups of the GAG are alkylated, after which the sulfate groups are removed by heating of the pyridinium salt in DMSO. The sites of sulfation are then labeled by peracetylation of the desulfated GAG. This modification has been shown to enhance separation, and is also effective in locating sites of sulfation in an  $\text{MS}^n$  type approach in an ion trap mass spectrometer.

#### *Electron-based Ion Activation*

The era of modern biomolecule analysis by tandem mass spectrometry started based on the combination of two separate technological developments, electrospray ionization (ESI) [43] and electron capture dissociation (ECD) [44]. ESI enabled the generation of multiply charged ions while maintaining labile modifications such as glycosylation, phosphorylation, or sulfation [45]. ECD also enabled the retention of the aforementioned labile modifications in a site-specific manner, but during the tandem mass spectrometry experiment, allowing for the identification of a modification's location to a particular position. As discussed in previous application to GAG MS/MS, upon ion activation, labile modifications are often lost. Due to a non-ergodic mechanism, ECD provided the ability to cleave bonds and produce sequence information. Although ECD has shown application for sequencing peptides and proteins, it is limited to the

tandem mass spectrometry of cationic species. GAGs are highly acidic biomolecules due to the occurrence of sulfate and carboxylate moieties and readily form anions. Pairing of metal cations with GAGs to generate positive ions for ECD has been demonstrated, but the resultant spectra defy interpretation (unpublished work - Amster). Due to repulsion between like charges, the low energy electrons ( $\sim 1$  eV) utilized in ECD are not sufficient for anionic activation in GAGs and higher energy electrons are required. Recently negative ion electron capture dissociation (niECD) has been demonstrated for sulfated peptides by irradiation with lower energy electrons (4-6 eV) (Unpublished work – Hakansson). Bond cleavage was observed without the loss of sulfate groups. The mechanism of this activation is still under investigation, but the most likely ability for electron capture in the peptide system may be due to the low charge density when compared to GAGs or a zwitterion state in which sites of both positive and negative charge are located on the same ion, providing a site of positive charge for electron capture.

Electron detachment dissociation [46] (EDD), the negative ion complement of ECD has recently been applied to the activation of acidic biomolecules for tandem mass spectrometry [46-51]. For EDD, multiply-charged anions are irradiated with moderate energy ( $\sim 19$  eV) electrons, detaching an electron and producing a radical species. This activation method has demonstrated value for the analysis of GAG oligosaccharides [50]. EDD produces more abundant glycosidic and cross-ring fragmentation than low energy or threshold type dissociation methods, and has been shown to effectively dissociate GAGs up to 10 saccharides in length [52], suggesting GAG sequencing can be performed with a single MS/MS experiment as opposed to an MS<sup>n</sup> approach which requires continual supervision based on experimental outcomes.

The initial publication for the EDD of GAGs was based on the application to non- or lowly sulfated (1 or less per disaccharide) HS tetrasaccharides [50]. EDD results were compared to threshold activation by both CID and IRMPD and results were presented that similar product ion distributions were achieved by each and these were a subset of products from EDD, which included increased assignments of cross-ring cleavage. Fragmentation mechanisms were also outlined to rationalize the generation of common products ions such as  $^{0,2}A_3$  and  $^{3,5}A_3$ . When the spectra of two epimers containing a unique hexuronic acid stereocenter were compared, EDD was shown to distinguish glucuronic acid (GlcA) from iduronic acid (IdoA) based on the occurrence of diagnostic product ions [53]. These ions were assigned as  $^{0,2}A_3$ ,  $B_3'$ , and  $B_3'-CO_2$  and were rationalized based on a hydrogen rearrangement mechanism present in GlcA residues where electron detachment from an ionized carboxyl group led to radical site migration and subsequent stereo-specific fragmentation.

Later work focused on the EDD of dermatan sulfate oligosaccharides ranging from dp4-10 [54]. EDD was shown to generate more informative cleavages when compared to threshold activation, but these were largely located on the hexuronic acid residues and limited the ability to assign the site of sulfation on hexosamine residues. This result was most likely due to the mobilization of protons, which led to an ionized carboxyl group. Investigation of the effect of DS precursor ion charge state and degree of sodiation later revealed that increasing the charge state and/or number of sodium counter ions to one greater than the number of sulfate groups greatly minimized or even eliminated the loss of sulfate during EDD [38].

### *Mechanistic Aspects of Electron-based Activation*

Although the name implies a singular process, two processes occur simultaneously during irradiation with moderate energy electrons (15-20 eV), electron detachment and electronic excitation, and are shown as solid lines in Figure 1.5.

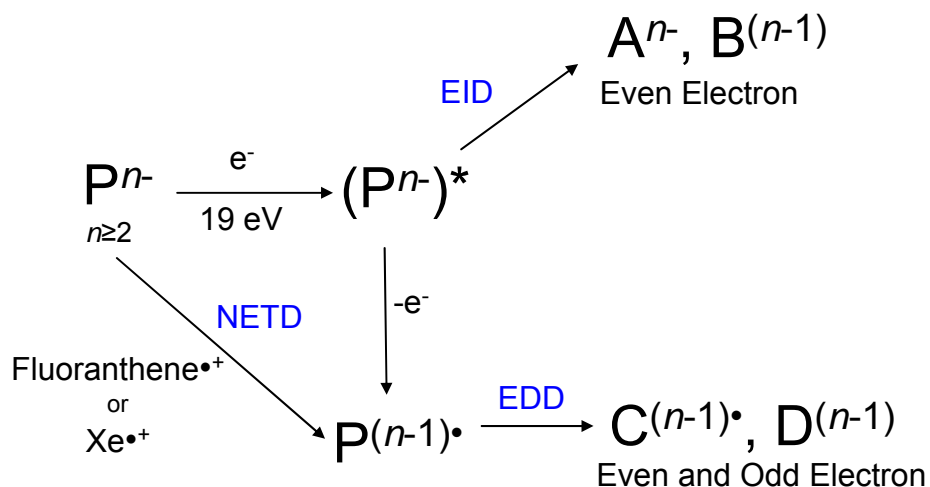


**Figure 1.5** Proposed pathways for the electron-based ion activation of anionic precursor ions by moderate energy electrons.

These two channels generate unique product distributions, which are both present in an EDD tandem mass spectrum. Upon irradiation with moderate energy electrons (15-20 eV), the multiply deprotonated precursor ion reaches an excited state intermediate that can undergo either electron detachment or electron induced dissociation (EID) through electronic excitation channels, previously described as electron impact excitation of ions from organics (EIEIO) [55]. The products generated by electron detachment are reduced in absolute charge magnitude, e.g. activation of a  $2^-$  precursor ion results in  $1^-$  products. These species can either be odd-electron or even-electron. EID results in both charge

conserved and charge reduced product ions and are largely even electron, although examples of odd-electron product ions in GAG precursor ions have been assigned [56].

To examine fragmentation mechanisms or pathways during EDD, it is possible to effectively separate the two processes. EID can be performed on the singly charged precursor ion of a given analyte, but this charge state becomes increasingly difficult to generate as the sulfate density increases due to their high acidity. Irradiation of a singly charged species by moderate energy electrons will result in the observation of only products arising from the electronic excitation channel as detachment from a  $1^-$  ion results in a neutral, which is not observable by MS-based detection. To bypass the excited state and generate products due only to detachment, ion-ion reactions can be employed to transfer an electron between the analyte precursor and a reagent cation.

#### *Negative Electron Transfer Dissociation*

In the first applications of electron-based ion activation by ECD and EDD, the experiments could only be performed in the Penning trap of a FT-ICR mass spectrometer, and the ability to activate biomolecules for tandem mass spectrometry and determine sites of labile modifications, such as phosphorylation and glycosylation, on peptides and proteins made ECD a very desirable technique to adapt to more widespread mass spectrometers. Both ECD and EDD have been demonstrated on 3D ion traps modified with magnets to assist in electron trapping [57, 58] and in a digital ion trap without an external magnetic field [59]. To overcome the difficulties of performing electron-ion reactions in the high pressure, RF region of the ion trap, trapping regions external to the mass analyzer have been implemented. Baba and co-workers have demonstrated this

technique for ECD in linear ion traps where both RF and magnetic fields were applied [60, 61] and others have performed ECD in a linear radio-frequency-free cell utilizing static electric and magnetic fields [62].

Ion-ion reactions were developed to initiate electron transfer and facilitate electron-ion reactions in quadrupole ion trap mass spectrometers. Electron transfer dissociation (ETD) employs radical anions generated in a chemical ionization (CI) source external to the mass analyzer [63]. Multiply-charged precursor ions are reacted with the radical anions in a linear ion trap, and an electron is transferred from the radical anion to the precursor ion producing an odd-electron species that undergoes further fragmentation. Compared to activation by ECD, ETD produces similar fragmentation on a shorter time scale and therefore is more ideal time-limited applications such as LC-MS/MS.

Negative electron transfer dissociation (NETD) is the negative ion complement of ETD. The gas phase electron transfer from a multiply charged oligonucleotide anion to a rare gas cation was initially demonstrated by McLuckey and co-workers [64] and later applied to peptide anions [65]. In this later work, the utility of xenon as well as fluoranthene was examined as an electron acceptor. Abundant EDD-like fragmentation of a phosphopeptide was observed using xenon radical cations ( $\text{Xe}^{+\bullet}$ ), while NETD using fluoranthene produced only loss of  $\text{CO}_2$  from the precursor ion. The absence of EDD-like fragmentation was attributed to using protonated fluoranthene instead of the fluoranthene radical cation. Recently Polfer and co-workers have examined the energetics of NETD between phosphopeptide anions and the radical cations of either fluoranthene or xenon [66]. NETD with fluoranthene retains the labile phosphorylation site whereas the reaction with xenon results in the neutral losses of  $\text{CO}_2$  and  $\text{H}_3\text{PO}_4$  and

adds complexity to the spectrum. This result was rationalized in the difference in recombination energy between the two radical cations with xenon  $\sim 4$  eV more energetic.

In addition to rare gas cations and fluoranthene, metal ions have also been employed to promote electron transfer. Negative electron transfer has been reported between the  $[M-5H]^{5-}$  charge state of insulin and  $Fe^+$  resulting in disulfide bond cleavage and formation of the A-chain and B-chain anions [67]. Metal ion complexes with phenanthroline have also shown utility in accepting an electron from peptide anions, but this reaction can also result in proton transfer depending upon the reagent metal [68].

More recently, electron photodetachment dissociation (EPD) has been demonstrated for GAG structural characterization [69, 70]. These studies have been conducted on a modified ion trap mass spectrometer to allow for the irradiation of the trapped ion cloud with an OPO laser to induce photodetachment. To date, only disaccharides and a tetrasaccharide have been examined.

### *Chemometric Approaches*

Tandem mass spectra regardless of ion activation method provide a wealth of information. The most apparent is the presence or absence of peaks corresponding to a particular product ion. The intensity of a given peak relative to others within the same spectrum or when compared to another spectrum can also provide valuable information. Binary mixture analysis can be employed in more straightforward cases to generate standard curves based on known mixtures and subsequent characterization of an unknown by comparison. EDD spectra often contain many peaks, which can be utilized for analysis, and it is necessary to employ more reliable, objective statistical tool that

makes use of a multiple number of product ions such as multivariate analysis (MVA) [71-73]. MVA has been widely applied in many scientific disciplines, including mass spectrometry, to extract valuable information from complicated data sets.

Early applications of MVA in mass spectrometry were based on factor analysis and ranged from the elucidation of basic chemical interactions in gas chromatography to the interpretation of fragmentation patterns in electron impact mass spectrometry and mixture analysis [74-77]. MVA has also been successfully applied to discern the characteristic features of large data sets in proteomics and generate peptide lists for targeted LC-MS/MS [78-80] as well as carbohydrate structure analysis [81, 82]. The application for carbohydrate analysis was at the mono- and disaccharide level to distinguish structural isomers and linkage position. Recent work has extended MVA, specifically principal component analysis (PCA), to differentiate the hexuronic acid stereochemistry in four synthetic HS epimers through the analysis of EDD and IRMPD spectra that contain peaks assigned to both glycosidic and cross-ring cleavages [83].

**Chapter 2** describes the experimental procedures employed for the preparation of glycosaminoglycan samples by enzymatic digestion of naturally-derived polysaccharides as well as modular chemical synthesis. Methods for the mass spectrometric characterization of GAG structure by tandem mass spectrometry are presented for both threshold and electron-based ion activation. Supplementary tools for EDD spectrum analysis are also discussed.

Optimization of the experimental parameters for the EDD of GAGs is detailed in **Chapter 3**. The EDD experiment is controlled by four parameters and presents a modest dimensional space to examine. These variables are the electron energy, extraction lens

voltage, current applied to the cathode heater element, and pulse duration. As each parameter is varied the optimum value is selected by monitoring the electron current entering the mass analyzer through a custom designed electronic circuit and conversion efficiency to assignable products.

The application of EDD to synthetic heparan sulfate tetrasaccharides varying in degree of sulfation and hexuronic acid stereochemistry is presented in **Chapter 4**. Synthetic compounds provide an attractive platform to systematically examine the effect of sulfate position on EDD spectra. As the sulfate density increases for a given oligomer length, it becomes increasingly difficult to ionize all of the sulfate groups and supplemental pairing with metal counter ions is required to minimize sulfate loss. Appropriate precursor ion selection results in the ability to locate sites of sulfation in compounds with sulfated hexosamine and hexuronic acid residues. When available, epimers pairs differing in hexuronic acid stereochemistry are also differentiated.

The differentiation of chondroitin sulfate (CS) epimers, varying in hexuronic acid stereochemistry, by electron-based ion activation is examined in **Chapter 5**. This capability has been demonstrated by collisional activation in an ion trap, but extension of stereochemical specific results from the EDD of HS is not consistent with results for CS glycoforms. EDD, EID, and NETD are employed independently to rationalize product distributions for the epimer pair. Multivariate statistical methods are applied to differentiate the EDD spectra of the epimers based on the absence of prior stereo-specific product ions.

The extension of EDD to heparin tetrasaccharides including 5-6 sites of sulfation is presented in **Chapter 6**. Due to the high sulfate density in heparin oligomers, the

analytical characterization of heparin remains challenging. To minimize sulfate loss, a combination of ionized and sodium paired sites is required as the occurrence of more than one ionized site per monosaccharide is energetically un-favored due to charge repulsion. The combination of various degrees of ionization and sodiation is examined. To extend the oligomerization beyond the tetrasaccharide level, the incorporation of a divalent metal counter ion ( $\text{Ca}^{2+}$ ) is shown to simplify the MS spectrum.

The NETD FT-ICR MS of GAGs is demonstrated in **Chapter 7**. The NETD of GAGs has been achieved in ion trap mass spectrometers, but the limited mass accuracy and resolving power of the instrument precludes the application to degrees of polymerization higher than tetra- to hexasaccharide or in highly sulfated GAGs where precursor ions are highly charged and charge reduction during fragmentation results in many products occupying a small mass range. To overcome these limitations, NETD has been performed on a commercially available FTMS instrument that includes the capability for ion-ion reactions.

Appendices include work on based on fundamental phenomena in FT-ICR MS yet not directly applicable to GAG structural characterization. **Section A** details the basis of FT-ICR MS in an encyclopedic context. **Sections B and C** detail efforts to study frequency shifts in FT-ICR MS by multi-particle ion trajectory simulations. Supplemental data is included in **Section D**.

## REFERENCES

1. Perrimon, N. and Bernfield, M., Cellular functions of proteoglycans--an overview. *Semin. Cell Dev. Biol.* **2001**, *12*, 65-67.
2. Fannon, M.; Forsten, K. E. and Nugent, M. A., Potentiation and Inhibition of bFGF Binding by Heparin: A Model for Regulation of Cellular Response. *Biochemistry* **2000**, *39*, 1434-1445.
3. Wu, Z. L.; Zhang, L.; Yabe, T.; Kuberan, B.; Beeler, D. L.; Love, A. and Rosenberg, R. D., The Involvement of Heparan Sulfate (HS) in FGF1/HS/FGFR1 Signaling Complex. *J. Biol. Chem.* **2003**, *278*, 17121-17129.
4. Lindahl, U.; Backstrom, G.; Hook, M.; Thunberg, L.; Fransson, L. A. and Linker, A., Structure of the antithrombin-binding site in heparin. *Proc. Natl. Acad. Sci. U. S. A.* **1979**, *76*, 3198-3202.
5. Gotte, M., Syndecans in Inflammation. *FASEB J.* **2003**, *17*, 575-591.
6. Batinic, D. and Robey, F. A., The V3 region of the envelope glycoprotein of human immunodeficiency virus type 1 binds sulfated polysaccharides and CD4-derived synthetic peptides. *J. Biol. Chem.* **1992**, *267*, 6664-6671.
7. Chen, Y.; Maguire, T.; Hileman, R. E.; Fromm, J. R.; Esko, J. D.; Linhardt, R. J. and Marks, R. M., Dengue virus infectivity depends on envelope protein binding to target cell heparan sulfate. *Nature Med.* **1997**, *3*, 866-871.
8. Williams, R. K. and Straus, S. E., Specificity and affinity of binding of herpes simplex virus type 2 glycoprotein B to glycosaminoglycans. *J. Virol.* **1997**, *71*, 1375-1380.

9. Liu, D. F.; Shriver, Z.; Gi, Y. W.; Venkataraman, G. and Sasisekharan, R., Dynamic regulation of tumor growth and metastasis by heparan sulfate glycosaminoglycans. *Semin. Throm. Hemost.* **2002**, *28*, 67-78.
10. Chi, L. L.; Amster, J. and Linhardt, R. J., Mass spectrometry for the analysis of highly charged sulfated carbohydrates. *Curr. Anal. Chem.* **2005**, *1*, 223-240.
11. Bulow, H. E. and Hobert, O., Differential Sulfations and Epimerization Define Heparan Sulfate Specificity in Nervous System Development. *Neuron* **2004**, *41*, 723-736.
12. Gama, C. I. and Hsieh-Wilson, L. C., Chemical approaches to deciphering the glycosaminoglycan code. *Curr. Opin. Chem. Biol.* **2005**, *9*, 609-619.
13. Staples, G. O.; Shi, X. F. and Zaia, J., Extended N-Sulfated Domains Reside at the Nonreducing End of Heparan Sulfate Chains. *J. Biol. Chem.* **2010**, *285*, 18336-18343.
14. Habuchi, H.; Habuchi, O. and Kimata, K., Sulfation pattern in glycosaminoglycan: Does it have a code? *Glycoconjugate J.* **2004**, *21*, 47-52.
15. Rosenberg, R. D. and Lam, L., Correlation between structure and function of heparin. *Proc. Natl. Acad. Sci. U. S. A.* **1979**, *76*, 1218-1222.
16. Lindahl, U.; Kusche-Gullberg, M. and Kjellen, L., Regulated Diversity of Heparan Sulfate. *J. Biol. Chem.* **1998**, *273*, 24979-24982.
17. Feyzi, E.; Saldeen, T.; Larsson, E.; Lindahl, U. and Salmivirta, M., Age-dependent Modulation of Heparan Sulfate Structure and Function. *J. Biol. Chem.* **1998**, *273*, 13395-13398.

18. Shi, X. and Zaia, J., Organ-specific Heparan Sulfate Structural Phenotypes. *J. Biol. Chem.* **2009**, *284*, 11806-11814.
19. Raman, R.; Raguram, S.; Venkataraman, G.; Paulson, J. C. and Sasisekharan, R., Glycomics: an integrated systems approach to structure-function relationships of glycans. *Nat Meth* **2005**, *2*, 817-824.
20. Horne, A. and Gettins, P., H-1-NMR Spectral Assignments for 2 Series of Heparin-Derived Oligosaccharides. *Carbohydr. Res.* **1992**, *225*, 43-57.
21. Dai, Y.; Whittal, R. M.; Bridges, C. A.; Isogai, Y.; Hindsgaul, O. and Li, L., Matrix-assisted laser desorption ionization mass spectrometry for the analysis of monosulfated oligosaccharides. *Carbohydr. Res.* **1997**, *304*, 1-9.
22. Juhasz, P. and Biemann, K., Utility of non-covalent complexes in the matrix-assisted laser desorption ionization mass spectrometry of heparin-derived oligosaccharides. *Carbohydr. Res.* **1995**, *270*, 131-147.
23. Schiller, J.; Arnhold, J.; Benard, S.; Reichl, S. and Arnold, K., Cartilage degradation by hyaluronate lyase and chondroitin ABC lyase: a MALDI-TOF mass spectrometric study. *Carbohydr. Res.* **1999**, *318*, 116-122.
24. Takagaki, K.; Kojima, K.; Majima, M.; Nakamura, T.; Kato, I. and Endo, M., Ion-Spray Mass-Spectrometric Analysis of Glycosaminoglycan Oligosaccharides. *Glycoconjugate J.* **1992**, *9*, 174-179.
25. Laremore, T. N. and Linhardt, R. J., Improved matrix-assisted laser desorption/ionization mass spectrometric detection of glycosaminoglycan disaccharides as cesium salts. *Rapid Commun. Mass Spectrom.* **2007**, *21*, 1315-1320.

26. Laremore, T. N.; Murugesan, S.; Park, T. J.; Avci, F. Y.; Zagorevski, D. V. and Linhardt, R. J., Matrix-assisted laser desorption/ionization mass spectrometric analysis of uncomplexed highly sulfated oligosaccharides using ionic liquid matrices. *Anal. Chem.* **2006**, *78*, 1774-1779.
27. Laremore, T. N.; Zhang, F. M. and Linhardt, R. J., Ionic liquid matrix for direct UV-MALDI-TOF-MS analysis of dermatan sulfate and chondroitin sulfate oligosaccharides. *Anal. Chem.* **2007**, *79*, 1604-1610.
28. Viseux, N.; de Hoffmann, E. and Domon, B., Structural Assignment of Permethylated Oligosaccharide Subunits Using Sequential Tandem Mass Spectrometry. *Anal. Chem.* **1998**, *70*, 4951-4959.
29. Saad, O. M. and Leary, J. A., Heparin Sequencing Using Enzymatic Digestion and ESI-MS with HOST: A Heparin/HS Oligosaccharide Sequencing Tool. *Anal. Chem.* **2005**, *77*, 5902-5911.
30. Zaia, J. and Costello, C. E., Tandem Mass Spectrometry of Sulfated Heparin-Like Glycosaminoglycan Oligosaccharides. *Anal. Chem.* **2003**, *75*, 2445-2455.
31. Little, D. P.; Speir, J. P.; Senko, M. W.; O'Connor, P. B. and McLafferty, F. W., Infrared Multiphoton Dissociation of Large Multiply Charged Ions for Biomolecule Sequencing. *Anal. Chem.* **1994**, *66*, 2809-2815.
32. Zaia, J., Principles of Mass Spectrometry of Glycosaminoglycans. *Journal of Biomolecular Mass Spectrometry* **2005**, *1*, 3-36.
33. Zaia, J.; McClellan, J. E. and Costello, C. E., Tandem Mass Spectrometric Determination of the 4S/6S Sulfation Sequence in Chondroitin Sulfate Oligosaccharides. *Anal. Chem.* **2001**, *73*, 6030-6039.

34. McClellan, J. E.; Costello, C. E.; O'Conno, P. B. and Zaia, J., Influence of Charge State on Product Ion Mass Spectra and the Determination of 4S/6S Sulfation Sequence of Chondroitin Sulfate Oligosaccharides. *Anal. Chem.* **2002**, *74*, 3760-3771.
35. Zaia, J.; Li, X.-Q.; Chan, S.-Y. and Costello, C. E., Tandem mass spectrometric strategies for determination of sulfation positions and uronic acid epimerization in chondroitin sulfate oligosaccharides. *J. Am. Soc. Mass Spectrom.* **2003**, *14*, 1270-1281.
36. Miller, M. J. C.; Costello, C. E.; Malmstrom, A. and Zaia, J., A tandem mass spectrometric approach to determination of chondroitin/dermatan sulfate oligosaccharide glycoforms. *Glycobiology* **2006**, *16*, 502-513.
37. Hitchcock, A. M.; Costello, C. E. and Zaia, J., Glycoform Quantification of Chondroitin/Dermatan Sulfate Using a Liquid Chromatography-Tandem Mass Spectrometry Platform. *Biochemistry* **2006**, *45*, 2350-2361.
38. Wolff, J. J.; Laremore, T. N.; Busch, A. M.; Linhardt, R. J. and Amster, I. J., Influence of Charge State and Sodium Cationization on the Electron Detachment Dissociation and Infrared Multiphoton Dissociation of Glycosaminoglycan Oligosaccharides. *J. Am. Soc. Mass Spectrom.* **2008**, *19*, 790-798.
39. Saad, O. M. and Leary, J. A., Compositional Analysis and Quantification of Heparin and Heparan Sulfate by Electrospray Ionization Ion Trap Mass Spectrometry. *Anal. Chem.* **2003**, *75*, 2985-2995.

40. Saad, O. M. and Leary, J. A., Delineating mechanisms of dissociation for isomeric heparin disaccharides using isotope labeling and ion trap tandem mass spectrometry. *J. Am. Soc. Mass Spectrom.* **2004**, *15*, 1274-1286.
41. Sweeney, M. D.; Yu, Y. and Leary, J. A., Effects of Sulfate Position on Heparin Octasaccharide Binding to CCL2 Examined by Tandem Mass Spectrometry. *J. Am. Soc. Mass Spectrom.* **2006**, *17*, 1114-1119.
42. Huang, R.; Pomin, V. H. and Sharp, J. S., LC-MS<sup>n</sup> Sequencing of Isomeric Chondroitin Sulfate Oligosaccharides Using a Chemical Derivatization Strategy. *Anal. Chem.* **In Review**,
43. Fenn, J. B.; Mann, M.; Meng, C. K.; Wong, S. F. and Whitehouse, C. M., Electrospray ionization for mass spectrometry of large biomolecules. *Science* **1989**, *246*, 64-71.
44. Zubarev, R. A.; Kelleher, N. L. and McLafferty, F. W., Electron capture dissociation of multiply charged protein cations. A nonergodic process. *J. Am. Chem. Soc.* **1998**, *120*, 3265-3266.
45. Zaia, J. and Costello, C. E., Compositional Analysis of Glycosaminoglycans by Electrospray Mass Spectrometry. *Anal. Chem.* **2001**, *73*, 233-239.
46. Budnik, B. A.; Haselmann, K. F. and Zubarev, R. A., Electron detachment dissociation of peptide di-anions: an electron-hole recombination phenomenon. *Chem. Phys. Lett.* **2001**, *342*, 299-302.
47. McFarland, M. A.; Marshall, A. G.; Hendrickson, C. L.; Nilsson, C. L.; Fredman, P. and Mansson, J. E., Structural Characterization of the GM1 Ganglioside by Infrared Multiphoton Dissociation, Electron Capture Dissociation, and Electron

- Detachment Dissociation Electrospray Ionization FT-ICR MS/MS. *J. Am. Soc. Mass Spectrom.* **2005**, *16*, 752-762.
48. Yang, J.; Mo, J. J.; Adamson, J. T. and Hakansson, K., Characterization of oligodeoxynucleotides by electron detachment dissociation Fourier transform ion cyclotron resonance mass spectrometry. *Anal. Chem.* **2005**, *77*, 1876-1882.
49. Adamson, J. T. and Hakansson, K., Electron capture dissociation of oligosaccharides ionized with alkali, alkaline earth, and transition metals. *Anal. Chem.* **2007**, *79*, 2901-2910.
50. Wolff, J. J.; Amster, I. J.; Chi, L. and Linhardt, R. J., Electron Detachment Dissociation of Glycosaminoglycan Tetrasaccharides. *J. Am. Soc. Mass Spectrom.* **2007**, *18*, 234-244.
51. Yang, J. and Hakansson, K., Fragmentation of Oligoribonucleotides from Gas-Phase Ion-Electron Reactions. *J. Am. Soc. Mass Spectrom.* **2006**, *17*, 1369-1375.
52. Wolff, J. J.; Laremore, T. N.; Busch, A. M.; Linhardt, R. J. and Amster, I. J., Electron Detachment Dissociation of Dermatan Sulfate Oligosaccharides. *J. Am. Soc. Mass Spectrom.* **2008**, *19*, 294-304.
53. Wolff, J. J.; Chi, L. L.; Linhardt, R. J. and Amster, I. J., Distinguishing glucuronic from iduronic acid in glycosaminoglycan tetrasaccharides by using electron detachment dissociation. *Anal. Chem.* **2007**, *79*, 2015-2022.
54. Wolff, J. J.; Laremore, T. N.; Busch, A. M.; Linhardt, R. J. and Amster, I. J., Electron Detachment Dissociation of Dermatan Sulfate Oligosaccharides. *J. Am. Soc. Mass Spectrom.* **2008**, *19*, 294-304.

55. Cody, R. B. and Freiser, B. S., Electron impact excitation of ions from organics: an alternative to collision induced dissociation. *Anal. Chem.* **1979**, *51*, 547-551.
56. Wolff, J. J.; Laremore, T. N.; Aslam, H.; Linhardt, R. J. and Amster, I. J., Electron-Induced Dissociation of Glycosaminoglycan Tetrasaccharides. *J. Am. Soc. Mass Spectrom.* **2008**, *19*, 1449-1458.
57. Savitski, M. M.; Nielsen, M. L.; Kjeldsen, F. and Zubarev, R. A., Proteomics-grade de novo sequencing approach. *J. Proteome Res.* **2005**, *4*, 2348.
58. Kjeldsen, F.; Silivra, O. A.; Ivonin, I. A.; Haselmann, K. F.; Gorshkov, M. and Zubarev, R. A., C $\alpha$ -C Backbone Fragmentation Dominates in Electron Detachment Dissociation of Gas-Phase Polypeptide Polyanions. *Chem. Eur. J.* **2005**, *11*, 1803-1812.
59. Ding, L. and Brancia, F. L., Electron capture dissociation in a digital ion trap mass spectrometer. *Anal. Chem.* **2006**, *78*, 1995-2000.
60. Baba, T.; Hashimoto, Y.; Hasegawa, H.; Hirabayashi, A. and Waki, I., Electron capture dissociation in a radio frequency ion trap. *Anal. Chem.* **2004**, *76*, 4263-4266.
61. Satake, H.; Hasegawa, H.; Hirabayashi, A.; Hashimoto, Y. and Baba, T., Fast multiple electron capture dissociation in a linear radio frequency quadrupole ion trap. *Anal. Chem.* **2007**, *79*, 8755-8761.
62. Voinov, V. G.; Beckman, J. S.; Deinzer, M. L. and Barofsky, D. F., Electron-capture dissociation (ECD), collision-induced dissociation (CID) and ECD/CID in a linear radiofrequency-free magnetic cell. *Rapid Commun. Mass Spectrom.* **2009**, *23*, 3028-3030.

63. Syka, J. E. P.; Coon, J. J.; Schroeder, M. J.; Shabanowitz, J. and Hunt, D. F., Peptide and protein sequence analysis by electron transfer dissociation mass spectrometry. *Proc. Natl. Acad. Sci. U. S. A.* **2004**, *101*, 9528-9533.
64. Herron, W. J.; Goeringer, D. E. and McLuckey, S. A., Gas-phase electron transfer reactions from multiply-charged anions to rare gas cations. *J. Am. Chem. Soc.* **1995**, *117*, 11555-11562.
65. Coon, J. J.; Shabanowitz, J.; Hunt, D. F. and Syka, J. E. P., Electron transfer dissociation of peptide anions. *J. Am. Soc. Mass Spectrom.* **2005**, *16*, 880-882.
66. Huzarska, M.; Ugalde, I.; Kaplan, D. A.; Hartmer, R.; Easterling, M. L. and Polfer, N. C., Negative electron transfer dissociation of de-protonated phosphopeptide anions: choice of radical cation reagent and competition between electron and proton transfer. *Submitted to Analytical Chemistry* **2010**,
67. Payne, A. H. and Glish, G. L., Gas-phase ion/ion interactions between peptides or proteins and iron ions in a quadrupole ion trap. *Intl. J. Mass Spectrom.* **2001**, *204*, 47-54.
68. Crizer, D. M.; Xia, Y. and McLuckey, S. A., Transition Metal Complex Cations as Reagents for Gas-Phase Transformation of Multiply Deprotonated Polypeptides. *J. Am. Soc. Mass Spectrom.* **2009**, *20*, 1718-1722.
69. Racaud, A.; Antoine, R.; Dugourd, P. and Lemoine, J., Photoinduced Dissociation of Heparin-Derived Oligosaccharides Controlled by Charge Location. *J. Am. Soc. Mass Spectrom.* *21*, 2077-2084.
70. Racaud, A.; Antoine, R.; Joly, L.; Mesplet, N.; Dugourd, P. and Lemoine, J., Wavelength-Tunable Ultraviolet Photodissociation (UVPD) of Heparin-Derived

- Disaccharides in a Linear Ion Trap. *J. Am. Soc. Mass Spectrom.* **2009**, *20*, 1645-1651.
71. Feinstein, A. R., *Multivariable Analysis*, Yale University Press: New Haven, CT, 1996.
72. Kowalski, B. R., *Chemometrics. Anal. Chem.* **1980**, *52*, 112R-122R.
73. Brereton, R. G., *Introduction to multivariate calibration in analytical chemistry. Analyst* **2000**, *125*, 2125-2154.
74. Rozett, R. W. and Petersen, E. M., *Classification of compounds by the factor analysis of their mass spectra. Anal. Chem.* **1976**, *48*, 817-825.
75. Justice, J. B. and Isenhour, T. L., *Factor analysis of mass spectra. Anal. Chem.* **1975**, *47*, 2286-2288.
76. Ritter, G. L.; Lowry, S. R.; Isenhour, T. L. and Wilkins, C. L., *Factor analysis of the mass spectra of mixtures. Anal. Chem.* **1976**, *48*, 591-595.
77. Knorr, F. J. and Futrell, J. H., *Separation of mass spectra of mixtures by factor analysis. Anal. Chem.* **1979**, *51*, 1236-1241.
78. Gaspari, M.; Verhoeckx, K. C. M.; Verheij, E. R. and van der Greef, J., *Integration of Two-Dimensional LC-MS with Multivariate Statistics for Comparative Analysis of Proteomic Samples. Anal. Chem.* **2006**, *78*, 2286-2296.
79. America, A. H. P.; Cordewener, J. H. G.; van Geffen, M. H. A.; Lommen, A.; Vissers, J. P. C.; Bino, R. J. and Hall, R. D., *Alignment and statistical difference analysis of complex peptide data sets generated by multidimensional LC-MS. Proteomics* **2006**, *6*, 641-653.

80. Gottfries, J.; Sjogren, M.; Holmberg, B.; Rosengren, L.; Davidsson, P. and Blennow, K., Proteomics for drug target discovery. *Chemom. Intell. Lab. Syst.* **2004**, *73*, 47-53.
81. Berman, E. S. F.; Kulp, K. S.; Knize, M. G.; Wu, L.; Nelson, E. J.; Nelson, D. O. and Wu, K. J., Distinguishing Monosaccharide Stereo- and Structural Isomers with TOF-SIMS and Multivariate Statistical Analysis. *Anal. Chem.* **2006**, *78*, 6497-6503.
82. Fangmark, I.; Jansson, A. and Nilsson, B., Determination of Linkage Position and Anomeric Configuration in Glucose-Containing Disaccharide Alditols by Multivariate Analysis of Data from Mass Spectrometry. *Anal. Chem.* **1999**, *71*, 1105-1110.
83. Oh, H. B.; Leach III, F. E.; Arungundram, S.; Al-Mafraji, K.; Venot, A.; Boons, G.-J. and Amster, I. J., Multivariate Analysis of Electron Detachment Dissociation Mass Spectra for Synthetic Heparan Sulfate Tetrasaccharides Differing Only in Hexuronic Acid Stereochemistry. *Accepted to J. Am. Soc. Mass Spectrom.* **2010**,

## **CHAPTER 2**

### **EXPERIMENTAL METHODS**

### *Synthetic Heparan Sulfate Oligosaccharide Preparation*

Heparan sulfate tetrasaccharides were synthesized by a modular approach [1] and purified by silica gel column chromatography. Prepared structures were confirmed by  $^1\text{H}$  NMR and accurate mass measurement by FT-ICR MS. Compounds were prepared as tetrasaccharides with varying degrees and positions of sulfation as well as hexuronic acid stereochemistry.

### *Preparation of Chondroitin Sulfate Oligosaccharides*

Chondroitin sulfate A (CS-A) and dermatan sulfate (DS) oligosaccharides were independently prepared by partial enzymatic depolymerization of bovine trachea chondroitin sulfate A (Celsus Laboratories, Cincinnati, OH) and porcine intestinal mucosa dermatan sulfate (Celsus Laboratories, Cincinnati, OH). A 20 mg/mL solution of each, in 50 mM Tris-HCl/60 mM sodium acetate buffer, pH 8 was incubated at 37°C with chondroitin ABC lyase from *Proteus vulgaris*, EC 4.2.2.4. (Seikagaku, Japan). After the absorbance at 232 nm indicated the digestion was 50% completed, the digestion mixture was heated at 100°C for 3 min. High-molecular-weight oligosaccharides and the enzyme were removed by ultra-filtration using a 5000 MWCO membrane. The resulting oligosaccharide mixture was concentrated by rotary evaporation and fractionated by low pressure GPC on a Bio-Gel P10 (Bio-Rad, Richmond, CA) column. Fractions containing oligosaccharides of interest were desalted by GPC on a Bio-Gel P2 column and freeze-dried [2]. Further purification was carried out using strong anion exchange high-pressure liquid chromatography (SAX-HPLC) on a semi-preparative SAX S5 Spherisorb column (Waters Corp, Milford, MA). The SAX-HPLC fractions containing > 90% of selected

oligosaccharides were collected, desalted by GPC, and freeze-dried. The solid was reconstituted in water and purified a second time by SAX-HPLC. Only the top 30% of the chromatographic peak was collected, desalted, and freeze-dried. Concentration of the oligosaccharide solutions was determined by measuring the absorbance at 232 nm ( $\epsilon = 3800 \text{ M}^{-1} \text{ cm}^{-1}$ ). The resulting fractions containing individual oligosaccharides were characterized by PAGE, ESI-MS, and high-field nuclear magnetic resonance (NMR) spectroscopy [3].

#### *GAG Oligosaccharide Desulfation*

The pyridinium salts of selected tetrasaccharides were dissolved in 10 % aqueous MeOH and heated for 6 hrs at 60° C [4] to produce the desulfated tetrasaccharides. The mass-selective quadrupole of the FT-ICR MS instrument was employed to isolate the desulfated compounds in lieu of additional laboratory based purification. The desulfation reaction does not affect the stereochemistry of the hexuronic acid residue, and so the chirality of the product is the same as that of the reactant as established by NMR analysis.

#### *Heparin Oligosaccharide Preparation*

Heparin sodium salt was obtained from porcine intestinal mucosa (Celsus Laboratories, Cincinnati, OH). Recombinant heparinase 1 (E.C. 4.2.2.7) from *F. heparinum* and expressed in *Escherichia coli* was used to partially depolymerize heparin sodium salt (6g) to 30% completion by ultraviolet absorbance and quenched in a water 100°C water bath. The reaction mixture was concentrated on a rotary evaporator and filtered through a 0.22  $\mu\text{m}$  filter prior to loading on a 1.5 m x 5.0 cm Bio-Gel P10

(BioRad, Hercules, CA) column. The column eluted at 1.2 mL/min using 0.2 M NaCl in distilled water to obtain uniform-sized oligosaccharides. After desalting separate peaks on a 100 cm x 2.0 cm P2 (BioRad, Hercules, CA) column, samples were concentrated and lyophilized. Fractionated samples were then separated on a 2.0 x 25 cm<sup>2</sup> semi-preparative strong anion exchange (SAX) high performance liquid chromatography (HPLC) (Shimadzu, Kyoto, Japan) column (Waters Spherisorb S5, Milford, MA) eluted with a salt gradient over 60 mins at a flow rate of 4.0 mL/min with absorbance detection at 232 nm [2]. Repurification was carried out for some fractions according to whether or not they were considered impure by analytical SAX-HPLC on a 5 µm Spherisorb -.46 x 25 cm<sup>2</sup> analytical column. Each of the oligosaccharides were prepared from HPLC determined to be >95% pure by analytical SAX-HPLC, PAGE analysis, RPIP-HPLC-ESI-MS, high resolution MS, and 1D and 2D NMR [5].

### *Mass Spectrometry Analysis*

Experiments (excluding NETD) were performed with a 9.4 T Bruker Apex Ultra QeFTMS (Billerica, MA), shown in Figure 2.1, fitted with an MTP dual ion source, 25 W CO<sub>2</sub> laser (Synrad model J48-2, Mukilteo, WA) for IRMPD, and an indirectly heated hollow cathode (HeatWave, Watsonville, CA) to generate electrons for EDD. The sample solutions were infused at a rate of 120 µL/hour and ionized by electrospray using a metal capillary (Agilent Technologies, Santa Clara, CA, #G2427A) or at 10 µL/hour and ionized by nanospray (pulled fused silica tip model FS360-75-15-D-20; New Objective, Woburn, MA, USA). Based on the extent of sulfation and desired charge state or degree of sodiation, the ESI solvent was varied. Solutions of each di-sulfated

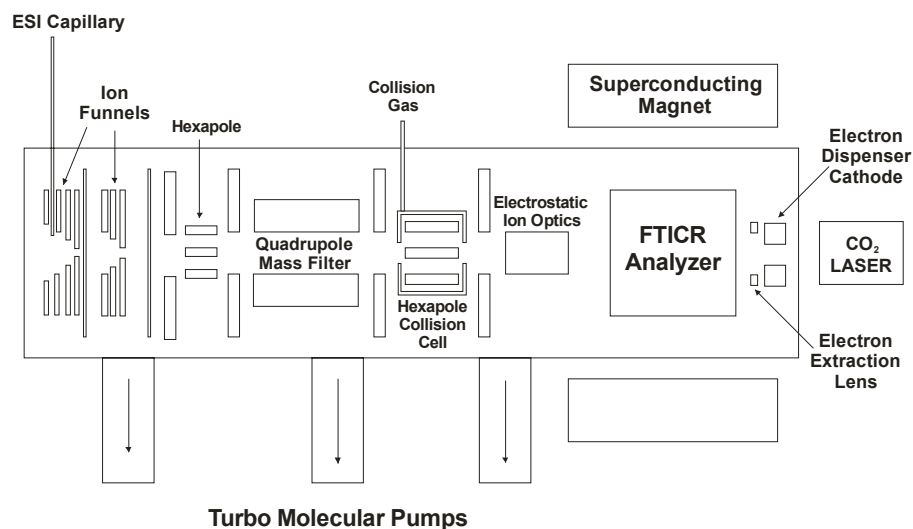


**Figure 2.1** Diagram of the Bruker Apex FTMS mass spectrometer.

oligosaccharide were introduced at a concentration of 0.1 mg/mL in 50:50:0.1 methanol:H<sub>2</sub>O:FA (Sigma, St. Louis, MO) to generate doubly deprotonated ions and 0.2 mg/mL in 50:50 methanol:H<sub>2</sub>O with 1% 100 μM NaOH to generate triply deprotonated ions and sodium adduct ions. To achieve quadruply deprotonated precursor ions for the tetra-sulfated tetrasaccharides, 105 mM sulfolane in acetonitrile was introduced to the ESI line via a line splitter [6]. A secondary syringe pump controlled the relative amount of sulfolane introduced to the ESI solvent. All oligosaccharides were examined in negative ion mode.

#### *Electron Detachment Dissociation (EDD)*

For EDD experiments, precursor ions were isolated in the external quadrupole and accumulated for 1-3 seconds in an rf only hexapole before injection into the FT-ICR MS cell. One or two quadrupole isolation/analyzer cell fills were utilized per scan. The selection of the precursor ion was further refined by using in-cell isolation with a

coherent harmonic excitation frequency (CHEF) event [7]. For electron irradiation the cathode bias was set to -19 V. The extraction lens was set to  $-18.5 \pm 0.1$  V, and the cathode heater was set to 1.5 A. The precursor ions were then irradiated with electrons for 1 second. 24-36 acquisitions were signal averaged per mass spectrum. For each mass spectrum, 1M points were acquired, padded with one zero fill, and apodized using a sinebell window. Background spectra were acquired by leaving all parameters the same but setting the cathode bias to 0 V to ensure that no electrons reached the analyzer cell. External calibration of mass spectra produced mass accuracy of 5 ppm. Internal calibration was also performed using confidently assigned glycosidic bond cleavage products as internal calibrants, providing mass accuracy of  $<1$  ppm. Due to the large number of low intensity products formed by EDD, only peaks with  $S/N > 10$  are reported. Product ions were assigned using accurate mass measurement and Glycoworkbench [8]. All products are reported using the Wolff-Amster annotation [9] of the Domon and Costello nomenclature [10]. To account for additional sulfate loss observed during analysis of highly sulfated GAGs, a filled circle has been added to the annotation to indicate a loss of 2 or more sulfates. In annotated spectra, charge states are assigned as  $1^-$  unless indicated otherwise.

#### *Electron Induced Dissociation (EID)*

EID experiments are performed with the same parameters as EDD, except a singly charged species is irradiated. 24 acquisitions were signal averaged per mass spectrum. For each mass spectrum, 512K points were acquired, padded with one zero fill, and apodized using a sinebell window. Background spectra were acquired by leaving

all parameters the same but setting the cathode bias to 0 V to ensure that no electrons reached the analyzer cell. External calibration of mass spectra produced mass accuracy of 5 ppm. Internal calibration was also performed using confidently assigned glycosidic bond cleavage products as internal calibrants, providing mass accuracy of <1 ppm.

### *Negative Electron Transfer Dissociation (NETD)*

NETD experiments were performed on a 12.0 T Bruker solariX FTMS instrument (Bruker Daltonics, Billerica, MA) depicted in Figure 2.2. In addition to higher magnetic field, the solariX instrument differs in several aspects when compared to the Apex cart utilized for all other experiments. The solariX FTMS cart adds the capability for

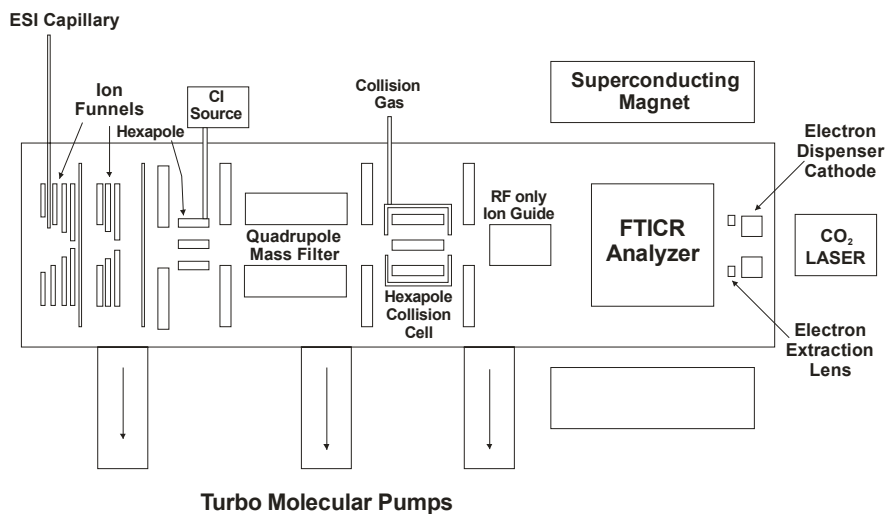


**Figure 2.2** Diagram of the Bruker solariX FTMS mass spectrometer.

ion-ion reactions in the hexapole collision region by modification of the supporting electronics to generate a 3-D ion trap. Analyte ions generated by ESI are accumulated in the collision cell trap and subsequently reacted with reagent ions generated by a chemical

ionization source (CI) adjacent to the primary ion flight path. For NETD, fluoranthene radical cations are generated in the CI source under a background pressure of either methane or nitrogen gas. The use of nitrogen promotes the formation of the radical species, whereas methane generates both radical and protonated cations. Prior to injection into the ion trap, the reagent radical cation is mass filtered. An additional difference is the replacement of the accelerating ion optics prior to the magnetic field by an rf-only ion guide.

For NETD experiments, precursor ions were isolated in the external quadrupole and accumulated for 1-3 seconds in the 3-D ion trap before reaction with the reagent radical cation. The fluoranthene radical cation was generated in the CI source and accumulated for 500 -1000 ms prior to mass filtering and injection into the 3-D ion trap. Ion-ion reactions were conducted for 1.5 s. The precursor ion and NETD products were then injected into the mass analyzer through an rf-only ion guide. One analyzer cell fill was utilized per scan. 24-36 acquisitions were signal averaged per mass spectrum. For each mass spectrum, 1M points were acquired, padded with one zero fill, and apodized using a sinebell window. Background spectra were acquired by leaving all parameters the same without the generation of the radical cation. External calibration of mass spectra produced mass accuracy of 5 ppm. Internal calibration was also performed using confidently assigned glycosidic bond cleavage products as internal calibrants, providing mass accuracy of <1 ppm. Due to the large number of low intensity products formed by NETD, only peaks with S/N > 10 are reported. Product ions were assigned using accurate mass measurement and Glycoworkbench [8]. All products are reported using

the Wolff-Amster annotation [9] of the Domon and Costello nomenclature [10]. In annotated spectra, charge states are assigned as 1<sup>-</sup> unless indicated otherwise.

### *Infrared Multiphoton Dissociation*

In selected cases, ions were activated by infrared multiphoton dissociation (IRMPD) to compare electron-based activation results with those from threshold activation. In those experiments, IRMPD was conducted with a 25 W CO<sub>2</sub> laser (Synrad model J48-2, Mukilteo, WA). Ions were irradiated for 0.025 s to 0.075 s at 65 % laser attenuation. Data acquisition and reduction was conducted in the same manner described earlier.

### *Multivariate Statistical Analysis*

Principal component analysis (PCA) was performed using PLS Toolbox (Eigenvector Research, Inc., Wenatchee, WA). The abundances of assigned fragment ions were normalized with respect to total ion abundance in each EDD spectrum. An input data matrix was constructed with each row containing the mass spectrum of a single tetrasaccharide epimer (samples) and each column, the normalized abundance of an assigned fragment ion (variables). For each sample, five replicates were acquired. Prior to PCA, each data set was mean-centered and cross-validated. For comparison, the abundances of assigned peaks from IRMPD spectra were also treated in the same manner as the EDD data. Partial least squares (PLS) analysis was also performed with PLS Toolbox on the same data sets selected for PCA.

## REFERENCES

1. Arungundram, S.; Al-Mafraji, K.; Asong, J.; Leach, F. E.; Amster, I. J.; Venot, A.; Turnbull, J. E. and Boons, G.-J., Modular Synthesis of Heparan Sulfate Oligosaccharides for Structure-Activity Relationship Studies. *J. Am. Chem. Soc.* **2009**, *131*, 17394-17405.
2. Pervin, A.; Gallo, C.; Jandik, K. A.; Han, X.-J. and Linhardt, R. J., Preparation and structural characterization of large heparin-derived oligosaccharides. *Glycobiology* **1995**, *5*, 83-95.
3. Munoz, E.; Xu, D.; Avci, F.; Kemp, M.; Liu, J. and Linhardt, R. J., Enzymatic synthesis of heparin related polysaccharides on sensor chips: Rapid screening of heparin-protein interactions. *Biochem. Biophys. Res. Commun.* **2006**, *339*, 597-602.
4. Nagasawa, K.; Inoue, Y. and Kamata, T., Solvolytic desulfation of glycosaminoglycuronan sulfates with dimethyl sulfoxide containing water or methanol. *Carbohydr. Res.* **1977**, *58*, 47-55.
5. Xiao, Z.; Zhao, W.; Yang, B.; Zhang, Z.; Guan, H. and Linhardt, R. J., Heparinase 1 selectivity for the 3,6-di-O-sulfo-2-deoxy-2-sulfamido- $\alpha$ -D-glucopyranose (1,4) 2-O-sulfo-  $\alpha$ -L-idopyranosyluronic acid (GlcNS3S6S-IdoA2S) linkages. *Glycobiology*
6. Huang, Y.; Shi, X.; Yin, H.; Killeen, K. and Zaia, J., Improvement of ESI Behavior of Heparan Sulfate Oligosaccharides by Using a Chip-based Pulsed Post-Column Makeup Flow for Online LC/MS, *58th ASMS Conference on Mass Spectrometry and Allied Topics*, Salt Lake City, UT, 2010.

7. Heck, A. J. R.; de Koning, L. J.; Pinkse, F. A. and Nibbering, N. M. M., Mass-specific selection of ions in Fourier-transform ion cyclotron resonance mass spectrometry. Unintentional off-resonance cyclotron excitation of selected ions. *Rapid Commun. Mass Spectrom.* **1991**, *5*, 406-414.
8. Ceroni, A.; Maass, K.; Geyer, H.; Geyer, R.; Dell, A. and Haslam, S. M., GlycoWorkbench: A Tool for the Computer-Assisted Annotation of Mass Spectra of Glycans. *Journal of Proteome Research* **2008**, *7*, 1650-1659.
9. Wolff, J. J.; Laremore, T. N.; Busch, A. M.; Linhardt, R. J. and Amster, I. J., Influence of Charge State and Sodium Cationization on the Electron Detachment Dissociation and Infrared Multiphoton Dissociation of Glycosaminoglycan Oligosaccharides. *J. Am. Soc. Mass Spectrom.* **2008**, *19*, 790-798.
10. Domon, B. and Costello, C. E., A systematic nomenclature for carbohydrate fragmentations in FAB-MS/MS spectra of glycoconjugates. *Glycoconjugate J.* **1988**, *5*, 397-409.

## CHAPTER 3

# EVALUATION OF THE EXPERIMENTAL PARAMETERS WHICH CONTROL ELECTRON DETACHMENT DISSOCIATION AND THEIR EFFECT ON THE FRAGMENTATION EFFICIENCY OF GLYCOSAMINOGLYCAN CARBOHYDRATES<sup>1</sup>

---

<sup>1</sup> Leach III, F. E.; Wolff, J. J.; Laremore, T. N.; Linhardt, R.J. and Amster, I. J. 2008. *International Journal of Mass Spectrometry*. 276:110-115. Reprinted here with permission of publisher.

## ABSTRACT

The efficiency of conversion of precursor ions to observable products for electron detachment dissociation (EDD) was measured as a function of the key experimental parameters to determine their optimal values for the Fourier transform mass spectrometry analysis of anionic glycosaminoglycan carbohydrates. These parameters include electron current, electron energy, dispenser cathode heater current, electron beam duration, charge state of the precursor ion, oligomer length, and precursor ion number accumulated in an external radio frequency multipole trap. Precursor conversion is most efficient at an electron current of 15  $\mu\text{A}$ , and decreases at higher and lower values. The conversion of precursor to product ions increases in efficiency as the electron pulse duration is increased. Together, these data suggest that a radially repulsive electric field is produced between the electron beam and negative ions during EDD which causes the reaction cross section to decrease at higher electron current values ( $>15 \mu\text{A}$ ). Elevating the heater current of the dispenser cathode increases the electron flux, but also causes ion activation, presumably by blackbody infrared irradiation. An electronic circuit is described that allows the electron current produced by the dispenser cathode to be measured during an EDD or electron capture dissociation (ECD) experiment.

## INTRODUCTION

Electron capture dissociation (ECD) [1] has proven to be a valuable tool for the analysis of a diverse array of biomolecules, particularly for peptide sequencing [2-4] and for the identification of labile modifications [5] that are difficult to retain during conventional ion activation methods. The negative ion complement of this ion activation method, electron detachment dissociation (EDD) has also been utilized for the analysis of deprotonated biomolecules including peptides [6], oligonucleotides [7, 8], gangliosides [9], and carbohydrates [10-13]. Like ECD, EDD produces a radical site in a charge-reduced precursor ion, and this leads to fragmentation processes that are complementary to those exhibited by other methods of ion activation, namely collisionally induced dissociation (CID) and infrared multiphoton dissociation (IRMPD).

With the development of these electron activation techniques, there has been an effort to characterize the key experimental parameters that control the yield of product ions and to gain further insight into the fundamental processes underlying electron induced fragmentation [2, 4, 14-22]. The majority of this work has been directed toward ECD. The chief parameters that affect ion production are electron beam current (controlled by the dispenser cathode heater current and the voltage applied to the electron extraction lens or grid), electron kinetic energy (determined by the voltage applied to the dispenser cathode), and the duration of the electron pulse. By manipulating these variables, the energy and flux of electrons entering the analyzer cell can be controlled.

As the initial step in ECD/EDD requires the interaction of an electron with a mass-selected precursor ion, the majority of work in this area has focused on maximizing the overlap of the electron beam with the trapped ions within the FT-ICR analyzer cell by

manipulation of the electron flux or the spatial distribution of ions [16, 17, 23, 24]. Initially, directly heated filaments were utilized as the electron source, but given their limited current sourcing capability and difficulties in tuning the appropriate electron energy, they were soon replaced by indirectly heated dispenser cathodes. This advance provides for an increased electron emission current and therefore a decrease in irradiation time [16]. Additionally, on and off-resonance excitation have been employed to manipulate the trapped ions and increase the ion-electron interaction [23, 24]. The utility of external ion accumulation for ECD has also been examined. Not only does accumulation in an external multipole increase the precursor ion population available for irradiation, it has been observed that external accumulation results in the axialization of the trapped ions, and therefore increases the beam-ion overlap, resulting in decreased irradiation times [17].

The impact of electron energy has been studied in both ECD and EDD. Typically, electrons are less than 0.2 eV in standard ECD [1]. This range has expanded to 3-13 eV through the development of hot electron capture dissociation (HECD) [18] which produces secondary ion fragments such as w-type ions for peptides. Tysbin et al. have also observed ECD products at electron kinetic energies of 0-50 eV by utilizing the increased sensitivity attained by implementing gas-assisted dynamic trapping [19]. Electron energy studies have covered a smaller range in EDD. Initial reports of EDD in peptide di-anions covered a range of 10-27 eV [6], whereas oligonucleotides were irradiated with 16-18 eV [7, 8] and carbohydrates with 19 eV [10-12] and 20-30 eV [13].

We have recently demonstrated the effectiveness of EDD for the analysis of anionic glycosaminoglycan (GAG) carbohydrates. EDD produces crossring and

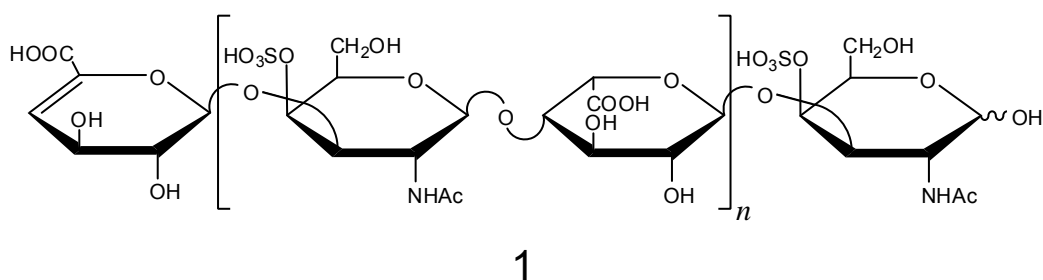
glycosidic bond fragmentation while minimizing the loss of SO<sub>3</sub> from sulfated GAG oligosaccharides [10-12]. To establish a quantitative basis for improving our fragmentation efficiency, we examine here the effect of key parameters on the efficiency of the EDD process. By calculating the efficiency of conversion to observable products, we are able to identify the optimal parameters for electron-based fragmentation of anionic glycosaminoglycans. We also examine the effect of oligosaccharide length, charge state of the precursor ion, and accumulation time in an external hexapole on the efficiency of conversion of precursors into product ions.

## **EXPERIMENTAL**

### *Preparation of DS Oligosaccharides*

Dermatan sulfate (DS) oligosaccharides (Structure 1) were prepared by partial enzymatic depolymerization of porcine intestinal mucosa dermatan sulfate (Celsus Laboratories, Cincinnati, OH). A 20 mg/mL dermatan sulfate solution in 50 mM Tris-HCl/60 mM sodium acetate buffer, pH 8 was incubated at 37 °C with chondroitin ABC lyase from *Proteus vulgaris*, EC 4.2.2.4. (Seikagaku, Japan). After the absorbance at 232 nm indicated the digestion was 50 % completed, the digestion mixture was heated at 100 °C for 3 min. High-molecular-weight oligosaccharides and the enzyme were removed by ultra-filtration using a 5000 MWCO membrane. The resulting oligosaccharide mixture was concentrated by rotary evaporation and fractionated by low pressure GPC on a Bio-Gel P10 (Bio-Rad, Richmond, CA) column. Fractions containing tetra- to decasaccharides (dp4 – dp10) were desalted by GPC on a Bio-Gel P2 column and freeze-dried [25]. Further purification of these compounds was carried out using strong anion exchange high-pressure liquid chromatography (SAX-HPLC) on a semi-preparative SAX

S5 Spherisorb column (Waters Corp, Milford, MA). The SAX-HPLC fractions containing > 90 % of the desired oligosaccharides were collected, desalted by GPC, and freeze-dried. The solid was reconstituted in water and purified a second time by SAX-HPLC. Only the top 30 % of the chromatographic peak was collected, desalted, and freeze-dried. Concentration of the oligosaccharide solutions was determined by measuring the absorbance at 232 nm ( $\epsilon = 3800 \text{ M}^{-1}\text{cm}^{-1}$ ). The resulting fractions containing individual DS oligosaccharides were characterized by PAGE, ESI-MS, and high-field nuclear magnetic resonance (NMR) spectroscopy.



### *Mass Spectrometry Analysis*

Experiments were performed with a 9.4 T Bruker Apex Ultra QeFTMS (Billerica, MA) fitted with an Apollo II dual source, and an indirectly heated hollow cathode for generating electrons for EDD. Solutions of each oligosaccharide were introduced at a concentration of 0.1 – 0.2 mg/mL in 50:50:0.1 methanol:H<sub>2</sub>O:FA (Sigma, St. Louis, MO) and ionized by electrospray using a metal capillary (Agilent Technologies, Santa Clara, CA, #G2427A). Formic acid was utilized to reduce the presence of additional charge states and sodium-hydrogen heterogeneity. The sample solutions were infused at a rate of 120  $\mu\text{L}/\text{hour}$ . All DS oligosaccharides were examined in negative ion mode.

For the EDD experiments, precursor ions were isolated in the external quadrupole and accumulated for 3-6 seconds before injection into the FTMS cell. One isolation/cell fill was utilized per scan. The selection of the precursor ion was further refined by using in-cell isolation with a coherent harmonic excitation frequency (CHEF) event [26]. For electron irradiation the cathode bias was set to -19 V. During scans of electron current, the extraction lens was varied from -18.75 V to -19.70 V, and the cathode heater was set to either 1.3 A or 1.6 A. The precursor ions were then irradiated with electrons for 1 second. During experiments varying the electron irradiation pulse duration, a constant cell current of 15  $\mu$ A was maintained by setting the extraction lens to -18.31 V for a heater current of 1.3 A and -18.79 V for a heater current of 1.6 A. 24 acquisitions were averaged per mass spectrum. For each mass spectrum, 512K points were acquired, padded with one zero fill, and apodized using a sinebell window. Background spectra were acquired by leaving all parameters the same but setting the cathode bias to 0 V to ensure that no electrons reached the analyzer cell. External calibration of mass spectra produced a mass accuracy of 5 ppm. Internal calibration was also performed using confidently assigned glycosidic bond cleavage products as internal calibrants, providing a mass accuracy of <1 ppm. Due to the large number of low intensity products formed by EDD, only peaks with S/N > 10 are reported. Product ions were assigned using accurate mass measurement. All products are reported using the Domon and Costello nomenclature [27].

To measure the cathode electron emission current and electron current incident upon the extraction lens during the EDD experiment, a pair of analog circuits is employed, shown in Figures 3.1A and 3.1B. A circuit for monitoring current is inserted

in series between the electron dispenser cathode and its voltage source, and a second circuit is inserted between the electron extraction lens and its voltage source.

For each series of experiments, the formulation of Gorshkov et al. [23] was employed to calculate the efficiency of conversion of precursor ions to observable products for the dermatan sulfate samples. Efficiency refers to the formation of all product ions, including those resulting from EDD, EID [28], and precursor activation due to blackbody irradiation. All efficiency calculations for electron current and pulse duration are presented as the average and associated

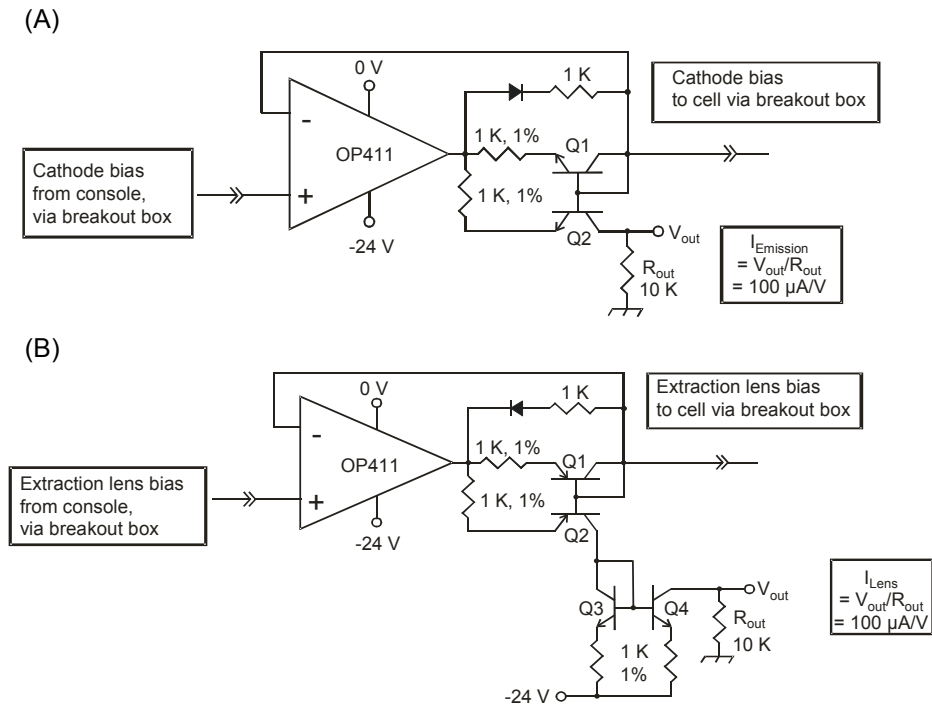


**Figure 3.1** (A) Analog circuit designed to measure the emission current of the EDD cathode. Q1 and Q2 are a matched pair of npn transistors. (B) Analog circuit designed to measure the extraction lens current. Q1/Q2 are a matched pair of npn transistors, and

Q3/Q4 are a matched pair of npn transistors. The electron current sourced by the cathode and sunk by the lens are mirrored and converted to a voltage by 10K resistors.

standard deviation of spectra taken in triplicate for each data point. Efficiency calculations for experiments that utilize hexapole accumulation are based on single measurements. We express our conversion efficiency as:

$$\xi = \frac{\sum_{j=1}^N I_j / z_j}{I_o / z_o}$$

$I_j$  is the fragment ion intensity of the  $j^{\text{th}}$  peak,  $z_j$  is its charge state, excluding the precursor ion intensity but including the charge-reduced precursor intensity,  $I_o$  is the non-irradiated precursor ion intensity and  $z_o$  is the precursor ion charge. As the ions are detected by the measurement of an image current in FTICR-MS, the observed signal intensity is directly proportional to the charge state of a given precursor or product ion. In dividing by a given peak's charge state, the intensities are normalized, allowing for direct summation across the products present in the  $MS^2$  spectrum.

For the two chosen dermatan sulfate samples, precursor ions of charge states  $2^-$  and  $4^-$ , corresponding to dp4 and dp8 respectively, were isolated and irradiated for each experiment. Based on the theoretical framework presented by Gorshkov, the maximum efficiency that can be achieved is given by:

$$\xi = \frac{n-1}{n} \left[ 1 - 0.5 \times \frac{(n-1)^2}{n^2} \right]$$

where  $n$  is the precursor charge state; the expected maximum attainable efficiency for a  $2^-$  ion is 43.75 % and approaches 50 % as the charge state is increased to  $4^-$ .

## RESULTS AND DISCUSSION

### *Measurement of Electron Current*

Other researchers have previously reported measuring the electron current that passes through the cell by capturing electrons at an ion focusing element on the opposing side of the cell from the electron emitters [16, 20, 21]. Kaiser and Bruce have recently reported measuring the electron current during EPIC by the difference in emission and lens current [29]. However, with previously reported approaches electron current cannot be measured during an ECD or EDD experiment. We have developed a method for measuring electron current during an experiment. Two analog circuits were designed to allow for a direct measurement of the cathode emission current and electron current incident upon the extraction lens, as shown in Figure 3.1A and 3.1B. The face of the hollow dispenser cathode is approximately  $36 \text{ mm}^2$  but only  $19 \text{ mm}^2$  of the cathode is exposed to the analyzer cell. Therefore some portion of the emitted electron flux is incident upon the face of the extraction lens and never reaches the cell. Thus, we need to measure both the electron current emitted by the dispenser cathode, and that captured by the extraction lens to determine, by difference, the current reaching the analyzer cell. We denote the measured currents as follows: emission current – the total electron current produced by the dispenser cathode; lens current – the electron current impinging on the face of the extraction lens; and cell current – the electron current entering the FT-ICR analyzer cell, deduced from the difference between emission and lens current.

The electron currents produced at the cathode and captured by the extraction lens are passed by a current mirror circuit in which an equivalent current is driven through a resistor to ground, producing a measurable voltage. The voltages are proportional to the electron current sourced by the cathode and sunk by the lens, and are recorded with an oscilloscope, which provides the values of electron current during the short pulse duration used for EDD or ECD. The current mirror circuit does not alter the voltage applied to the cathode and lens, in contrast to the use of a series resistor for monitoring the current. This is an important advantage, as even small changes in the bias voltage of the dispenser cathode or the extraction lens can produce large changes in the electron current.

Prior to our application of the circuit to the EDD experiment, we established a series of baseline curves shown in Figure 3.2, to measure the actual output of the cathode. From these measurements, we find that 80-90 % of the emitted electrons are captured by the lens, and therefore fail to reach the FT-ICR analyzer cell. At standard conditions for EDD experiments conducted to date (heater current of 1.6 A and  $-0.2$  V potential difference between the cathode and lens), only 7 % of emitted electrons enter the cell, resulting in a cell current of approximately 15-20  $\mu\text{A}$ . This low value is surprising, as the hollow cathode dispenser/extraction lens design exposes 19  $\text{mm}^2$  of the 36  $\text{mm}^2$  cathode surface area, and the expected transmission efficiency into the cell should be approximately 50 %. To confirm the value measured by our circuit, we have also measured the electron current captured by the high voltage focusing element on the opposing side of the analyzer cell as proposed by Polfer and Tsybin [16, 21] and find it to be in agreement with the value determined by the difference in emission and lens current.

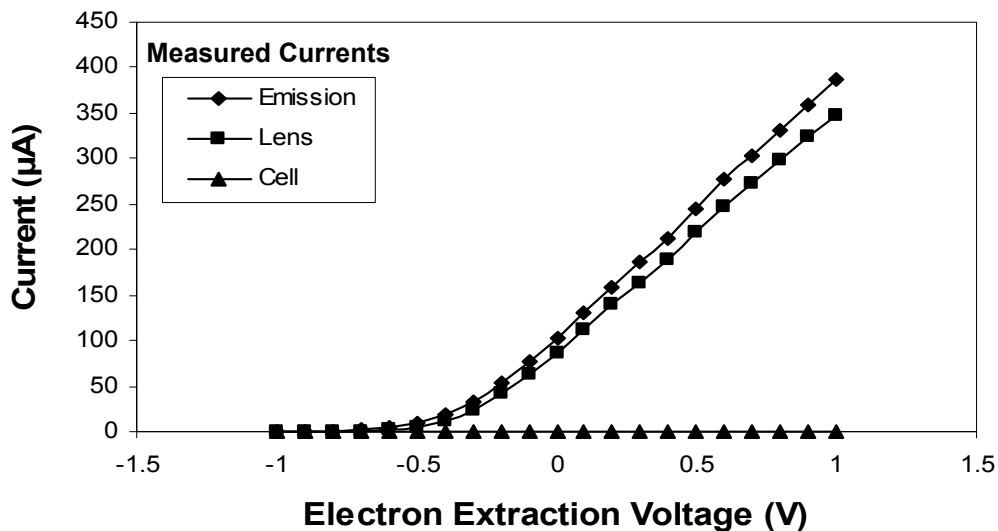


**Figure 3.2** Electron currents ( $\mu\text{A}$ ) as a function of the potential difference between the extraction lens and dispenser cathode,  $\Delta V$ , at a heater current of 1.6A. A sub-optimal transmission efficiency is observed for electrons entering the FTICR analyzer cell.

#### *Effect of Oligosaccharide Length and Precursor Ion Charge State*

To examine the effect of oligosaccharide length on fragmentation efficiency, dermatan sulfate dp4 and dp8 were analyzed, shown in Figure 3.3. In both samples, a maximum efficiency is observed at 15  $\mu\text{A}$  of cell current. In doubling the length of the oligomer, the conversion efficiency increases from 18 % to 29 %. The dp8 oligosaccharide has twice the number of sulfate groups than does dp4, and the principal charge state of dp8 is twice that of dp4. Zubarev *et al.* [2] have previously observed an increase in cross-section to be dependent on  $z^2$  during ECD. The higher efficiency of dissociation of dp8 suggests a doubling in the collision cross-section for the interaction of

electrons and precursor ions, resulting from the higher charge of the longer oligosaccharide. This interaction produces both electron detachment and electron induced dissociation.

### *Heater Current*

To examine the effect of heater current on the EDD of dermatan sulfate glycosaminoglycans, spectra were analyzed at heater current settings of 1.3 A and 1.6 A for dermatan sulfate dp8, shown in Figure 3.4. At a cell current of 15  $\mu\text{A}$ , a maximum conversion efficiency of approximately 28-29 % was observed for both heater current values. As the heater current value does not affect the energy of the electrons entering the cell, it should be expected that a similar maximum should be observed for each. The conversion efficiency decreases sharply at cell current values below 15  $\mu\text{A}$ , although products have been observed at cell current values of only 1  $\mu\text{A}$ . Above 15  $\mu\text{A}$  there is also a decrease in efficiency. We do not ascribe much significance to the secondary maximum observed at 30  $\mu\text{A}$  for the data collected with a heater current of 1.3 A, as the dispenser cathode is operating close to the temperature threshold for electron emission. EDD products have been observed at cell current values up to 75  $\mu\text{A}$ . At higher cell currents, the precursor is depleted in intensity and the conversion to products is reduced. Several possible mechanisms could account for the decline in efficiency above the optimal electron current of 15  $\mu\text{A}$ . First is that as the electron cell current increases, there is an increase in radial repulsion between the electron beam and negative charge of the trapped ions. This repulsion could result in decreased overlap between the electron beam

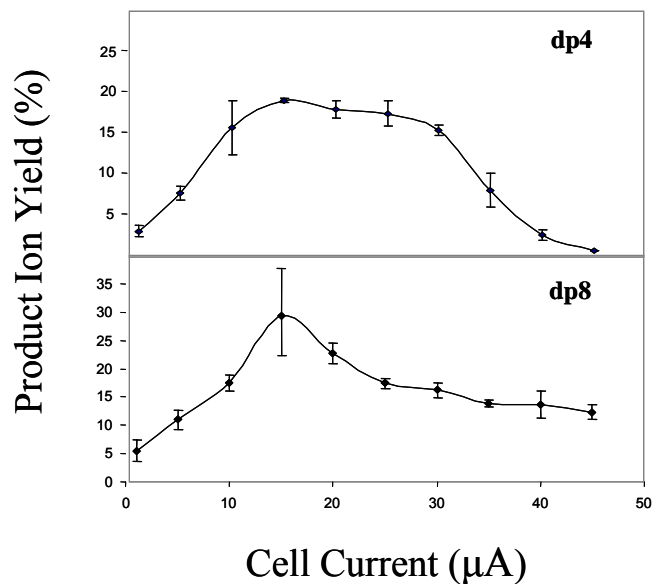


**Figure 3.3** Efficiencies of product formation versus electron current for dermatan sulfate dp4 and dp8 at a heater current of 1.6A, showing a maximum at 15 µA.

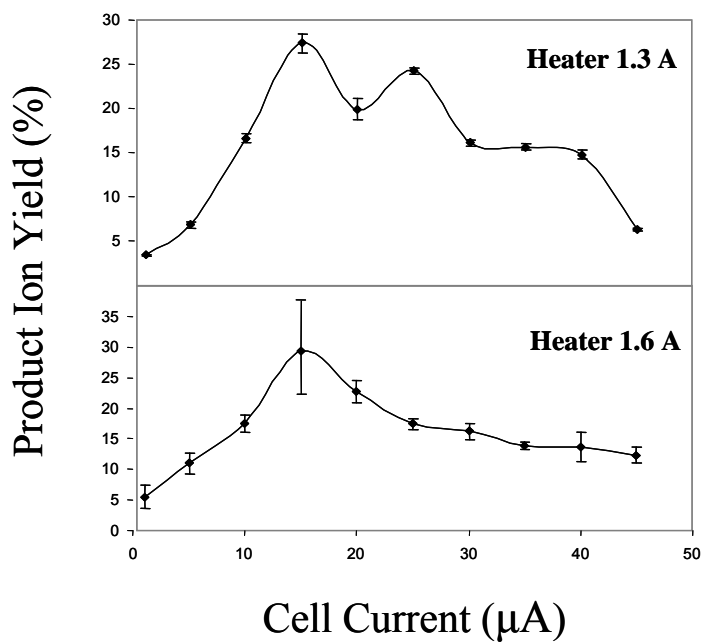


**Figure 3.4** Efficiency of product formation for dermatan sulfate dp8 as a function of cell current at heater currents of 1.3A and 1.6A.

and the ions, resulting in lower fragmentation efficiencies. Consistent with this argument, the dp8 oligomer is observed to have a sharper maximum than dp4, as seen in Figure 3.3. One expects a larger repulsive interaction for the longer dp8 oligomer, as it carries twice the charge as does dp4. A second possibility is that with higher electron current, sequential dissociation reactions produce fragment ions with intensities or mass-to-charge values below the detection limit. A third possibility is ion loss by neutralization from multiple electron detachment, which is expected to increase with higher electron flux. These latter two possibilities are discounted by other observations (vide infra.)

In order to achieve the same cell current at different heater current settings, the voltage applied to the extraction lens must be altered. As the heater current is lowered, the extraction voltage, the potential difference between the extraction lens and dispenser cathode ( $\Delta V$ ), must be increased to maintain a constant cell current. In our study, the cathode was held at -19.0 V and the extraction voltage increased from -0.19 V at 1.6 A to +0.26 V at 1.3 A. Identical EDD mass spectra of DS dp8, shown in Figure 3.5, were obtained at these settings, demonstrating that cell current is the principle parameter that controls the extent of fragmentation in EDD, and that by monitoring this parameter, one can obtain identical EDD mass spectra for a variety of heater current values.

### *Pulse Duration*

Our previous EDD studies of glycosaminoglycan carbohydrates have used an electron pulse duration of 1.0 s [10-12]. Having established that the maximum efficiency occurs at a cell current of 15  $\mu\text{A}$ , the effect of electron pulse duration was investigated while holding constant the electron current delivered to the cell. Fragmentation

efficiency is observed to increase as the electron beam interaction time increases from 0.1 s to 2.0 s, as shown in Figure 3.6.

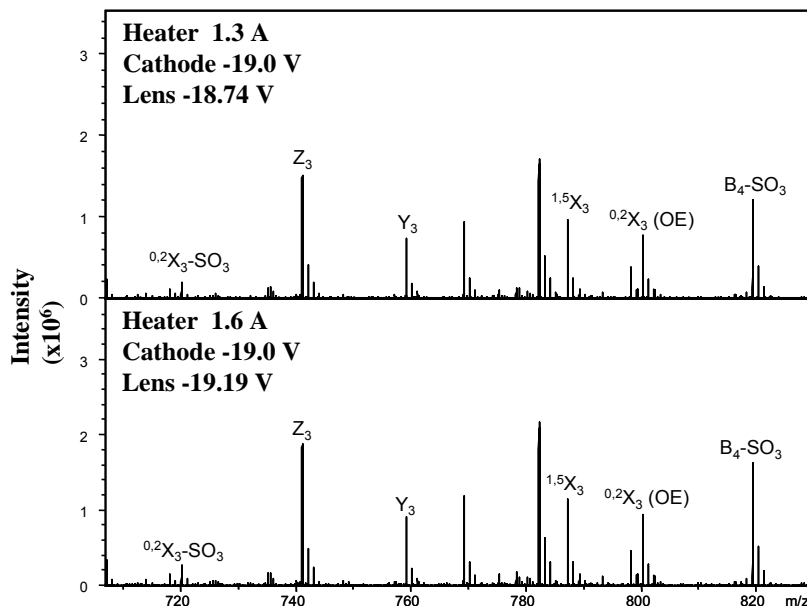


**Figure 3.5** EDD mass spectra acquired at heater current settings of 1.3 A and 1.6 A showing identical fragmentation obtained by adjusting the electron extraction voltage.

This behavior is quite different from the cell current measurements, in which efficiency peaks at an intermediate value and then decreases as the cell current increases. Together these data suggest that the decrease in efficiency at higher cell currents is not a result of converting ions into neutrals through multiple electron detachment events, or promoting secondary fragmentation that reduces products to  $m/z$  or intensity values that are below the threshold for detection. If these mechanisms were active, then increasing pulse duration would have an effect similar to increasing the cell current, as both expose the

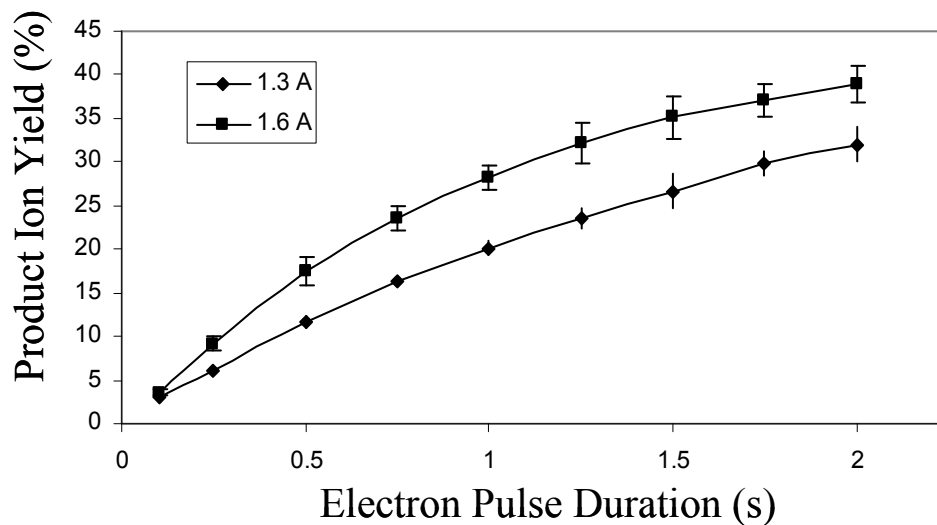


**Figure 3.6** Efficiency of product formation as a function of electron pulse duration at heater currents of 1.3 A and 1.6 A.

ions to a larger number of electrons. Rather, these data suggest that the loss in efficiency from raising the electron beam current above the optimal value ( $15 \mu\text{A}$ ) is a result of radial repulsion between the electron beam and the negatively charged precursor ions, which reduces the overlap of the two.

In order to couple EDD MS to online liquid chromatography (HPLC), the pulse duration should be reduced to 10-100 milliseconds, to allow acquisition on the peak elution time scale. Our present results indicate that sub-optimal conversion efficiencies are achieved on this time scale. Short irradiation times have been attained in ECD by increasing the flux of low energy electrons entering the analyzer cell [16]. However, for ECD, there is an attractive force between the positively-charged precursor ions and the electron beam that improves efficiency as the electron current increases. This approach

has an opposite result for EDD because by increasing the electron current, the repulsion between the electron beam and the negatively charged precursor ions also increases, reducing EDD efficiency.

As the value of electron current at the cell is identical for both series of experiments (heater current settings of 1.3 A and 1.6 A), the efficiency curves should be similar. We observe a difference of approximately 10 % between the two curves. This small difference may be a result of blackbody radiation from the dispenser cathode. By increasing the heater current from 1.3 A to 1.6 A, the cathode glows considerably brighter, and the number of emitted infrared photons is expected to increase, resulting in additional ion activation that can increase the EDD fragmentation. To observe true EDD species resulting from the lowest energy radical pathway, the heater current should be minimized to reduce blackbody activation.

### *Hexapole Accumulation*

Prior to entering the analyzer cell, the mass-selected precursor ion is accumulated in a hexapole collision cell. Typically, the time for ion accumulation is selected to maximize the precursor intensity. On the other hand, the minimum time required per scan is desired to increase the duty cycle of the measurement. To quantitatively determine the optimal hexapole accumulation time, conversion efficiencies were calculated at the optimal cell current of 15  $\mu\text{A}$  and for accumulation times ranging from 1.0 s to 6.0 s. As shown in Figure 3.7, the precursor ion intensity is observed to increase with hexapole storage time in asymptotic fashion, suggesting that the space charge limit of the hexapole is being reached after 6.0 s. There is an increase in efficiency up to 3.0 s

but a decline at longer hexapole accumulation times. Both the precursor and product ion intensities continue to increase with longer accumulation times but product ion formation increases more slowly than precursor ion intensity leading to a decrease in conversion efficiency. This result is most likely due to a decrease in overlap between an expanding ion cloud and the static shape of the electron beam. As the number of ions in the

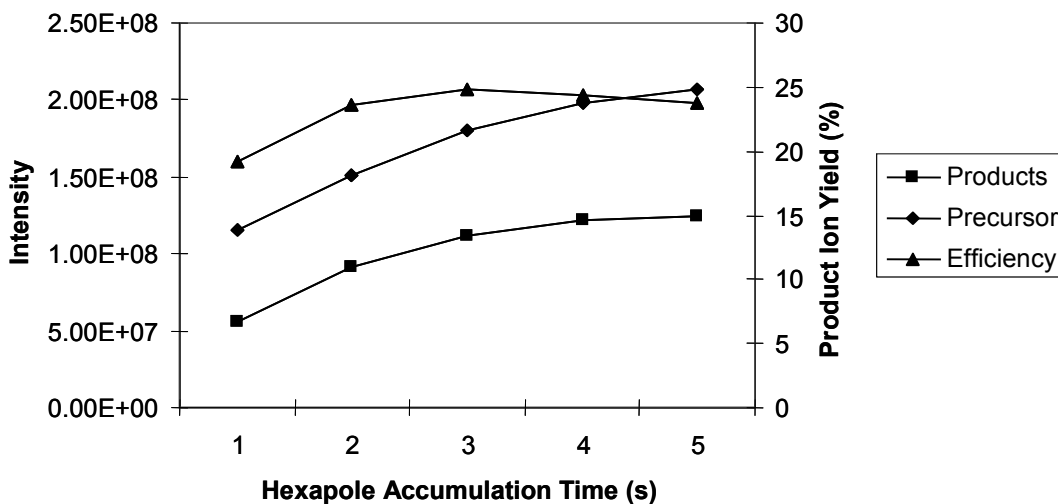


**Figure 3.7** Efficiency of product formation (right axis) and precursor/product intensities (left axis) as a function of precursor accumulation time in the external hexapole.

hexapole increases, the volume of the ion cloud is expected to increase, producing a wider radial distribution of ions after transfer to the analyzer cell. For accumulation times longer than 3.0 s, it appears that the majority of additional precursor ions are distributed outside the interaction region defined by the electron beam.

### *Electron Energy*

Prior EDD studies of anionic GAGs have employed 19 eV electrons for precursor irradiation [10-12]. We examine here the effect of varying electron energy over the range of 15-20 eV, while maintaining a constant electron cell current of 15  $\mu$ A. A threshold of 16 eV was observed for the onset of odd-electron products that can be attributed to the radical EDD fragmentation mechanism. Consistent product ion distributions have been observed over the range of 16-20 eV as seen in Figure 3.8. Product ion distributions observed at energies as high as 75 eV (data not shown) are

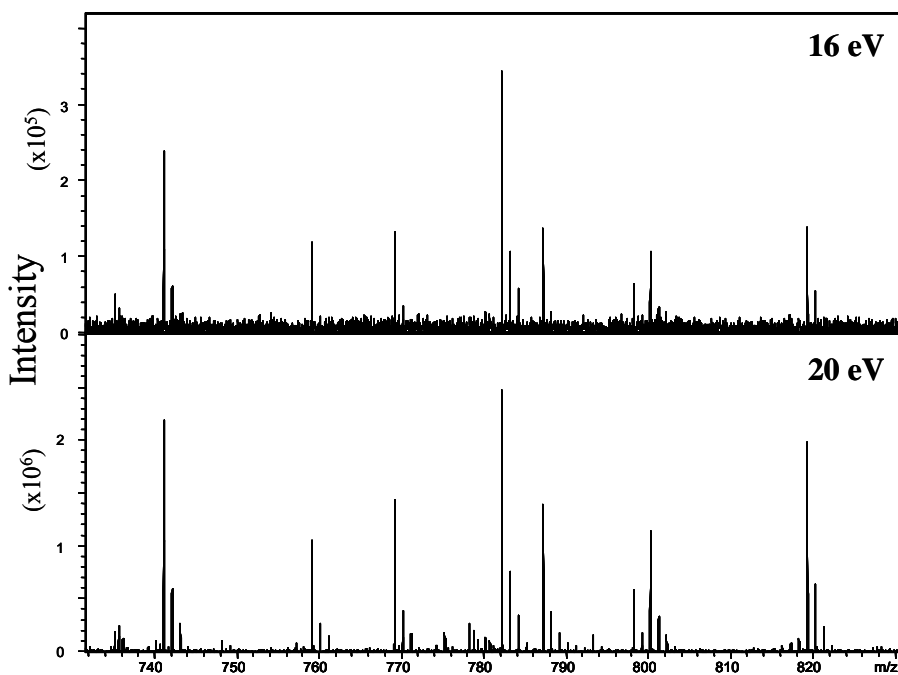


**Figure 3.8** EDD mass spectra obtained at 16 eV and 20 eV showing similar product ion distributions.

similar to our observations at 19 eV, although it appears that increasing rates of glycosidic bond cleavage and losses of  $\text{SO}_3$  and  $\text{CO}_2$  occur as the energy is increased.

We have previously observed preferential radical-induced loss of SO<sub>3</sub> over CO<sub>2</sub> at 19 eV. At higher electron energy, both loss channels appear to be equally likely, suggesting electronic activation pathways of dissociation in addition to radical mechanisms.

## **CONCLUSIONS**

The measurement of the electron current entering the analyzer cell enables the optimization of parameters required to obtain the most efficient precursor conversion efficiency for anionic glycosaminoglycan carbohydrates. These studies provide insight into the manner in which electrons interact with negative ions. The current obstacle to increasing the efficiency of EDD appears to be the repulsive interaction of the negative ion cloud with the electron beam. Under the current electron extraction configuration greater than 50 % of the electrons are captured by the lens. Additional work will seek to increase the electron transmission efficiency and allow for operation at lower heater currents, thereby reducing additional blackbody IR ion activation.

## **ACKNOWLEDGEMENTS**

The authors gratefully acknowledge financial support from the National Institutes of Health grant #2R01-GM038060-16.

## REFERENCES

1. Zubarev, R. A.; Kelleher, N. L. and McLafferty, F. W., Electron capture dissociation of multiply charged protein cations. A nonergodic process. *J. Am. Chem. Soc.* **1998**, *120*, 3265-3266.
2. Zubarev, R. A.; Horn, D. M.; Fridriksson, E. K.; Kelleher, N. L.; Kruger, N. A.; Lewis, M. A.; Carpenter, B. K. and McLafferty, F. W., Electron capture dissociation for structural characterization of multiply charged protein cations. *Anal. Chem.* **2000**, *72*, 563-573.
3. Hakansson, K.; Cooper, H. J.; Emmett, M. R.; Costello, C. E.; Marshall, A. G. and Nilsson, C. L., Electron capture dissociation and infrared multiphoton dissociation MS/MS of an N-glycosylated tryptic peptide to yield complementary sequence information. *Anal. Chem.* **2001**, *73*, 4530-4536.
4. Hakansson, K.; Emmett, M. R.; Hendrickson, C. L. and Marshall, A. G., High-sensitivity electron capture dissociation tandem FTICR mass spectrometry of microelectrosprayed peptides. *Anal. Chem.* **2001**, *73*, 3605-3610.
5. Kelleher, N. L.; Zubarev, R. A.; Bush, K.; Furie, B.; Furie, B. C.; McLafferty, F. W. and Walsh, C. T., Localization of Labile Posttranslational Modifications by Electron Capture Dissociation: The Case of Carboxyglutamic Acid. *Anal. Chem.* **1999**, *71*, 4250-4253.
6. Budnik, B. A.; Haselmann, K. F. and Zubarev, R. A., Electron detachment dissociation of peptide di-anions: an electron-hole recombination phenomenon. *Chem. Phys. Lett.* **2001**, *342*, 299-302.

7. Yang, J.; Mo, J. J.; Adamson, J. T. and Hakansson, K., Characterization of oligodeoxynucleotides by electron detachment dissociation Fourier transform ion cyclotron resonance mass spectrometry. *Anal. Chem.* **2005**, *77*, 1876-1882.
8. Yang, J. and HÅkansson, K., Fragmentation of Oligoribonucleotides from Gas-Phase Ion-Electron Reactions. *J. Am. Soc. Mass Spectrom.* **2006**, *17*, 1369-1375.
9. McFarland, M. A.; Marshall, A. G.; Hendrickson, C. L.; Nilsson, C. L.; Fredman, P. and MÅnsson, J.-E., Structural Characterization of the GM1 Ganglioside by Infrared Multiphoton Dissociation, Electron Capture Dissociation, and Electron Detachment Dissociation Electrospray Ionization FT-ICR MS/MS. *J. Am. Soc. Mass Spectrom.* **2005**, *16*, 752-762.
10. Wolff, J. J.; Chi, L. L.; Linhardt, R. J. and Amster, I. J., Distinguishing glucuronic from iduronic acid in glycosaminoglycan tetrasaccharides by using electron detachment dissociation. *Anal. Chem.* **2007**, *79*, 2015-2022.
11. Wolff, J. J.; Amster, I. J.; Chi, L. and Linhardt, R. J., Electron Detachment Dissociation of Glycosaminoglycan Tetrasaccharides. *J. Am. Soc. Mass Spectrom.* **2007**, *18*, 234-244.
12. Wolff, J. J.; Laremore, T. N.; Busch, A. M.; Linhardt, R. J. and Amster, I. J., Electron Detachment Dissociation of Dermatan Sulfate Oligosaccharides. *J. Am. Soc. Mass Spectrom.* **2008**, *19*, 294-304.
13. Adamson, J. T. and HÅkansson, K., Electron Detachment Dissociation of Neutral and Sialylated Oligosaccharides. *J. Am. Soc. Mass Spectrom.* **2007**, *18*, 2162-2172.

14. Tsybin, Y. O.; Hendrickson, C. L.; Beu, S. C. and Marshall, A. G., Impact of ion magnetron motion on electron capture dissociation Fourier transform ion cyclotron resonance mass spectrometry. *Int. J. Mass Spectrom.* **2006**, *255*, 144-149.
15. Tsybin, Y. O.; Witt, M.; Baykut, G.; Kjeldsen, F. and Hakansson, P., Combined infrared multiphoton dissociation and electron capture dissociation with a hollow electron beam in Fourier transform ion cyclotron resonance mass spectrometry. *Rapid Commun. Mass Spectrom.* **2003**, *17*, 1759-1768.
16. Tsybin, Y. O.; Håkansson, P.; Budnik, B. A.; Haselmann, K. F.; Kjeldsen, F.; Gorshkov, M. and Zubarev, R. A., Improved low-energy electron injection systems for high rate electron capture dissociation in Fourier transform ion cyclotron resonance mass spectrometry. *Rapid Commun. Mass Spectrom.* **2001**, *15*, 1849-1854.
17. Haselmann, K. F.; Budnik, B. A.; Olsen, J. V.; Nielsen, M. L.; Reis, C. A.; Clausen, H.; Johnsen, A. H. and Zubarev, R. A., Advantages of external accumulation for electron capture dissociation in Fourier transform mass spectrometry. *Anal. Chem.* **2001**, *73*, 2998-3005.
18. Kjeldsen, F.; Haselmann, K. F.; Budnik, B. A.; Jensen, F. and Zubarev, R. A., Dissociative capture of hot (3-13 eV) electrons by polypeptide polycations: an efficient process accompanied by secondary fragmentation. *Chem. Phys. Lett.* **2002**, *356*, 201-206.
19. Tsybin, Y. O.; Witt, M.; Baykut, G. and Hakansson, P., Electron capture dissociation Fourier transform ion cyclotron resonance mass spectrometry in the

- electron energy range 0-50 eV. *Rapid Commun. Mass Spectrom.* **2004**, *18*, 1607-1613.
20. Yang, J. and Håkansson, K., Characterization and optimization of electron detachment dissociation Fourier transform ion cyclotron resonance mass spectrometry. *Int. J. Mass Spectrom.* **2008**, *276*, 144-148.
  21. Polfer, N. C.; Haselmann, K. F.; Zubarev, R. A. and Langridge-Smith, P. R. R., Electron capture dissociation of polypeptides using a 3 Tesla Fourier transform ion cyclotron resonance mass spectrometer. *Rapid Commun. Mass Spectrom.* **2002**, *16*, 936-943.
  22. McFarland, M. A.; Chalmers, M. J.; Quinn, J. P.; Hendrickson, C. L. and Marshall, A. G., Evaluation and Optimization of Electron Capture Dissociation Efficiency in Fourier Transform Ion Cyclotron Resonance Mass Spectrometry. *J. Am. Soc. Mass Spectrom.* **2005**, *16*, 1060-1066.
  23. Gorshkov, M. V.; Masselon, C. D.; Nikolaev, E. N.; Udseth, H. R.; Pasa-Tolic, L. and Smith, R. D., Considerations for electron capture dissociation efficiency in FTICR mass spectrometry. *Int. J. Mass Spectrom.* **2004**, *234*, 131-136.
  24. Mormann, M. and Peter-Katalinić, J., Improvement of electron capture efficiency by resonant excitation. *Rapid Commun. Mass Spectrom.* **2003**, *17*, 2208-2214.
  25. Pervin, A.; Gallo, C.; Jandik, K. A.; Han, X.-J. and Linhardt, R. J., Preparation and structural characterization of large heparin-derived oligosaccharides. *Glycobiology* **1995**, *5*, 83-95.
  26. Heck, A., J. R.; de Koning, L., J. ; Pinkse, F. A. and Nibbering, N. M. M., Mass-specific selection of ions in Fourier-transform ion cyclotron resonance mass

- spectrometry. Unintentional off-resonance cyclotron excitation of selected ions. *Rapid Commun. Mass Spectrom.* **1991**, *5*, 406-414.
27. Domon, B. and Costello, C. E., A systematic nomenclature for carbohydrate fragmentations in FAB-MS/MS spectra of glycoconjugates. *Glycoconjugate J.* **1988**, *5*, 397-409.
  28. Cody, R. B. and Freiser, B. S., Electron impact excitation of ions from organics: an alternative to collision induced dissociation. *Anal. Chem.* **1979**, *51*, 547-551.
  29. Kaiser, N. K. and Bruce, J. E., Reduction of ion magnetron motion and space charge using radial electric field modulation. *Int. J. Mass Spectrom.* **2007**, *265*, 271-280.

## CHAPTER 4

### **ELECTRON DETACHMENT DISSOCIATION OF SYNTHETIC HEPARAN SULFATE GLYCOSAMINOGLYCAN TETRASACCHARIDES VARYING IN DEGREE OF SULFATION AND HEXURONIC ACID STEREOCHEMISTRY<sup>1</sup>**

---

<sup>1</sup> Leach III, F. E., Arungundram, S., Al-Mafraji, K., Venot, A., Boons, G.-J., and I.J. Amster. To be submitted to *Analytical Chemistry*.

## **ABSTRACT**

Glycosaminoglycan (GAG) carbohydrates provide a challenging analytical target for structural determination due to a polydisperse nature inherent to a non-template based biosynthesis and presence of the labile sulfate modification. The resultant structures, although heterogeneous, contain domains which indicate a sulfation pattern or code that correlates to specific function. Mass spectrometry, in particular electron detachment dissociation Fourier transform ion cyclotron resonance (EDD FT-ICR MS), provides a highly sensitive platform for GAG structural analysis by providing cross-ring cleavages for sulfation location and product ions specific to hexuronic acid stereochemistry. To investigate the effect of sulfation pattern and variations in stereochemistry on EDD spectra, a series of synthetic heparan sulfate tetrasaccharides are examined.

## INTRODUCTION

Glycosaminoglycan (GAG) carbohydrates are sulfated linear biopolymers that are typically covalently associated with a protein core as proteoglycans. These polydisperse biomolecules are involved in the regulation of biochemical pathways [1-5] and disease progression [6-8] and are largely found in the extracellular matrix and cell surface [9, 10]. The associated GAG chains can be categorized based upon constituent hexose residues, glycosidic linkage between hexoses, extent of O- or N-sulfation and N-acetylation, and hexuronic acid stereochemistry into specific glycoform classes i.e. chondroitin sulfate, heparan sulfate, hyaluronan, etc. The heparinoid (heparan sulfate (HS) and heparin) glycosaminoglycans represent one of the most analytically challenging classes of biomolecules based on the high degree of variability in oligomer length, extent and location of sites of sulfation, and hexuronic acid stereochemistry.

The relationship between variability in heparinoid sulfation and epimerization and cellular function [11, 12] has led to increased interest in the characterization of domain structure [13] and sulfation patterns [14]. The most notable of these domains is the five residue heparin sequence for binding to antithrombin [5, 15]. The binding motif consists of eight sulfate groups specifically distributed along the pentasaccharide, of which the tri-sulfated disaccharide (IdoA2S-GlcNS6S) is a key element in protein recognition [16]. Additional variation of domain structure has been observed based upon organism age [17] as well as specificity to organ-type [18]. To fully understand these patterns and variations, there has been increased interest in the full characterization of structure-function relationships, generally known as glycomics [19].

The inherent heterogeneity of these acidic biomolecules, due to a non-template based synthesis in the Golgi apparatus, has encouraged the application of a variety of analytical techniques for their structural determination. Mass spectrometry has recently been demonstrated as a highly sensitive method for the characterization of GAGs [20-22] based on the combination of accurate mass measurement of intact oligomers [23, 24] as well as tandem mass spectrometric determination of the locations of labile sulfate modifications [25-35] and the assignment of the hexuronic acid C-5 stereochemistry [27, 36].

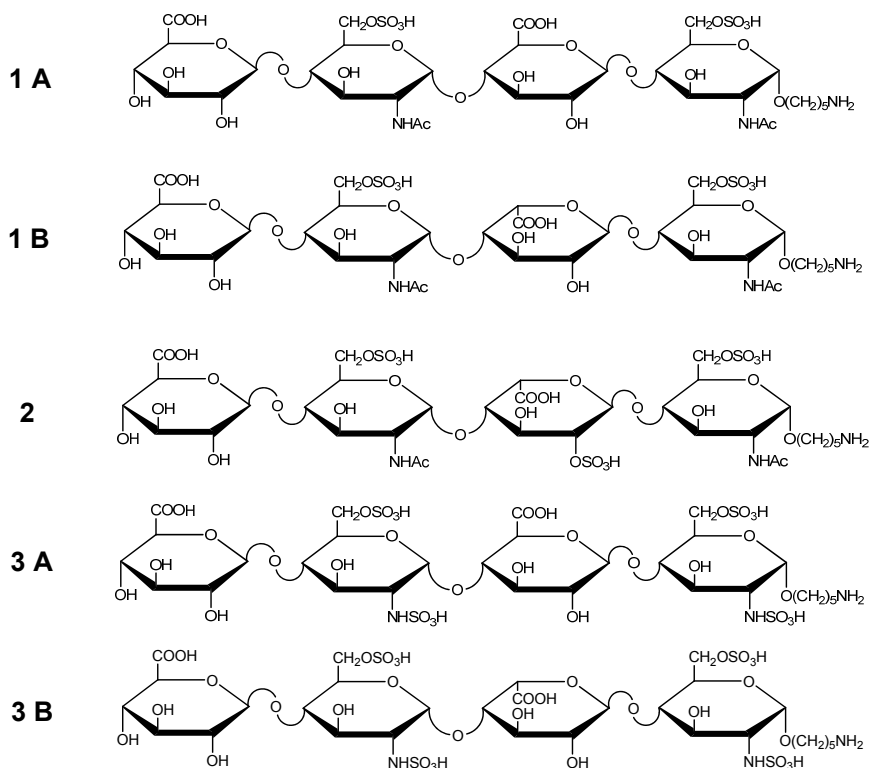
Recently developed synthetic methods [37] have provided a unique opportunity to systematically examine the effect of sulfate position and hexuronic acid stereochemistry on electron detachment dissociation (EDD) spectra in a controlled fashion at the tetrasaccharide level. We show here that as the positions and extent of sulfation are varied, appropriate precursor ion selection is required to produce bond cleavages that precisely locate the sites of sulfation as well as to generate product ions that can assign C-5 stereoisomerism in hexuronic acid residues.

## **EXPERIMENTAL METHODS**

### *Heparan Sulfate Oligosaccharide Preparation*

Heparan sulfate tetrasaccharides were synthesized by a modular approach [37] and purified by silica gel column chromatography. Prepared structures were confirmed by <sup>1</sup>H NMR and accurate mass measurement by FT-ICR MS. Compounds were prepared as tetrasaccharides with varying degrees and positions of sulfation as well as hexuronic acid stereochemistry are depicted in Scheme 1 as structures: 1A – GlcA-GlcNAc6S-

GlcA-GlcNAc6S-(CH<sub>2</sub>)<sub>5</sub>NH<sub>2</sub>, 1B - GlcA-GlcNAc6S-IdoA-GlcNAc6S-(CH<sub>2</sub>)<sub>5</sub>NH<sub>2</sub>; 2 - GlcA-GlcNAc6S-IdoA2S-GlcNAc6S-(CH<sub>2</sub>)<sub>5</sub>NH<sub>2</sub>; 3A - GlcA-GlcNS6S-GlcA-GlcNS6S-(CH<sub>2</sub>)<sub>5</sub>NH<sub>2</sub>, 3B - GlcA-GlcNS6S-IdoA-GlcNS6S-(CH<sub>2</sub>)<sub>5</sub>NH<sub>2</sub>.



### *Tetrasaccharide Desulfation*

The pyridinium salts of structures 1A/B were dissolved in 10 % aqueous MeOH and heated for 6 hrs at 60° C [38] to produce the desulfated tetrasaccharides GlcA-GlcNAc-GlcA-GlcNAc-(CH<sub>2</sub>)<sub>5</sub>NH<sub>2</sub> and GlcA-GlcNAc-IdoA-GlcNAc-(CH<sub>2</sub>)<sub>5</sub>NH<sub>2</sub>, respectively. The mass-selective quadrupole of the FT-ICR MS instrument was employed to isolate the desulfated compounds in lieu of additional laboratory based purification.

### *Mass Spectrometry Analysis*

Experiments were performed with a 9.4 T Bruker Apex Ultra QeFTMS (Billerica, MA) fitted with an MTP dual ion source, 25 W CO<sub>2</sub> laser (Synrad model J48-2, Mukilteo, WA) for IRMPD, and an indirectly heated hollow cathode (HeatWave, Watsonville, CA) to generate electrons for EDD. The sample solutions were infused at a rate of 120  $\mu$ L/hour and ionized by electrospray using a metal capillary (Agilent Technologies, Santa Clara, CA, #G2427A) or at 10  $\mu$ L/hour and ionized by nanospray (pulled fused silica tip model FS360-75-15-D-20; New Objective, Woburn, MA, USA). Based on the extent of sulfation and desired charge state or degree of sodiation, the ESI solvent was varied. Solutions of each di-sulfated oligosaccharide were introduced at a concentration of 0.1 mg/mL in 50:50:0.1 methanol:H<sub>2</sub>O:FA (Sigma, St. Louis, MO) to generate doubly deprotonated ions and 0.2 mg/mL in 50:50 methanol:H<sub>2</sub>O with 1% 100  $\mu$ M NaOH to generate triply deprotonated ions and sodium adduct ions. To achieve quadruply deprotonated precursor ions for the tetra-sulfated tetrasaccharides, 105 mM sulfolane in acetonitrile was introduced to the ESI line via a line splitter [39]. A secondary syringe pump controlled the relative amount of sulfolane introduced to the ESI solvent. All HS oligosaccharides were examined in negative ion mode.

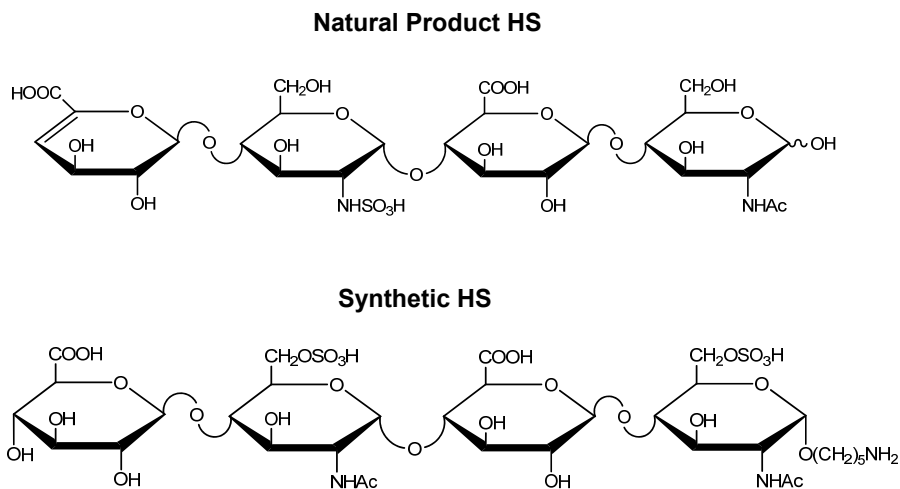
For EDD experiments, precursor ions were isolated in the external quadrupole and accumulated for 1-3 seconds in an rf only hexapole before injection into the FT-ICR MS cell. One or two quadrupole isolation/analyzer cell fills were utilized per scan. The selection of the precursor ion was further refined by using in-cell isolation with a coherent harmonic excitation frequency (CHEF) event [40]. For electron irradiation the cathode bias was set to -19 V. The extraction lens was set to  $-18.5 \pm 0.1$  V, and the

cathode heater was set to 1.5 A. The precursor ions were then irradiated with electrons for 1 second. 24-36 acquisitions were signal averaged per mass spectrum. For each mass spectrum, 1M points were acquired, padded with one zero fill, and apodized using a sinebell window. Background spectra were acquired by leaving all parameters the same but setting the cathode bias to 0 V to ensure that no electrons reached the analyzer cell. External calibration of mass spectra produced mass accuracy of 5 ppm. Internal calibration was also performed using confidently assigned glycosidic bond cleavage products as internal calibrants, providing mass accuracy of <1 ppm. Due to the large number of low intensity products formed by EDD, only peaks with S/N > 10 are reported. Product ions were assigned using accurate mass measurement and Glycoworkbench.[41] All products are reported using the annotation proposed by Wolff and Amster[35], derived from the Domon and Costello nomenclature [42]. To account for additional sulfate loss observed during analysis of highly sulfated GAGs, a filled circle has been added to the annotation to indicate a loss of 2 or more sulfate groups as SO<sub>3</sub> (an open circle indicates the loss of one SO<sub>3</sub>) from a sulfate half ester. In annotated spectra, the charge states of all ions are 1<sup>-</sup> unless otherwise indicated.

## **RESULTS AND DISCUSSION**

Electron detachment dissociation (EDD) has previously been applied to the structural characterization of enzymatically prepared heparan sulfate tetrasaccharides ranging in degree of sulfation from zero to two (1 per disaccharide repeat unit) [32, 33]. The examined synthetic heparan sulfate tetrasaccharides contain two to four sulfate

modifications and a C-5 stereo-center on each hexuronic acid. Shown in Scheme 2, the synthetic compounds are also modified at the reducing end to provide targets for



protein-GAG interaction screening assays. Although the reducing end modification is unnatural, it does provide a mass shift in fragments that contain the reducing end and enables the assignment of GAG product ions that would otherwise be isobaric due to the symmetric nature of oligosaccharides with a constant repeat unit. EDD activation of synthetic compounds without the linker reveal that the modification has minimal effect on the MS/MS results. The synthetic oligosaccharide non-reducing end has a chiral center at C-5, which is absent in the  $\Delta$ -uronic acid residues produced by enzymatic cleavage of natural materials previously studied in our laboratory.

Consistent with previous findings for enzymatically prepared GAG oligosaccharides, EDD results in an information rich tandem mass spectrum containing glycosidic and cross-ring bond cleavages [32, 33] that provides more structural information than vibrational activation of the same precursor ion, shown in Figure 4.1.

We previously reported that the application of EDD to HS tetramers produced ions specific to assigned as  $^{0,2}A_3$ ,  $B_3'$ , and  $B_3'-CO_2$  as well as  $^{3,5}A_3$  when an N-sulfo group is present on the amino sugar to the non-reducing side of the acidic residue. The tetrasaccharides chosen for this prior study contained only one sulfate moiety. Selection of a doubly de-protonated precursor ion for EDD therefore resulted in an ionized sulfate and carboxyl, which provided a site for electron detachment and generated stereo-specific product ions based on a proposed radical mechanism. Increasing the degree of sulfation reduces the likelihood that a carboxyl will be ionized as the sulfate group is more acidic. To produce the desired product ions, it is necessary to select a precursor ion with an ionized state corresponding to one more than the number of sulfate groups.

***EDD of di-sulfated tetrasaccharides [GlcA-GlcNAc6S-HexA-GlcNAc6S-(CH<sub>2</sub>)<sub>5</sub>NH<sub>2</sub>]***

EDD of the doubly de-protonated precursor ion for Structures 1A and 1B results in complete glycosidic bond cleavage as well as abundant cross-ring cleavages as shown in Figure 4.2. As these tetrasaccharides differ in only the stereochemistry of one hexuronic acid residue, it is not surprising that the fragmentation observed is nearly identical. In each case, the 6-O-sulfation in the GlcNAc residues can be assigned by the presence of cross-ring cleavages. For the reducing end hexosamine residue, the occurrence of  $^{2,4}X_0$  and  $^{0,2}A_4$  unambiguously locate the site of sulfation to C-6 instead of N. On the central hexosamine residue, the occurrence of five cross-ring cleavages, specifically  $^{3,5}A_2$ , enables the assignment of 6-O-sulfation.

Although the doubly de-protonated precursor ion should possess two ionized sulfate sites and therefore preclude the possibility of  $SO_3$  loss due to mechanisms known

from collisional induced dissociation [22], SO<sub>3</sub> loss is nevertheless observed as minor products, most likely due to electronic excitation channels which are not eliminated by

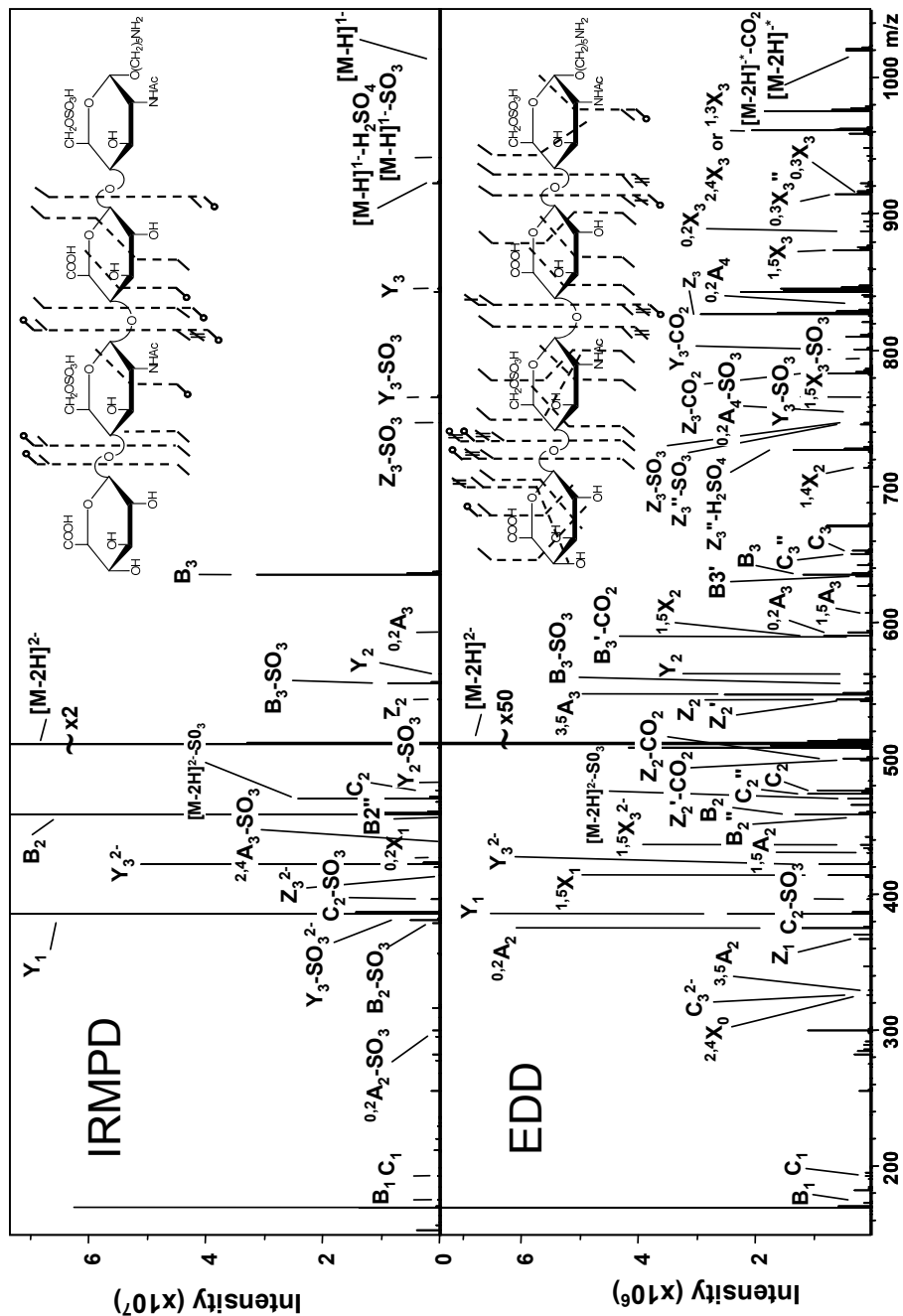


**Figure 4.1** Comparison between threshold and electron-based activation of a di-sulfated synthetic GAG tetrasaccharide, structure 1A.

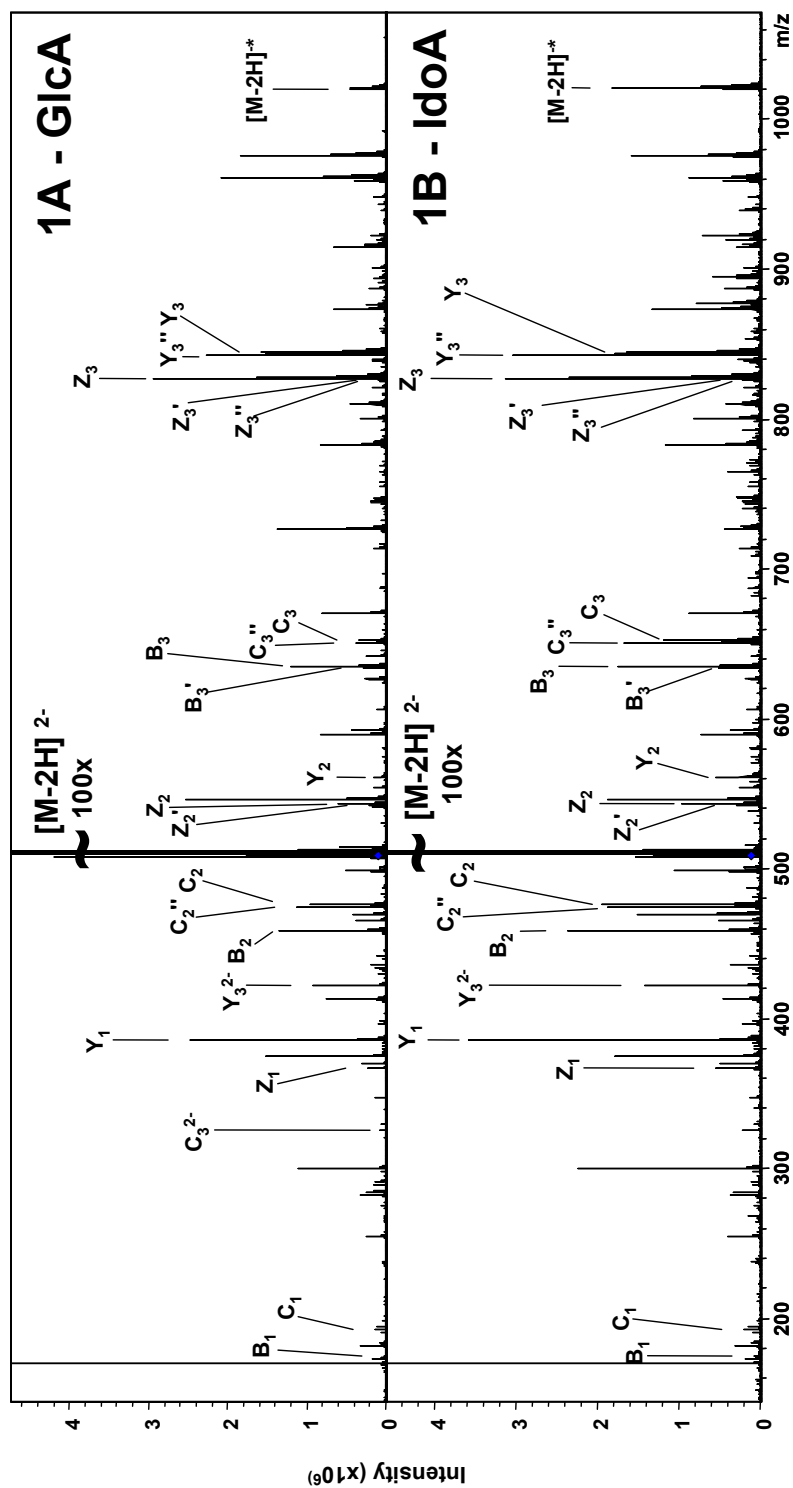


**Figure 4.2** EDD spectra of the epimer pair 1A/B. Only glycosidic bond cleavages are annotated. Complete cleavage information is shown in the Figure 4.1 inset for EDD and is representative of both epimers.

the presence of an ionized sulfate.  $\text{SO}_3$  loss occurs largely from glycosidic bond fragments but also from the precursor ion, charge-reduced precursor, and selected cross-ring cleavages ( $^{0,2}\text{A}_4$ ,  $^{0,2}\text{A}_2$ , and  $^{1,5}\text{X}_3$ ). Additional losses of one or two hydrogen atoms are also observed from glycosidic bond cleavages as well as the loss of  $\text{CO}_2$  from the charge reduced species and the  $\text{Z}_2$  fragment ion. These products are not found by threshold methods of activation, such as IRMPD or CID.

#### *Determination of Hexuronic Acid Stereochemistry*

Contrary to previous EDD results specific to hexuronic acid stereochemistry in HS, the  $^{0,2}\text{A}_3$  and  $\text{B}_3'$  ions are present in both the GlcA spectrum as well as the IdoA spectrum, possibly due to the presence of 6-O-sulfation which may introduce new fragmentation pathways.  $\text{B}_3'-\text{CO}_2$  is not observed in either spectrum. These fragments could arise from a radical mechanism due to electron detachment or from electronic excitation of the precursor ion. To determine the responsible fragmentation mechanism, negative electron transfer dissociation (NETD) [43] of the doubly de-protonated precursor ion can be applied to assign products due to electron detachment while electron induced dissociation (EID) [34] of the singly de-protonated precursor ion produce fragments due only to electronic excitation. NETD of the doubly de-protonated precursor ions for Structures 1A/B also produces the  $^{0,2}\text{A}_3$  and  $\text{B}_3'$  ions in each epimer (data not shown) and indicates the existence of a detachment initiated mechanism not established in the original publication [36].

Selection of a charge state corresponding to the number of sulfates minimizes the loss of  $\text{SO}_3$  during ion activation, but it does not lead to stereo-specific product ion

formation because carboxyl groups are not ionized. To insure that the occurrence or absence of these product ions is due to a specific stereochemistry, a precursor ion must be selected where the charge state is  $3^-$  (two ionized sulfates and one ionized carboxyl) or a proton has been exchanged for a sodium cation [35]. In the case of direct infusion, these two precursor ions can be generated by addition of NaOH to the ESI solvent.

Although both possibilities place an ionized site at a carboxyl, the resultant EDD spectra differ. The  $[M-3H]^{3-}$  precursor for both epimers produces the  $^{0,2}A_3$  and  $B_3'$  ions whereas  $B_3'-CO_2$  is only observed for the GlcA epimer at low intensity, shown in Figure 4.3. To generate product ions indicative of the hexuronic acid stereochemistry, the  $[M-3H+1Na]^{2-}$  precursor must be selected.

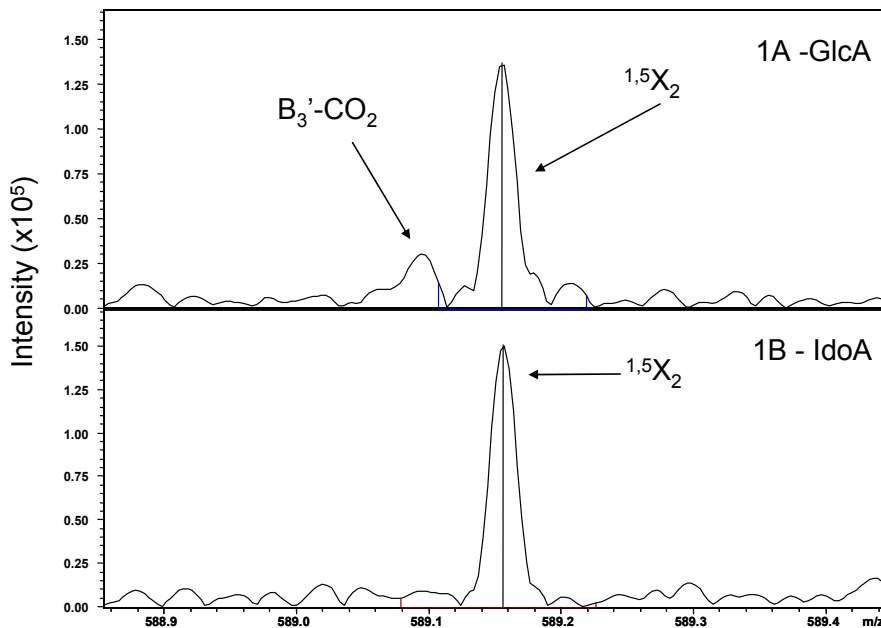


**Figure 4.3** Enlarged region of the EDD spectra for the  $[M-3H]^{3-}$  precursor of both 1A and 1B showing the presence of the minor product,  $B_3'-CO_2$ , in the GlcA epimer.

Shown in Figure 4.4, a product ion distribution consistent with prior stereo-specific EDD results is obtained. For the GlcA containing epimer,  $^{0,2}A_3$  and  $^{0,2}A_3+Na$  are observed while these ions are absent in the IdoA epimer. Additionally,  $B_3'+Na$  is more intense in the GlcA epimer relative to the  $B_3+Na$  intensity.

### *Desulfation Approach*

A more direct approach to determine the hexuronic acid stereochemistry is to desulfate the oligosaccharide, which for a doubly de-protonated tetrasaccharide places an ionized site on each carboxyl and precludes the influence of sulfation on observed production ion distributions. This results in a two-step method for GAG oligosaccharide characterization. The first EDD experiment on the sulfate-intact oligosaccharide is used to determine the sites of sulfation while the second measurement, on desulfated oligosaccharides, provides the data needed to assign stereo-chemical information. Shown in Figure 4.5, the EDD spectra of the desulfated epimer pair results in unambiguous assignment based upon the occurrence/absence of diagnostic ions known from prior EDD experiments.  $^{0,2}A_3$  is observed in the GlcA tetrasaccharide and  $B_3'$  is higher in intensity than the  $B_3$  ion. Secondly, in the IdoA tetrasaccharide,  $C_3''$  is more intense than  $C_3$  which is consistent with prior report. Although this method is useful in the case of 6-O sulfation, caution is urged due to potential structural modifications inherent to the removal of N-sulfo groups.

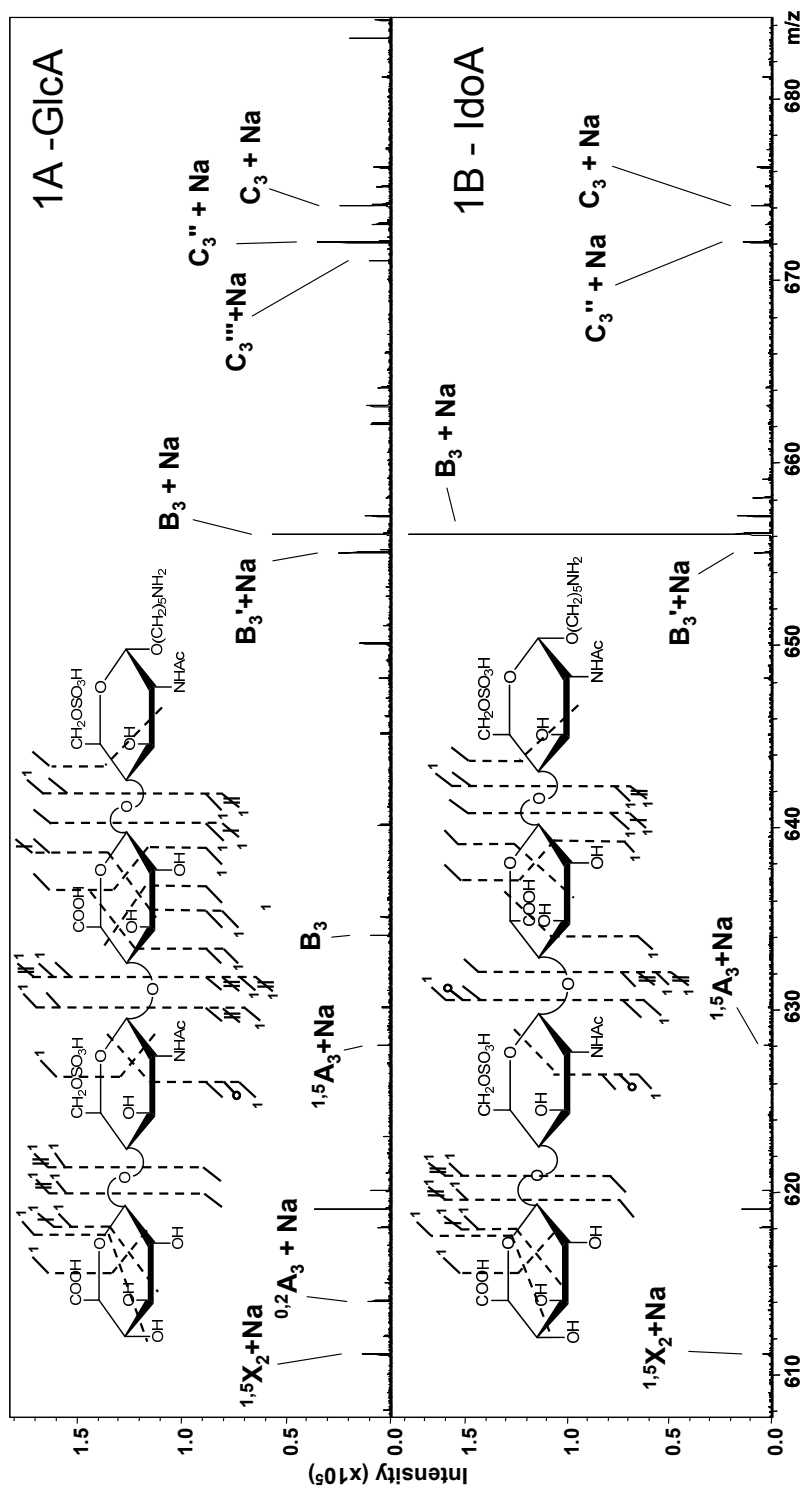


**Figure 4.4** Enlarged region of the EDD spectra for the  $[M-3H]^{3-}$  precursor of both 1A and 1B showing the presence of the minor product,  $B_3'$ -CO<sub>2</sub>, in the GlcA epimer.

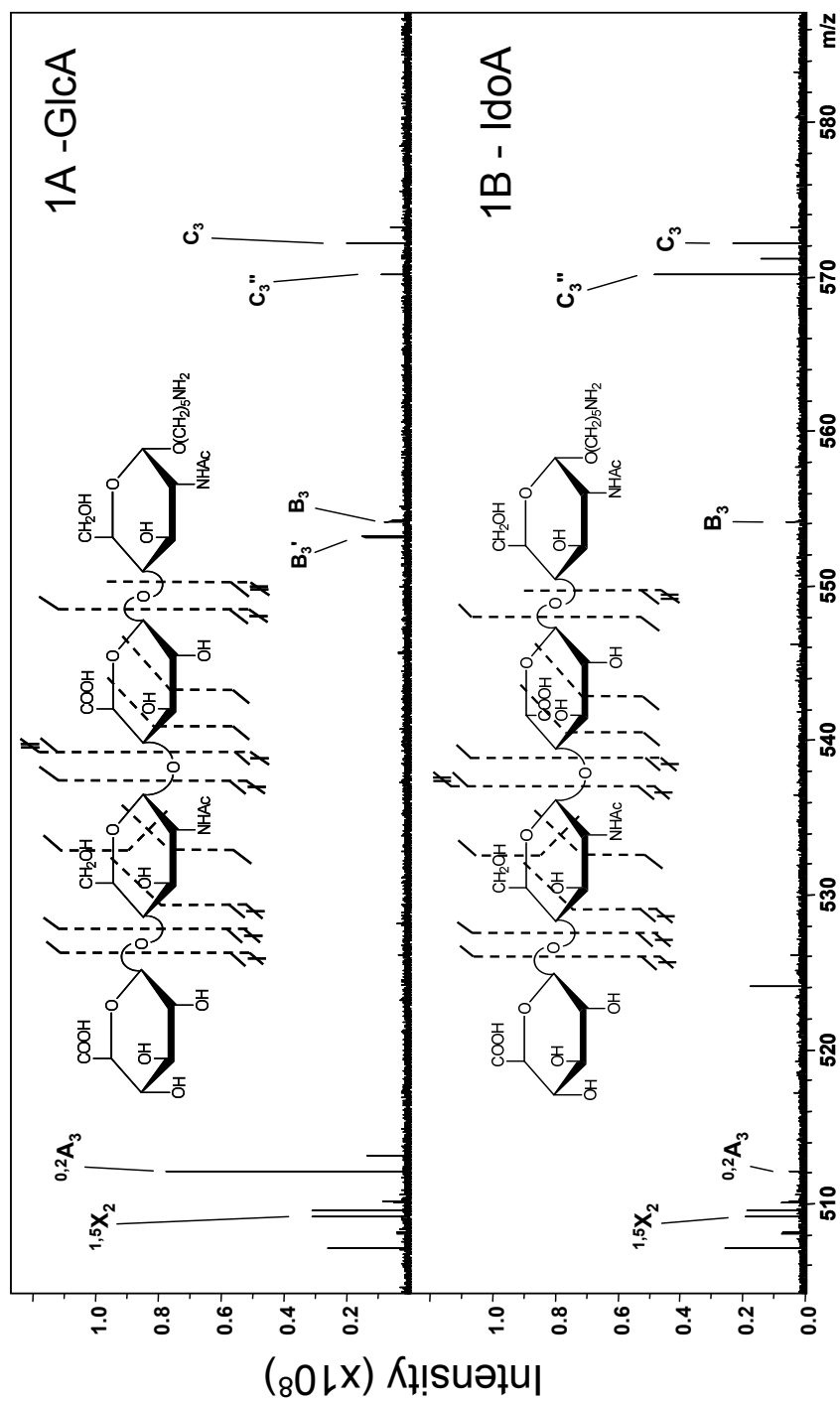


**Figure 4.5** The stereo-specific region EDD spectra obtained from the  $[M-2H]^{2-}$  precursor ion of the desulfated compounds for 1A and 1B. Intense  $0,2A_3$  and  $B_3'$  ions are assigned in the GlcA epimer, compared to IdoA, in addition an intense  $C_3''$  ion in IdoA.

***EDD of a tri-sulfated tetrasaccharide [GlcA-GlcNAc6S-IdoA2S-GlcNAc6S-(CH<sub>2</sub>)<sub>5</sub>NH<sub>2</sub>]***

Previous EDD experiments on GAGs have examined the fragmentation behavior when sulfates are present on a hexosamine residue. The occurrence of 4/6-O-sulfation is typical for chondroitin sulfate glycoforms and N-sulfation or 6-O-sulfation is typical for heparan sulfate or heparin glycoforms. The 2-O-sulfation of hexuronic acid residues, particularly IdoA, is a common motif in heparin and has not been previously studied by EDD. Increasing the degree of sulfation introduces inherent heterogeneity to the mass spectrum based on sodium exchange and variation in charge state; therefore, multiple precursor ions exist for MS/MS analysis and proper selection is required. It has been previously demonstrated for both threshold and electron-based GAG activation that the precursor should have an ionized state corresponding to at least the number of sulfate groups or pairing sulfates with a metal counter ion to minimize SO<sub>3</sub> loss (In dermatan sulfate oligosaccharides, n+1 ionized sites, where n is the number of sulfate groups, is typically required [35]). This precursor can be achieved in this case by selecting the [M-3H]<sup>3-</sup> or [M-4H+2Na]<sup>2-</sup> state.

EDD activation of the [M-3H]<sup>3-</sup> precursor ion results in the tandem mass spectrum shown in Figure 4.6. Product ions are observed from charge states ranging from 3<sup>-</sup> to 1<sup>-</sup>. Charge-conserved fragments due to direct electronic excitation of the [M-3H]<sup>3-</sup> precursor are assigned as <sup>1,5</sup>X<sub>3</sub>, <sup>0,2</sup>X<sub>3</sub>, <sup>1,5</sup>X<sub>3</sub>, as well as Y<sub>3</sub>/Y<sub>3</sub>-SO<sub>3</sub>. Similar to results obtained for DS oligosaccharides [33], the neutral loss of 1 or 2 SO<sub>3</sub> groups directly from the precursor ion is also observed even though the precursor should contain all ionized sulfates. Based on this observation, there must exist electronic excitation channels in increasingly sulfated HS oligosaccharides through which SO<sub>3</sub> loss can occur even though



the presence of an ionized sulfate shunts this channel during threshold activation.

Additionally, the loss of 2 SO<sub>3</sub> groups is observed from Y<sub>2</sub> and Y<sub>3</sub>. The first loss in each case results in charge conservation whereas the second results in charge reduction, e.g. Y<sub>3</sub><sup>3-</sup>, (Y<sub>3</sub>-SO<sub>3</sub>)<sup>3-</sup>, and (Y<sub>3</sub>-2SO<sub>3</sub>)<sup>2-</sup>.

The distribution of fragments based on charge state is largely due to the location of the sulfate groups and terminus (non-reducing end, NRE, or reducing end, RE) contained in the fragment. Due to the occurrence of 1 sulfate per residue in this tetrasaccharide, 1<sup>-</sup> product ions are assigned as cleavages ranging in oligomer length from B<sub>1</sub> to <sup>3,5</sup>A<sub>3</sub> from the NRE and Z<sub>1</sub>/Y<sub>1</sub> from the RE. Increasing the fragment length to C<sub>3</sub> from the NRE or <sup>0,2</sup>X<sub>1</sub> to Y<sub>3</sub> from the RE subsequently generates 2<sup>-</sup> product ions due to the presence of two sulfates. Charge reduction by SO<sub>3</sub> loss from an ionized sulfate also generates several 2<sup>-</sup> products such as <sup>1,5</sup>X<sub>3</sub>-SO<sub>3</sub> and <sup>0,2</sup>X<sub>3</sub>-SO<sub>3</sub>.

Complete glycosidic bond cleavage is observed which enables the location of two sites of sulfation, one each to an amino sugar, and the third to the central acidic sugar. The location on the acidic residue can be determined as the 2-O position by the occurrence of a <sup>0,2</sup>X<sub>1</sub> cross-ring cleavage. On the hexosamine residues the sulfation site can be assigned as either 6-O- or 3-O- by the <sup>0,2</sup>A<sub>2</sub> and <sup>0,2</sup>A<sub>4</sub> cross-ring cleavages, which precludes the possibility of N-sulfation by fragment mass. Although the [M-3H]<sup>3-</sup> precursor ion does not provide conclusive evidence for 6-O-sulfation, activation of the [M-3H+1Na]<sup>2-</sup> precursor produces a <sup>2,4</sup>A<sub>2</sub>+Na which eliminates the possibility of 3-O-sulfation on the central hexosamine and <sup>3,5</sup>A<sub>4</sub>+Na which supports 6-O-sulfation on the reducing end hexosamine. The complete sulfation pattern is therefore –GlcNAc6S-HexA2S-GlcNAc6S.

The continued ability to locate sulfation sites to a residue by glycosidic bond cleavage and assign the location on the hexose ring by cross-ring cleavage has been demonstrated, but the identification of hexuronic stereochemistry becomes more challenging as the sulfate density increases. To place an ionized site on a carboxyl group for subsequent electron detachment, the  $[M-4H]^{4-}$  must be generated or a sufficient number of protons must be exchanged for sodium cations to produce either the  $[M-4H+2Na]^{2-}$  or  $[M-4H+1Na]^{3-}$  ion. EDD of the  $[M-4H+2Na]^{2-}$  ion produces a more intense  $C_3''$  than  $C_3$ . As previously discussed, the absence of  $^{0,2}A_3$  and for the  $C_3''$  ion to be greater in intensity than  $C_3$  are the diagnostic conditions for IdoA assignment. This requirement is satisfied, but the GlcA epimer was not available for analysis and subsequent comparison.

An increase in the number of sodium counter ions can provide a means to control the stereochemical-dependent fragmentation, as shown for the di-sulfated and tri-sulfated tetrasaccharides, but there also appears to be a direct effect on the degree of electronic excitation for each precursor state. Electronic excitation is inferred in EDD by the presence of charge conserved product ions, e.g.  $2^-$  products generated by activation of the  $[M-2H]^{2-}$  precursor ion. Shown in Figure 4.7, the number and relative intensity of the electronic excitation products (indicated by circles) decreases as the number of sodium counter ions is increased from zero to three. At the maximum number of sodium cations allowable for the  $2^-$  precursor, no doubly deprotonated products are observed. This result could be due to the suppression of electronic excitation channels by addition of counter ions. This hypothesis is supported by the reduction in the total number of product ions observed.

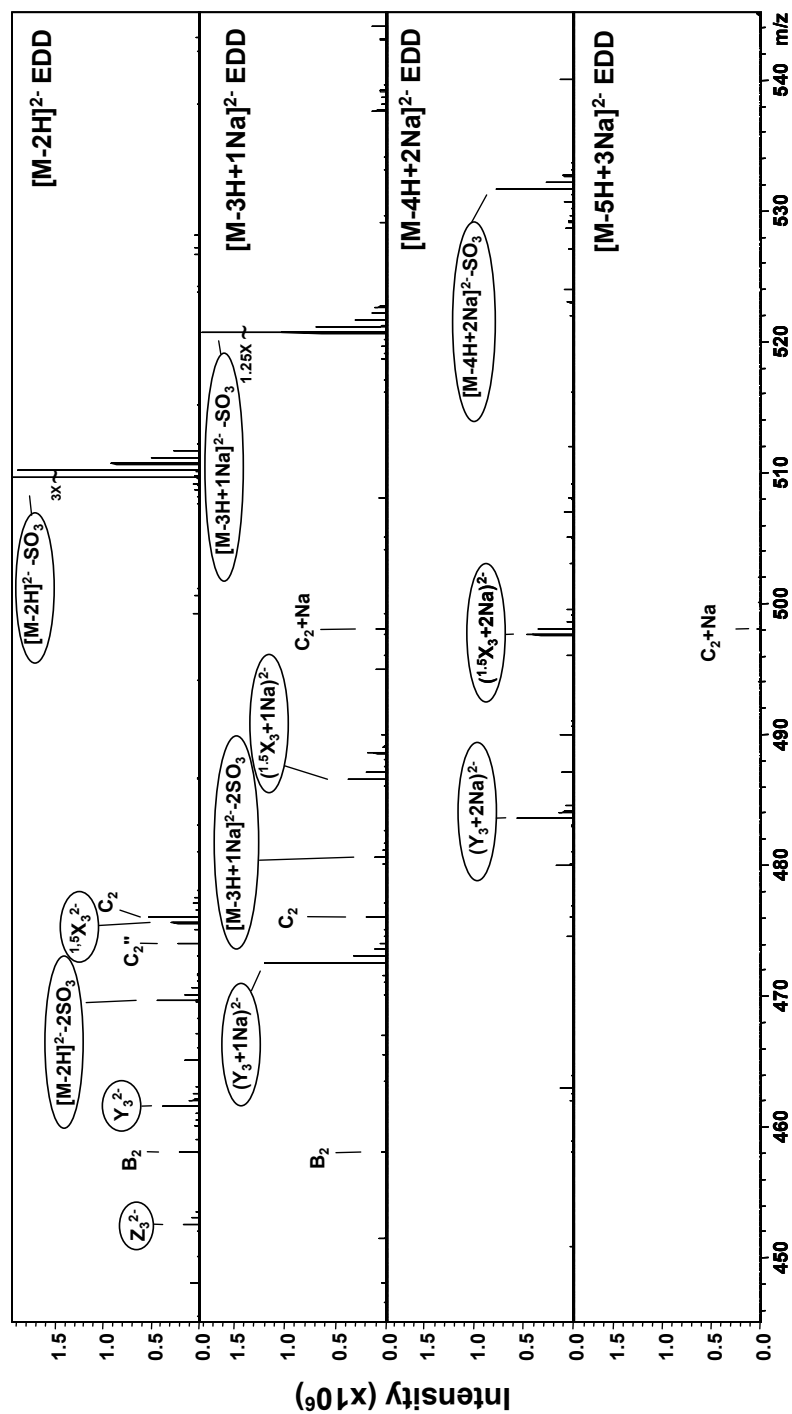


**Figure 4.7** The spectral region containing 2<sup>-</sup> product ions generated from the activation of [M-2H]<sup>2-</sup> precursor ions with an increasing degree of sodium exchange. Sulfate loss from the precursor in addition to the occurrence of charge conserved products is shown to decrease. (A positive mass shift occurs in each spectrum due to sodium exchange.)

***EDD of a Tetra-sulfated Tetrasaccharide [GlcA-GlcNS6S-HexA-GlcNS6S-(CH<sub>2</sub>)<sub>5</sub>NH<sub>2</sub>]***

The N-sulfo modification is also a common motif in heparinoid GAGs. Addition of N-sulfation to the previously examined di-6-O-sulfated tetrasaccharide produces a tetra-sulfated saccharide containing two sulfates on each amino sugar. Shown in Figure 4.8, the EDD spectra of the  $[M-4H]^{4-}$  precursor for the two epimeric possibilities of the central hexuronic acid residue, GlcA (top) and IdoA (bottom) further demonstrate the capability of EDD to generate glycosidic bond cleavage as well as cross-ring cleavage in the presence of a high degree of sulfation. As the sulfate density increases, the need for cross-ring cleavage to locate the sulfate position on the hexose ring is reduced as the possible sites for sulfation are occupied but still necessitated to fully confirm location unless all potential sites on a ring are sulfated.

In the case of the examined tetra-sulfated compounds, the observed glycosidic bond cleavages readily identify each amino sugar as di-sulfated. N-sulfo modification can be determined by the  $^{0,2}X_0$  cleavage for the reducing end hexosamine and by the difference in mass of the  $B_2$  and  $^{0,2}A_2$  cleavages for the central amino residue.

Alternatively, the extent of N-sulfation compared to N-acetylation can be determined by an accurate mass measurement of the precursor. In cases where there is a mixture of N-sulfo and N-acetyl, bond cleavage analysis is required to identify the residue location. Similar to the tri-sulfated tetrasaccharide, determination of 6-O-sulfation is also not absolute for the precursor containing all ionized sulfates. The addition of 1 sodium counter ion (data not shown) results in the required  $^{2,4}A_2$  cleavage which places the sulfate at 6-O instead of 3-O.

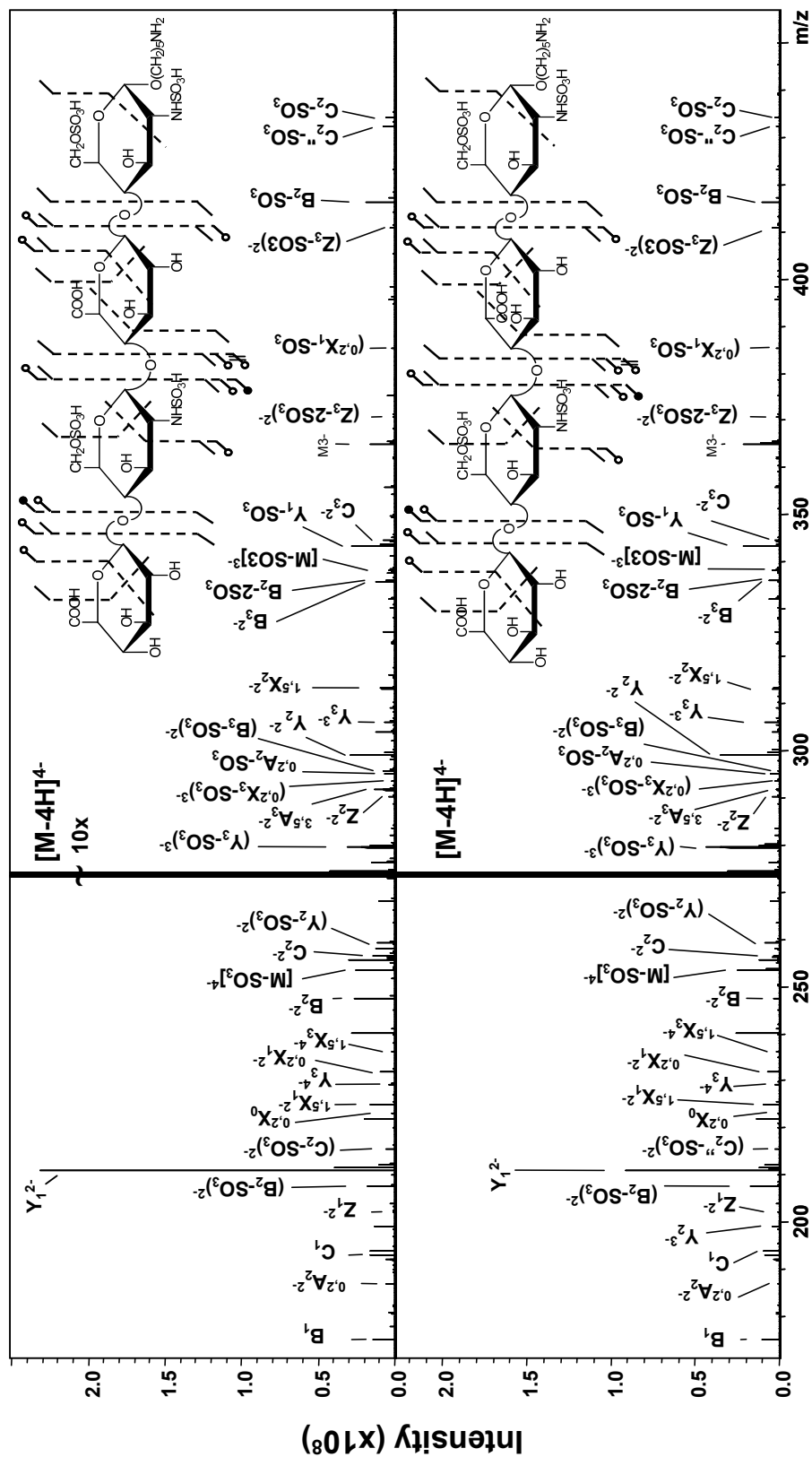


Figure 4.8 EDD spectra for the tetra-sulfated epimer pair, structures 3A and 3B.

Extension of C-5 hexuronic acid stereochemical determination is also possible at this degree of sulfation combining both O- and N-sulfo groups. Previous EDD-based stereochemical determination has been achieved for a tetrasaccharide with N-sulfation. The introduction of the N-sulfo modification generated a more intense  $^{3,5}A_3$  product ion in GlcA compared to IdoA by a factor of six [36]. The intensity difference present in the current epimer pair (factor of four) is in agreement and consistent with prior results where a proposed mechanism based on an  $\alpha$ -cleavage of an oxy-radical positioned at C3 or C4 generates the  $^{3,5}A_3$  cleavage with additional slow H-transfer for the cleavage to occur in IdoA with reduced intensity. Although the activated precursor ion charge state corresponded to the number of sulfate groups in this instance, it is hypothesized that an ionized site has moved to the hexuronic acid to facilitate this mechanism as the presence of two sites of negative charge on one residue would be unfavorable.

## CONCLUSIONS

Synthetic glycosaminoglycan tetrasaccharides provide a variable system for the examination of the effects of the degree and position of sulfation and hexuronic stereochemistry on EDD fragmentation. Consistent with threshold activation, selection of the appropriate precursor ion is necessary to minimize loss of the labile sulfate modification during EDD. The precursor ion typically possesses a charge state corresponding to the number of sulfate groups. EDD activation of tetrasaccharides ranging in sulfation from two to four produces glycosidic and cross-ring cleavage necessary to locate the sulfate moiety. To generate stereo-specific cleavages for GlcA/IdoA determination, the addition of sodium counter ions is required to move an

ionized site onto a carboxyl group. Sodium counter ions are also required to generate cross-ring cleavages for sulfation location in some instances.

## **ACKNOWLEDGEMENTS**

FEL III and IJA gratefully acknowledge financial support from the National Institutes of Health Grant #2R01-GM038060-20. FEL III/IJA/SA/KA/AV/GJB gratefully acknowledge financial support from the Center for Research Resource of the National Institutes of Health Grant # P41RR005351. FEL III personally acknowledges the University of Georgia Graduate School for current funding and Drs. Robert J. Linhardt and Tatiana N. Laremore (Rensselaer Polytechnic Institute) for helpful discussions regarding the nuances of desulfation chemistry.

## REFERENCES

1. Gotte, M., Syndecans in Inflammation. *The FASEB Journal* **2003**, *17*, 575-591.
2. Fannon, M.; Forsten, K. E. and Nugent, M. A., Potentiation and Inhibition of bFGF Binding by Heparin: A Model for Regulation of Cellular Response. *Biochemistry* **2000**, *39*, 1434-1445.
3. Lin, X., Functions of heparan sulfate proteoglycans in cell signaling during development. *Development* **2004**, *131*, 6009-6021.
4. Wu, Z. L.; Zhang, L.; Yabe, T.; Kuberan, B.; Beeler, D. L.; Love, A. and Rosenberg, R. D., The Involvement of Heparan Sulfate (HS) in FGF1/HS/FGFR1 Signaling Complex. *J. Biol. Chem.* **2003**, *278*, 17121-17129.
5. Lindahl, U.; Backstrom, G.; Hook, M.; Thunberg, L.; Fransson, L. A. and Linker, A., Structure of the antithrombin-binding site in heparin. *Proc. Natl. Acad. Sci. U. S. A.* **1979**, *76*, 3198-3202.
6. Williams, R. K. and Straus, S. E., Specificity and affinity of binding of herpes simplex virus type 2 glycoprotein B to glycosaminoglycans. *J. Virol.* **1997**, *71*, 1375-1380.
7. Batinic, D. and Robey, F. A., The V3 region of the envelope glycoprotein of human immunodeficiency virus type 1 binds sulfated polysaccharides and CD4-derived synthetic peptides. *J. Biol. Chem.* **1992**, *267*, 6664-6671.
8. Chen, Y.; Maguire, T.; Hileman, R. E.; Fromm, J. R.; Esko, J. D.; Linhardt, R. J. and Marks, R. M., Dengue virus infectivity depends on envelope protein binding to target cell heparan sulfate. *Nature Med.* **1997**, *3*, 866-871.

9. Selleck, S. B., Proteoglycans and pattern formation: sugar biochemistry meets developmental genetics. *Trends in Genetics* **2000**, *16*, 206-212.
10. Perrimon, N. and Bernfield, M., Cellular functions of proteoglycans--an overview. *Semin. Cell Dev. Biol.* **2001**, *12*, 65-67.
11. Bulow, H. E. and Hobert, O., Differential Sulfations and Epimerization Define Heparan Sulfate Specificity in Nervous System Development. *Neuron* **2004**, *41*, 723-736.
12. Gama, C. I. and Hsieh-Wilson, L. C., Chemical approaches to deciphering the glycosaminoglycan code. *Curr. Opin. Chem. Biol.* **2005**, *9*, 609-619.
13. Staples, G. O.; Shi, X. F. and Zaia, J., Extended N-Sulfated Domains Reside at the Nonreducing End of Heparan Sulfate Chains. *J. Biol. Chem.* **2010**, *285*, 18336-18343.
14. Habuchi, H.; Habuchi, O. and Kimata, K., Sulfation pattern in glycosaminoglycan: Does it have a code? *Glycoconjugate J.* **2004**, *21*, 47-52.
15. Rosenberg, R. D. and Lam, L., Correlation between structure and function of heparin. *Proc. Natl. Acad. Sci. U. S. A.* **1979**, *76*, 1218-1222.
16. Lindahl, U.; Kusche-Gullberg, M. and Kjellen, L., Regulated Diversity of Heparan Sulfate. *J. Biol. Chem.* **1998**, *273*, 24979-24982.
17. Feyzi, E.; Saldeen, T.; Larsson, E.; Lindahl, U. and Salmivirta, M., Age-dependent Modulation of Heparan Sulfate Structure and Function. *J. Biol. Chem.* **1998**, *273*, 13395-13398.
18. Shi, X. and Zaia, J., Organ-specific Heparan Sulfate Structural Phenotypes. *J. Biol. Chem.* **2009**, *284*, 11806-11814.

19. Raman, R.; Raguram, S.; Venkataraman, G.; Paulson, J. C. and Sasisekharan, R., Glycomics: an integrated systems approach to structure-function relationships of glycans. *Nat Meth* **2005**, *2*, 817-824.
20. Chi, L. L.; Amster, J. and Linhardt, R. J., Mass spectrometry for the analysis of highly charged sulfated carbohydrates. *Current Analytical Chemistry* **2005**, *1*, 223-240.
21. Zaia, J. and Costello, C. E., Compositional Analysis of Glycosaminoglycans by Electrospray Mass Spectrometry. *Anal. Chem.* **2001**, *73*, 233-239.
22. Zaia, J., Principles of Mass Spectrometry of Glycosaminoglycans. *J. Biomacromol. Mass Spectrom.* **2005**, *1*, 3-36.
23. Chi, L.; Wolff, J. J.; Laremore, T. N.; Restaino, O. F.; Xie, J.; Schiraldi, C.; Toida, T.; Amster, I. J. and Linhardt, R. J., Structural Analysis of Bikunin Glycosaminoglycan. *J. Am. Chem. Soc.* **2008**, *130*, 2617-2625.
24. Laremore, T. N.; Leach III, F. E.; Amster, I. J. and Linhardt, R. J., Electrospray ionization Fourier transform mass spectrometric analysis of intact bikunin glycosaminoglycan from normal human plasma. *Int. J. Mass Spectrom. In Press, Corrected Proof*,
25. Zaia, J.; McClellan, J. E. and Costello, C. E., Tandem Mass Spectrometric Determination of the 4S/6S Sulfation Sequence in Chondroitin Sulfate Oligosaccharides. *Anal. Chem.* **2001**, *73*, 6030-6039.
26. McClellan, J. E.; Costello, C. E.; O'Conno, P. B. and Zaia, J., Influence of Charge State on Product Ion Mass Spectra and the Determination of 4S/6S Sulfation

- Sequence of Chondroitin Sulfate Oligosaccharides. *Anal. Chem.* **2002**, *74*, 3760-3771.
27. Zaia, J.; Li, X.-Q.; Chan, S.-Y. and Costello, C. E., Tandem mass spectrometric strategies for determination of sulfation positions and uronic acid epimerization in chondroitin sulfate oligosaccharides. *J. Am. Soc. Mass Spectrom.* **2003**, *14*, 1270-1281.
28. Zaia, J. and Costello, C. E., Tandem Mass Spectrometry of Sulfated Heparin-Like Glycosaminoglycan Oligosaccharides. *Anal. Chem.* **2003**, *75*, 2445-2455.
29. Miller, M. J. C.; Costello, C. E.; Malmstrom, A. and Zaia, J., A tandem mass spectrometric approach to determination of chondroitin/dermatan sulfate oligosaccharide glycoforms. *Glycobiology* **2006**, *16*, 502-513.
30. Saad, O. M. and Leary, J. A., Compositional Analysis and Quantification of Heparin and Heparan Sulfate by Electrospray Ionization Ion Trap Mass Spectrometry. *Anal. Chem.* **2003**, *75*, 2985-2995.
31. Saad, O. M. and Leary, J. A., Heparin Sequencing Using Enzymatic Digestion and ESI-MS with HOST: A Heparin/HS Oligosaccharide Sequencing Tool. *Anal. Chem.* **2005**, *77*, 5902-5911.
32. Wolff, J. J.; Amster, I. J.; Chi, L. and Linhardt, R. J., Electron Detachment Dissociation of Glycosaminoglycan Tetrasaccharides. *J. Am. Soc. Mass Spectrom.* **2007**, *18*, 234-244.
33. Wolff, J. J.; Laremore, T. N.; Busch, A. M.; Linhardt, R. J. and Amster, I. J., Electron Detachment Dissociation of Dermatan Sulfate Oligosaccharides. *J. Am. Soc. Mass Spectrom.* **2008**, *19*, 294-304.

34. Wolff, J. J.; Laremore, T. N.; Aslam, H.; Linhardt, R. J. and Amster, I. J., Electron-Induced Dissociation of Glycosaminoglycan Tetrasaccharides. *J. Am. Soc. Mass Spectrom.* **2008**, *19*, 1449-1458.
35. Wolff, J. J.; Laremore, T. N.; Busch, A. M.; Linhardt, R. J. and Amster, I. J., Influence of Charge State and Sodium Cationization on the Electron Detachment Dissociation and Infrared Multiphoton Dissociation of Glycosaminoglycan Oligosaccharides. *J. Am. Soc. Mass Spectrom.* **2008**, *19*, 790-798.
36. Wolff, J. J.; Chi, L.; Linhardt, R. J. and Amster, I. J., Distinguishing Glucuronic from Iduronic Acid in Glycosaminoglycan Tetrasaccharides by Using Electron Detachment Dissociation. *Anal. Chem.* **2007**, *79*, 2015-2022.
37. Arungundram, S.; Al-Mafraji, K.; Asong, J.; Leach, F. E.; Amster, I. J.; Venot, A.; Turnbull, J. E. and Boons, G.-J., Modular Synthesis of Heparan Sulfate Oligosaccharides for Structure-Activity Relationship Studies. *J. Am. Chem. Soc.* **2009**, *131*, 17394-17405.
38. Nagasawa, K.; Inoue, Y. and Kamata, T., Solvolytic desulfation of glycosaminoglycuronan sulfates with dimethyl sulfoxide containing water or methanol. *Carbohydr. Res.* **1977**, *58*, 47-55.
39. Huang, Y.; Shi, X.; Yin, H.; Killeen, K. and Zaia, J., Improvement of ESI Behavior of Heparan Sulfate Oligosaccharides by Using a Chip-based Pulsed Post-Column Makeup Flow for Online LC/MS, *58th ASMS Conference on Mass Spectrometry and Allied Topics*, Salt Lake City, UT, 2010.
40. Heck, A. J. R.; de Koning, L. J.; Pinkse, F. A. and Nibbering, N. M. M., Mass-specific selection of ions in Fourier-transform ion cyclotron resonance mass

spectrometry. Unintentional off-resonance cyclotron excitation of selected ions.

*Rapid Commun. Mass Spectrom.* **1991**, *5*, 406-414.

41. Ceroni, A.; Maass, K.; Geyer, H.; Geyer, R.; Dell, A. and Haslam, S. M., GlycoWorkbench: A Tool for the Computer-Assisted Annotation of Mass Spectra of Glycans. *J. Prot. Res.* **2008**, *7*, 1650-1659.
42. Domon, B. and Costello, C. E., A systematic nomenclature for carbohydrate fragmentations in FAB-MS/MS spectra of glycoconjugates. *Glycoconjugate J.* **1988**, *5*, 397-409.
43. Wolff, J. J.; Leach, F. E.; Laremore, T. N.; Kaplan, D. A.; Easterling, M. L.; Linhardt, R. J. and Amster, I. J., Negative Electron Transfer Dissociation of Glycosaminoglycans. *Anal. Chem.* **2010**, *82*, 3460-3466.

## CHAPTER 5

# DETERMINATION OF HEXURONIC ACID STEREOCHEMISTRY IN CHONDROITIN SULFATE GLYCOSAMINOGLYCAN OLIGOSACCHARIDES BY ELECTRON DETACHMENT DISSOCIATION<sup>1</sup>

---

<sup>1</sup> Leach III, F.E., Ly, M., Laremore, T.N., Wolff, J.J., Perlow, J., Linhardt, R.J., and I.J. Amster. To be submitted to *Journal of the American Society for Mass Spectrometry*.

## ABSTRACT

To assign the stereochemistry in chondroitin sulfate (CS) epimers and investigate the mechanisms for product ion formation during electron detachment dissociation (EDD) in CS glycoforms, a series of experiments have been conducted in which precursor ions are independently activated by EDD, electron induced dissociation (EID), and negative electron transfer dissociation (NETD). This approach allows for the assignment of electronic excitation products formed by EID and detachment products to radical pathways in NETD, both of which occur simultaneously during EDD. Although a unique diagnostic ion based on presence/absence has not been assigned to differentiate the uronic acid stereochemistry in electron detachment spectra for the predominant  $[M-2H]^{2-}$  precursor, intensity differences do exist when assigned glycosidic and cross-ring cleavages are compared. The variations in the intensities of the doubly deprotonated  $^{0,2}X_3$  and  $Y_3$  ions have been shown to be indicative of CS-A/DS composition during the CID of binary mixtures. These ions can provide insight into the uronic acid composition of binary mixtures in EDD, but the relative abundances, although reproducible, are low when compared to those in a CID spectrum acquired on an ion trap. The application of principal component analysis (PCA) presents a multivariate approach to determining the uronic acid stereochemistry spectra of these GAGs by taking advantage of the reproducible peak distributions produced by electron detachment.

## INTRODUCTION

Glycosaminoglycan (GAG) carbohydrates are acidic linear polysaccharides that participate a variety of biological activities [1-7]. GAGs are biologically expressed in a variety of glycoforms, which vary in modifications to a disaccharide repeat unit consisting of hexuronic acid and hexosamine residues. These modifications include glycosidic bond linkage position and stereochemistry, position and extent of O- and N-sulfation and N-acetylation, and hexuronic acid stereochemistry. The analytical characterization of these modifications has been a standing challenge due to the natural poly-dispersivity of these biomolecules arising from a non-template based synthesis. Of the applied techniques, mass spectrometry [8-15] and tandem mass spectrometry [16-22] have presented highly sensitive methods of structural characterization.

The tandem mass spectrometry methods can be classified based upon the type of ion activation: threshold, which includes collisional induced dissociation (CID) [23] and infrared multiphoton dissociation (IRMPD) [24], and electron-based, which includes electron capture dissociation (ECD) [25], electron detachment dissociation (EDD) [26], electron transfer dissociation (ETD) [27], and negative electron transfer dissociation (NETD) [28]. Both classes of ion activation have been demonstrated for a variety of GAG glycoforms ranging in extent of sulfation and polymerization.

Chondroitin sulfate (CS) GAGs have largely been characterized by threshold activation [16-18, 29-33] as electron-based methods have only recently been applied to CS GAG analysis [34-36]. Threshold activation has afforded the ability to locate the sulfate modification (4-O or 6-O dependent upon CS type) in pure samples as well as mixtures [16-18]. Additionally, the ability to determine hexuronic acid stereochemistry

has been demonstrated based upon fragment ion intensities and rationalized based upon the differences in oligomeric flexibility inferred by the incorporation of IdoA residues [18].

Analysis of CS glycoforms by EDD has presented experimental results that differ from prior results in HS. This outcome is not entirely unexpected as the two glycoforms vary in sites of O-sulfation and are composed of differing hexosamine residues (glucosamine in HS and galactosamine in CS), which produces a glycosidic bond linkage unique to each. Prior EDD results for HS have provided information relevant to the location of sulfate groups [37] as well as the assignment of hexuronic acid stereochemistry [38] based on the presence or absence of diagnostic fragment ions such as  $^{0,2}A_3$ ,  $B_3'$ , and  $B_3'-CO_2$ . These ions are not sufficient for the assignment of hexuronic acid residue in CS glycoforms as some occur in both epimers and others are not present in either.

To fully characterize the electron-based ion activation of the epimer pair, CS-A and DS, EDD, as well as EID [35] and NETD [39] have been employed to activate the tetrasaccharide of each. The tandem mass spectra generated from each allow the assignment of products due to electronic excitation (EID) or radical-based mechanisms (NETD). Similar to threshold activation, the stereochemistry of the hexuronic acid residue can be inferred by the intensities of cleavages at the non-reducing terminus. Although their occurrence can provide insight into the composition, the intensities are low, albeit reproducible, compared to CID products generated in an ion trap. Multivariate statistical methods, namely principal component analysis (PCA), have previously been applied to HS tetrasaccharide epimer differentiation [40] and are

employed here to take advantage of the highly reproducible nature of EDD spectra and quantitatively assign the stereochemistry of hexuronic acid residues in 4-O sulfated CS epimers.

## **EXPERIMENTAL METHODS**

### *Preparation of GAG Oligosaccharides*

Chondroitin sulfate A (CS-A) and dermatan sulfate (DS) oligosaccharides were independently prepared by partial enzymatic depolymerization of bovine trachea chondroitin sulfate A (Celsus Laboratories, Cincinnati, OH) and porcine intestinal mucosa dermatan sulfate (Celsus Laboratories, Cincinnati, OH). A 20 mg/mL solution of each, in 50 mM Tris-HCl/60 mM sodium acetate buffer, pH 8 was incubated at 37°C with chondroitin ABC lyase from *Proteus vulgaris*, EC 4.2.2.4. (Seikagaku, Japan). After the absorbance at 232 nm indicated the digestion was 50% completed, the digestion mixture was heated at 100°C for 3 min. High-molecular-weight oligosaccharides and the enzyme were removed by ultra-filtration using a 5000 MWCO membrane. The resulting oligosaccharide mixture was concentrated by rotary evaporation and fractionated by low pressure GPC on a Bio-Gel P10 (Bio-Rad, Richmond, CA) column. Fractions containing oligosaccharides of interest were desalted by GPC on a Bio-Gel P2 column and freeze-dried [41]. Further purification of compounds was carried out using strong anion exchange high-pressure liquid chromatography (SAX-HPLC) on a semi-preparative SAX S5 Spherisorb column (Waters Corp, Milford, MA). The SAX-HPLC fractions containing > 90% of were collected, desalted by GPC, and freeze-dried. The solid was reconstituted in water and purified a second time by SAX-HPLC. Only the top 30% of

the chromatographic peak was collected, desalted, and freeze-dried. Concentration of the oligosaccharide solutions was determined by measuring the absorbance at 232 nm ( $\epsilon = 3800 \text{ M}^{-1}\text{cm}^{-1}$ ). The resulting fractions containing individual oligosaccharides were characterized by PAGE, ESI-MS, and high-field nuclear magnetic resonance (NMR) spectroscopy [42].

#### *Oligosaccharide Desulfation*

The pyridinium salts of CS-A and DS dp4 were independently dissolved in 10 % aqueous MeOH and heated for 6 hrs at 60° C [43] to produce the desulfated tetrasaccharides  $\Delta\text{UA-GalNAc-GlcA-GalNAc}$  and  $\Delta\text{UA-GalNAc-IdoA-GalNAc}$ , respectively. The mass-selective quadrupole of the FT-ICR MS instrument was employed to isolate the desulfated compounds in lieu of additional laboratory based purification. The desulfation reaction does not affect the stereochemistry of the hexuronic acid residue, and so the chirality of the product is the same as that of the reactant as established by NMR analysis.

#### *Mass Spectrometry Analysis*

Experiments were performed with a 9.4 T Bruker Apex Ultra QeFTMS (Billerica, MA) fitted with an Apollo II dual source, 25 W CO<sub>2</sub> laser (Synrad model J48-2, Mukilteo, WA) for IRMPD, and an indirectly heated hollow cathode (HeatWave, Watsonville, CA) to generate electrons for EDD. The sample solutions were infused at a rate of 120  $\mu\text{L}/\text{hour}$  and ionized by electrospray using a metal capillary (Agilent Technologies, Santa Clara, CA, #G2427A). Solutions of each oligosaccharide were

introduced at a concentration of 0.1 mg/mL in 50:50:0.1 methanol:H<sub>2</sub>O:FA (Sigma, St. Louis, MO) to generate doubly deprotonated ions and 0.2 mg/mL in 50:50 methanol:H<sub>2</sub>O with 1% 100  $\mu$ M NaOH to generate triply deprotonated ions and sodium adduct ions. All oligosaccharides were examined in negative ion mode.

For the EDD experiments, precursor ions were isolated in the external quadrupole and accumulated for 1-3 seconds before injection into the FT-ICR MS cell. One quadrupole isolation/cell fill was utilized per scan. The selection of the precursor ion was further refined by using in-cell isolation with a coherent harmonic excitation frequency (CHEF) event [44]. For electron irradiation the cathode bias was set to -19 V and the extraction lens was varied from -18.4 V to -18.6 V to optimize the electron current entering the analyzer cell. The cathode heater was set to 1.5 A. The precursor ions were then irradiated with electrons for 1 second. EID experiments are performed with the same parameters as EDD, except a singly charged species is irradiated. 24 acquisitions were signal averaged per mass spectrum. For each mass spectrum, 512K points were acquired, padded with one zero fill, and apodized using a sinebell window. Background spectra were acquired by leaving all parameters the same but setting the cathode bias to 0 V to ensure that no electrons reached the analyzer cell. External calibration of mass spectra produced mass accuracy of 5 ppm. Internal calibration was also performed using confidently assigned glycosidic bond cleavage products as internal calibrants, providing mass accuracy of <1 ppm. Due to the larger number of low intensity products formed by EDD, only peaks with S/N > 10 are reported. Product ions were assigned using accurate mass measurement and Glycoworkbench [45]. All products are reported using the Wolff-Amster annotation [36] of the Domon and Costello nomenclature [46].

NETD experiments were performed on a 12.0 T Bruker solarix FTMS instrument (Bruker Daltonics, Billerica, MA). For NETD experiments, precursor ions were isolated in the external quadrupole and accumulated for 1-3 seconds in the 3-D ion trap before reaction with the reagent radical cation. The fluoranthene radical cation was generated in the chemical ionization (CI) source and accumulated for 500 -1000 ms prior to mass filtering and injection into the 3-D ion trap. Ion-ion reactions were conducted for 1.5 s. The precursor ion and NETD products were then injected into the mass analyzer through an rf-only ion guide. One analyzer cell fill was utilized per scan. 24-36 acquisitions were signal averaged per mass spectrum. For each mass spectrum, 1M points were acquired, padded with one zero fill, and apodized using a sinebell window. Background spectra were acquired by leaving all parameters the same without the generation of the radical cation. Data reduction was conducted in the same manner described above.

#### *Multivariate Statistical Analysis*

Principal component analysis (PCA) was performed using PLS Toolbox (Eigenvector Research, Inc., Wenatchee, WA). The abundances of 34 assigned fragment ions were normalized with respect to total ion abundance in each EDD spectrum. An input data matrix was constructed with each row containing the mass spectrum of a single tetrasaccharide epimer (samples) and each column, the normalized abundance of an assigned fragment ion (variables). For each tetrasaccharide, five EDD spectra were obtained in the same day. Prior to PCA, each data set was mean-centered and cross-validated. For comparison, the abundances of 19 assigned peaks from IRMPD spectra were also treated in the same manner as the EDD data.

## RESULTS AND DISCUSSION

### *EDD of chondroitin sulfate A (CS-A) oligosaccharides*

Electron detachment dissociation (EDD) spectra of dermatan sulfate (DS) oligosaccharides ranging from degree of polymerization (dp) 4 to 10 have been previously reported [34]. The examined chondroitin sulfate A (CS-A) oligosaccharides only differ from those samples in the stereochemistry of the hexuronic acid residues. Both DS and CS-A have a uniform disaccharide repeat in reference to 4-O-sulfation on the hexosamine, whereas the DS oligosaccharides contain IdoA and the CS-A contain GlcA. Shown in Figure 5.1 are the annotated structures for the EDD activation of CS-A dp4-10.

Across the degrees of polymerization examined for CS-A, results consistent with the EDD of DS are observed. In summary, cleavage of all glycosidic bonds is observed except for  $C_2$  and  $Z_2$  in the dp6 oligomer. Due to the uniform repeat unit, the  $C_{n/2}$  and  $Z_{n/2}$  cleavages, where  $n$  is the degree of polymerization, are isobaric with the precursor ion and are not uniquely assigned. The loss of  $CO_2$  is observed from the  $Z_2$  cleavage and occurs in dp4-10. The loss of  $SO_3$  is observed from both glycosidic, with losses of H or 2H, and cross-ring cleavages, typically assigned as  $^{1,5}X_n$  or  $^{0,2}X_n$  of GlcA residues. Consistent with observations in DS, cross-ring cleavages are largely observed on hexuronic acid residues, indicating a propensity for mobile protons and radical site formation at the carboxylate, which leads to increased cross-ring fragment generation.

As the only difference between CS-A and DS is the stereochemistry of the hexuronic acid, it is not entirely unexpected that the EDD spectra look remarkably similar

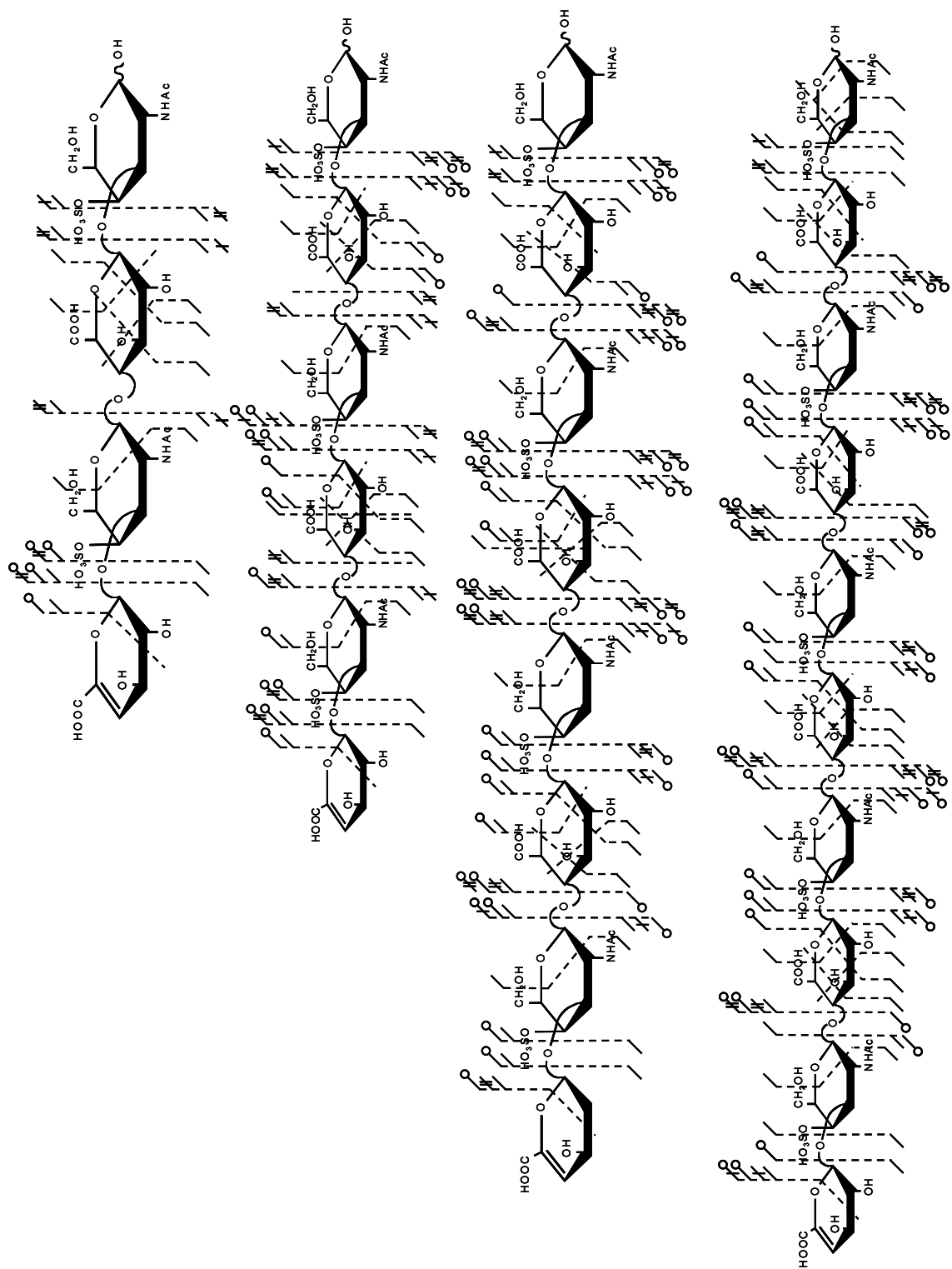


**Figure 5.1** EDD product assignments for CS-A dp4-10.

and no product ions are unique to one epimer when the activation of precursor ions of the same charge state and degree of polymerization are compared. Shown in Figure 5.2, the EDD of the  $[M-2H]^{2-}$  precursor ions for the CS-A and DS dp4 oligomers are compared. (Note: The EDD of DS has been previously published [34] and is shown here for the benefit of direct comparison.) Activation of each precursor ion under nearly the same experimental conditions produces spectra that contain the same suite of product ions but differing in intensities in some cases. These differences, specifically that of the charge conserved  $^{0,2}X_n$  and  $Y_n$  product ions on the non-reducing terminus, were exploited by Zaia and co-workers to identify the hexuronic acid stereochemistry in CID spectra generated in a quadrupole ion trap [18]. In the doubly deprotonated dp4 oligomers shown, these ions occur as  $^{0,2}X_3^{2-}$  and  $Y_3^{2-}$  and distinguishable intensity differences occur between the two epimers (denoted by squares in Figure 5.2).

#### *Hexuronic Acid Determination by EDD*

Direct tandem mass spectrometric evidence of hexuronic acid stereochemistry has previously been achieved in heparan sulfate (HS) tetrasaccharides by EDD [47]. The product ions diagnostic of GlcA containing tetrasaccharides were  $^{0,2}A_3$ ,  $B_3'$ , and  $B_3'-CO_2$  and secondary confirmation of IdoA was indicated by a more intense  $C_3''$  than  $C_3$ . The generation of these product ions is dependent upon detachment from an ionized carboxyl site. As the number of sulfates is increased on an oligosaccharide, the charge state must exceed the number of sulfate groups by at least one to satisfy this condition. Based on the hypothesis of mobile protons in CS glycoforms [48], the presence of an ionized carboxyl

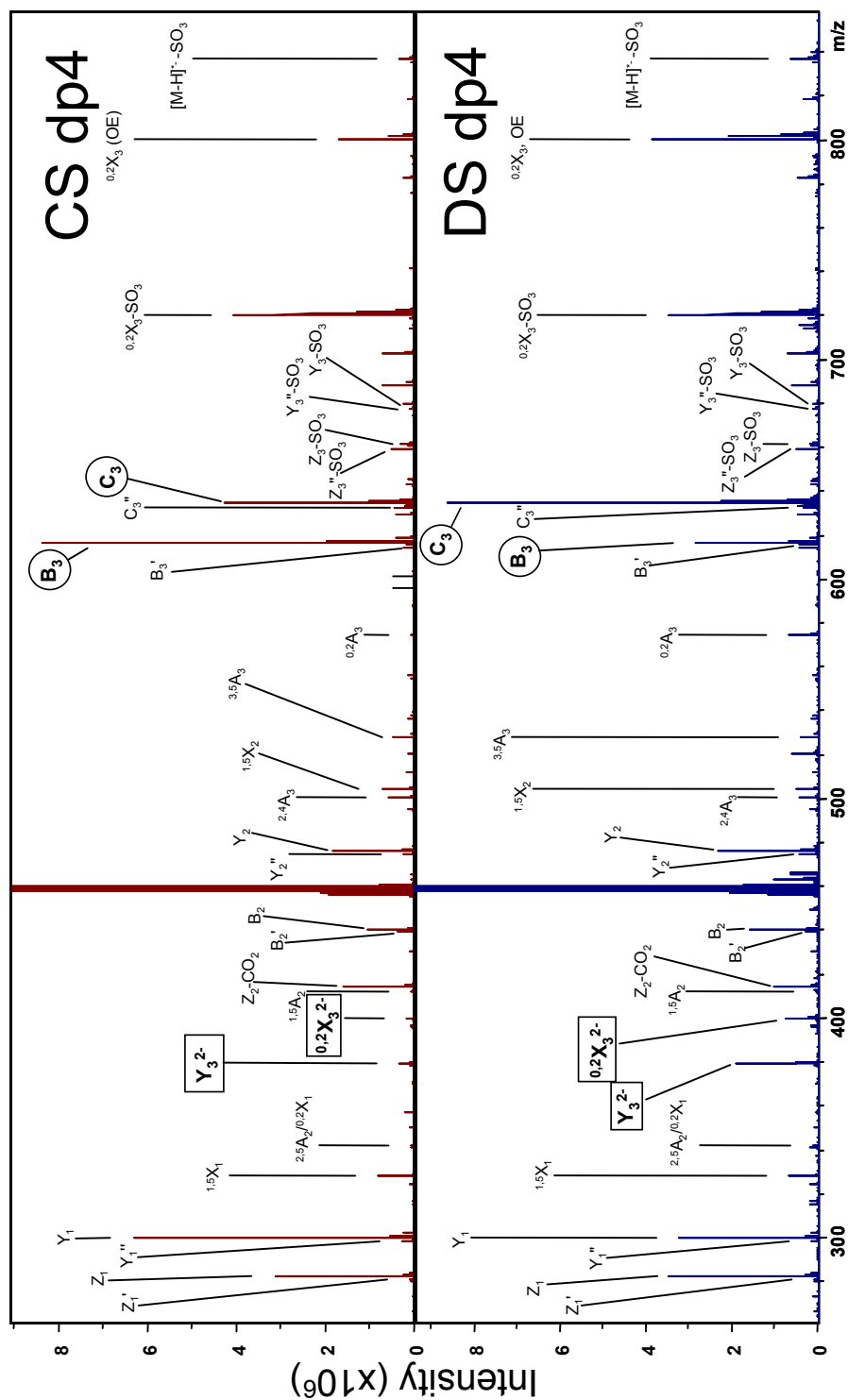


**Figure 5.2** Comparison of the EDD activation for the  $[M-2H]^{2-}$  precursor ion of the tetrasaccharide epimer pair, CS-A and DS.

carboxyl group may be inferred for the  $[M-2H]^{2-}$  precursor, but is not certain unless the  $[M-3H]^{3-}$  ion is generated.

Comparison of the EDD generated fragments depicted in Figure 5.2 for the  $[M-2H]^{2-}$  precursor reveals that the diagnostic  $^{0,2}A_3$  ion, previously indicative of GlcA, occurs in both epimers. This result was observed in the initial EDD study of DS oligosaccharides, as well as IRMPD. Additionally,  $B_3'$  and  $C_3''$  are also assigned in both, but  $B_3'-CO_2$  is not assigned in either. Examination of the relative intensities in each spectrum, though, can provide initial information for differentiation. When the intensities of the  $B_3$  and  $C_3$  glycosidic cleavages (denoted by circles in Figure 5.2) are compared within each epimer,  $B_3 > C_3$  in CS-A and  $B_3 < C_3$  in DS.  $B_3'$  and  $C_3''$  remain minor components in each epimer. Comparison between the two epimers reveals the  $^{0,2}A_3$  is more intense in DS than CS-A. A more quantitative method for epimer differentiation using multivariate statistics will be presented later in the text.

To insure the presence of an ionized carboxyl group, the EDD activation of the  $[M-3H]^{3-}$  precursor was conducted and generated the tandem mass spectra shown in Figure 5.3. A unique stereo-specific ion does not occur in either spectrum. Subtle intensity differences are observed when  $^{0,2}X_3^{2-}$  and  $Y_3^{2-}$  are compared between epimers yet the  $^{0,2}A_3$  nor  $B_3'$  and  $B_3'-CO_2$  cleavages do not occur. This result serves as further evidence that detachment initiated mechanisms play a less substantial role in CS glycoform epimer differentiation by EDD than in HS.

#### *Mechanistic Aspects*

The source of product ions observed during the electron-based ion activation of multiply de-protonated GAG ions can be rationalized by the schematic shown in Figure

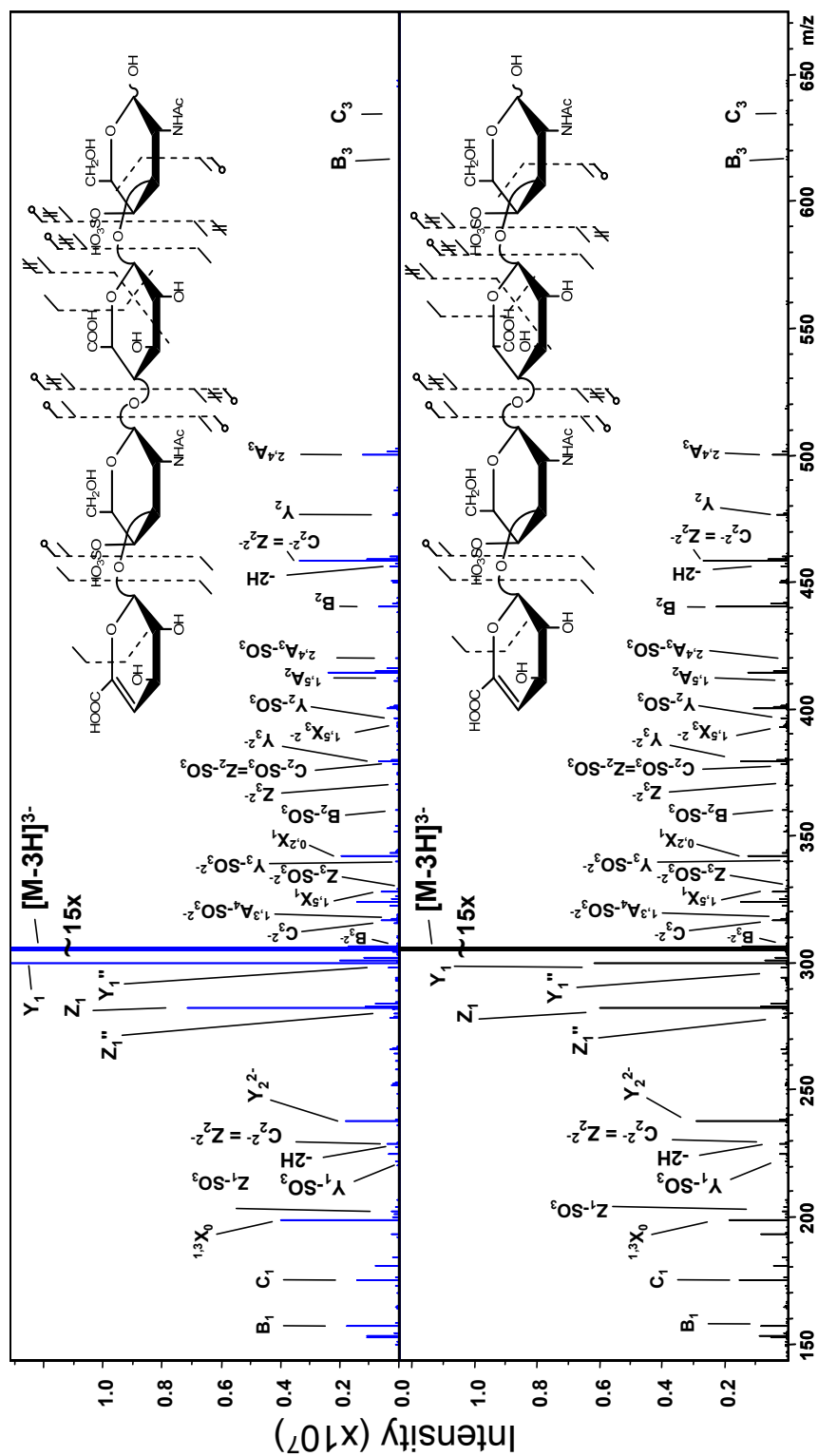


**Figure 5.3** Comparison of the EDD activation for the  $[M-3H]^{3-}$  precursor ion of the tetrasaccharide epimer pair, CS-A and DS.

5.4. The activation path during EDD is initiated by irradiation with moderate energy electrons (typically 19 eV), which produces an excited state intermediate.

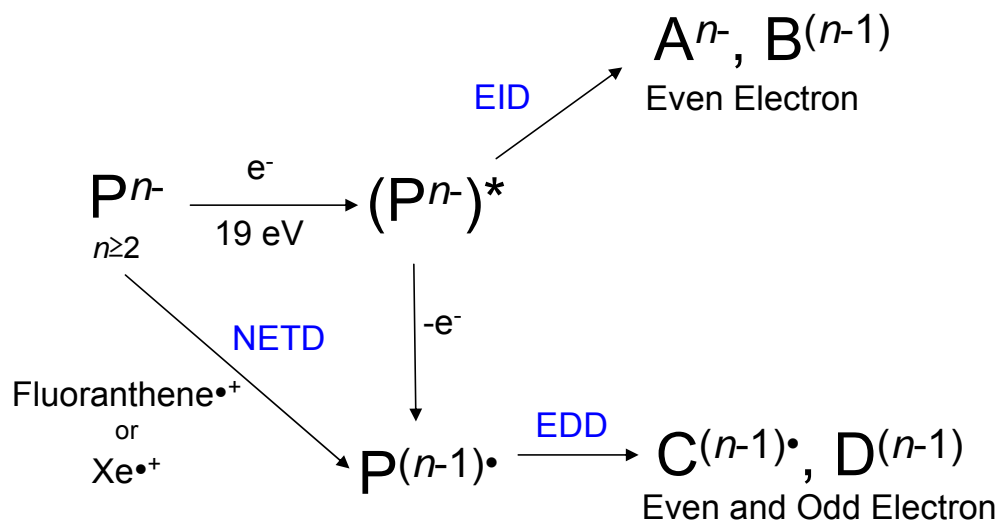


**Figure 5.4** Proposed pathway for the electron-based activation of multiply charged anions.

From this state, two independent processes, electron detachment and electron induced dissociation (EID) lead to the products observed in an EDD tandem mass spectrum. Electron detachment results in product ions, which are reduced in absolute charge (formally oxidized) and can be assigned as either odd-electron species or even electron species. EID products result from the direct electronic excitation of the precursor ion and may either be charge conserved or reduced, existing largely as even electron species but in some cases odd-electron species have been observed. To determine the activation channel responsible for a specific product ion, it is possible to conduct negative electron transfer dissociation (NETD) for the assignment of products due to detachment as the

excited state intermediate is avoided or the irradiation of a mass-selected singly de-protonated GAG anion by moderate energy electrons during which observed products will be solely due to EID processes. Additionally, the extent of ionized sites along the anion can be manipulated by the ESI spray solvent conditions as well as Na/H exchange.

*Negative Electron Transfer Dissociation (NETD) of Doubly De-protonated CS GAG Tetrasaccharides*

NETD has previously been applied to GAG structural characterization in ion traps [39], but this is the first published example of NETD coupled to the FT-ICR mass analyzer for GAG analysis. Briefly, ion-ion reactions between multiply de-protonated GAG analytes and radical cations of fluoranthene occur in the high-pressure region of the instrument, and the products are transported by an rf-only ion guide to the ICR mass analyzer. A detailed account of the NETD FT-ICR MS of GAGs will be the subject of a future manuscript in preparation.

The NETD of the  $[M-2H]^{2-}$  CS-A/DS dp4 epimer pair is shown in Figure 5.5. Comparison of the product ions in NETD with those from EDD experimentally confirms that they are a subset of EDD. Inspection of the previously stereo-specific region of the spectrum reveals that the  $^{0,2}A_3$ ,  $B_3'$ , and  $C_3''$  ions are present in both epimers; therefore, radical detachment mechanisms are involved in their generation but exist in both diastereomers. Interestingly, the  $B_3'$  ion is more intense when compared to  $B_3$  in DS, which contains the IdoA residue, and  $^{0,2}A_3$  is more intense in DS than CS-A. This result is opposite that found in HS and may indicate a more facile hydrogen rearrangement in the IdoA case for CS glycoforms.

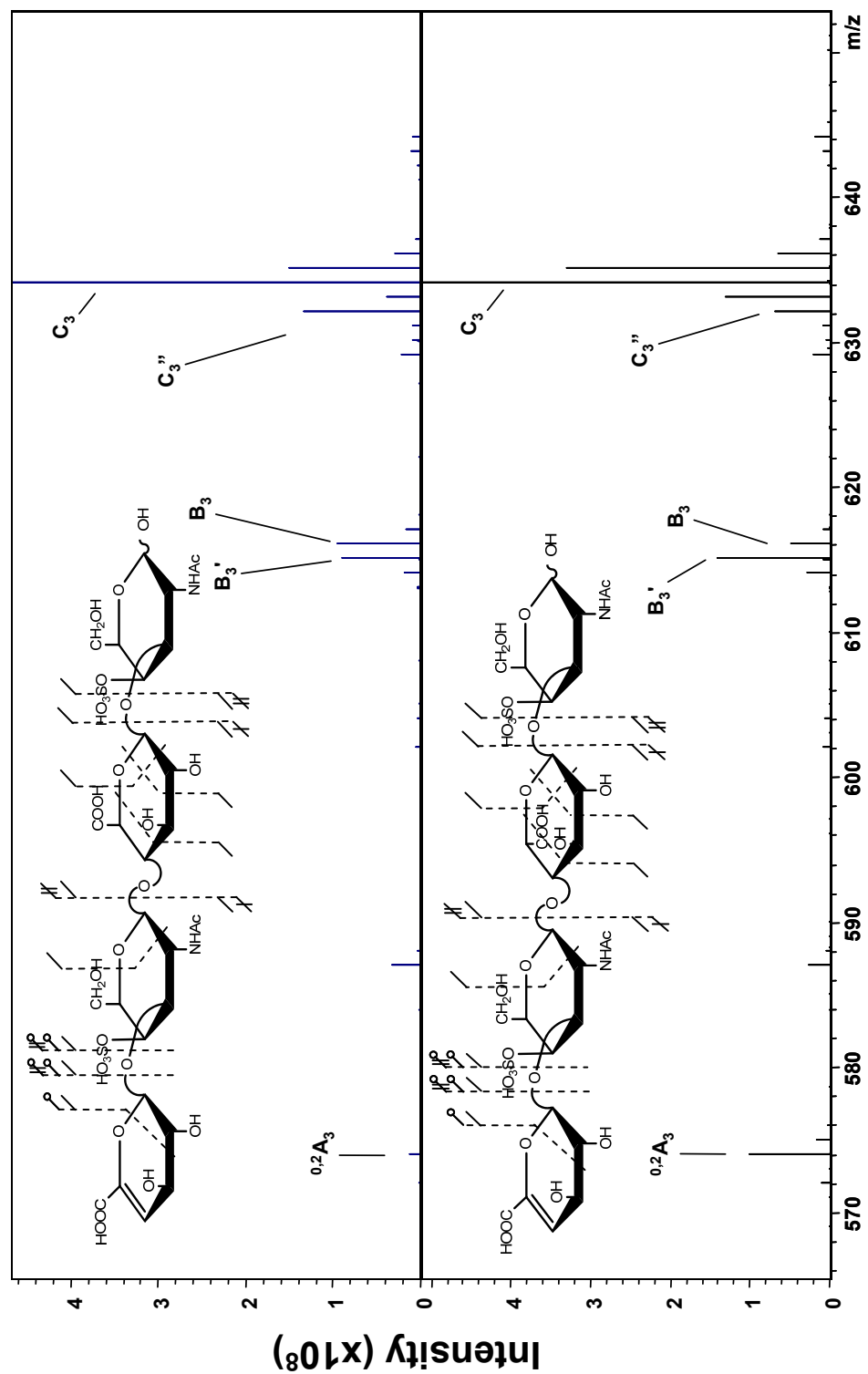


**Figure 5.5** NETD of the  $[M-2H]^{2-}$  precursor ion of the tetrasaccharide epimer pair, CS-A and DS, from 470  $m/z$  to 560  $m/z$ . Insets denote the assigned product ions.



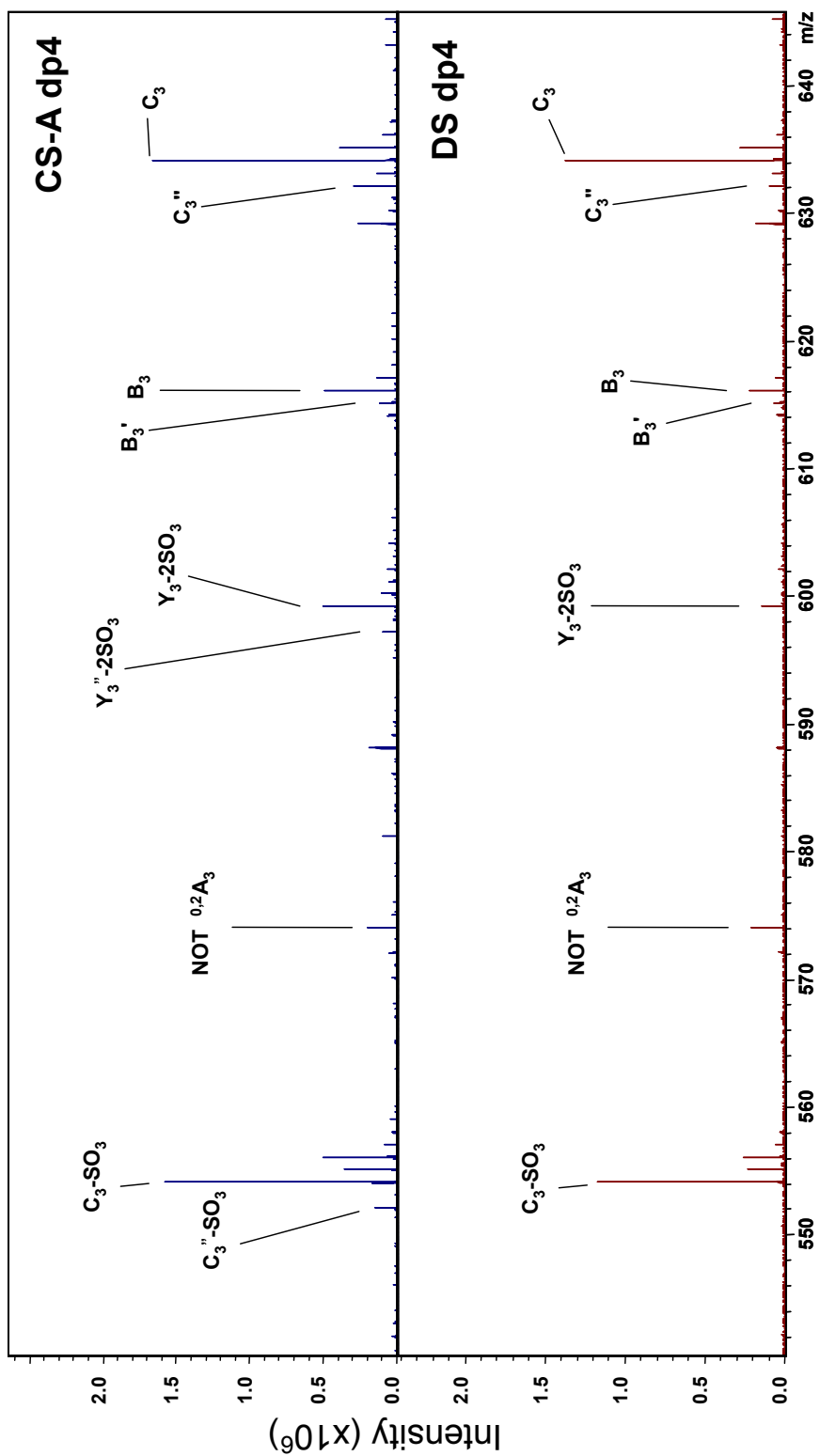


**Figure 5.7** The product ions in the previous stereo-specific region in the EID mass spectrum. (Based on accurate mass, the  $^{0,2}A_3$  ion is not observed.)

### Manipulation of Na/H Heterogeneity

The ability to control the fragmentation of GAG anions by selection of an appropriate precursor ion charge state and the addition of metal counter-ions, specifically  $\text{Na}^+$ , is well known within the threshold activation community and has been utilized to minimize and/or eliminate the loss of  $\text{SO}_3$  from sulfated GAGs [49]. These techniques have also been utilized to minimize the loss of  $\text{SO}_3$  by increasing the number of ionized sites above the total number of sulfates during the EDD of DS and synthetic HS GAGs, providing stereo-specific products in increasingly sulfated HS by previously proposed mechanisms. Application of this technique for CS epimer characterization introduces the possibility of an ionized carboxyl, yet no stereo-specific product ions are generated in either the  $[\text{M}-3\text{H}+1\text{Na}]^{2-}$  nor  $[\text{M}-4\text{H}+2\text{Na}]^{2-}$  precursor ion shown respectively in Figures 5.8 and 5.9.

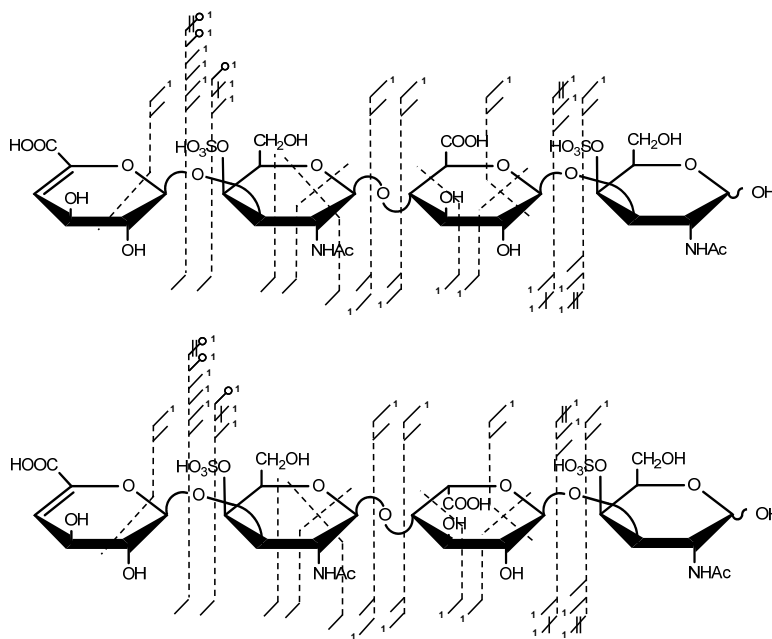


**Figure 5.8** Assigned product ions for the EDD of the  $[\text{M}-3\text{H}+1\text{Na}]^{2-}$  precursor ion for the CS-A/DS epimer pair.

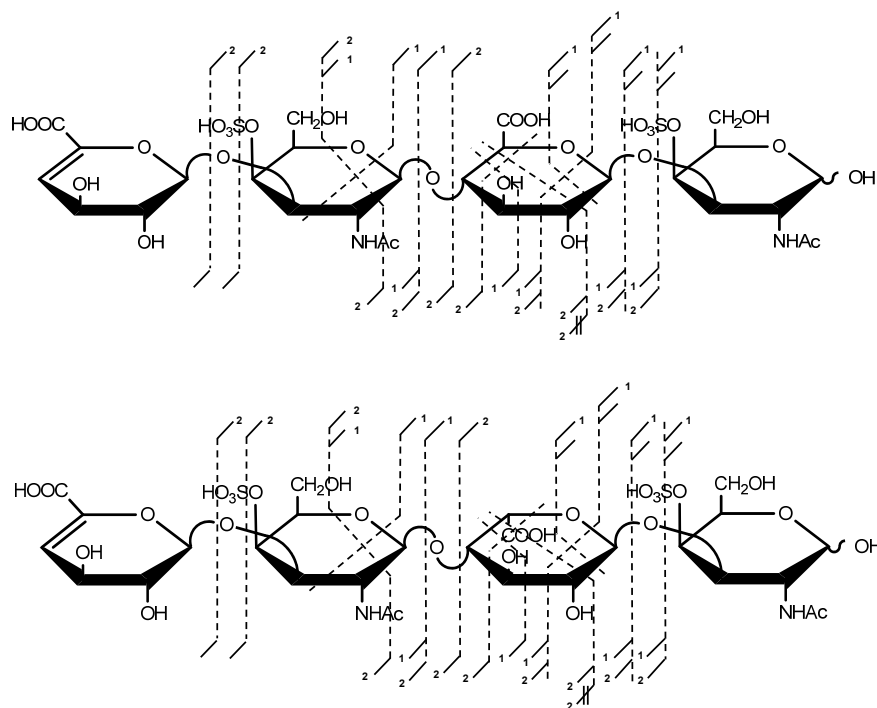


**Figure 5.9** Assigned product ions for the EDD of the  $[M-4H+2Na]^{2-}$  precursor ion for the CS-A/DS epimer pair.

### *Oligosaccharide Desulfation*

To remove the participation of sulfate groups and potentially identify stereo-specific product ions due solely to electron detachment from a carboxylate, the disulfated tetrasaccharide epimer pair of CS-A and DS were solvolytically desulfated by the method described earlier. The doubly deprotonated precursor ion,  $[M-2H]^{2-}$ , of each produces unambiguous ionization of both carboxyl groups. The spectral region containing the useful product ions generated in HS epimers is shown in Figure 5.10, with insets denoting the total fragmentation. When compared the two regions are nearly identical in terms of product ions observed and relative intensities. Also, the overall fragmentation depicted in the inset shows the occurrence of the same product ion suite for the epimers. This result provides direct evidence that the difference in the glycosidic

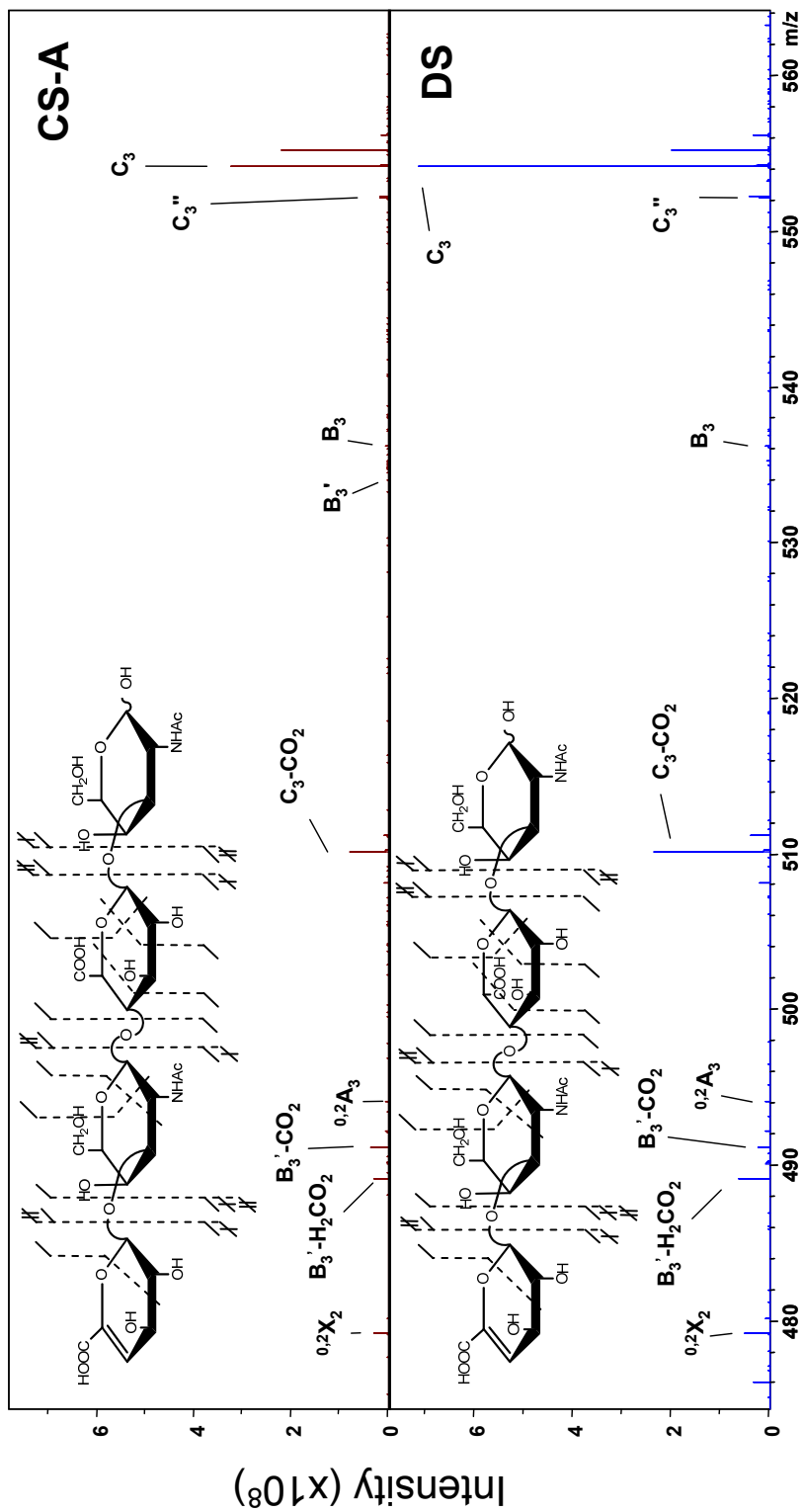


**Figure 5.10** EDD of the desulfated chondroitin epimer pair from 470 m/z to 570 m/z.

Insets denote the assigned product ions.

linkage between HS and CS/DS glycoforms negates the ability to identify the hexuronic acid stereochemistry as GlcA based on the occurrence of  $^{0,2}A_3$  and  $B_3'$ -CO<sub>2</sub> in CS/DS glycoforms and other product ions must be assigned or methods employed for this differentiation.

### *Multivariate Statistical Analysis*

Based upon the systematic investigation of electron-based CS GAG ion activation, the presence or absence of diagnostic products is not a reliable manner to identify the hexuronic acid stereochemistry by EDD. To quantitatively make this assignment, multivariate (MVA) statistical methods are employed. MVA methods have previously demonstrated the ability to separate synthetic HS GAG epimers at the tetrasaccharide oligomer length without the need for the identification of stereo-specific products [40]. The method selected for this study is principal component analysis (PCA). The most readily obtained charge state for CS/DS GAGs corresponds to the number of repeat units, for a mono-sulfated disaccharide repeat. In the examined tetrasaccharides, the  $[M-2H]^{2-}$  precursor satisfies this condition. Based on earlier qualitative descriptions of product ion intensity differences between epimers, the selection of this charge state for additional statistical examination is further validated.

EDD activation of the  $[M-2H]^{2-}$  precursor for each epimer results in 34 assigned product ions. The application of PCA to replicate data sets for three binary mixtures is demonstrated in Figure 5.11. Separation of the pure components is obtained by the first principal component plotted as the abscissa. Replicates for each mixture are well

grouped, and the projection of the 50/50 mixture lies at approximately the mid-point of the plot. Similar to results in synthetic HS tetrasaccharides, this result is due to the

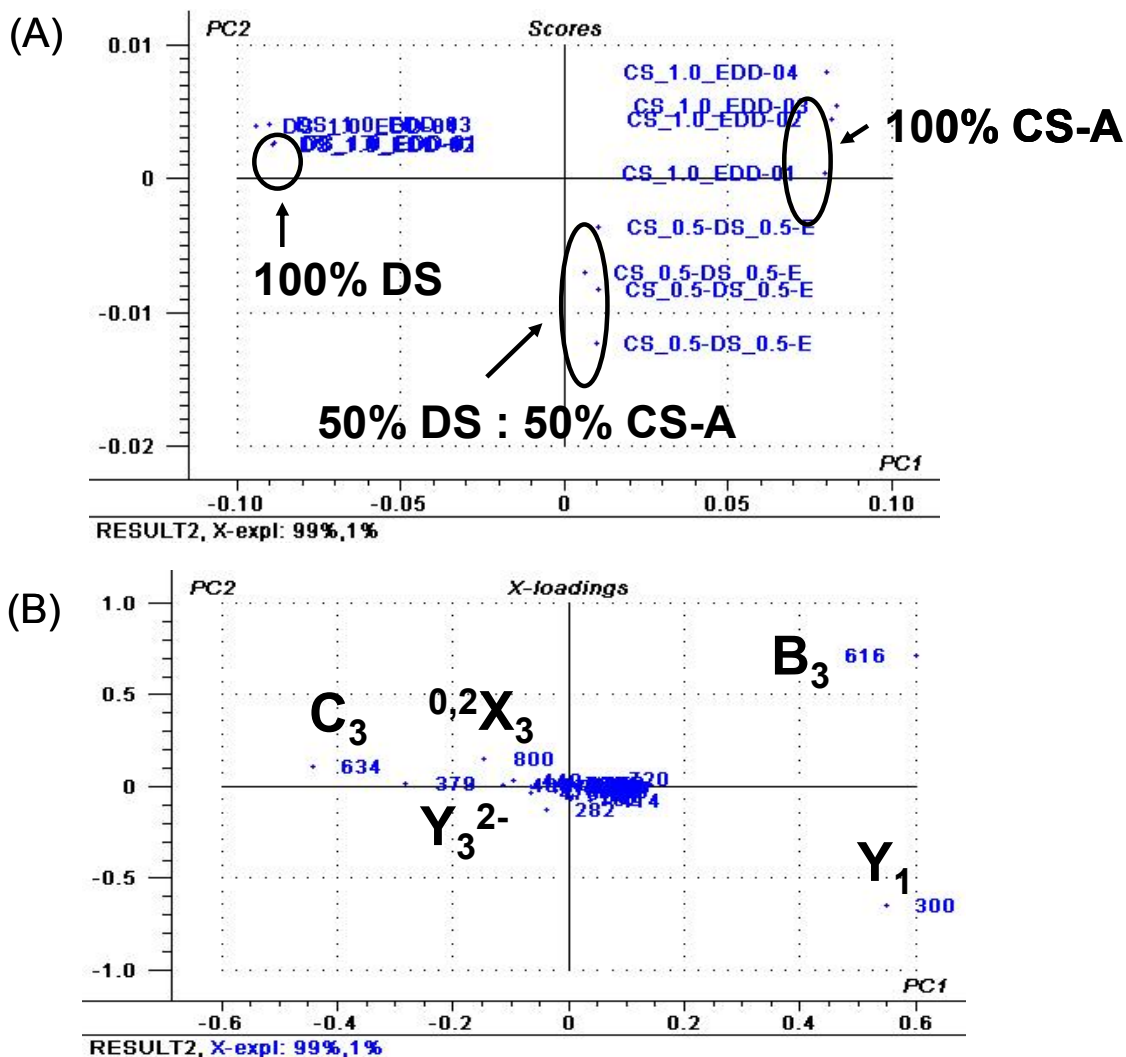


**Figure 5.11** PCA results for binary mixture analysis of the EDD product ions from the activation of the  $[M-2H]^{2-}$  precursor ion. The plot of PC2 vs PC1 is shown in (A) and the respective loadings values are shown in (B).

explanation of the majority of the data set variance by PC1 (99.13%). Examination of the loadings values allows for the assignment of component contributions to the separation. Similar to CID analysis, the  $Y_3^{2-}$  ion contributes highly to the separation. Interestingly, the singly deprotonated  $^{0,2}X_3^{1-}$  ion contributes more to the epimer distinction in EDD than the doubly deprotonated as in CID. Other significant loadings are the  $B_3$ ,  $C_3$ , and  $Y_1$  ions generated by glycosidic cleavage adjacent to the stereocenter. Although the losses of H from  $B_3$  and  $C_3$  resulting in the  $B_3'$  and  $C_3''$  ions are observed in CS glycoforms, these do not contribute to the statistical differentiation. For sake of comparison to threshold methods, the IRMPD activation of the  $[M-2H]^{2-}$  precursor was also performed. These spectra contained fewer assigned fragment ions (19), but PCA based differentiation was still possible. Shown in Figure 5.12, the first two principal components are plotted. Similar to results in EDD, PC1 results in an approximate binary mixture scale. Examination of the PC2 axis reveals a spread within each replicate group. This result is likely due to variation in the overlap between IR photons and the ion cloud as the ions undergo magnetron motion within the FT-ICR analyzer cell. Examination of the loading values for the PCA analysis of IRMPD spectra generates a similar list of product ions with high contributions, namely,  $Y_3^{2-}$ ,  $B_3$ , and  $Y_1$ , with additional contributions due to  $^{0,2}X_3^{2-}$ ,  $C_3$ , and  $Y_1$ . The negative loadings of the doubly deprotonated  $^{0,2}X_3$  and  $Y_3$  contribute to the separation of DS whereas  $Y_1$  and  $B_3$  denote CS-A. These results are consistent with the prior CID ion trap results based on peak intensity analysis and serve to validate the application of MVA methods to epimer characterization.

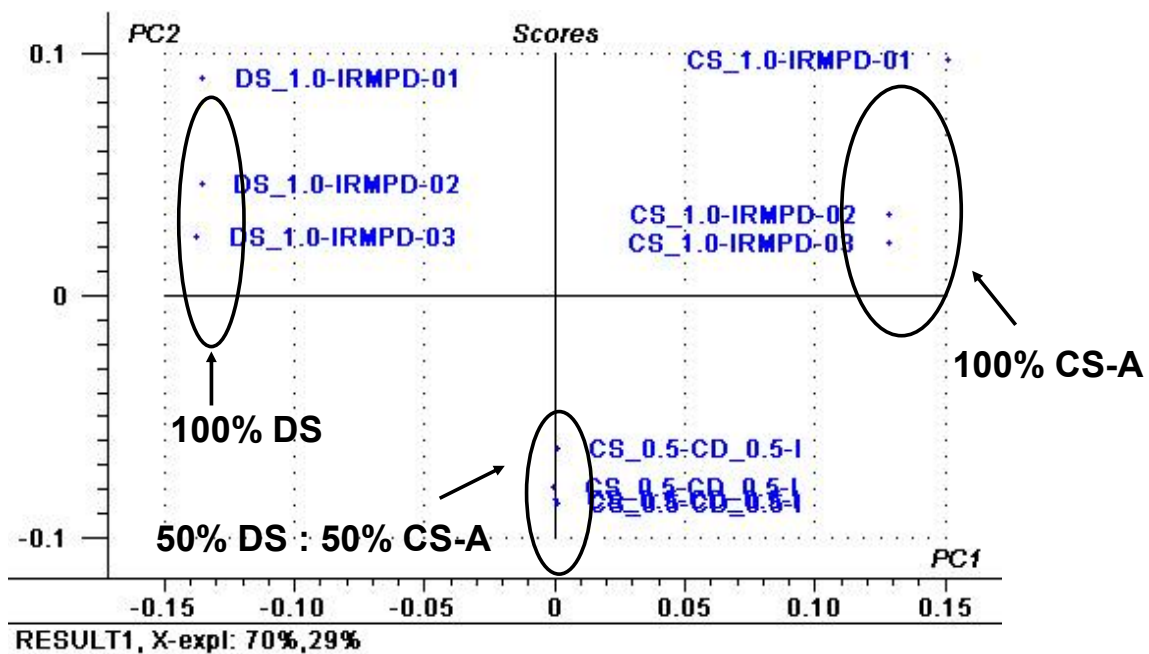


**Figure 5.12** PCA results for binary mixture analysis of the IRMPD product ions from the activation of the  $[M-2H]^{2-}$  precursor ion.

## CONCLUSIONS

Although CS and HS GAGs are structurally similar, the introduction of small stereochemical changes has a profound effect on the outcome of a tandem mass spectrometry experiment. Electron detachment dissociation (EDD) has previously shown dual utility in application to HS tetrasaccharides by providing increased cross-ring cleavage, which allows the location of the labile sulfate modification, and stereo-specific ions, which allows the identification of the hexuronic acid stereochemistry. When applied to CS glycoforms, the extent of cross-ring cleavage is diminished in comparison and the ability to differentiate GlcA from IdoA is not realized by a detachment-initiated

radical-mechanism. Instead, hexuronic stereochemistry can be inferred by the relative intensities of charge-conserved products due to electron excitation. Due to the reproducible nature of EDD spectra, the application of multivariate statistical methods can provide acidic stereochemical assignment and a quantitative measure in mixture analysis.

#### **ACKNOWLEDGEMENTS**

The authors gratefully acknowledge financial support from the National Institutes of Health grant #2R01-GM038060-16.

## REFERENCES

1. Fannon, M.; Forsten, K. E. and Nugent, M. A., Potentiation and Inhibition of bFGF Binding by Heparin: A Model for Regulation of Cellular Response. *Biochemistry* **2000**, *39*, 1434-1445.
2. Wu, Z. L.; Zhang, L.; Yabe, T.; Kuberan, B.; Beeler, D. L.; Love, A. and Rosenberg, R. D., The Involvement of Heparan Sulfate (HS) in FGF1/HS/FGFR1 Signaling Complex. *J. Biol. Chem.* **2003**, *278*, 17121-17129.
3. Lindahl, U.; Backstrom, G.; Hook, M.; Thunberg, L.; Fransson, L. A. and Linker, A., Structure of the antithrombin-binding site in heparin. *Proc. Natl. Acad. Sci. U. S. A.* **1979**, *76*, 3198-3202.
4. Chen, Y.; Maguire, T.; Hileman, R. E.; Fromm, J. R.; Esko, J. D.; Linhardt, R. J. and Marks, R. M., Dengue virus infectivity depends on envelope protein binding to target cell heparan sulfate. *Nature Med.* **1997**, *3*, 866-871.
5. Hoogewerf, A. J.; Kuschert, G. S. V.; Proudfoot, A. E. I.; Borlat, F.; Clark-Lewis, I.; Power, C. A. and Wells, T. N. C., Glycosaminoglycans Mediate Cell Surface Oligomerization of Chemokines. *Biochemistry* **1997**, *36*, 13570-13578.
6. Liu, D. F.; Shriver, Z.; Gi, Y. W.; Venkataraman, G. and Sasisekharan, R., Dynamic regulation of tumor growth and metastasis by heparan sulfate glycosaminoglycans. *Seminars in Thrombosis and Hemostasis* **2002**, *28*, 67-78.
7. Williams, R. K. and Straus, S. E., Specificity and affinity of binding of herpes simplex virus type 2 glycoprotein B to glycosaminoglycans. *J. Virol.* **1997**, *71*, 1375-1380.

8. Dai, Y.; Whittal, R. M.; Bridges, C. A.; Isogai, Y.; Hindsgaul, O. and Li, L., Matrix-assisted laser desorption ionization mass spectrometry for the analysis of monosulfated oligosaccharides. *Carbohydr. Res.* **1997**, *304*, 1-9.
9. Juhasz, P. and Biemann, K., Utility of non-covalent complexes in the matrix-assisted laser desorption ionization mass spectrometry of heparin-derived oligosaccharides. *Carbohydr. Res.* **1995**, *270*, 131-147.
10. Schiller, J.; Arnhold, J.; Benard, S.; Reichl, S. and Arnold, K., Cartilage degradation by hyaluronate lyase and chondroitin ABC lyase: a MALDI-TOF mass spectrometric study. *Carbohydr. Res.* **1999**, *318*, 116-122.
11. Takagaki, K.; Kojima, K.; Majima, M.; Nakamura, T.; Kato, I. and Endo, M., Ion-Spray Mass-Spectrometric Analysis of Glycosaminoglycan Oligosaccharides. *Glycoconjugate J.* **1992**, *9*, 174-179.
12. Reinhold, V. N.; Carr, S. A.; Green, B. N.; Petitou, M.; Choay, J. and Sinay, P., Structural characterization of sulfated glycosaminoglycans by fast atom bombardment mass spectrometry: application to heparin fragments prepared by chemical synthesis. *Carbohydr. Res.* **1987**, *161*, 305-313.
13. Lamb, D. J.; Wang, H. M.; Mallis, L. M. and Linhardt, R. J., Negative ion fast-atom bombardment tandem mass spectrometry to determine sulfate and linkage position in glycosaminoglycan-derived disaccharides. *J. Am. Soc. Mass Spectrom.* **1992**, *3*, 797-803.
14. Laremore, T. N.; Murugesan, S.; Park, T. J.; Avci, F. Y.; Zagorevski, D. V. and Linhardt, R. J., Matrix-assisted laser desorption/ionization mass spectrometric

- analysis of uncomplexed highly sulfated oligosaccharides using ionic liquid matrices. *Anal. Chem.* **2006**, *78*, 1774-1779.
15. Zaia, J. and Costello, C. E., Compositional Analysis of Glycosaminoglycans by Electrospray Mass Spectrometry. *Anal. Chem.* **2001**, *73*, 233-239.
  16. Zaia, J.; McClellan, J. E. and Costello, C. E., Tandem Mass Spectrometric Determination of the 4S/6S Sulfation Sequence in Chondroitin Sulfate Oligosaccharides. *Anal. Chem.* **2001**, *73*, 6030-6039.
  17. McClellan, J. E.; Costello, C. E.; O'Conno, P. B. and Zaia, J., Influence of Charge State on Product Ion Mass Spectra and the Determination of 4S/6S Sulfation Sequence of Chondroitin Sulfate Oligosaccharides. *Anal. Chem.* **2002**, *74*, 3760-3771.
  18. Zaia, J.; Li, X.-Q.; Chan, S.-Y. and Costello, C. E., Tandem mass spectrometric strategies for determination of sulfation positions and uronic acid epimerization in chondroitin sulfate oligosaccharides. *J. Am. Soc. Mass Spectrom.* **2003**, *14*, 1270-1281.
  19. Zaia, J. and Costello, C. E., Tandem Mass Spectrometry of Sulfated Heparin-Like Glycosaminoglycan Oligosaccharides. *Anal. Chem.* **2003**, *75*, 2445-2455.
  20. Saad, O. M. and Leary, J. A., Delineating mechanisms of dissociation for isomeric heparin disaccharides using isotope labeling and ion trap tandem mass spectrometry. *J. Am. Soc. Mass Spectrom.* **2004**, *15*, 1274-1286.
  21. Saad, O. M. and Leary, J. A., Heparin Sequencing Using Enzymatic Digestion and ESI-MS with HOST: A Heparin/HS Oligosaccharide Sequencing Tool. *Anal. Chem.* **2005**, *77*, 5902-5911.

22. Viseux, N.; de Hoffmann, E. and Domon, B., Structural Assignment of Permethylated Oligosaccharide Subunits Using Sequential Tandem Mass Spectrometry. *Anal. Chem.* **1998**, *70*, 4951-4959.
23. Cody, R. B. and Freiser, B. S., Collision-Induced Dissociation In A Fourier-Transform Mass-Spectrometer. *Int. J. Mass Spectrom. Ion Processes* **1982**, *41*, 199-204.
24. Little, D. P.; Speir, J. P.; Senko, M. W.; O'Connor, P. B. and McLafferty, F. W., Infrared Multiphoton Dissociation of Large Multiply Charged Ions for Biomolecule Sequencing. *Anal. Chem.* **1994**, *66*, 2809-2815.
25. Zubarev, R. A.; Kelleher, N. L. and McLafferty, F. W., Electron capture dissociation of multiply charged protein cations. A nonergodic process. *J. Am. Chem. Soc.* **1998**, *120*, 3265-3266.
26. Budnik, B. A.; Haselmann, K. F. and Zubarev, R. A., Electron detachment dissociation of peptide di-anions: an electron-hole recombination phenomenon. *Chem. Phys. Lett.* **2001**, *342*, 299-302.
27. Syka, J. E. P.; Coon, J. J.; Schroeder, M. J.; Shabanowitz, J. and Hunt, D. F., Peptide and protein sequence analysis by electron transfer dissociation mass spectrometry. *Proc. Natl. Acad. Sci. U. S. A.* **2004**, *101*, 9528-9533.
28. Herron, W. J.; Goeringer, D. E. and McLuckey, S. A., Gas-phase electron transfer reactions from multiply-charged anions to rare gas cations. *J. Am. Chem. Soc.* **1995**, *117*, 11555-11562.

29. Desaire, H. and Leary, J. A., Detection and quantification of the sulfated disaccharides in chondroitin sulfate by electrospray tandem mass spectrometry. *J. Am. Soc. Mass Spectrom.* **2000**, *11*, 916-920.
30. Desaire, H.; Sirich, T. L. and Leary, J. A., Evidence of Block and Randomly Sequenced Chondroitin Polysaccharides: Sequential Enzymatic Digestion and Quantification Using Ion Trap Tandem Mass Spectrometry. *Anal. Chem.* **2001**, *73*, 3513-3520.
31. Miller, M. J. C.; Costello, C. E.; Malmstrom, A. and Zaia, J., A tandem mass spectrometric approach to determination of chondroitin/dermatan sulfate oligosaccharide glycoforms. *Glycobiology* **2006**, *16*, 502-513.
32. Hitchcock, A. M.; Costello, C. E. and Zaia, J., Glycoform Quantification of Chondroitin/Dermatan Sulfate Using a Liquid Chromatography-Tandem Mass Spectrometry Platform. *Biochemistry* **2006**, *45*, 2350-2361.
33. Huang, R.; Pomin, V. H. and Sharp, J. S., LC-MS<sub>n</sub> Sequencing of Isomeric Chondroitin Sulfate Oligosaccharides Using a Chemical Derivatization Strategy. *Anal. Chem.* **In Review**,
34. Wolff, J. J.; Laremore, T. N.; Busch, A. M.; Linhardt, R. J. and Amster, I. J., Electron Detachment Dissociation of Dermatan Sulfate Oligosaccharides. *J. Am. Soc. Mass Spectrom.* **2008**, *19*, 294-304.
35. Wolff, J. J.; Laremore, T. N.; Aslam, H.; Linhardt, R. J. and Amster, I. J., Electron-Induced Dissociation of Glycosaminoglycan Tetrasaccharides. *J. Am. Soc. Mass Spectrom.* **2008**, *19*, 1449-1458.

36. Wolff, J. J.; Laremore, T. N.; Busch, A. M.; Linhardt, R. J. and Amster, I. J., Influence of Charge State and Sodium Cationization on the Electron Detachment Dissociation and Infrared Multiphoton Dissociation of Glycosaminoglycan Oligosaccharides. *J. Am. Soc. Mass Spectrom.* **2008**, *19*, 790-798.
37. Wolff, J. J.; Amster, I. J.; Chi, L. and Linhardt, R. J., Electron Detachment Dissociation of Glycosaminoglycan Tetrasaccharides. *J. Am. Soc. Mass Spectrom.* **2007**, *18*, 234-244.
38. Wolff, J. J.; Chi, L. L.; Linhardt, R. J. and Amster, I. J., Distinguishing glucuronic from iduronic acid in glycosaminoglycan tetrasaccharides by using electron detachment dissociation. *Anal. Chem.* **2007**, *79*, 2015-2022.
39. Wolff, J. J.; Leach, F. E.; Laremore, T. N.; Kaplan, D. A.; Easterling, M. L.; Linhardt, R. J. and Amster, I. J., Negative Electron Transfer Dissociation of Glycosaminoglycans. *Anal. Chem.* **2010**, *82*, 3460-3466.
40. Oh, H. B.; Leach III, F. E.; Arungundram, S.; Al-Mafraji, K.; Venot, A.; Boons, G.-J. and Amster, I. J., Multivariate Analysis of Electron Detachment Dissociation Mass Spectra for Synthetic Heparan Sulfate Tetrasaccharides Differing Only in Hexuronic Acid Stereochemistry. *Accepted to J. Am. Soc. Mass Spectrom.* **2010**,
41. Pervin, A.; Gallo, C.; Jandik, K. A.; Han, X.-J. and Linhardt, R. J., Preparation and structural characterization of large heparin-derived oligosaccharides. *Glycobiology* **1995**, *5*, 83-95.
42. Munoz, E.; Xu, D.; Avci, F.; Kemp, M.; Liu, J. and Linhardt, R. J., Enzymatic synthesis of heparin related polysaccharides on sensor chips: Rapid screening of

- heparin-protein interactions. *Biochem. Biophys. Res. Commun.* **2006**, 339, 597-602.
43. Nagasawa, K.; Inoue, Y. and Kamata, T., Solvolytic desulfation of glycosaminoglycuronan sulfates with dimethyl sulfoxide containing water or methanol. *Carbohydr. Res.* **1977**, 58, 47-55.
44. Heck, A. J. R.; de Koning, L. J.; Pinkse, F. A. and Nibbering, N. M. M., Mass-specific selection of ions in Fourier-transform ion cyclotron resonance mass spectrometry. Unintentional off-resonance cyclotron excitation of selected ions. *Rapid Commun. Mass Spectrom.* **1991**, 5, 406-414.
45. Ceroni, A.; Maass, K.; Geyer, H.; Geyer, R.; Dell, A. and Haslam, S. M., GlycoWorkbench: A Tool for the Computer-Assisted Annotation of Mass Spectra of Glycans. *Journal of Proteome Research* **2008**, 7, 1650-1659.
46. Domon, B. and Costello, C. E., A systematic nomenclature for carbohydrate fragmentations in FAB-MS/MS spectra of glycoconjugates. *Glycoconjugate J.* **1988**, 5, 397-409.
47. Wolff, J. J.; Chi, L.; Linhardt, R. J. and Amster, I. J., Distinguishing Glucuronic from Iduronic Acid in Glycosaminoglycan Tetrasaccharides by Using Electron Detachment Dissociation. *Anal. Chem.* **2007**, 79, 2015-2022.
48. Zaia, J.; Miller, M. J. C.; Seymour, J. L. and Costello, C. E., The Role of Mobile Protons in Negative Ion CID of Oligosaccharides. *J. Am. Soc. Mass Spectrom.* **2007**, 18, 952-960.
49. Zaia, J., Principles of Mass Spectrometry of Glycosaminoglycans. *Journal of Biomolecular Mass Spectrometry* **2005**, 1, 3-36.

## CHAPTER 6

### ELECTRON DETACHMENT DISSOCIATION AND INFRARED MULTIPHOTON DISSOCIATION OF HEPARIN TETRASACCHARIDES<sup>1</sup>

---

<sup>1</sup> Leach III, F.E., Xiao, Z., Ly, M., Laremore, T.N., Linhardt, R.J., and I.J. Amster. To be submitted to *International Journal of Mass Spectrometry*.

## **ABSTRACT**

Heparin glycosaminoglycans present the most difficult glycoform for analytical characterization due to high levels of sulfation and heterogeneity. Recent contamination of the clinical heparin supply and subsequent fatalities has highlighted the need of sensitive methodologies for analysis. In the last decade, tandem mass spectrometry has been increasingly applied for the analysis of GAGs, but developments in the characterization of highly sulfated compounds have been minimal due to the low number of cross-ring cleavages generated by threshold ion activation by collisional induced dissociation (CID). In the current work, electron detachment dissociation (EDD) and infrared multiphoton dissociation (IRMPD) are applied to a series of heparin tetrasaccharides. In both activation techniques, abundant glycosidic and cross-ring cleavages are observed.

## INTRODUCTION

The analytical characterization of sulfated glycosaminoglycan (GAG) carbohydrates has remained topical. Sulfated GAGs are linear, acidic biopolymers that are synthesized on a non-template basis. This mechanism results in high polydispersivity in natural samples and presents a challenging system for analytical characterization. Of the established glycoform classes, the heparin and heparan sulfates are the most diverse, demonstrating high variability in sites of O-sulfation, N-sulfation or –acetylation, and hexuronic acid stereochemistry. Specifically, heparin poses a daunting challenge by direct analysis due to high molecular weight ( $M_w$ : range 5 kDa - 40kDa, average 15 kDa) [1] and polydispersivity has continued for nearly 100 years, starting with its discovery in 1916 . Heparin is known to interact with a variety of proteins [1] through domains containing sequence motifs such as the pentasaccharide sequence for heparin binding to antithrombin III [2, 3].

The characterization of heparin is of vital importance due to clinical applications where it is employed for anticoagulant activity by inhibition of serine proteases in the blood coagulation cascade [1]. Recently, the heparin market suffered high levels of contamination, resulting in several fatalities. The source of the contaminant was traced to a highly sulfated chondroitin oligomer that was not differentiated by the current quality control protocol [4]. In light of this event, sensitive methods are needed to determine any impurities within a sample lot. The purification of heparin oligosaccharides and subsequent characterization by 2-D NMR has been applied to heparin dp2-40 [5]. NMR has also been shown to differentiate heparin from over-sulfated chondroitin during the previously described contamination event based on unique signals generated by the N-

acetyl group found in chondroitin [4]. Historically, the characterization of heparin has been conducted at the oligosaccharide level by preparation with heparin lyases [6] and separation by liquid chromatography [7, 8] or capillary zone electrophoresis [9].

Mass spectrometry based analysis has followed these methods and have eliminated the need for chemical modification of the sample, a common preliminary step for separation. Both MALDI-MS [10] and ESI-MS<sup>n</sup> [11-16] methods have been developed. MALDI-MS in combination with enzymology has presented a powerful approach for sequencing due to the charge-deconvoluted nature of MALDI and sensitivity (~ fmol), but requires the non-covalent complexation with a peptide to ionize in positive ion mode [10, 17, 18]. ESI-MS approaches have provided the ability to ionize heparin and heparin-like GAGs (HLGAGs) directly into the negative ion mode, producing high charge states while retaining the labile sulfate groups. Ion traps have largely been employed for these efforts to conduct CID-MS<sup>n</sup> and oligomer lengths have varied from di- to octasaccharide with a combination of enzymatic steps [11-16].

Several difficulties exist in the MS-based analysis of highly sulfated GAG oligomers. The first is the polydisperse nature of GAGs, which results in a complex mixture of oligomer lengths and sulfation states, but can be resolved by chromatographic methods before ionization. The second is MS-level heterogeneity due to Na/H exchange [19], which results in the division of a single GAG chain into many mass channels. This effect is especially pronounced in highly sulfated GAGs such as heparin where Na exchange states can match the number of sulfates for a given charge state. Lastly, it is difficult to ionize all of the sulfates on a given oligosaccharide due to multiple charges existing on a given residue. It is well known in the ESI-MS of GAGs that all sulfate

groups should be ionized and/or paired with a metal counter ion to reduce the facile loss of the modification as  $\text{SO}_3$  through H-rearrangement [20]. Therefore, the ESI solvent conditions should be adjusted such that Na exchange can occur at an acceptable level to produce a suitable precursor ion yet not to the point of reducing the ionization efficiency.

Tandem mass spectrometry can be employed to locate the sites of sulfation in HLGAGs, but difficulty arises when assignment of the hexuronic acid stereochemistry is needed. Previously, electron detachment dissociation (EDD) [21] has demonstrated a duality in GAG ion activation [22] where sites of sulfation and hexuronic acid stereochemistry could be determined during a single tandem mass spectrometry experiment when applied to heparan sulfate tetrasaccharides [23]. This provision becomes increasingly difficult as the sulfate density increases as the ionized sites will preferentially exist at a sulfate than a carboxylate due to pKa and the proposed mechanism for the generation of stereo-specific products by EDD is based on detachment from a carboxylate. Fortunately, a correlation between 2-O-sulfation and hexuronic acid stereochemistry has been demonstrated that can assist in the stereochemical assignment [24]. Although heparin may contain either IdoA or GlcA, the dominant disaccharide repeat unit is (IdoA2S-GlcNS6S). The IdoA constituents, to date, are always found as 2-O-sulfated whereas the GlcA residues are unsulfated [24]. Knowledge of sample origin is critical though as the ability to biologically 2-O-sulfate GlcA residues in murine mastocytoma has been demonstrated, but not in porcine intestinal mucosa heparin [25].

The following work has extended the application of EDD and infrared multiphoton dissociation (IRMPD) in GAG oligosaccharides to heparin tetrasaccharides derived from porcine mucosa. The selection of a precursor ion for MS/MS activation

where all sulfates are ionized or paired with a metal counter ion minimizes the loss of sulfate groups as  $\text{SO}_3$  and subsequent fragmentation by either method is shown to provide sufficient provide ion suites for the assignment of sulfate position, except in the hexasulfated tetrasaccharide case (GlcNS6S-IdoA2S) where the question of 3-O- or 6-O-sulfation remains (although the occurrence of 3-O is low abundance when compared to 6-O, occurring at 1 in 50 GlcN residues [25]). Based on the knowledge of sample origin, hexuronic acid stereochemistry can be determined by the assignment of 2-O-sulfation from cross-ring cleavage product ions. Conversely, the absence of 2-O-sulfation cannot definitively assign GlcA as the occurrence of un-sulfated IdoA is approximately 10 % in heparin [25].

## **EXPERIMENTAL METHODS**

### *Heparin Oligosaccharide Preparation*

Heparin sodium salt was obtained from porcine intestinal mucosa (Celsus Laboratories, Cincinnati, OH). Recombinant heparinase 1 (E.C. 4.2.2.7) from *F. heparinum* and expressed in *Escherichia coli* was used to partially depolymerize heparin sodium salt (6g) to 30% completion by ultraviolet absorbance and quenched in a water 100°C water bath. The reaction mixture was concentrated on a rotary evaporator and filtered through a 0.22  $\mu\text{m}$  filter prior to loading on a 1.5 m x 5.0 cm Bio-Gel P10 (BioRad, Hercules, CA) column. The column eluted at 1.2 mL/min using 0.2 M NaCl in distilled water to obtain uniform-sized oligosaccharides. After desalting separate peaks on a 100 cm x 2.0 cm P2 (BioRad, Hercules, CA) column, samples were concentrated and lyophilized. Fractionated samples were then separated on a 2.0 x 25  $\text{cm}^2$  semi-

preparative strong anion exchange (SAX) high performance liquid chromatography (HPLC) (Shimadzu, Kyoto, Japan) column (Waters Spherisorb S5, Milford, MA) eluted with a salt gradient over 60 mins at a flow rate of 4.0 mL/min with absorbance detection at 232 nm [5]. Repurification was carried out for some fractions according to whether or not they were considered impure by analytical SAX-HPLC on a 5  $\mu\text{m}$  Spherisorb -46 x 25  $\text{cm}^2$  analytical column. Each of the oligosaccharides were prepared from HPLC determined to be >95% pure by analytical SAX-HPLC, PAGE analysis, RPIP-HPLC-ESI-MS, high resolution MS, and 1D and 2D NMR [24].

#### *Mass Spectrometry Analysis*

Experiments were performed with a 9.4 T Bruker Apex Ultra QeFTMS (Billerica, MA) fitted with an MTP dual ion source, 25 W CO<sub>2</sub> laser (Synrad model J48-2, Mukilteo, WA) for IRMPD, and an indirectly heated hollow cathode (HeatWave, Watsonville, CA) to generate electrons for EDD. The sample solutions were infused at a rate of 120  $\mu\text{L}/\text{hour}$  and ionized by electrospray using a metal capillary (Agilent Technologies, Santa Clara, CA, #G2427A) or at 10  $\mu\text{L}/\text{hour}$  and ionized by nanospray (pulled fused silica tip model FS360-75-15-D-20; New Objective, Woburn, MA, USA). Based on the extent of sulfation and desired charge state or degree of sodiation, the ESI solvent was varied. Solutions of each di-sulfated oligosaccharide were introduced at a concentration of 0.1 mg/mL in 50:50:0.1 methanol:H<sub>2</sub>O:FA (Sigma, St. Louis, MO) to generate doubly deprotonated ions and 0.2 mg/mL in 50:50 methanol:H<sub>2</sub>O with 1% 100  $\mu\text{M}$  NaOH to generate triply deprotonated ions and sodium adduct ions. To achieve quadruply deprotonated precursor ions for the tetra-sulfated tetrasaccharides, 105 mM

sulfolane in acetonitrile was introduced to the ESI line via a line splitter [26]. A secondary syringe pump controlled the relative amount of sulfolane introduced to the ESI solvent. All HS oligosaccharides were examined in negative ion mode.

For EDD experiments, precursor ions were isolated in the external quadrupole and accumulated for 1-3 seconds in an rf only hexapole before injection into the FT-ICR MS cell. One or two quadrupole isolation/analyzer cell fills were utilized per scan. The selection of the precursor ion was further refined by using in-cell isolation with a coherent harmonic excitation frequency (CHEF) event [27]. For electron irradiation the cathode bias was set to -19 V. The extraction lens was set to  $-18.5 \pm 0.1$  V, and the cathode heater was set to 1.5 A. The precursor ions were then irradiated with electrons for 1 second. 24-36 acquisitions were signal averaged per mass spectrum. IRMPD was conducted with a 25 W CO<sub>2</sub> laser (Synrad model J48-2, Mukilteo, WA). Ions were irradiated for 0.025 s to 0.075 s at 65 % laser attenuation.

For each mass spectrum, 1M points were acquired, padded with one zero fill, and apodized using a sinebell window. Background spectra were acquired by leaving all parameters the same but setting the cathode bias to 0 V to ensure that no electrons reached the analyzer cell. External calibration of mass spectra produced mass accuracy of 5 ppm. Internal calibration was also performed using confidently assigned glycosidic bond cleavage products as internal calibrants, providing mass accuracy of <1 ppm. Due to the large number of low intensity products formed by EDD, only peaks with S/N > 10 are reported. Product ions were assigned using accurate mass measurement and Glycoworkbench [28]. All products are reported using the Wolff-Amster annotation [29] of the Domon and Costello nomenclature [30]. To account for additional sulfate loss

observed during analysis of highly sulfated GAGs, a filled circle has been added to the annotation to indicate a loss of 2 or more sulfates. In annotated spectra, charge states are assigned as 1<sup>-</sup> unless indicated otherwise.

## RESULTS AND DISCUSSION

Highly sulfated GAG oligosaccharides readily form ionic salts (e.g. sodium).

This chemistry introduces additional heterogeneity at the MS level shown in Figure 6.1.

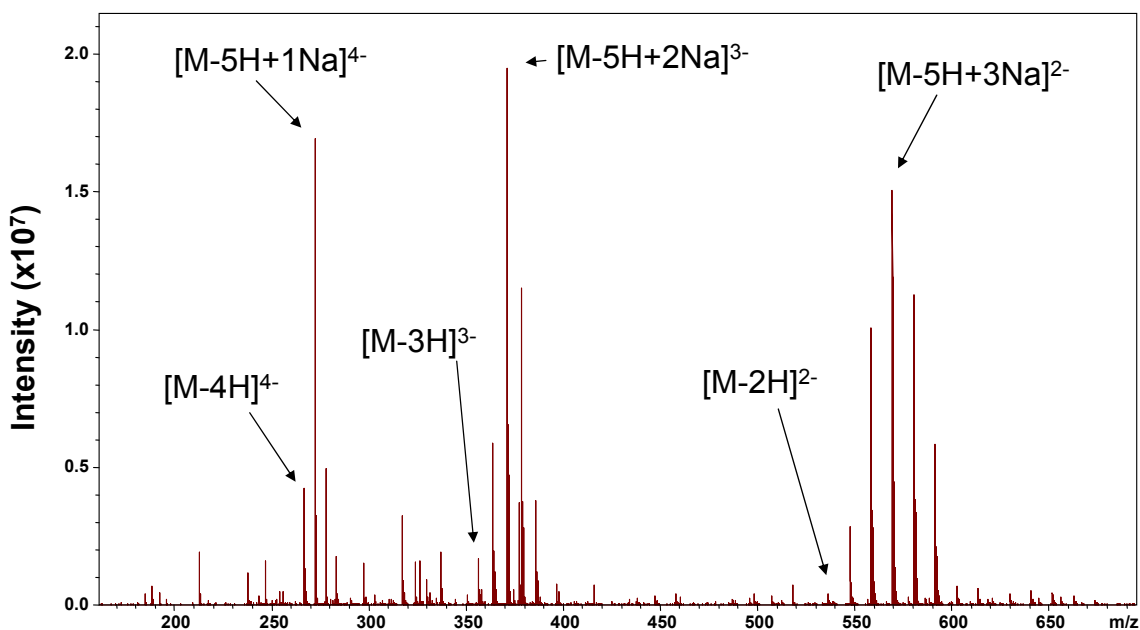


**FIGURE 6.1.** MS of the pentasulfated heparin tetrasaccharide, T1, demonstrating spectral heterogeneity due to charge state variation and sodium exchange.

In purified compounds, this splits the ion signal between many channels, reducing the precursor intensity in any one channel for tandem mass spectrometry. Sodium exchange can arise due to ESI line contamination as well as solvent introduction. The addition of

0.1 % formic acid has been shown to reduce this heterogeneity in CS glycoforms, but has limited success when applied to highly sulfated heparin or HS oligosaccharides.

Conveniently, the affinity for sodium is beneficial in that it enables the generation of precursor ions where the total number of ionized sites and metal counter-ions equals the number of sulfate groups. To shunt the loss of sulfate moieties, it is desirable to ionize all sulfates, but this is unfavorable when multiple sites of sulfation are present on one hexose ring due to charge repulsion; therefore the addition of sites of sodiation fulfills the initial criterion.

To readily convey this concept, the notion of an ionized sulfated criteria (ISC) is introduced. The ISC value of a GAG precursor is calculated by the difference in total sites of sulfation from the summed number of charges and sodium counter-ions. For example, a pentasulfated GAG ion with a charge state of 4 and 1 Na ion, would have an ISC of 0. Increasing the ISC to 1 would in theory place an ionized site on a carboxyl group and introduce the potential for EDD generated products that differentiate GlcA from IdoA. An ISC of  $< 1$  would leave a protonated sulfate moiety, increasing the potential for loss as  $\text{SO}_3$ . Due to charge repulsion effects and proton mobility in highly sulfated GAGs, it is difficult to preferentially locate the ionized site. In the current work, precursor ions will be selected to satisfy an ISC of 0 to minimize sulfate loss. In future work where sulfate densities are reduced, ISC values of 0 or greater will be selected.

*T1 ( $\Delta\text{UA}2\text{S-GlcNS}6\text{S-GlcA-GlcNS}6\text{S}$ )*

Based on the MS data presented in Figure 6.1, three potential precursors ions are available where the precursor ion satisfies the  $\text{ISC} = 0$ . The EDD activation of each

precursor state enables the evaluation of the degree of ionization/sodiation for highly sulfated tetrasaccharides. Additional threshold activation by IRMPD is made for comparison in certain cases.

The highest degree of ionization for a tetrasaccharide without introducing charge repulsion effects is achieved at 4<sup>-</sup>. With four ionized sites, it is hypothesized that an ionized site will exist on each hexose ring. For T1 containing five sulfates, the addition of one Na<sup>+</sup> ions satisfies the ISC = 0. The EDD of this precursor ion, [M-5H+1Na]<sup>4+</sup>, is shown in Figure 6.2. Abundant glycosidic and cross-ring bond cleavage products are observed, ranging in charge state from 1<sup>-</sup> to 4<sup>-</sup>. The masses of glycosidic bond cleavages can be utilized to deduce the location of sites of sulfation as follows: one on the non-reducing hexuronic acid, two on the central glucosamine, and two on the reducing end glucosamine.

The knowledge of sample origin in combination with an accurate mass measurement of the precursor ion can directly assign the positions of three sulfate groups. On hexuronic acid residues, only 2-O-sulfation is known to occur and the difference in precursor ion mass due to N-sulfo modification instead of N-acetylation assigns the second and third positions. The remaining two sites of sulfation cannot be assigned directly at the MS level, even though it is highly likely that 6-O-sulfation occurs on both glucosamine residues based on the known 1-4 glycosidic bond linkage in heparin oligosaccharides and rare occurrence of 3-O-sulfation. Cross-ring cleavage assignments can validate this hypothesis. The assignment of 6-O-sulfation on the reducing end glucosamine can be confirmed by the generation of the <sup>2,4</sup>X<sub>0</sub> cross-ring product as well as the <sup>3,5</sup>A<sub>4</sub> ion. The occurrence of 6-O-sulfation on the central glucosamine can be

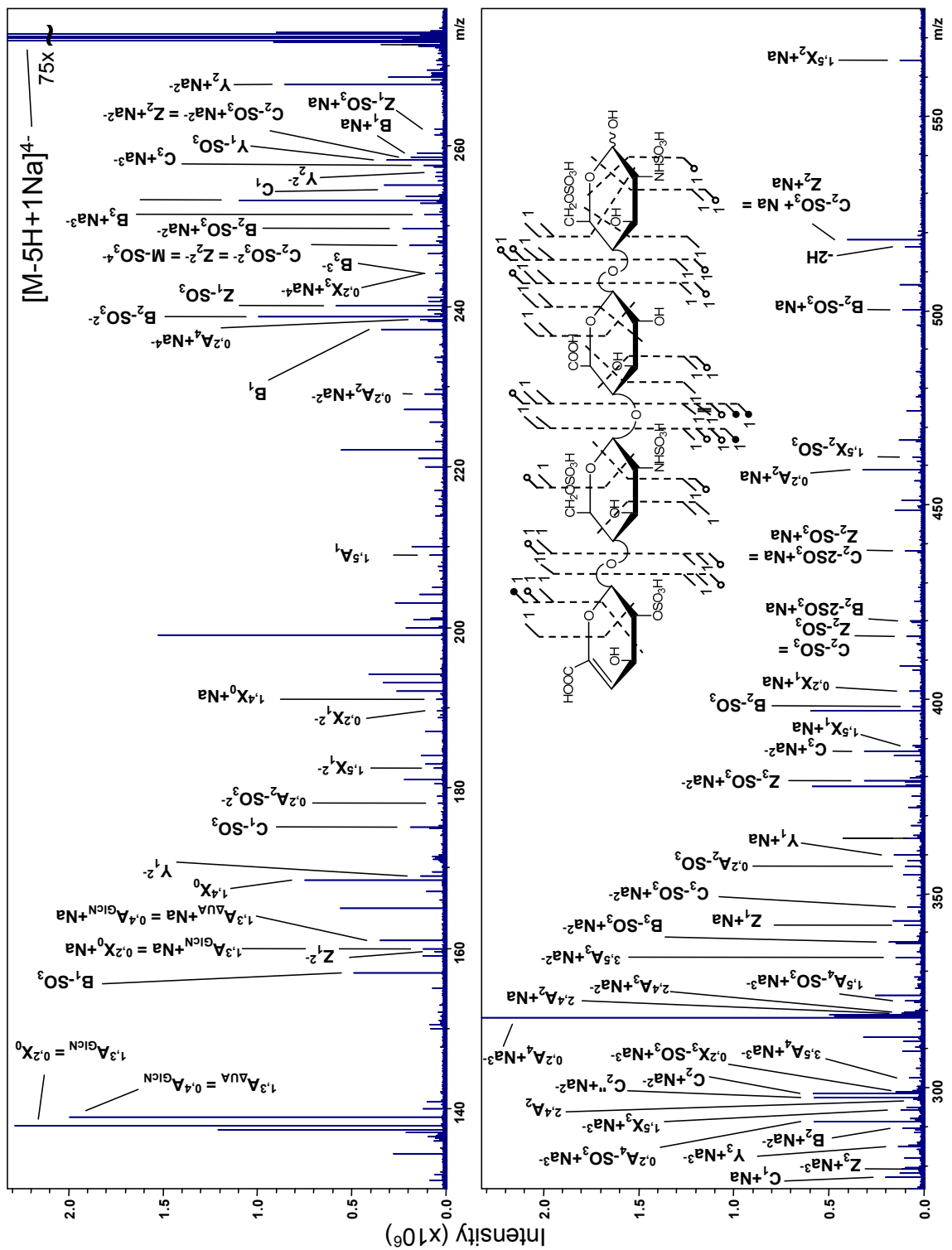
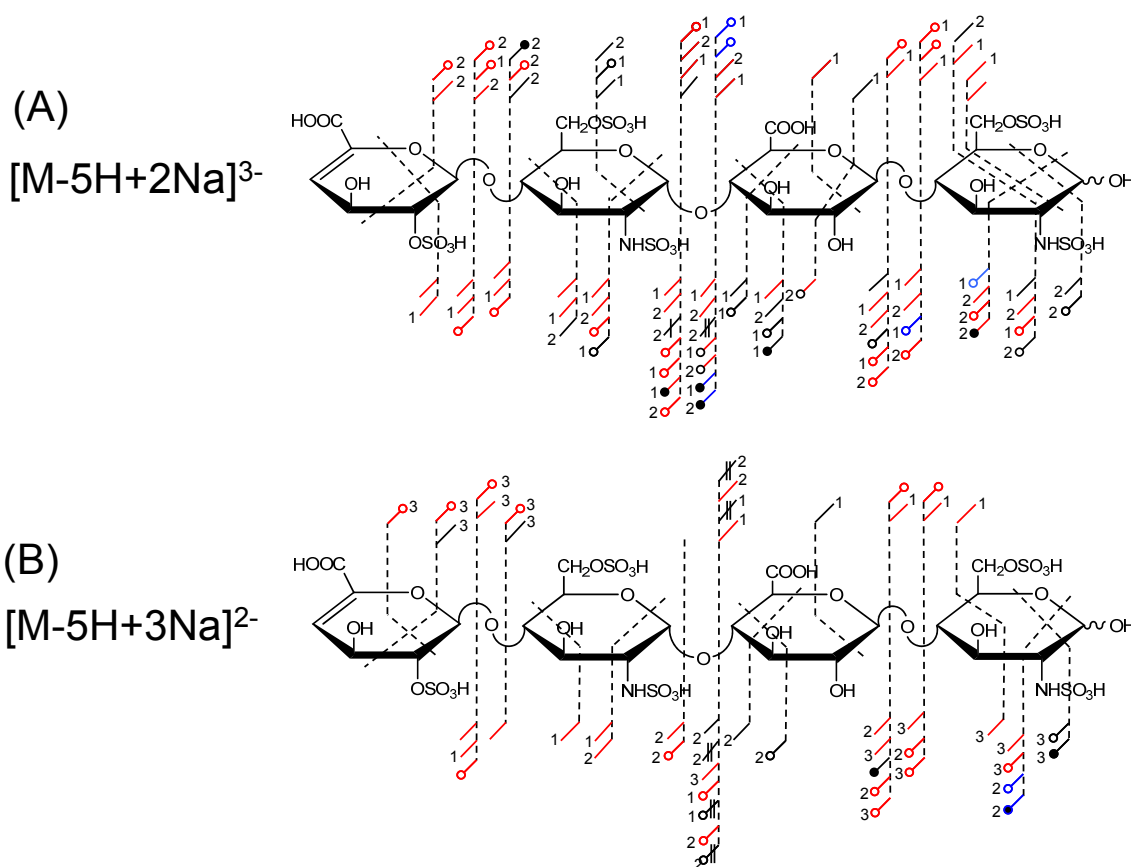


FIGURE 6.2 EDD spectrum of T1. Structural inset denotes the assigned product ions.

assigned by the difference in mass due to  $\text{SO}_3$  between the  $^{0,2}\text{A}_2$  and  $^{2,4}\text{A}_2$  cross-ring products.

As described previously, two other ions,  $[\text{M}-5\text{H}+2\text{Na}]^{3-}$  and  $[\text{M}-5\text{H}+3\text{Na}]^{2-}$  satisfy the  $\text{ISC} = 0$ . The annotated structures indicating both EDD and IRMPD fragmentation [31] for each precursor are shown in Figure 6.3. A precursory examination of both 6.3A and 6.3B reveal that EDD and IRMPD generate the previously denoted product ions



**FIGURE 6.3** Annotated structures denoting the assigned EDD and IRMPD product ions for the  $[\text{M}-5\text{H}+2\text{Na}]^{3-}$  AND  $[\text{M}-5\text{H}+3\text{Na}]^{2-}$  precursor ions of T1.

employed to assign the five sites of sulfation in T1. When the product ion sets are compared based on activation method, the majority of assigned products are observed in both EDD and IRMPD spectra (indicated by red) with additional cross-ring (<sup>1,5</sup>X and <sup>1,5</sup>A) and glycosidic bond cleavages with the loss of 1H or 2H present only in the EDD data set (black). This observation is consistent with prior results in DS GAGs where threshold activation products were shown to be a subset of EDD [31].

Consistent behavior is observed in Figure 6.3B for the  $[M-5H+3Na]^{2-}$  where both EDD and IRMPD can be employed independently to locate the five sites of sulfation, although the absolute number of cleavages is reduced when compared to the discussed 4<sup>-</sup> and 3<sup>-</sup> precursor ions. This decrease in observed fragmentation with increasing sodium exchange has been documented in both DS [29] and HS GAG oligosaccharides [32]. The addition of the Na<sup>+</sup> counter-ion reduces the number of sulfate loss fragments, but concurrently eliminates fragment ions that are presumably due to the presence of an ionized site.

#### *T2 (ΔUA2S-GlcNS6S-IdoA2S-GlcNS)*

Based on the evaluation of the observed decrease in product ions with increasing sodium exchange for T1, the  $[M-5H+1Na]^{4+}$  precursor ion was activated for T2. Both T1 and T2 are penta-sulfated, but T2 is sulfated on the IdoA residue and only N-sulfated on the reducing end (RE) glucosamine. This sulfation sequence is one sulfate group less than that of the typical heparin disaccharide repeat which will be examined in the following section. Depicted in Figure 6.4, are product ions assigned for EDD and/or IRMPD. Examination of the product ions generated by both activation methods reveals

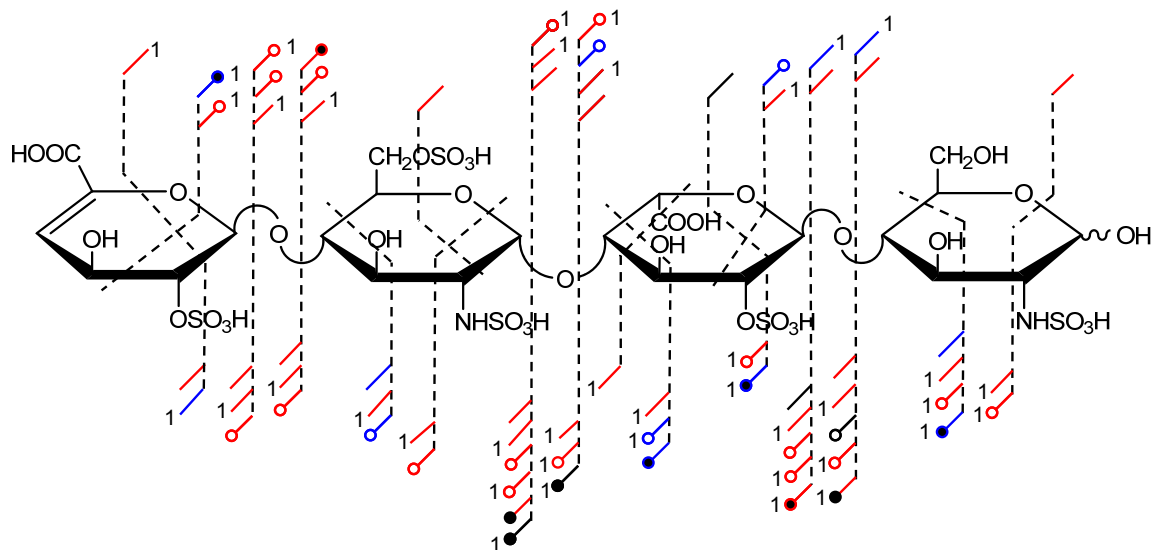


**FIGURE 6.4** Annotated structure indicating the assigned EDD and IRMPD products ions from the activation of the  $[M-5H+1Na]^{4-}$  precursor ion for T2.

that sufficient cleavages are generated to locate all of the sulfation sites by a combination of glycosidic and cross-ring cleavages by the reductive method utilized in the prior section. Although the loss of  $SO_3$  is observed in the majority of product ions, in only one case ( $^{0,2}X_3$ ) is the sulfate-intact ion not observed. Losses of 2 sulfate groups are largely observed from glycosidic bonds for both activation methods and only for IRMPD generated cross-ring cleavages.

### *T3 ( $\Delta UA2S$ -GlcNS6S-IdoA2S-GlcNS6S)*

The highest degree of sulfation examined to date by EDD and/or IRMPD is the tri-sulfated disaccharide repeat unit present in T3. This increase in sulfation introduced further heterogeneity at the MS level when compared to T1 or T2, but precursor ions still

exist where the  $ISC = 0$ . Shown in Figure 6.5 are the product ions assigned due to activation by both EDD and IRMPD of the  $[M-6H+2Na]^{4+}$  ion. Annotated spectra for the EDD of T3 is shown in Figure 6.6. Consistent with results in samples T1 and T2, the majority of product ions are consistent within both activation types.

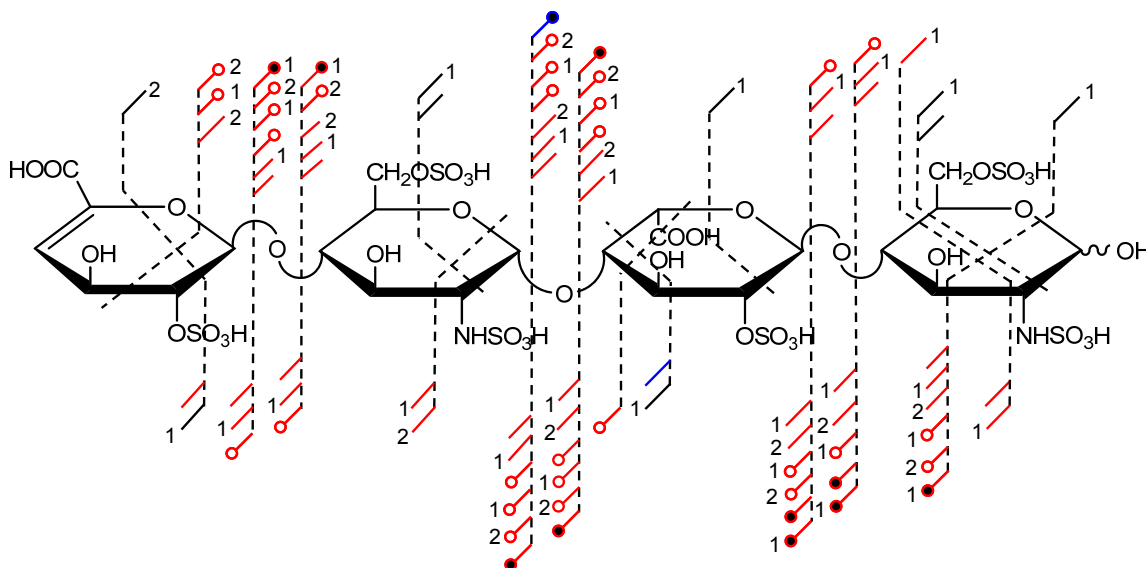


**FIGURE 6.5** Annotated structure indicating the assigned EDD and IRMPD products ions from the activation of the  $[M-6H+2Na]^{4+}$  precursor ion for T3.

Both IRMPD and EDD result in the cleavage of all glycosidic bonds. In either case, each glycosidic bond product ion is paired with at least one sulfate loss with the number increasing to two losses as the fragment length is increased. As described previously, as the number of sulfation sites increases for a given oligomer length, the possible structures decreases due to the finite number of O-sulfo possibilities. Analysis



of glycosidic bond cleavage products places 1 sulfate on each hexuronic acid and 2 sulfates on each glucosamine, which by accurate mass is known to be N-sulfo. Location of the O-sulfo group on the RE N-sulfo-glucosamine can be established by the occurrence of  $^{2,4}X_0$  in both EDD and IRMPD. Due to the lack of additional cross-ring cleavage on the central N-sulfo-glucosamine, the exact location to 6-O-sulfation cannot be determined by MS/MS, but is known due to complimentary NMR data. Subtle differences do exist between the two data sets, such as the occurrence of a  $^{1,5}X$  cleavage on each hexose ring in only EDD and additional losses of sulfates as  $SO_3$  in IRMPD.

#### *Envelope EDD*

In highly sulfated GAGs, separation of ion signal into distinct mass channels presents difficulty when combined with the low conversion efficiency of EDD. In an attempt to collect sufficient information to locate sites of sulfation from such a sample, an entire charge state envelope can be activated. An example of this method is demonstrated in Figure 6.7, where the 4 minus charge state distribution of Arixtra is isolated with a sufficiently large quadrupole window and subsequently activated by EDD. Even though no cross-ring cleavages are assigned, the generation of glycosidic bond cleavages in combination with accurate mass is sufficient to assign the positions of 6 of 8 sulfate groups along the pentasaccharide sequence. The only sites in question are the 6-O-sulfates.

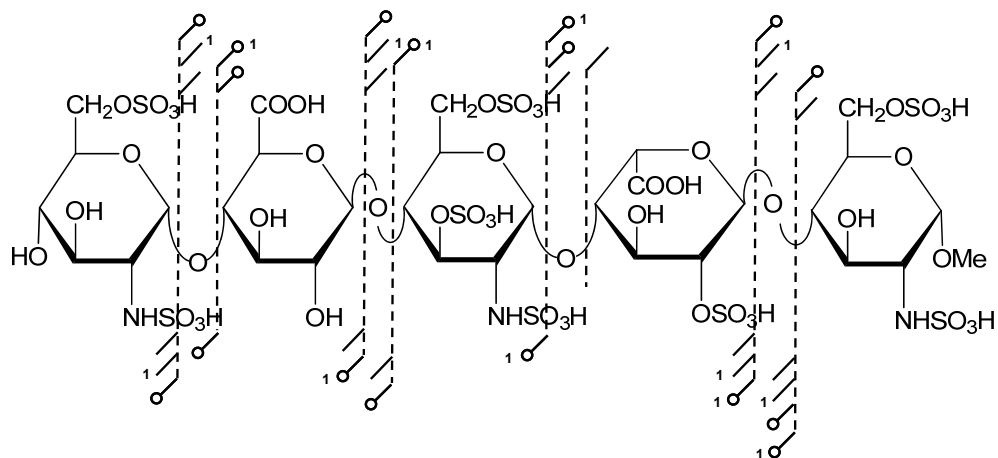


**FIGURE 6.7** Annotated structure indicating the product ions assigned during the irradiation of the 4<sup>-</sup> charge state distribution of Arixtra.

#### *Determination of Hexuronic Acid Stereochemistry*

In the examined tetrasaccharides, the ability of EDD to assign the hexuronic acid stereochemistry has not been fully realized. Due to the distribution of ion signal between many product ion channels, many are low intensity. The previous indicators of hexuronic acid stereochemistry, e.g. B<sub>3</sub>' , B<sub>3</sub>'-CO<sub>2</sub>, nor <sup>0,2</sup>A<sub>3</sub> are not assigned in T2 (GlcA) nor C<sub>3</sub>' in T1 or T3 (both containing IdoA). The EDD of a sufficiently desulfated precursor produced by solvolytic means may result in that determination [32], but insight can be achieved by known biology where 2-O-sulfation is known to only occur on iduronic acid residues [24]. The generation of sufficient cross-ring cleavage on hexuronic acid residues can lead to the assignment of 2-O-sulfation as shown in T1 and T3; therefore, in combination with the known biology, IdoA can be inferred.

### *Divalent Counter-ion Exchange*

The MS spectrum shown in Figure 6.1 demonstrates a high level of heterogeneity due to variations in charge state and sodium exchange. The cation exchange of  $\text{Ca}^{2+}$  for  $\text{Na}^+$ , displayed in Figure 6.8, reduces the separation of ion signal into unique mass channels from 15 to 4, therefore increasing the precursor signal available for MS/MS.

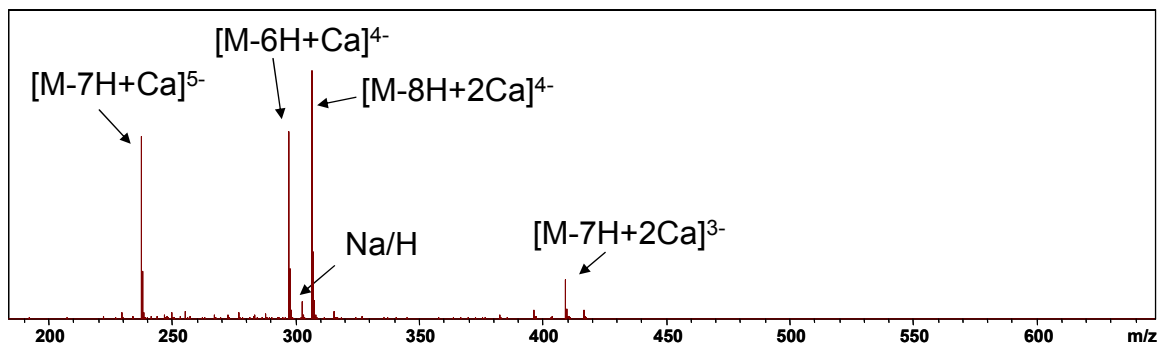


**FIGURE 6.8** MS spectrum of a heparin tetrasaccharide after cation exchange.

### **CONCLUSIONS**

The selection of the appropriate precursor ion for the tandem mass spectrometry of GAG oligosaccharides is critical to the generation of informative mass spectra. This case is especially true in highly sulfated GAGs such as heparin. To minimize sulfate loss as  $\text{SO}_3$  and maximize the number of product ions observed, the highest charge state should be selected with the minimal number of sodium counter-ions (if needed). Slight differences in the product ion distributions generated by EDD and IRMPD are observed, but both provide sufficient information to locate sites of sulfation. This result contradicts prior results in ion trap mass spectrometers where CID proved to generate minimal bond

cleavage in HLGAGs. Although previous detachment generated products are not observed, the combination of the knowledge of sulfate location and sample origin can be utilized to some extent to identify hexuronic acid stereochemistry.

## **ACKNOWLEDGEMENTS**

The authors gratefully acknowledge financial support from the National Institutes of Health grant #2R01-GM038060-16. FEL III personally acknowledges the University of Georgia Graduate School for funding from a Dissertation Completion Award.

## REFERENCES

1. Capila, I. and Linhardt, R. J., Heparin-Protein Interactions. *Angew. Chem. Intl. Ed.* **2002**, *41*, 390-412.
2. Lindahl, U.; Backstrom, G.; Hook, M.; Thunberg, L.; Fransson, L. A. and Linker, A., Structure of the antithrombin-binding site in heparin. *Proc. Natl. Acad. Sci. U. S. A.* **1979**, *76*, 3198-3202.
3. Lindahl, U.; Kusche-Gullberg, M. and Kjellen, L., Regulated Diversity of Heparan Sulfate. *J. Biol. Chem.* **1998**, *273*, 24979-24982.
4. Guerrini, M.; Beccati, D.; Shriver, Z.; Naggi, A.; Viswanathan, K.; Bisio, A.; Capila, I.; Lansing, J. C.; Guglieri, S.; Fraser, B.; Al-Hakim, A.; Gunay, N. S.; Zhang, Z.; Robinson, L.; Buhse, L.; Nasr, M.; Woodcock, J.; Langer, R.; Venkataraman, G.; Linhardt, R. J.; Casu, B.; Torri, G. and Sasisekharan, R., Oversulfated chondroitin sulfate is a contaminant in heparin associated with adverse clinical events. *Nat Biotech* **2008**, *26*, 669-675.
5. Pervin, A.; Gallo, C.; Jandik, K. A.; Han, X.-J. and Linhardt, R. J., Preparation and structural characterization of large heparin-derived oligosaccharides. *Glycobiology* **1995**, *5*, 83-95.
6. Lohse, D. L. and Linhardt, R. J., Purification and characterization of heparin lyases from *Flavobacterium heparinum*. *J. Biol. Chem.* **1992**, *267*, 24347-24355.
7. Bienkowski, M. J. and Conrad, H. E., Structural characterization of the oligosaccharides formed by depolymerization of heparin with nitrous acid. *J. Biol. Chem.* **1985**, *260*, 356-365.

8. Guo, Y. and Conrad, H. E., The disaccharide composition of heparins and heparan sulfates. *Anal. Biochem.* **1989**, *176*, 96-104.
9. Ampofo, S. A.; Wang, H. M. and Linhardt, R. J., Disaccharide compositional analysis of heparin and heparan sulfate using capillary zone electrophoresis. *Anal. Biochem.* **1991**, *199*, 249-255.
10. Venkataraman, G.; Shriver, Z.; Raman, R. and Sasisekharan, R., Sequencing Complex Polysaccharides. *Science* **1999**, *286*, 537-542.
11. Saad, O. M. and Leary, J. A., Compositional Analysis and Quantification of Heparin and Heparan Sulfate by Electrospray Ionization Ion Trap Mass Spectrometry. *Anal. Chem.* **2003**, *75*, 2985-2995.
12. Saad, O. M. and Leary, J. A., Delineating mechanisms of dissociation for isomeric heparin disaccharides using isotope labeling and ion trap tandem mass spectrometry. *J. Am. Soc. Mass Spectrom.* **2004**, *15*, 1274-1286.
13. Saad, O. M.; Ebel, H.; Uchimura, K.; Rosen, S. D.; Bertozzi, C. R. and Leary, J. A., Compositional profiling of heparin/heparan sulfate using mass spectrometry: assay for specificity of a novel extracellular human endosulfatase. *Glycobiology* **2005**, *15*, 818-826.
14. Saad, O. M. and Leary, J. A., Heparin Sequencing Using Enzymatic Digestion and ESI-MS with HOST: A Heparin/HS Oligosaccharide Sequencing Tool. *Anal. Chem.* **2005**, *77*, 5902-5911.
15. Sweeney, M. D.; Yu, Y. and Leary, J. A., Effects of Sulfate Position on Heparin Octasaccharide Binding to CCL2 Examined by Tandem Mass Spectrometry. *J. Am. Soc. Mass Spectrom.* **2006**, *17*, 1114-1119.

16. Zaia, J. and Costello, C. E., Tandem Mass Spectrometry of Sulfated Heparin-Like Glycosaminoglycan Oligosaccharides. *Anal. Chem.* **2003**, *75*, 2445-2455.
17. Juhasz, P. and Biemann, K., Mass spectrometric molecular-weight determination of highly acidic compounds of biological significance via their complexes with basic polypeptides. *Proc. Natl. Acad. Sci. U. S. A.* **1994**, *91*, 4333-4337.
18. Juhasz, P. and Biemann, K., Utility of non-covalent complexes in the matrix-assisted laser desorption ionization mass spectrometry of heparin-derived oligosaccharides. *Carbohydr. Res.* **1995**, *270*, 131-147.
19. Chi, L.; Wolff, J. J.; Laremore, T. N.; Restaino, O. F.; Xie, J.; Schiraldi, C.; Toida, T.; Amster, I. J. and Linhardt, R. J., Structural Analysis of Bikunin Glycosaminoglycan. *J. Am. Chem. Soc.* **2008**, *130*, 2617-2625.
20. Zaia, J., Principles of Mass Spectrometry of Glycosaminoglycans. *Journal of Biomolecular Mass Spectrometry* **2005**, *1*, 3-36.
21. Budnik, B. A.; Haselmann, K. F. and Zubarev, R. A., Electron detachment dissociation of peptide di-anions: an electron-hole recombination phenomenon. *Chem. Phys. Lett.* **2001**, *342*, 299-302.
22. Wolff, J. J.; Amster, I. J.; Chi, L. and Linhardt, R. J., Electron Detachment Dissociation of Glycosaminoglycan Tetrasaccharides. *J. Am. Soc. Mass Spectrom.* **2007**, *18*, 234-244.
23. Wolff, J. J.; Chi, L.; Linhardt, R. J. and Amster, I. J., Distinguishing Glucuronic from Iduronic Acid in Glycosaminoglycan Tetrasaccharides by Using Electron Detachment Dissociation. *Anal. Chem.* **2007**, *79*, 2015-2022.

24. Xiao, Z.; Zhao, W.; Yang, B.; Zhang, Z.; Guan, H. and Linhardt, R. J., Heparinase 1 selectivity for the 3,6-di-O-sulfo-2-deoxy-2-sulfamido- $\alpha$ -D-glucopyranose (1,4) 2-O-sulfo-  $\alpha$ -L-idopyranosyluronic acid (GlcNS3S6S-IdoA2S) linkages. *Glycobiology*
25. Kusche, M. and Lindahl, U., Biosynthesis of heparin. O-sulfation of D-glucuronic acid units. *J. Biol. Chem.* **1990**, 265, 15403-15409.
26. Huang, Y.; Shi, X.; Yin, H.; Killeen, K. and Zaia, J., Improvement of ESI Behavior of Heparan Sulfate Oligosaccharides by Using a Chip-based Pulsed Post-Column Makeup Flow for Online LC/MS, *58th ASMS Conference on Mass Spectrometry and Allied Topics*, Salt Lake City, UT, 2010.
27. Heck, A. J. R.; de Koning, L. J.; Pinkse, F. A. and Nibbering, N. M. M., Mass-specific selection of ions in Fourier-transform ion cyclotron resonance mass spectrometry. Unintentional off-resonance cyclotron excitation of selected ions. *Rapid Commun. Mass Spectrom.* **1991**, 5, 406-414.
28. Ceroni, A.; Maass, K.; Geyer, H.; Geyer, R.; Dell, A. and Haslam, S. M., GlycoWorkbench: A Tool for the Computer-Assisted Annotation of Mass Spectra of Glycans. *Journal of Proteome Research* **2008**, 7, 1650-1659.
29. Wolff, J. J.; Laremore, T. N.; Busch, A. M.; Linhardt, R. J. and Amster, I. J., Influence of Charge State and Sodium Cationization on the Electron Detachment Dissociation and Infrared Multiphoton Dissociation of Glycosaminoglycan Oligosaccharides. *J. Am. Soc. Mass Spectrom.* **2008**, 19, 790-798.

30. Domon, B. and Costello, C. E., A systematic nomenclature for carbohydrate fragmentations in FAB-MS/MS spectra of glycoconjugates. *Glycoconjugate J.* **1988**, *5*, 397-409.
31. Wolff, J. J.; Laremore, T. N.; Busch, A. M.; Linhardt, R. J. and Amster, I. J., Electron Detachment Dissociation of Dermatan Sulfate Oligosaccharides. *J. Am. Soc. Mass Spectrom.* **2008**, *19*, 294-304.
32. Leach III, F. E.; Oh, H. B.; Arungundram, S.; Al-Mafraji, K.; Venot, A.; Boons, G.-J. and Amster, I. J., Electron Detachment Dissociation of Synthetic Heparan Sulfate Tetrasaccharides Varying in Degree of Sulfation and Hexuronic Acid Stereochemistry. Manuscript in Preparation. **2011**.

## CHAPTER 7

# NEGATIVE ELECTRON TRANSFER DISSOCIATION FOURIER TRANSFORM MASS SPECTROMETRY OF GLYCOSAMINOGLYCAN OLIGOSACCHARIDES<sup>1</sup>

---

<sup>1</sup> Leach III, F.E., Wolff, J.J., Xiao, Z., Ly, M., Laremore, T.N., Arungundram, S., Al-Mafraji, K., Venot, A., Boons, G.-J., Linhardt, R.J., and I.J. Amster. To be submitted to *Journal of the American Society for Mass Spectrometry*.

## **ABSTRACT**

Electron transfer through gas phase ion-ion reactions has led to the widespread application of electron-based techniques once only capable in ion trapping mass spectrometers. Although any mass analyzer can in theory be coupled to an ion-ion reaction device (typically a 3-D ion trap), some systems of interest exceed the capabilities of most mass spectrometers. This case is particularly true in the structural characterization of glycosaminoglycan (GAG) oligosaccharides. To adequately characterize highly sulfated GAGs or oligosaccharides above the tetrasaccharide level, a high resolution mass analyzer is required. To extend previous efforts on an ion trap mass spectrometer, negative electron transfer dissociation (NETD) coupled with a Fourier transform ion cyclotron resonance (FT-ICR) mass spectrometer has been applied to increasingly sulfated heparan sulfate and heparin tetrasaccharides as well as a dermatan sulfate octasaccharide. Results similar to those obtained by electron detachment dissociation (EDD) are observed.

## INTRODUCTION

The implementation of ion-ion reactions for tandem mass spectrometry applications in commercial mass spectrometers has extended the ability to conduct electron-based ion activation to a variety of platforms through electron transfer dissociation (ETD) [1] and negative electron transfer dissociation (NETD) [2, 3]. Previously, the capabilities of electron capture dissociation (ECD) [4] and electron detachment dissociation (EDD) [5] were only possible in Fourier transform ion cyclotron resonance mass spectrometers (FT-ICR MS) [6] and enabled the generation of complementary cleavages to threshold activation and retention of labile modifications such as glycosylation [7], phosphorylation [8], and sulfation [9] during biomolecule sequencing efforts.

NETD has previously been demonstrated for glycosaminoglycan (GAG) oligosaccharide structural characterization in an ion trap mass spectrometer for tetrasaccharides with low levels of sulfation [10] and a detailed account of the development of anion specific electron transfer reactions can be found in that report. The ion trap has limited mass accuracy and resolving power and to extend the utility of NETD for GAG analysis to molecules of high sulfation or polymerization, which produce many products within a narrow mass range [11-14], it is necessary to employ a mass analyzer capable of increased resolving power, such as FT-ICR MS.

In combination with the high performance aspects of FT-ICR MS, NETD presents an attractive alternative to EDD where ion conversion efficiencies are fundamentally limited by the radial repulsion between a negative charged ion cloud and electron beam [15]. By monitoring the electron current entering the mass analyzer, the optimum value

for the electron extraction from the cathode can be achieved, but increasing the pulse duration results in an asymptotic return in the efficiency increase; therefore, EDD cannot be conducted efficiently at timescales shorter than  $\sim 1$  s and online coupling for the tandem mass spectrometry of chromatographically separated analytes where the peak window is on the order of milli-seconds is not feasible. The application of NETD is only limited by the generation of the reagent radical cation species and subsequent reaction coordinate. Although chemical ionization (CI) sources in electron transfer capable mass spectrometers can generate ions for both ETD and NETD, the generation of radical cations for NETD is much less efficient and presently NETD activation is on order of  $\sim 1$  s. Further instrumental developments are possible and should allow for the reaction times on the order of milli-seconds, similar to ECD and ETD.

The present work further extends the application of NETD for GAG sequencing into the regimes of high sulfation and polymerization. Although NETD presents a subset of the products generated by EDD with the other due to direct electronic excitation of the precursor ion [16, 17], the product ions generated by an electron-transfer initiated mechanism include glycosidic bond cleavages and cross-ring cleavages and produce remarkably similar spectra when compared to those generated by the EDD of the same precursor ion [10] while the coupling with the FT-ICR mass analyzer allows for the isotopic resolution and mass accuracy necessary to characterize more complex GAG tandem mass spectra.

## **EXPERIMENTAL METHODS**

### *Synthetic Heparan Sulfate Oligosaccharide Preparation*

Heparan sulfate tetrasaccharides were synthesized by a modular approach [18] and purified by silica gel column chromatography. Prepared structures were confirmed by  $^1\text{H}$  NMR and accurate mass measurement by FT-ICR MS. Compounds were prepared as tetrasaccharides with varying degrees and positions of sulfation as well as hexuronic acid stereochemistry.

#### *Preparation of Chondroitin Sulfate Oligosaccharides*

Chondroitin sulfate A (CS-A) and dermatan sulfate (DS) oligosaccharides were independently prepared by partial enzymatic depolymerization of bovine trachea chondroitin sulfate A (Celsus Laboratories, Cincinnati, OH) and porcine intestinal mucosa dermatan sulfate (Celsus Laboratories, Cincinnati, OH). A 20 mg/mL solution of each, in 50 mM Tris-HCl/60 mM sodium acetate buffer, pH 8 was incubated at 37°C with chondroitin ABC lyase from *Proteus vulgaris*, EC 4.2.2.4. (Seikagaku, Japan). After the absorbance at 232 nm indicated the digestion was 50% completed, the digestion mixture was heated at 100°C for 3 min. High-molecular-weight oligosaccharides and the enzyme were removed by ultra-filtration using a 5000 MWCO membrane. The resulting oligosaccharide mixture was concentrated by rotary evaporation and fractionated by low pressure GPC on a Bio-Gel P10 (Bio-Rad, Richmond, CA) column. Fractions containing oligosaccharides of interest were desalted by GPC on a Bio-Gel P2 column and freeze-dried [19]. Further purification was carried out using strong anion exchange high-pressure liquid chromatography (SAX-HPLC) on a semi-preparative SAX S5 Spherisorb column (Waters Corp, Milford, MA). The SAX-HPLC fractions containing > 90% of selected oligosaccharides were collected, desalted by GPC, and freeze-dried. The solid

was reconstituted in water and purified a second time by SAX-HPLC. Only the top 30% of the chromatographic peak was collected, desalted, and freeze-dried. Concentration of the oligosaccharide solutions was determined by measuring the absorbance at 232 nm ( $\epsilon = 3800 \text{ M}^{-1}\text{cm}^{-1}$ ). The resulting fractions containing individual oligosaccharides were characterized by PAGE, ESI-MS, and high-field nuclear magnetic resonance (NMR) spectroscopy [20].

#### *Heparin Oligosaccharide Preparation*

Heparin sodium salt was obtained from porcine intestinal mucosa (Celsus Laboratories, Cincinnati, OH). Recombinant heparinase 1 (E.C. 4.2.2.7) from *F. heparinum* and expressed in *Escherichia coli* was used to partially depolymerize heparin sodium salt (6g) to 30% completion by ultraviolet absorbance and quenched in a water 100°C water bath. The reaction mixture was concentrated on a rotary evaporator and filtered through a 0.22  $\mu\text{m}$  filter prior to loading on a 1.5 m x 5.0 cm Bio-Gel P10 (BioRad, Hercules, CA) column. The column eluted at 1.2 mL/min using 0.2 M NaCl in distilled water to obtain uniform-sized oligosaccharides. After desalting separate peaks on a 100 cm x 2.0 cm P2 (BioRad, Hercules, CA) column, samples were concentrated and lyophilized. Fractionated samples were then separated on a 2.0 x 25 cm<sup>2</sup> semi-preparative strong anion exchange (SAX) high performance liquid chromatography (HPLC) (Shimadzu, Kyoto, Japan) column (Waters Spherisorb S5, Milford, MA) eluted with a salt gradient over 60 mins at a flow rate of 4.0 mL/min with absorbance detection at 232 nm [19]. Repurification was carried out for some fractions according to whether or not they were considered impure by analytical SAX-HPLC on a 5  $\mu\text{m}$  Spherisorb -.46

x 25 cm<sup>2</sup> analytical column. Each of the oligosaccharides were prepared from HPLC determined to be >95% pure by analytical SAX-HPLC, PAGE analysis, RPIP-HPLC-ESI-MS, high resolution MS, and 1D and 2D NMR [21].

### *Mass Spectrometry Analysis*

Experiments were performed on a 12.0 T Bruker solariX FTMS instrument (Bruker Daltonics, Billerica, MA) fitted with an MTP dual ion source. The sample solutions were ionized by static nano-electrospray (pulled fused silica tip model FS360-75-15-D-20; New Objective, Woburn, MA, USA). Based on the extent of sulfation and desired charge state or degree of sodiation, the ESI solvent was varied. Solutions of each oligosaccharide were introduced at a concentration of 0.1 mg/mL in 50:50 acetonitrile:water (Sigma, St. Louis, MO). All oligosaccharides were examined in negative ion mode.

For NETD experiments, precursor ions were isolated in the external quadrupole and accumulated for 1-3 seconds in the 3-D ion trap before reaction with the reagent radical cation. The fluoranthene radical cation was generated in the CI source and accumulated for 500 -1000 ms prior to mass filtering and injection into the 3-D ion trap. Ion-ion reactions were conducted for 1.5 s. The precursor ion and NETD products were then injected into the mass analyzer through an rf-only ion guide. One analyzer cell fill was utilized per scan. 24-36 acquisitions were signal averaged per mass spectrum except for DS dp8 for which 100 scans were acquired. For each mass spectrum, 1M points were acquired, padded with one zero fill, and apodized using a sinebell window. Background spectra were acquired by leaving all parameters the same without the generation of the

radical cation. External calibration of mass spectra produced mass accuracy of 5 ppm. Internal calibration was also performed using confidently assigned glycosidic bond cleavage products as internal calibrants, providing mass accuracy of <1 ppm. Due to the large number of low intensity products formed by NETD, only peaks with S/N > 10 are reported. Product ions were assigned using accurate mass measurement and Glycoworkbench [22]. All products are reported using the Wolff-Amster annotation [12] of the Domon and Costello nomenclature [23]. In annotated spectra, charge states are assigned as 1<sup>-</sup> unless indicated otherwise.

## RESULTS AND DISCUSSION

Negative electron transfer dissociation (NETD) is proposed to encompass the low-energy radical based reaction pathway during EDD [10, 24]. As such, the loss of labile sulfate groups as SO<sub>3</sub> is observed in all examined cases and warrants explanation. This result may be due to a combination of several factors, both instrumental and GAG-specific. The instrumental induced loss of SO<sub>3</sub> may arise from the conditions of the 3-D ion trap generated from the hexapole collision cell. The pressure in this region is relatively high when compared to the mass analyzer (10<sup>-6</sup> torr vs 10<sup>-10</sup> torr). The increased frequency of collisions and DC potentials present before and after the rf-only conditions induced for the ion-ion reaction period could lead to low energy CID events. Alternatively, the high pressure conditions could also lead to the protonation of ionized sulfate groups which would result in the facile loss as SO<sub>3</sub> due to the known H-rearrangement mechanism [25]. The latter is more likely and supported by the observation of fragment ions containing more protonated sulfate groups than the original

precursor, a point that will be discussed during the NETD of dermatan sulfate (DS) dp8. A final possibility is the mobilization of acidic protons along the GAG oligomer. In all examined cases, the precursor ions correspond to instances where all sulfates are ionized or paired with a sodium counter ion, producing an ionized sulfate condition (ISC) of zero [13]. In the following analyses, increased cross-ring cleavage is observed on hexuronic acid residues. Based on pKa, the sulfate groups are ionized and carboxyl groups protonated in these precursor ions. To generate an ionized carboxyl and produce a site for electron transfer, it is necessary for the proton to mobilize [26] and migrate, therefore protonating the sulfate group and leading to the pathway for neutral loss as SO<sub>3</sub>. It is likely that a combination of the above pathways occurs and further mechanistic studies are warranted.

#### *HS1 (GlcA-GlcNAc6S-IdoA-GlcNAc6S)*

The NETD of lowly sulfated GAG tetrasaccharides (1 or less per disaccharide unit) has been reported [10] and the inclusion of data for the case of HS1 is performed for the sake of generating a sulfation gradient in the current work. Shown in Figure 7.1 is the NETD mass spectrum for the [M-2H]<sup>2-</sup> precursor of HS1. Consistent with results from GAG NETD in an ion trap, both the charge reduced precursor ([M-2H]<sup>\*-</sup>) and protonated precursor ([M-H]<sup>1-</sup>) are assigned [10], indicating both electron transfer and protonation events in the 3-D ion trap of the FTMS instrument. Abundant bond cleavage is observed, including glycosidic and cross-ring products, but not all glycosidic bond possibilities are present in the spectrum (B<sub>1</sub>, C<sub>1</sub>, and Z<sub>1</sub> are absent). The assignment of 6-O-sulfation on the central N-acetylglucosamine can be determined by the mass difference

between the  $^{1,4}X_2$  and  $^{1,5}X_2$  cross-ring cleavages, but is not possible on the reducing end due to only one cross-ring cleavage assignment. Cross-ring cleavages are located largely on the hexuronic acid residues, which indicates proton mobility and relocation of the ionized site from the sulfate groups to the carboxyl where electron transfer can occur. Interestingly, the  $^{0,2}A_3$  product ion that is indicative of GlcA in tetrasaccharides with no or one site of sulfation occurs in this IdoA containing compound through a solely radical-based ion fragmentation pathway. The occurrence of this ion in di-sulfated tetrasaccharides containing either GlcA or IdoA has been reported for the EDD of this epimer pair [14].

#### *HS2 (GlcA-GlcNAc6S-IdoA2S-GlcNAc6S)*

The addition of 2-O-sulfation to HS1 leads to HS2, increasing the sites of sulfation from two to three. Shown in Figure 7.2, is the NETD of the  $[M-3H]^{3-}$  precursor ion. Abundant fragmentation of the precursor is observed with highest densities of bond cleavage on the hexuronic acids. On the non-reducing end (NRE) terminus, five cross-ring cleavages are assigned and four on the central iduronic acid. Consistent with prior results during the NETD of GAGs [10], instances of both charge reduction by protonation and electron transfer are observed. From the HS2  $[M-3H]^{3-}$  precursor ion, two transfer events occur and produce the  $[M-3H]^{2*-}$  and  $[M-3H]^{*-}$  ions as well as the protonated  $[M-2H]^{2-}$  and  $[M-H]^{1-}$  ions. Losses of 1H and 2H are observed from both glycosidic and cross-ring bond cleavages.

NETD only provides the definitive assignment of two sites of sulfation in this case, the 2-O-sulfation on the central IdoA residue by the difference in mass of the  $^{0,2}A_3$

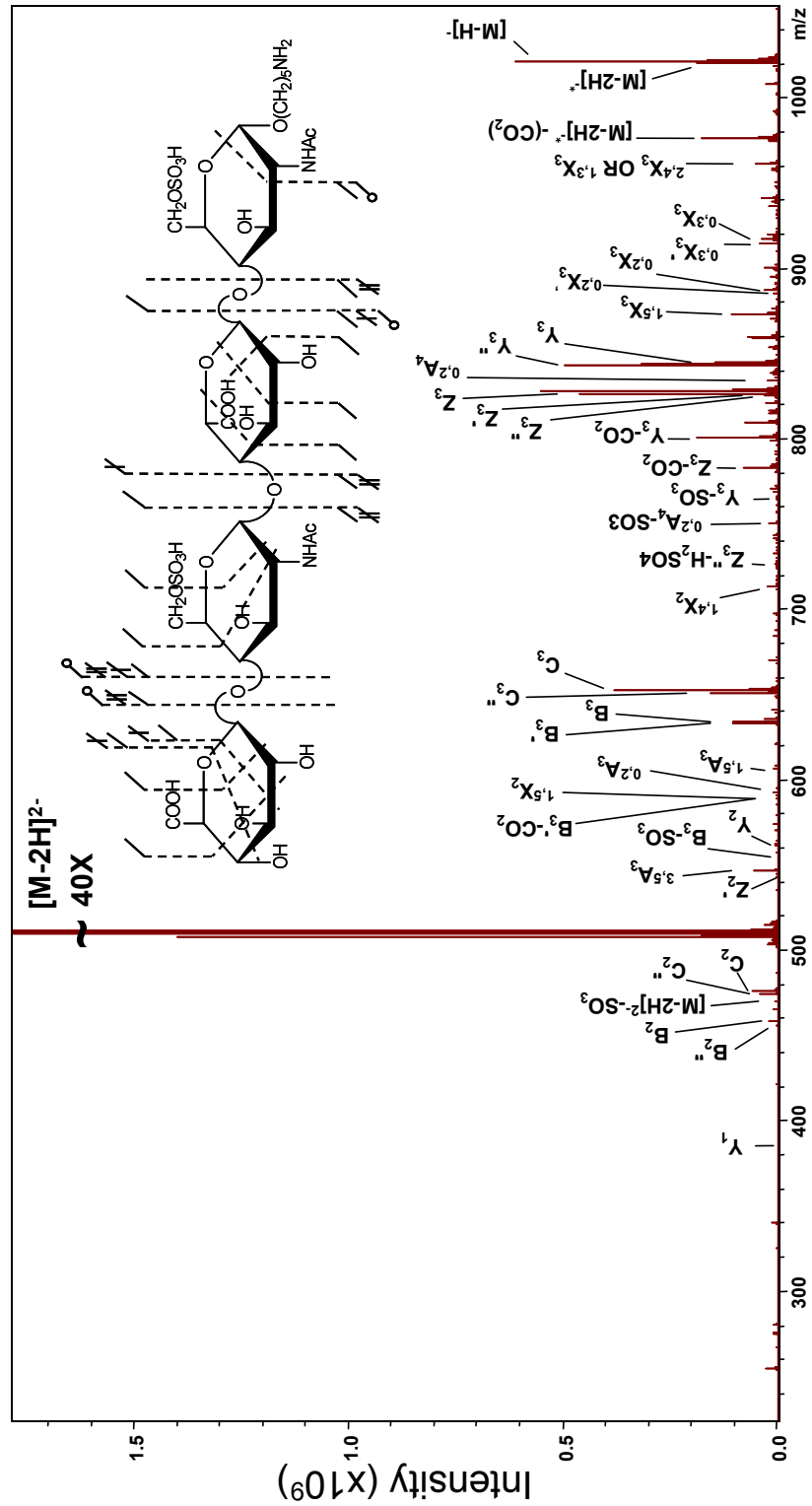


FIGURE 7.1 NETD of the  $[M-2H]^{2-}$  precursor ion for HS1.

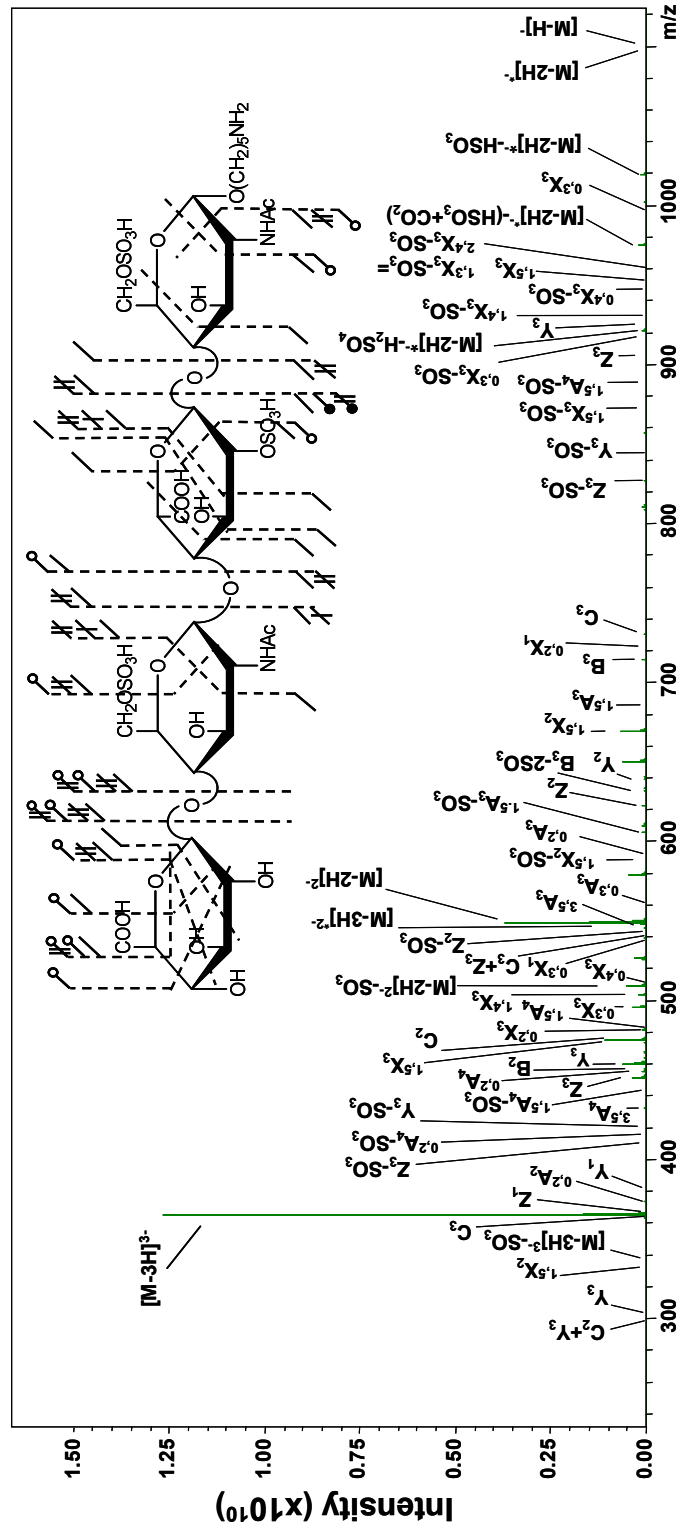
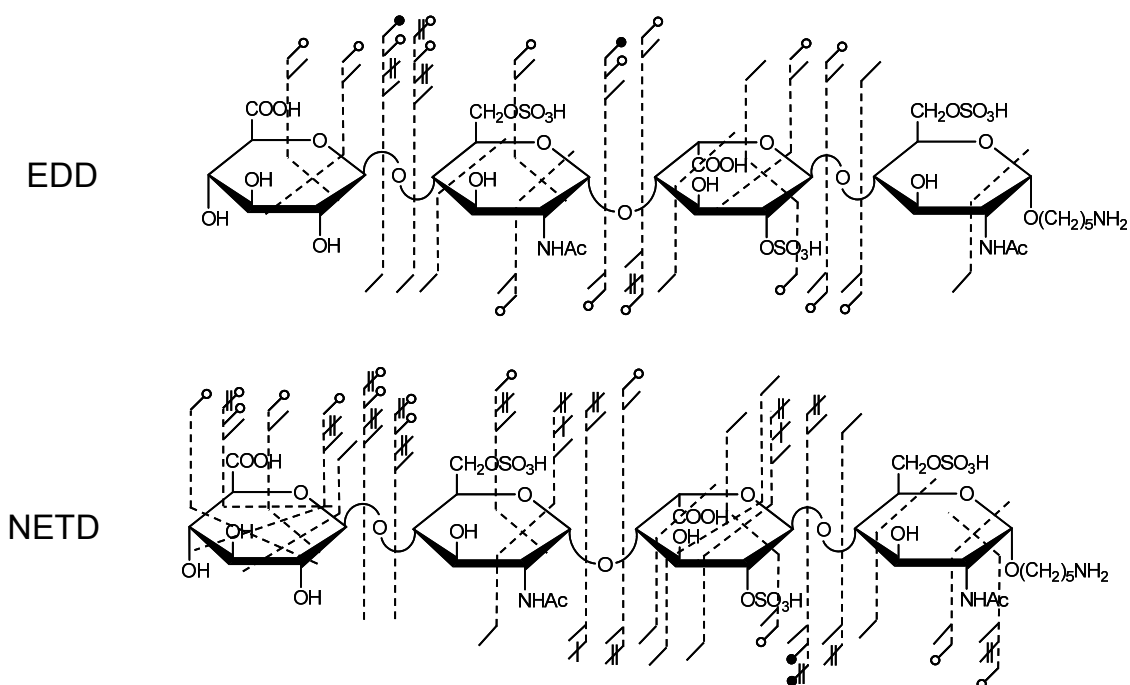


FIGURE 7.2 NETD of the  $[M-3H]^{3-}$  precursor ion for HS2.

and  $^{1,5}A_3$  ions and 6-O-sulfation of the reducing end (RE) N-acetylglucosamine by the difference in mass for the  $^{3,5}A_4$  and  $C_3$  ions. Insufficient cross-ring cleavages are generated on the central N-acetylglucosamine for definitive 6-O assignment. For comparison, the annotated structure for the EDD of the same precursor [14] is shown in Figure 7.3. EDD provides the ability to locate the 6-O-sulfation by the generation of the



**FIGURE 7.3** Comparison of the product ion distributions generated by EDD and NETD for HS2.

$^{3,5}A_2$  cross-ring cleavage, presumably by electronic excitation events, but does not provide the RE sulfate location. Although detachment processes occur during EDD, not all products from NETD are observed in the EDD fragmentation. This difference is especially true when the number of acidic residue cleavages is compared between the two activation methods, where EDD generates five total and NETD nine total.

### *H3 (ΔUA2S-GlcNS6S-IdoA2S-GlcNS6S)*

The most highly charged and sulfated GAG oligosaccharides belong to the heparin glycoform class. Due to the high charge density (2.7 ionized sites per disaccharide) [27], the precursor ions appear at low  $m/z$  (200-300) and products due to charge reduction span a range from approximately 150-550  $m/z$  during an MS/MS event, shown in Figure 7.4 for the NETD of the hexasulfated tetrasaccharide, H3. The mass accuracy and resolving power necessary to confidently assign the multiply-charged products of such an experiment is not foreseeable in an ion trap mass spectrometer and only available in an instrument such as an FT-ICR mass spectrometer.

The annotated tandem mass spectrum for the NETD of the  $[M-6H+2Na]^{4-}$  precursor is depicted in Figure 7.4. Due to the high peak density, a simple annotation has been employed to denote the cleavage type and loss of sulfate. Assigned product ions are annotated with the letter of the cleavage type, e.g. A for  $^{0,2}A_3$  and a circled letter is indicative of the loss of sulfate from a product ion. A supplemental list including peak assignments and  $m/z$  values is included in Appendix D. Product ions are assigned that correspond to cleavage of all glycosidic bonds. Losses of sulfate are observed for all glycosidic bond product ions except  $C_1$  and  $Z_2$ . Compared to the distribution of cross-ring cleavage product ions in heparan sulfate tetrasaccharides with lower sulfation, the cross-ring products are more uniform across the length of the oligomer. The coverage of cross-ring cleavages allows for the assignment of all six sites of sulfation. In contrast to the EDD of the same precursor ion, only five sites could be definitively assigned [13]. As seen in Figure 7.4, the NETD of H3 also includes the neutral losses of  $SO_3$ ,  $CO_2$ ,

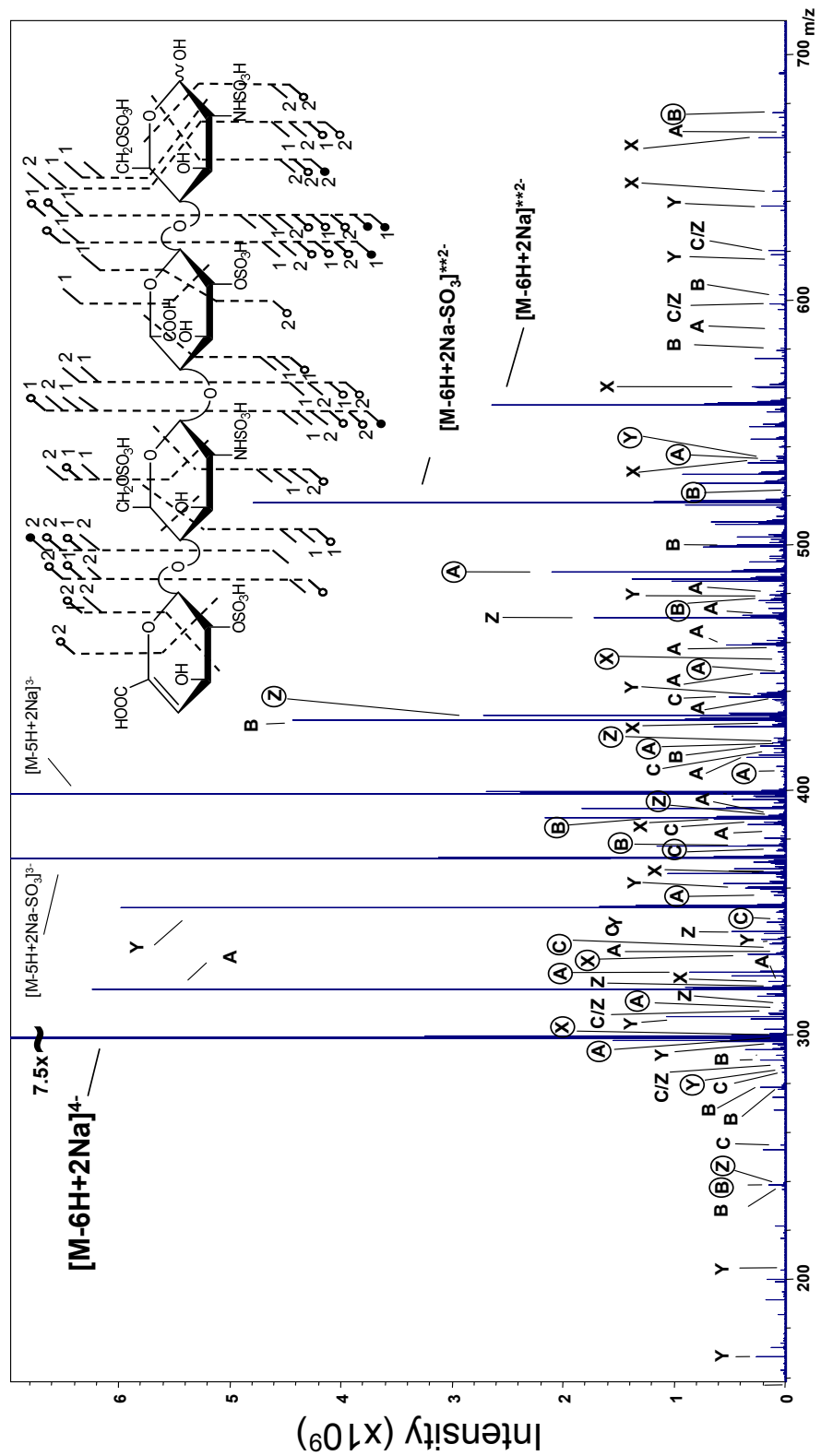
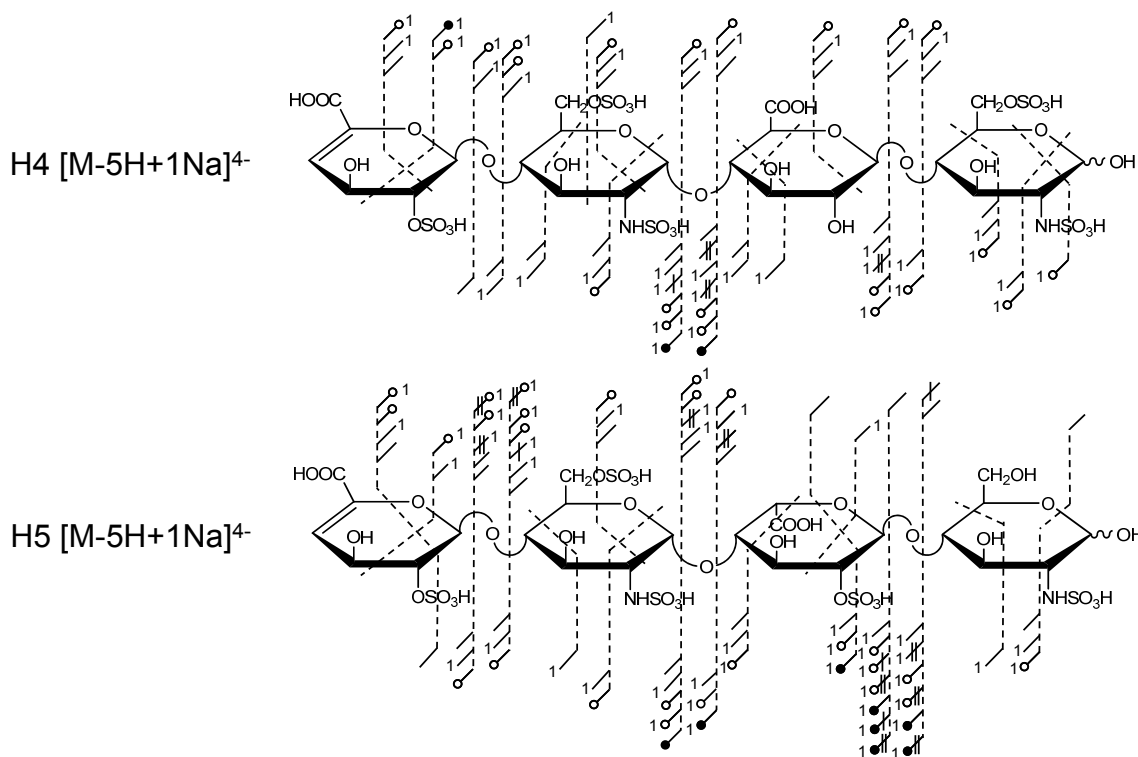


FIGURE 7.4 NETD mass spectrum of the  $[M-6H+2Na]^{4+}$  precursor of H3.

and H<sub>2</sub>O (only SO<sub>3</sub> is annotated) from the doubly reduced species, [M-6H+2Na]<sup>2-\*\*\*</sup>.

*H4 (ΔUA2S-GlcNS6S-GlcA-GlcNS6S) and H5 (ΔUA2S-GlcNS6S-IdoA2S-GlcNS)*

The NETD product ion assignments of two penta-sulfated heparin tetrasaccharides are shown in Figure 7.5 for the inclusion of variation in hexuronic acid



**FIGURE 7.5** Annotated structures for the NETD of H4 and H5.

stereochemistry and sulfation when compared to H3. Consistent with the NETD of H3, complete glycosidic and sufficient cross-ring cleavage is observed to locate all sites of sulfation on each tetrasaccharide. Comparison between the three heparin tetrasaccharides

reveals a variation in sulfate loss. In particular, the NETD of H4 indicates decreased levels of sulfate loss, specifically multiple losses of SO<sub>3</sub> from higher cleavages. Close examination of the structures reveals that H3 and H5 contain IdoA2S residues that present a pathway for proton movement from the carboxyl to the ionized sulfate, whereas H4 contains an un-sulfated GlcA. Unfortunately, a true epimer pair is not currently available to enable direct comparison.

*DS dp8 [ $\Delta$ UA-(GalNAc4S-IdoA)<sub>3</sub>-GalNAc4S]*

The EDD of DS dp8 generates a complex tandem mass spectrum [11] that requires a mass analyzer capable of high resolving power. By extension, the NETD of the same octasaccharide ([M-4H]<sup>4+</sup> precursor) should produce a similar spectrum and is shown in Figure 7.6. Abundant cleavage is observed for both glycosidic and cross-ring bonds with accompanying losses of H and 2H. No ions are assigned in the NETD spectrum that are not present during EDD. The loss of one sulfate group is observed for most glycosidic bond cleavages and in several cross-ring cleavages (mainly <sup>1,5</sup>X<sub>n</sub>). In no instance are more than two sulfate groups lost from a product ion. Cross-ring cleavages are largely assigned to hexuronic acid residues and are consistent with the observation during EDD of the same precursor ion [11] and of mobile protons in CS GAGs during tandem mass spectrometry [26].

Of note is the low number of product ions in the low m/z region below the precursor ion. Due to the lack of electronic excitation products that are charge conserved, i.e. 4<sup>-</sup> products from a 4<sup>-</sup> precursor, during NETD and possible protonation of high mass

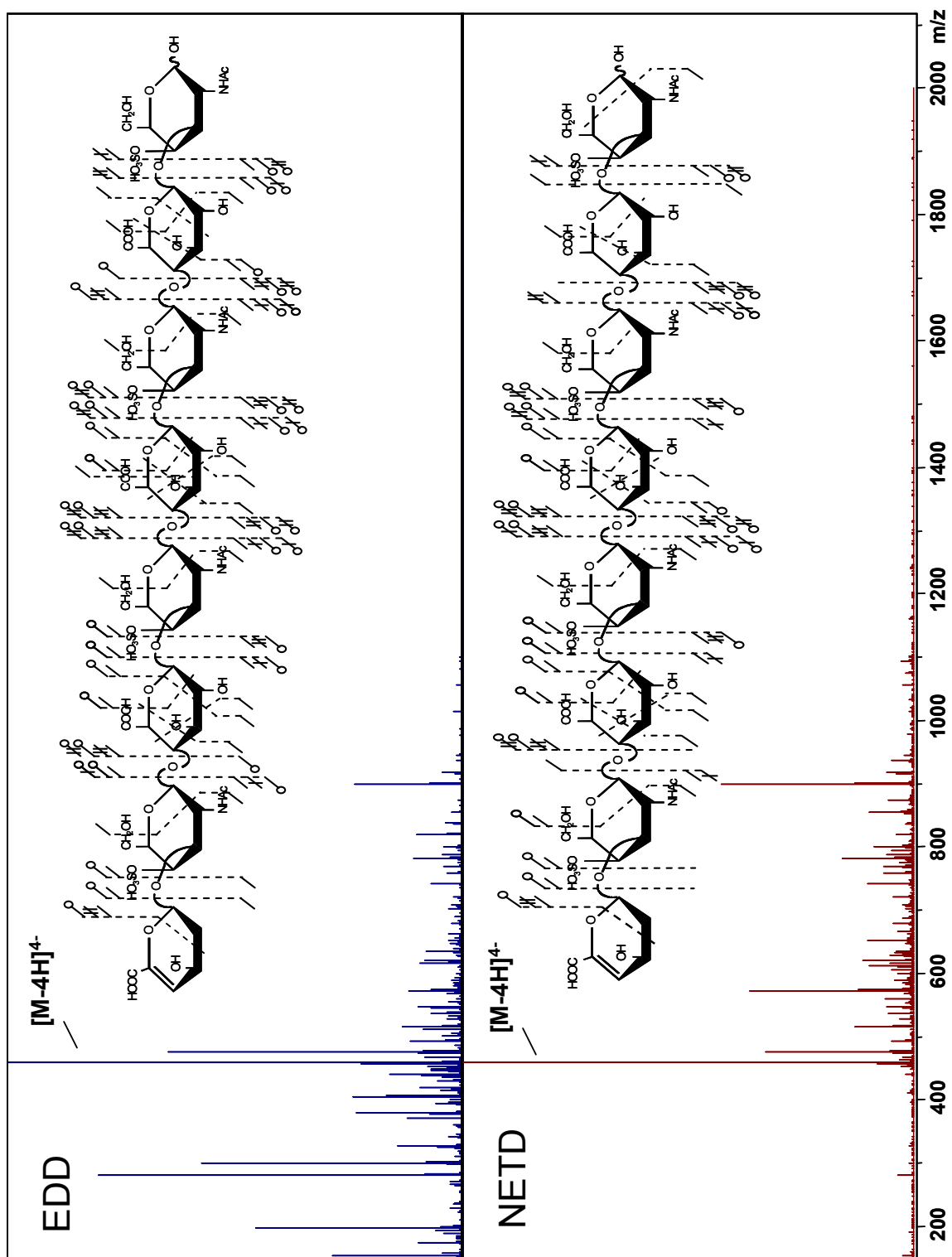
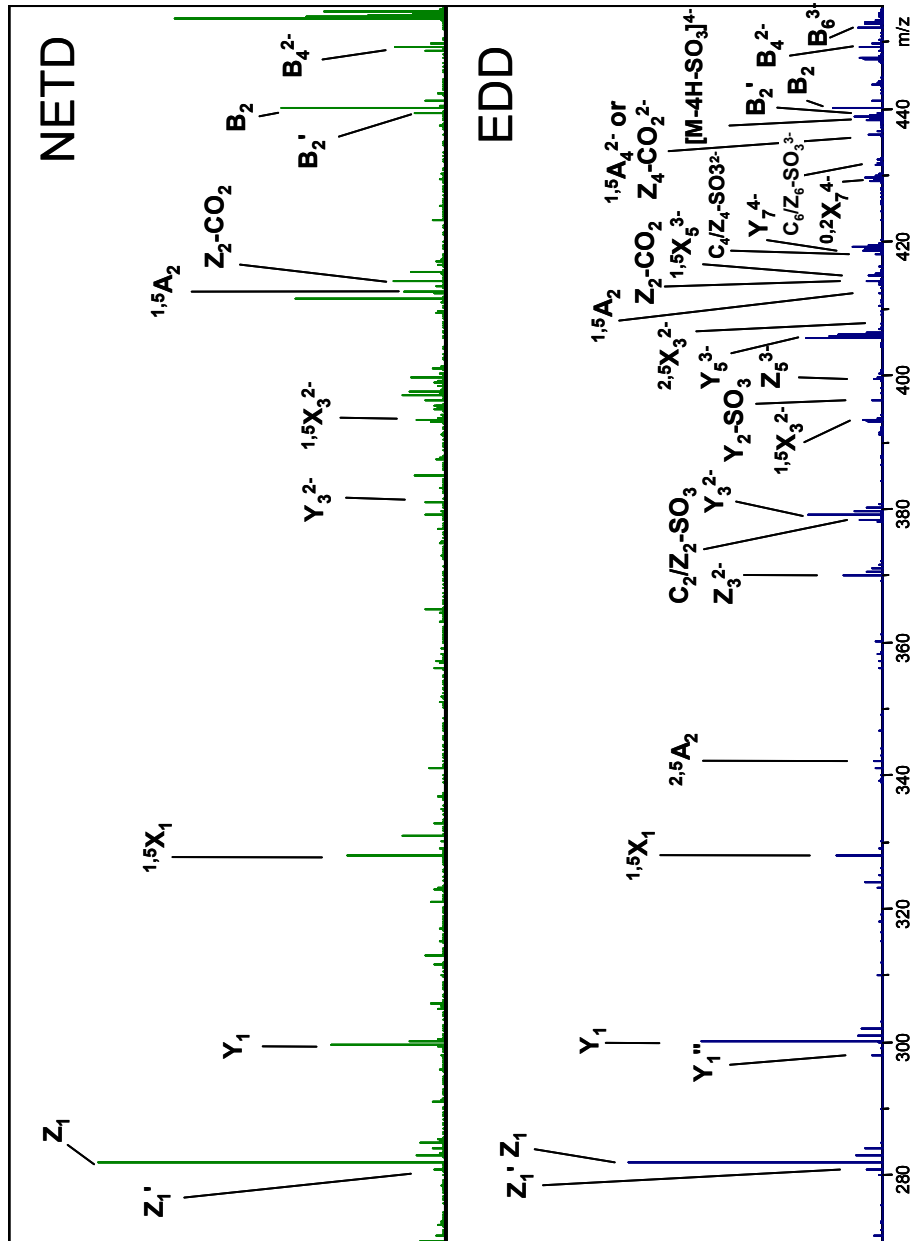


FIGURE 7.6 Spectra and annotated structures for the EDD and NETD DS dp8.

ions that bore multiple charges and results in a higher  $m/z$  than in EDD, this region of the mass spectrum appears vacant as shown in Figure 7.7. The relative intensity of odd-



**FIGURE 7.7** Annotated spectra showing the low  $m/z$  region of the EDD and NETD for the  $[M-4H]^{4-}$  precursor of DS dp8.

electron (OE) products is increased in the NETD spectrum. These include the charge-reduced species,  $[M-4H]^{3-*}$ ,  $^{0,2}X_7$ ,  $^{0,2}X_5$ , and  $B_3'$ , shown in Figure 7.8.

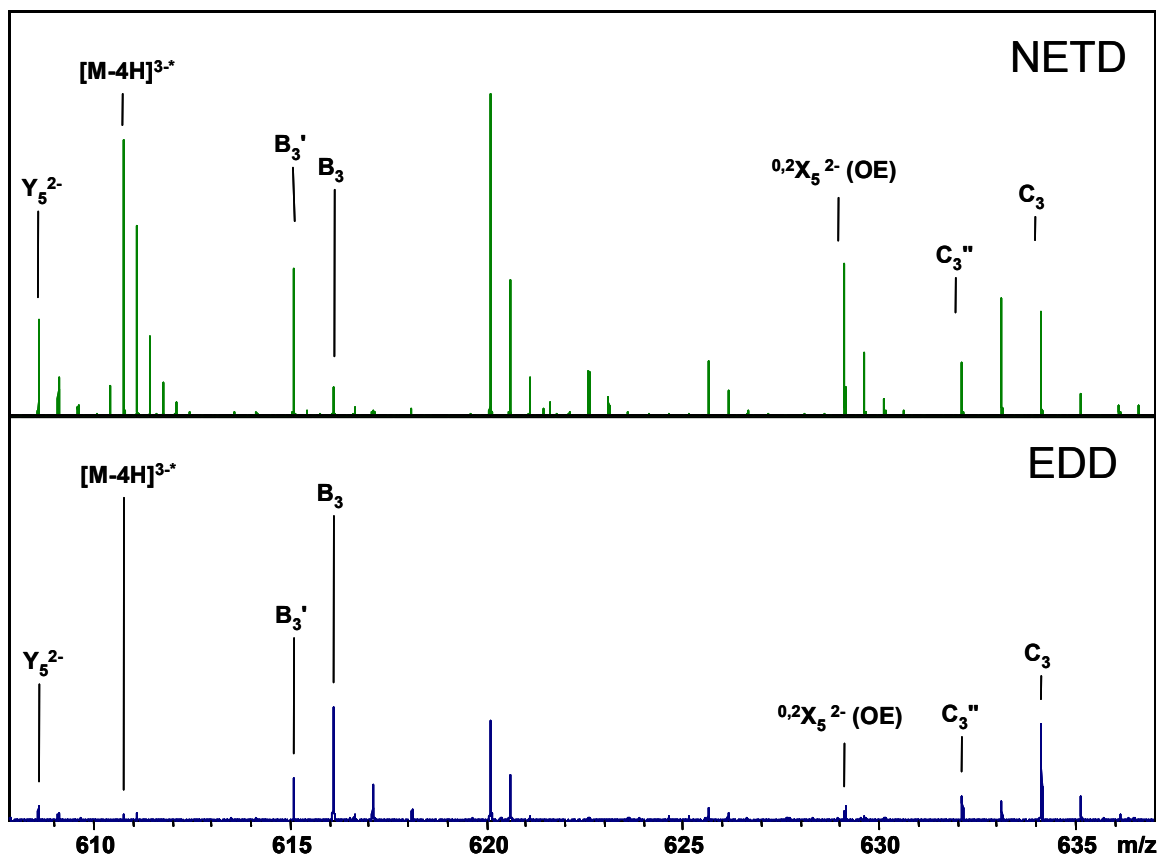


**FIGURE 7.8** Annotated spectra showing selected odd-electron products assigned from the EDD and NETD of the  $[M-4H]^{4+}$  precursor of DS dp8.

## CONCLUSIONS

The combination of ion-ion reactions for tandem mass spectrometry ion activation and subsequent mass analysis by FT-ICR MS is highly suited for the structural

characterization of sulfated glycosaminoglycan oligosaccharides. NETD provides the ability to generate sufficient cross-ring cleavages for location of sites of sulfation while FT-ICR provides the mass accuracy and resolving power necessary to confidently assign the large number of product ions distributed in a narrow  $m/z$  window. Although slight differences are observed when EDD and NETD products are compared due to the lack of electronic excitation products, NETD presents a pathway to apply electron-based ion activation to online-chromatographic separation as it is not limited to longer time scales as is EDD.

## **ACKNOWLEDGEMENTS**

FEL III, ZX, ML, TL, RJL, and IJA gratefully acknowledge financial support from the National Institutes of Health grant #2R01-GM038060-16. FEL III, SA, KM, AV, GJB, and IJA gratefully acknowledge financial support from the Center for Research Resource of the National Institutes of Health Grant # P41RR005351. FEL III personally acknowledges the University of Georgia Graduate School for funding from a Dissertation Completion Award and Bruker Daltonics (Billerica, MA) for solariX instrument time.

## REFERENCES

1. Syka, J. E. P.; Coon, J. J.; Schroeder, M. J.; Shabanowitz, J. and Hunt, D. F., Peptide and protein sequence analysis by electron transfer dissociation mass spectrometry. *Proc. Natl. Acad. Sci. U. S. A.* **2004**, *101*, 9528-9533.
2. Herron, W. J.; Goeringer, D. E. and McLuckey, S. A., Gas-phase electron transfer reactions from multiply-charged anions to rare gas cations. *J. Am. Chem. Soc.* **1995**, *117*, 11555-11562.
3. Coon, J. J.; Shabanowitz, J.; Hunt, D. F. and Syka, J. E. P., Electron transfer dissociation of peptide anions. *J. Am. Soc. Mass Spectrom.* **2005**, *16*, 880-882.
4. Zubarev, R. A.; Kelleher, N. L. and McLafferty, F. W., Electron Capture Dissociation of Multiply Charged Protein Cations. A Nonergodic Process. *J. Am. Chem. Soc.* **1998**, *120*, 3265-3266.
5. Budnik, B. A.; Haselmann, K. F. and Zubarev, R. A., Electron detachment dissociation of peptide di-anions: an electron-hole recombination phenomenon. *Chem. Phys. Lett.* **2001**, *342*, 299-302.
6. Marshall, A. G.; Hendrickson, C. L. and Jackson, G. S., Fourier transform ion cyclotron resonance mass spectrometry: A primer. *Mass Spectrom. Rev.* **1998**, *17*, 1-35.
7. Mirgorodskaya, E.; Roepstorff, P. and Zubarev, R. A., Localization of O-Glycosylation Sites in Peptides by Electron Capture Dissociation in a Fourier Transform Mass Spectrometer. *Anal. Chem.* **1999**, *71*, 4431-4436.

8. Shi, S. D. H.; Hemling, M. E.; Carr, S. A.; Horn, D. M.; Lindh, I. and McLafferty, F. W., Phosphopeptide/Phosphoprotein Mapping by Electron Capture Dissociation Mass Spectrometry. *Anal. Chem.* **2000**, *73*, 19-22.
9. Wolff, J. J.; Amster, I. J.; Chi, L. and Linhardt, R. J., Electron Detachment Dissociation of Glycosaminoglycan Tetrasaccharides. *J. Am. Soc. Mass Spectrom.* **2007**, *18*, 234-244.
10. Wolff, J. J.; Leach, F. E.; Laremore, T. N.; Kaplan, D. A.; Easterling, M. L.; Linhardt, R. J. and Amster, I. J., Negative Electron Transfer Dissociation of Glycosaminoglycans. *Anal. Chem.* **2010**, *82*, 3460-3466.
11. Wolff, J. J.; Laremore, T. N.; Busch, A. M.; Linhardt, R. J. and Amster, I. J., Electron Detachment Dissociation of Dermatan Sulfate Oligosaccharides. *J. Am. Soc. Mass Spectrom.* **2008**, *19*, 294-304.
12. Wolff, J. J.; Laremore, T. N.; Busch, A. M.; Linhardt, R. J. and Amster, I. J., Influence of Charge State and Sodium Cationization on the Electron Detachment Dissociation and Infrared Multiphoton Dissociation of Glycosaminoglycan Oligosaccharides. *J. Am. Soc. Mass Spectrom.* **2008**, *19*, 790-798.
13. Leach III, F. E.; Xiao, Z.; Laremore, T. N.; Wolff, J. J.; Linhardt, R. J. and Amster, I. J., Electron Detachment Dissociation and Infrared Multiphoton Dissociation of Heparin Glycosaminoglycan Tetrasaccharides. *Manuscript in Preparation* **2010**,
14. Leach III, F. E.; Oh, H. B.; Arungundram, S.; Al-Mafraji, K.; Venot, A.; Boons, G.-J. and Amster, I. J., Electron Detachment Dissociation of Synthetic Heparan

Sulfate Tetrasaccharides Varying in Degree of Sulfation and Hexuronic Acid Stereochemistry. *Manuscript in Preparation*. **2010**,

15. Leach III, F. E.; Wolff, J. J.; Laremore, T. N.; Linhardt, R. J. and Amster, I. J., Evaluation of the experimental parameters which control electron detachment dissociation, and their effect on the fragmentation efficiency of glycosaminoglycan carbohydrates. *Int. J. Mass Spectrom.* **2008**, 276, 110-115.
16. Leach III, F. E.; Ly, M.; Laremore, T. N.; Wolff, J. J.; Linhardt, R. J. and Amster, I. J., Electron Detachment Dissociation and Hexuronic Acid Determination in Chondroitin Sulfate Glycosaminoglycan Oligosaccharides. *Manuscript in Preparation* **2010**,
17. Wolff, J. J.; Laremore, T. N.; Aslam, H.; Linhardt, R. J. and Amster, I. J., Electron-Induced Dissociation of Glycosaminoglycan Tetrasaccharides. *J. Am. Soc. Mass Spectrom.* **2008**, 19, 1449-1458.
18. Arungundram, S.; Al-Mafraji, K.; Asong, J.; Leach, F. E.; Amster, I. J.; Venot, A.; Turnbull, J. E. and Boons, G.-J., Modular Synthesis of Heparan Sulfate Oligosaccharides for Structure-Activity Relationship Studies. *J. Am. Chem. Soc.* **2009**, 131, 17394-17405.
19. Pervin, A.; Gallo, C.; Jandik, K. A.; Han, X.-J. and Linhardt, R. J., Preparation and structural characterization of large heparin-derived oligosaccharides. *Glycobiology* **1995**, 5, 83-95.
20. Munoz, E.; Xu, D.; Avci, F.; Kemp, M.; Liu, J. and Linhardt, R. J., Enzymatic synthesis of heparin related polysaccharides on sensor chips: Rapid screening of

- heparin-protein interactions. *Biochem. Biophys. Res. Commun.* **2006**, 339, 597-602.
21. Xiao, Z.; Zhao, W.; Yang, B.; Zhang, Z.; Guan, H. and Linhardt, R. J., Heparinase 1 selectivity for the 3,6-di-O-sulfo-2-deoxy-2-sulfamido- $\beta$ -D-glucopyranose (1,4) 2-O-sulfo-  $\beta$ -L-idopyranosyluronic acid (GlcNS3S6S-IdoA2S) linkages. *Glycobiology*
  22. Ceroni, A.; Maass, K.; Geyer, H.; Geyer, R.; Dell, A. and Haslam, S. M., GlycoWorkbench: A Tool for the Computer-Assisted Annotation of Mass Spectra of Glycans. *Journal of Proteome Research* **2008**, 7, 1650-1659.
  23. Domon, B. and Costello, C. E., A systematic nomenclature for carbohydrate fragmentations in FAB-MS/MS spectra of glycoconjugates. *Glycoconjugate J.* **1988**, 5, 397-409.
  24. Leach III, F. E.; Ly, M.; Laremore, T. N.; Wolff, J. J.; Linhardt, R. J. and Amster, I. J., Electron Detachment Dissociation and Hexuronic Acid Determination in Chondroitin Sulfate Glycosaminoglycan Oligosaccharides. Manuscript in Preparation **2011**.
  25. Zaia, J., Principles of Mass Spectrometry of Glycosaminoglycans. *Journal of Biomolecular Mass Spectrometry* **2005**, 1, 3-36.
  26. Zaia, J.; Miller, M. J. C.; Seymour, J. L. and Costello, C. E., The Role of Mobile Protons in Negative Ion CID of Oligosaccharides. *J. Am. Soc. Mass Spectrom.* **2007**, 18, 952-960.
  27. Capila, I. and Linhardt, R. J., Heparin-Protein Interactions. *Angew. Chem. Intl. Ed.* **2002**, 41, 390-412.

## **CHAPTER 8**

### **CONCLUSIONS**

The electron based ion activation of glycosaminoglycan (GAG) oligosaccharides varying in degree of sulfation and hexuronic acid stereochemistry has been performed for GAGs from the three major sulfated glycoform classes (heparan sulfate, heparin, and chondroitin sulfate). To optimize the parameters for the electron detachment dissociation (EDD) of GAGs, the electron current was monitored by a custom-designed electronic circuit and a maximum conversion efficiency was calculated for a current of 15  $\mu$ A entering the analyzer cell. In conjunction with an asymptotic increase in conversion efficiency as the electron pulse duration is increased, radial repulsion between the negative ion cloud and electron beam is inferred; therefore fundamentally limiting the EDD experiment.

Although these biomolecules share a common backbone constituted by iterating uronic acid and hexosamine monosaccharides, the outcome of a tandem mass spectrometry experiment is shown to be highly dependent upon the specific glycoform class and level of sulfation. For example, in lowly (or non-) sulfated heparan sulfate tetrasaccharides, direct evidence of hexuronic acid stereochemistry is observed in both EDD and negative electron transfer dissociation (NETD) spectra based upon diagnostic product ions that occur in glucuronic acid (GlcA) containing GAGs and not iduronic acid (IdoA). When the same method is applied to chondroitin sulfate epimers, the same product ion distributions are not sufficient to distinguish the two diastereomers, although they differ in the location of only one glycosidic bond linkage and site of sulfation, and products due to electronic excitation of the precursor ion in conjunction with multivariate statistics must be employed for differentiation.

Increasing the degree of sulfation at the tetrasaccharide level from lowly sulfated heparan sulfates to heparin poses a challenge due to the lability of the sulfate half ester and additional heterogeneity at the MS level due to Na/H exchange which minimizes the precursor ion signal available in a given mass channel. Although it is desirable to activate a GAG precursor ion in which an additional ionized site is included above the total number of sulfates to lead to an ionized carboxyl group that would provide a detachment initiated radical pathway for stereo-specific product ions in GlcA/IdoA epimers, these precursor ions are difficult to generate and the necessary product ions are generated at levels presumably below the limit of detection. Even though this presents a difficulty, the mobility of protons along the GAG oligomer, in some instances, places an ionized site at a carboxyl enabling the assignment of stereo-specific product ions. Additional information such as sample origin can also be utilized to identify the hexuronic acid stereochemistry.

For highly sulfated GAGs, i.e. heparin, where 2-3 sulfate groups are present per disaccharide, threshold activation by infrared multiphoton dissociation (IRMPD) is demonstrated to provide sufficient cross-ring cleavage to locate sites of sulfation on both hexuronic acid and hexosamine residues. In lowly sulfated GAGs (1 sulfate per disaccharide), threshold activation has been demonstrated to produce fewer cross-ring cleavages. This result is most likely due to the presence of a large number of charges on the precursor ion, possibly introducing lower energy pathways for product ion formation.

Extension of ion activation by NETD to highly sulfated GAGs requires coupling with a high resolution mass analyzer. NETD has been conducted on ion trap mass spectrometers for tetrasaccharides containing 1-2 sulfates which result in a product ion

distribution spanning a wide mass range. The NETD of highly sulfated GAGs reduces this mass range and increases the need for resolving power. In precursor ions where only sulfates are hypothesized to be ionized, abundant cross-ring cleavage is observed on non-sulfated hexuronic acid residues, indicating the movement of a proton from a carboxyl group to a sulfate, therefore placing an ionized site for electron transfer. This mechanism also provides a pathway for sulfate loss as  $\text{SO}_3$  (through protonation) during a low energy activation method.

The presented work demonstrates the capability of electron-based ion activation (EDD and NETD) for locating sites of sulfation on GAG glycoforms from all sulfated classes. Although the generation of stereo-specific product ions for the determination of hexuronic acid stereochemistry becomes increasingly difficult for highly sulfated compounds (and in specific glycoforms e.g. chondroitin sulfates), supplementary information from multivariate statistical analysis of peak intensities or sample origin can be employed. To overcome the physical limitation of repulsion between like charges, the implementation of ion-ion reactions for NETD in GAG analysis provides a pathway to reduce the activation time required and couple electron-based ion activation to LC methods, enabling the online analysis of complex GAG mixtures.

## APPENDIX A

### THE FT-ICR MASS ANALYZER<sup>1</sup>

---

<sup>1</sup> Leach III, F.E. and I.J. Amster. Submitted to Volume 7 Elsevier *Encyclopedia of Mass Spectrometry: The m/z Analyzer*, 8/6/2010.

## **ABSTRACT**

Fourier transform ion cyclotron resonance mass spectrometry (FT-ICR MS) provides a high performance platform for biomolecule and complex mixture characterization based on the combined provision of high mass accuracy and resolving power. The origins of FT-ICR MS can be traced to the early 20<sup>th</sup> century with major technological developments occurring since the 1970s. These modern advancements build upon a fundamental knowledge of ion physics and now provide highly sensitive instrumentation with the capability for elemental composition determination by accurate mass measurement and structural determination through utilization of varied tandem mass spectrometry techniques.

## INTRODUCTION

Fourier transform ion cyclotron resonance mass spectrometry (FT-ICR MS) has seen increasing application since its inception in 1974 [1], based on the current provision of the highest mass accuracy ( $\sim 500$  ppb or better) and resolving power ( $m/\Delta m_{50\%} > 100,000$ ) as well as implementation of a variety of tandem mass spectrometry techniques for the structural analysis of biomolecules. The combination of high mass accuracy and resolution in FT-ICR enable the assignment of elemental composition based solely on an accurate mass measurement, even in complex mixtures where several components may have the same nominal mass. This aspect of FT-ICR, in conjunction with the ability to detect components over a large dynamic range, has seen widespread application in proteomics [2-4] and more recently in petroleomics [5, 6].

Beyond the basis of an accurate mass measurement, the modern FT-ICR platform presents the ability to conduct experiments not only in spatially distinct regions of the instrument but also temporally by repeated ion isolation and activation events in the analyzer to conduct  $MS^n$  experiments. Tandem mass spectrometry techniques based on threshold activation (collisional induced dissociation, CID, and infrared multiphoton dissociation, IRMPD) and electron based activation (electron capture dissociation, ECD, electron detachment dissociation, EDD, and electron transfer dissociation, ETD) have been demonstrated on FT-ICR instruments for the structural characterization of biomolecules including peptides, intact proteins, carbohydrates, and oligonucleotides, generated from variety of ion sources such as electrospray ionization (ESI) [7] and matrix assisted laser desorption ionization (MALDI) [8, 9].

In the post-genomic era, the FT-ICR mass analyzer has come into widespread prominence, advancing initially from an instrument centered on ion-molecule chemistry [10, 11] to an indispensable tool in modern bio-molecular analysis [12] utilized for the determination of elemental composition as well as structure. Since the introduction of the first FT-ICR MS in 1974, over 700 systems have been deployed worldwide.

## **HISTORICAL**

The beginnings of FT-ICR MS can be traced back to E.O. Lawrence, who developed the theory of ion cyclotron resonance (ICR) in the 1930s [13]. The basis of which is that the motion of a charged particle, when perpendicular to a magnetic field, is constrained to a circular orbit with a defined frequency. This relationship is known as the cyclotron equation and will be discussed in detail in the following section. The first cyclotron accelerator based on this principle was constructed by Lawrence during this time to accelerate light ions for the study of nuclear structure [14]. In this first implementation of cyclotron resonance shown in Figure A.1, ions were subjected to a pulsed radiofrequency (rf) electric field imposed on two semi-circular electrodes, which were orthogonal to the field of an electromagnet. In order for an ion's orbital frequency to come into resonance, the magnet field was adjusted so that the time required for an ion to traverse one of the electrodes corresponded to half of the waveform's period. When this condition was satisfied, the ion was accelerated. Based on the conservation of angular momentum, the ion's radius must increase with an increase in angular velocity. With continual passing of the electrode gap, the ion's trajectory subsequently approached the electrodes. This experimental configuration is the converse of modern instruments

where the magnetic field is static and the rf field is scanned. The physical basis of ICR will be discussed in subsequent sections.

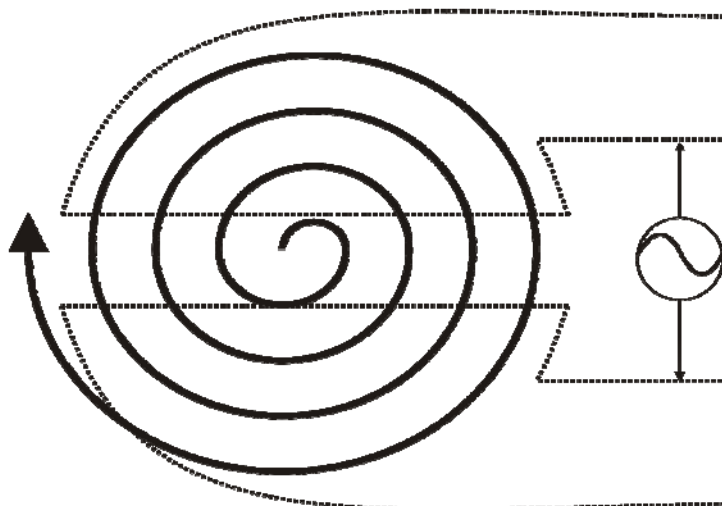


**FIGURE A.1** Diagram of Lawrence's cyclotron. An alternating electric field is applied to the two semi-circular electrodes which are inserted into a magnetic field.

The next major development in ICR was the coupling of ICR to mass spectrometry in the omegatron [15, 16]. Instead of pulsing the electric field, the rf was continuously applied to the electrodes, and the mass-to-charge ( $m/z$ ) could be recorded as the magnetic field was scanned. As a particular ion's cyclotron frequency would come into resonance with the applied field, it would continuously spiral outward and be collected for detection. The next series of developments were made in the 1960s by the laboratories of Wobschall [17], Llewellyn, and Baldeschwieler [10], while studying ion-molecule reactions. The first advance was the measurement of an ion's resonant power

absorption as opposed to collection on a plate for detection. The second was the introduction of double resonance techniques to study reaction intermediates in ion-molecule reactions [18]. This technique would later become the basis for tandem mass spectrometry [19].

The application of Fourier transform methods, borrowed from nuclear magnetic resonance (NMR) [20], to ion cyclotron resonance by Comisarow and Marshall in 1974 [1] marked the beginning of FTICR-MS. These first experiments necessitated new technology to measure the large bandwidth present in an ICR mass spectrum. This broadband aspect required a low amplitude fast frequency sweep [21] and conversion of the signal current to a single voltage by a broadband RC circuit [1, 22]. These initial developments are still the basis of the modern FT-ICR MS experiment and provide the desired aspects of high resolution and wide mass range [23].

## **ION PHYSICS**

Although the FT-ICR mass analyzer is intrinsically complex, it is based on relatively simple physics. These fundamental principles have been reviewed extensively in the literature [24-28]. At its core, the FT-ICR analyzer is a Penning Trap [29-31]. Ions are confined in three dimensions, radially by the application of a static magnetic field and axially by the application of electric potentials.

The motion of ions in the FT-ICR analyzer can be described by classical electromagnetic theory, where the ion experiences static magnetic and electric fields. In the fundamental case of an applied static magnetic field, the Lorentz force experienced by an ion can be expressed via Newtonian mechanics as:

$$F = ma = q(v \times B) \quad (\text{Equation 1})$$

where an ion of charge,  $q$ , experiences the force of a magnetic field,  $B$ . The magnetic force is expressed as a cross product because an ion is only affected by the magnetic field if a portion of its velocity vector is perpendicular to the field. Additional forces such as that due to an applied electric field and to space charge due to coulombic interactions between ions can also be added to this expression, but will be addressed later.

The primary influence of the Lorentz force is ion cyclotron motion, shown in Figure A.2. Upon interaction with the static magnetic field, the ion's linear trajectory is converted into a circular orbit. This periodic orbit due to the magnetic field is known as cyclotron motion and is the fundamental basis for FT-ICR MS. The periodic motion of the ion can also be expressed as a frequency that is characteristic of a particular ion and is determined by the cyclotron equation. The cyclotron frequency ( $f_c$ ) is dependent upon three values: the strength of the static magnetic field,  $B$ , the mass of a given ion,  $m$ , and its respective charge,  $q$ , and is expressed as:

$$f_c = \frac{qB}{2\pi m} \quad \text{or} \quad \omega_c = \frac{qB}{m} \quad (\omega_c = 2\pi f_c) \quad (\text{Equation 2})$$

where the terms are in SI units ( $f_c$  is expressed in Hz,  $q$  in Coulombs,  $B$  in Tesla, and  $m$  in kg).

### Ion Cyclotron Motion

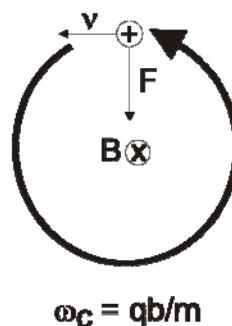


**FIGURE A.2** An illustration of the forces acting upon an ion as it undergoes cyclotron motion.

From this equation, the mass-to-charge ratio ( $m/q$ , more often expressed as  $m/z$  where  $z$  is also charge) is determined by measuring the cyclotron frequency of a given ion. For example, the amino acid lysine (nominal mass of 146 Da) with a charge state of 1+ undergoing cyclotron motion in a magnetic field of 1 T would have a cyclotron frequency of 105 kHz, whereas the protein BSA (bovine serum albumin, nominal mass of 66432 Da) with a charge state of 50+ in the same magnetic field would have a frequency of 12 kHz.

Of key importance to FT-ICR MS, the cyclotron frequency measured during an experiment is independent of its kinetic energy. Other mass analyzers such as time-of-flight (TOF), rely on detection methods that are dependent on an ion's velocity and subsequently its kinetic energy. In these analyzers, there is a fundamental maximum resolution that can be achieved due to the spread in the velocity of a given ion during

detection. This initial difference of FT-ICR MS gives rise to a marked improvement in resolving power, which can routinely approach 100,000 ( $m/\Delta m_{50\%}$ ) or greater in broadband operation. Alternatively, the high resolving power of FT-ICR MS can be rationalized based on the number of cyclotron orbits an ion undergoes during measurement [32].

Although the ion's trajectory is confined to an orbit due to the magnetic field, it is not confined axially as no magnetic force is experienced during motion along magnetic field lines. To restrict movement along the z-axis of the magnetic field, electric potentials are applied. These trapping potentials give rise to a second type of ion motion known as trapping motion.

Early experiments in ion cyclotron resonance lacked trapping potentials. In these drift cells, ions moved unrestricted along the primary axis through the magnetic field and were detected as they passed through the ICR cell. The time available for detection in this configuration was on the order of milliseconds. To increase the detection time, the first application of an axially confining trapping potential, the trapped ICR cell, was developed by McIver in 1970 [33]. Plates were applied to the ends of the ICR cell, perpendicular to the primary magnetic field axis, and a small, symmetric voltage ( $\sim 1V$ ) was then applied to confine ions, which in turn undergo simple harmonic oscillations within the cell [34].

Combining the forces of the magnetic field and applied trapping potentials, Eqn. 1 now becomes:

$$F = q(v \times B) + qE \quad (\text{Equation 3})$$

The idealized electric isopotential formed in this case is perfectly quadrupolar, shown in Figure A.3, in that the electric field gradient is uniform regardless of position in the trap. In reality, the potential is only approximately quadrupolar at the center of the analyzer with deviations from the ideal case varying based on the cell design. These imperfections result in a positional dependence for an ion's frequency within the analyzer.

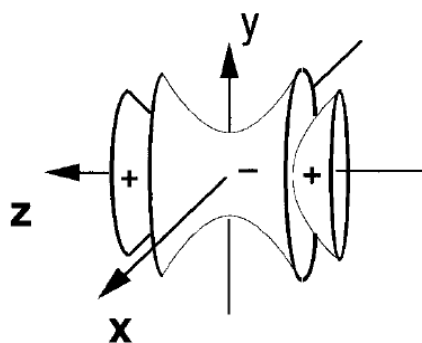


**FIGURE A.3** The isopotential surface of the desired three-dimensional axial quadrupolar potential. (*Adapted from Marshall 1998 [25]*)

The third form of ion motion in the FT-ICR analyzer cell arises from the combination of the applied magnetic and electric fields, and is known as magnetron motion [35]. These two forces act upon the ions in opposing directions. The magnetic field confines the ions along the Z-axis near the center of the analyzer cell, whereas the electric field is radially repulsive directing ions away from the center of the cell as seen in Figure A.4. When

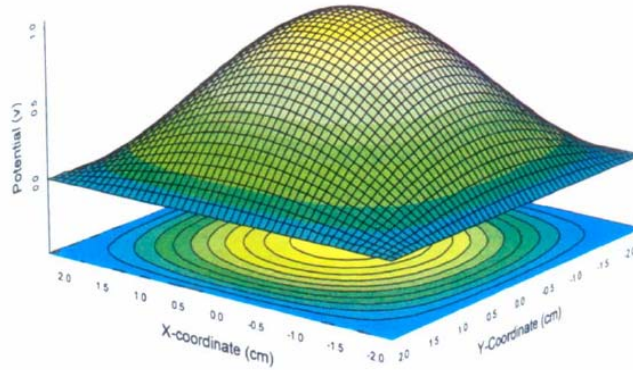


**FIGURE A.4** The isopotential surface due to the application of trapping plates to the ICR analyzer. A radially repulsive force directing ions away from the cell's center is present. (From Amster 1996 [24])

these two independent forces are combined, the ultimate effect on the ion motion is a precession in orbit around the center of the cell. When compared in terms of frequency there is a difference of several orders of magnitude between cyclotron motion and magnetron motion. Cyclotron frequencies are normally in the range of KHz to MHz where as magnetron frequencies are on the order of Hz. The magnetron shift in measured frequency ( $f_m$ ) can be expressed as:

$$f_m = \frac{\alpha V}{\pi a^2 B} \quad \text{(Equation 4)}$$

where  $\alpha$  is a constant based on the geometry of the analyzer cell,  $V$  is the applied trapping potential,  $a$  is the distance between the two trapping plates, and  $B$  is the magnetic field

strength. It should be noted that the magnetron shift is independent of  $m/z$  and is constant for a specific instrumental configuration. For example in a cubic cell with an  $\alpha$  of 1.39, trapping potential of 1 V and plate spacing of 5 cm the magnetron frequency will be 172 Hz at 1 T and 25 Hz at 7 T.

The observed cyclotron frequency is therefore reduced by the addition of magnetron motion. A correction can then be applied to the measured or observed cyclotron frequency,  $f_{obs}$ , to arrive at the true cyclotron frequency,  $f_c$ .

$$f_c = f_{obs} + f_m \quad \text{(Equation 5)}$$

Although there are now three forms of ion motion, the cyclotron motion is still the dominant mode and the trapping and magnetron motions can be treated as perturbations. If this were not the case, a measurement of the cyclotron frequency would not allow an accurate calculation of an ion's mass-to-charge. It is still possible for the magnetron motion to alter the measured cyclotron frequency and leads to mass shifts, radial ion diffusion [36], and sidebands [37, 38].

An additional term due to collisions can also be added to Eqn. 3. This term has the general effect of frictional damping of ion motion. During a typical FT-ICR MS experiment, the pressure of the analyzer cell is held at pressures of  $10^{-9}$  to  $10^{-10}$  Torr. Collisions are infrequent in this pressure regime, but it may be desirable to introduce a collision gas into the analyzer cell at some point during the experiment, as during in-cell collisionally activated dissociation (CAD) [39, 40]. The initial effect of a collision gas is a reduction in its velocity and subsequently an ion's kinetic energy. As the velocity is

reduced, all three of the ion's motions in the FT-ICR analyzer cell are affected. The Lorentz force is a cross product of velocity, therefore the cyclotron frequency is reduced and ions begin to lose orbital radius due to the presence of the magnetic field. The collision gas also reduces movement within the harmonic oscillator created by the trapping potentials and ions condense towards the center of the cell. Thirdly, the reduction in velocity leads to an increase in the magnetron radius due to the radially repulsive field. The end result is a drift towards the perimeter of the analyzer cell where ions are neutralized by collisions with the electrodes.

Ion motion within the FT-ICR analyzer primarily depends upon externally applied electric potentials and magnetic field, but the coulombic interaction between ions can also affect ion motion. This general effect is known as space charge [41, 42]. In the typically inhomogeneous electrostatic field of an FT-ICR analyzer, the coulombic repulsion between ions of like charge can perturb the measured cyclotron frequency. A shift in frequency will introduce an error in mass accuracy while a spread in frequency broadens the spectral peak and results in a decrease in spectral resolution. This effect can be accounted for mathematically by taking into account the ion cloud density,  $\rho$ , and a constant defining the ion cloud shape,  $G_i$ . The shift in cyclotron frequency due to space charge ( $f_{sc}$ ) becomes

$$f_{sc} = \frac{q\rho G_i}{\epsilon_o B} \quad (\text{Equation 6})$$

This additional correction can be accounted for in equation 4 and can be expanded to include this space charge term

$$f_c = f_{obs} + f_m + f_{sc} \quad (\text{Equation 7})$$

Taking into account these deviations from the true cyclotron frequency, the mass-to-charge of a given ion can be precisely measured in the FT-ICR MS mass analyzer. As we have covered the motion of ions within the cell, it is now necessary to describe the experimental configuration used to measure the cyclotron frequency of a desired ion or ions.

## **DETECTION**

As stated earlier, the FT-ICR analyzer is unique in that the cyclotron frequency of an ion is measured and converted to a mass-to-charge value based on the cyclotron equation (Eqn 2). A second feature unique to FT-ICR is the measurement of an image current to detect ions trapped in the analyzer [22]. This process is non-destructive, and ions remain available for further experiments in the cell. Most traditional mass analyzers, such as a quadrupole or time-of-flight, rely on electron multipliers for detection where the ion is neutralized. A detailed description of the principles and configurations of FT-ICR detection beyond the scope of the current discussion can be found in the work of Marshall and Hendrickson [43]

Within the FT-ICR analyzer, there are two pairs of opposing plates upon which potentials are applied as shown in Figure A.5. One pair of plates is utilized for excitation

while the other is for detection. Upon entering the analyzer cell and initializing a cyclotron orbit, the ions are moving in a non-coherent fashion. Detection at this stage would not produce a meaningful signal. Due to incoherent ion motion, a distribution of phases will be observed resulting in deconstructive interference. Before an image current can be measured, the ions must first orbit coherently. To achieve this state, a sinusoidal

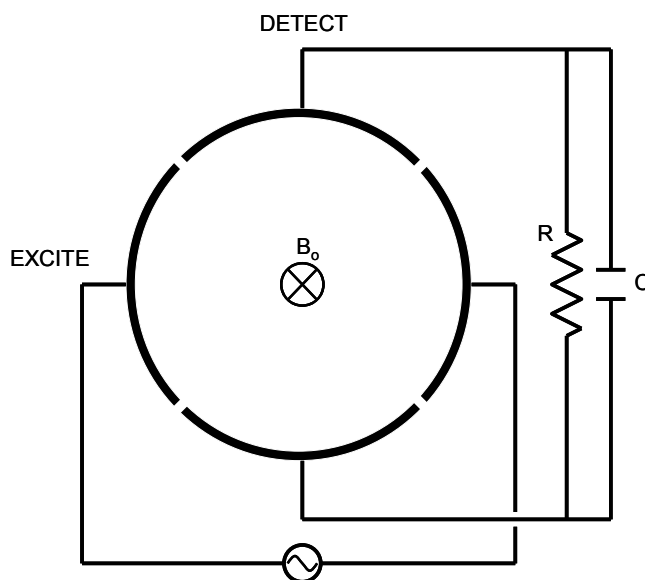


**FIGURE A.5** A typical ICR cell design indicating the pairs of electrodes for excitation (connected to an rf oscillator) and for detection (connected to a broadband RC circuit).

radio frequency (rf) voltage is applied to the excitation plates. If an ion's cyclotron frequency is equal to the applied rf signal, the resonant energy will be absorbed, increasing the radius of cyclotron orbit, and the ions will move closer to the perimeter of the cell. When this resonance voltage is applied continuously, the ion will achieve an orbit that exceeds that diameter of the FT-ICR cell and will be neutralized by striking the

cell walls or be axially ejected from the trap by energy converted into the trapping motion. While this effect may seem detrimental, it becomes useful when the need to eject a desired ion or range of ions from the analyzer cell arises. As the applied rf electric field is rapidly scanned, ions move coherently outward towards the detection plates and return towards the center of the cell when the frequency is off-resonance with the ion's cyclotron frequency. During the period when they approach the cell perimeter, positive ions will attract electrons towards one of the detection plates and then the other as it passes in orbit. Conversely, negative ions will repel electrons away from the plates. This alternating current between the two plates is measured by a connected RC circuit and is known as an image current. The measured current is proportional to the number of charges on a given ion. For a doubly charged ion, the current will be twice that of a singly charged ion given the populations are the same size. This nuance must be taken into account to properly compare signal intensities of varying charge state.

As described, the previous experiment would measure a single mass-to-charge value for an ion with a frequency in-resonance with the applied rf voltage. In practice, many ions are detected simultaneously by rapidly scanning a specified frequency range. This broadband scan excites all ions with cyclotron frequencies in the applied frequency spectrum. The measured image current then becomes a superposition of sinusoidal waveforms, one for each mass-to-charge value present within the analyzer cell. This time domain transient [22] displayed in Figure A.6 would appear to be of minimal value to a mass spectrometrists but contains the respective cyclotron frequencies for any detected ion

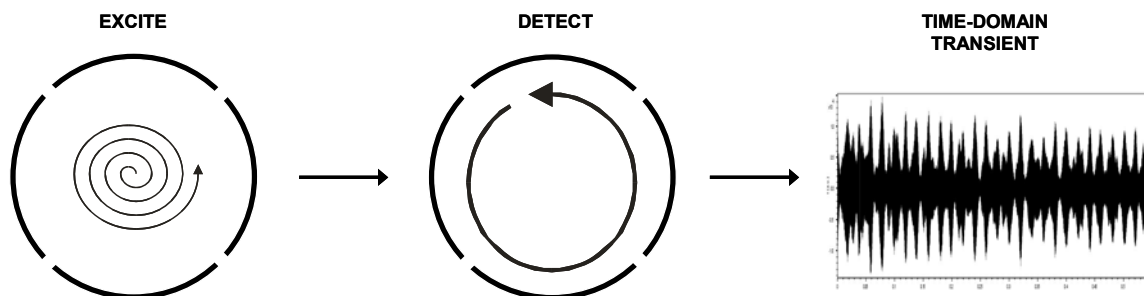


**FIGURE A.6** The FT-ICR experimental sequence of excitation of the trapped ions population's cyclotron radius, detection of an image current, and recording of a time domain transient or FID (free induction decay).

in the cell. These frequencies are resolved by applying a Fourier transform to the transient [1, 27]. The associated mass-to-charge values and intensities are then derived from a calibration equation [44], shown below, based on the cyclotron equation.

$$\left(\frac{m}{z}\right)_i = \frac{A}{f_i} + \frac{B}{f_i^2} \quad (\text{Equation 8})$$

where the mass-to-charge of a given ion,  $i$ , is calculated from its frequency and by two constants,  $A$  and  $B$ , based on the applied magnetic field and trapping potentials. This generalized procedure is shown in Figure A.7. Space charge can also be accounted for in

## Multichannel Detection

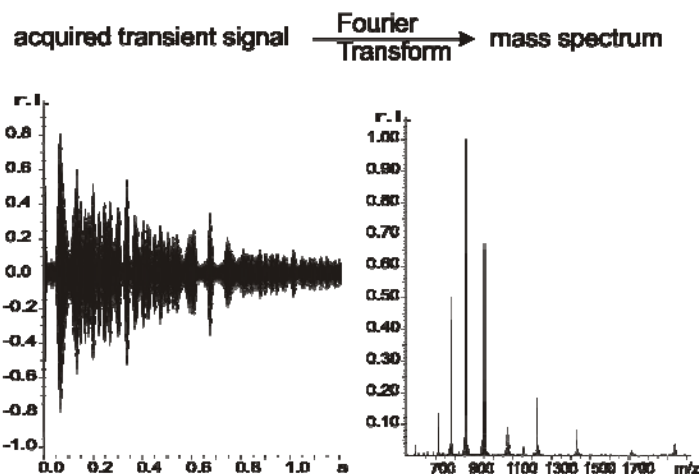


**FIGURE A.7** Multi-channel or broadband detection in FT-ICR MS results in a time domain transient. To produce a mass spectrum, the Fourier transform is applied to the transient producing a frequency spectrum that is converted to a mass spectrum by mass calibration. (From Amster 1996 [24])

the calibration equation [45, 46] incorporating a third term which includes the respective ion intensity,  $I_i$ , and a third constant  $C$ . Equation 8 then becomes,

$$\left(\frac{m}{z}\right)_i = \frac{A}{f_i} + \frac{B}{f_i^2} + C \left(\frac{I_i}{f_i^2}\right) \quad (\text{Equation 9})$$

Although the broadband excitation and detection of ions is suitable for a variety of FT-ICR MS experiments, increased resolution is required for specific applications.

The most direct method to obtain high-resolution data is to increase the duration of the time domain transient acquired. This solution is not practical due to two problems that arise. The first is the measured image current is not infinite in duration. The signal is only observed for maximum period of minutes due to damping by gas phase collisions. The second is the limitation of electronics. If it were possible to acquire an extended transient, the resulting data would be limited by the memory available for the digitizer to acquire the transient and the computer memory available for the Fourier transform. The latter limitation is more of a historical footnote as electronics have progressed substantially since the beginnings of FT-ICR MS.

Initially developed to overcome the stated electronics limitation during the advent of FT-ICR MS, heterodyne detection allows for high resolution data collection under the current limitation of available image current signal duration [43]. By multiplying a reference time domain signal that is close to the ICR time domain signal of interest, a mixed or composite signal in the frequency domain is acquired with one signal due to the sum of the two frequencies and the other due to the difference seen in Figure A.8. By applying a low-pass filter, the sum frequency is removed and the lower frequency difference signal is available for acquisition at a lower rate, allowing for a longer transient to be acquired. After application of the Fourier transform, the reference frequency is added to the calculated frequency value to produce the actual cyclotron frequency.

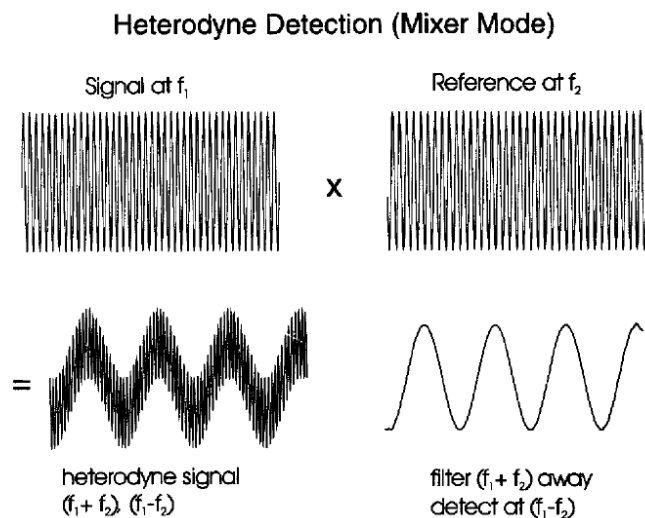


**FIGURE A.8** A schematic representation of heterodyne detection. A measured signal,  $f_1$ , is multiplied by a reference signal,  $f_2$ . This heterodyne signal contains both sum and difference components. The sum component is filtered away in order to detect at the lower difference component. (From Amster 1996 [24])

The previously described excitation methods are dipolar in nature as opposite phases of the rf signal are applied to two opposing plates in the FT-ICR analyzer. It is also possible to apply a quadrupolar excitation (QE) during an FT-ICR MS experiment [47]. Unlike dipolar excitation which increases an ion's cyclotron orbit and drives an ion towards the perimeter of the cell, quadrupolar excitation, in combination with the introduction of a collision gas, reduces the cyclotron orbit leading to ion coalescence and axialization in the center of the cell. During quadrupolar excitation, an rf signal that is resonant with a given ion's cyclotron frequency is applied to opposing plates. A second rf signal that is  $180^\circ$  out of phase is applied to the second pair of opposing plates, as

shown in Figure A.9. By applying a quadrupolar electric field, the cyclotron and magnetron motions of an ion will periodically interconvert [48]. The initial effect of the

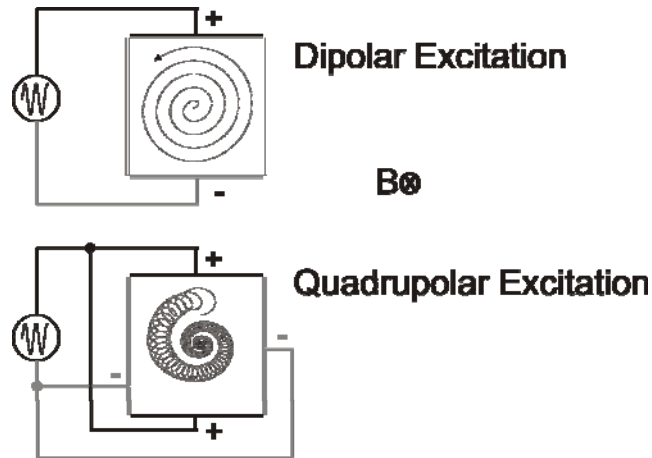


**FIGURE A.9** A comparison ion trajectories due to dipolar excitation (top) and quadrupolar excitation (bottom). Dipolar excitation results in an increase in the cyclotron radius whereas quadrupolar results in a periodic interconversion between cyclotron motion and magnetron motion. (*From Amster 1996 [24]*)

collision gas leads to a reduction in an ion's velocity and therefore the cyclotron orbit decreases in radius as well as the magnetron orbit increasing due to radial repulsion from the trapping potential. As the frequency of cyclotron orbit is much larger than that of the magnetron motion, it will experience more collisions and will dampen faster than the magnetron mode will increase in radius. The end result of the excitation is a diminished cyclotron orbit, resulting in the x-y centering and z-axialization of an ion population in the middle of the cell.

As described, the addition of quadrupolar excitation to a standard FT-ICR cell requires electronic or mechanical alterations. Typically one pair of cell plates is utilized for excitation and the other for detection. Two solutions have been presented to implement quadrupolar excitation as initially described. To perform QE, dipolar excitation, and detect within the same cell, a relay must be inserted to alternate the function of one pair of cell plates between quadrupolar and dipolar modes [49]. This solution allows for QE without mechanical alterations of the analyzer cell. A second alternative involves the use of two analyzer cells in tandem [47]. The first cell is specialized for the quadrupolar excitation, while the second is configured for the standard dipolar excite and detect. This solution poses one disadvantage in that only one quadrupolar excitation can be performed with a given ion population before detection in the second cell. To increase the resolution in a measurement, multiple quadrupolar excitations can be performed allowing for ions to be excited to higher cyclotron orbit for detection and then regrouped at the center of the cell for additional excite/detect events [49]. The application of QE can be further simplified by applying only one phase of the rf signal to a pair of plates and then grounding the second pair [50]. This solution reduces the overall complexity of the QE application while producing potentials nearly identical to those produced by the original configuration when compared in SIMION [51] simulations.

Excitation and detection are two central elements of an FT-ICR MS experimental sequence. The entire sequence can be visualized as a series of events or pulses that occur during an experiment as portrayed in Figure A.10. The first pulse corresponds to the quench event. Asymmetric voltages are applied to the trapping plates resulting in an

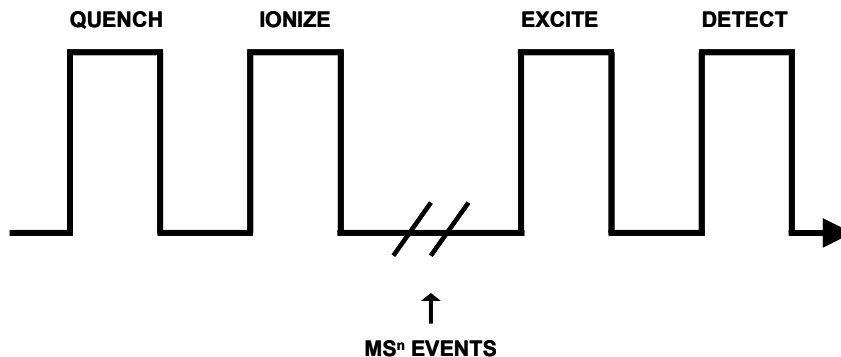


**FIGURE A.10** A typical experimental pulse sequence in FT-ICR MS.

unstable potential that will eject any ions present in the cell. The second pulse is an ionization event. Ion formation is fundamental to the FT-ICR pulse program and to mass spectrometry as neutral species cannot be detected. Traditionally, ionization occurred within the magnetic field via matrix assisted laser desorption ionization (MALDI) [8, 9, 52] or electron ionization (EI) [53]. The presence of a magnetic mirror [54], or barrier to ions entering the field from sources external to the magnet, initially precluded the concept of external ionization. This difficulty has been overcome by the introduction of ion injection devices [55-58], which will be discussed later.

In the simplest FT-ICR MS experiment, the quench and ionization pulses are followed by pulses for excitation and detection. This basic pulse sequence is sufficient to obtain an MS spectrum, or detection of ions generated from the primary ionization event. In order to develop more complex experiments additional pulses are required. The pulses are inserted between the primary ionization event and excitation pulses. These events lead to  $MS^n$  experiments where a precursor ion is fragmented into secondary ion

products, which can be further fragmented. The application of various  $MS^n$  techniques will be addressed later.

The previously described events of a broadband excitation event are also known as an rf chirp [21] shown in Figure A.11. The major drawback of the rf chirp is a lack of

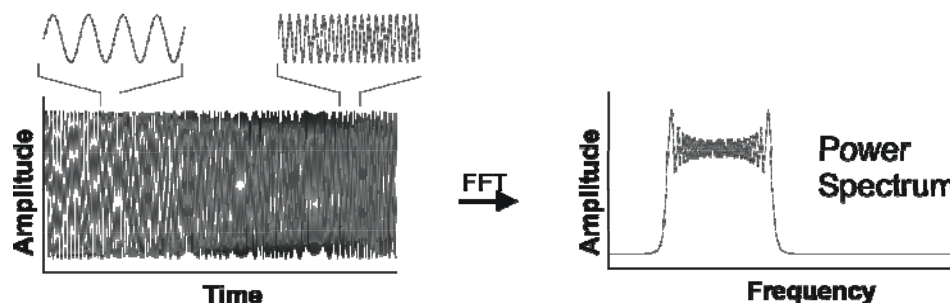


**FIGURE A.11** An rf chirp waveform utilized for excitation. The frequency sweep appears uniform in the time domain but the power spectrum resulting from a FT contains a non-uniform distribution that decreases slowly outside of the applied frequency range. (From Amster 1996 [24])

resolution and nearby ions will be excited even if they are outside of the specified frequency range because the excitation power decreases slowly at the edge of the waveform. Additionally, the excitation power applied within the chirp range is non-uniform, leading to a variation in excitation radius and excitation into fields of varying intensity if the applied field is inhomogeneous.

If the amplitude of an applied chirp was large enough, all resonant ions in the frequency range would be ejected from the cell. To leave a desired ion in the cell during

such an event, the frequency corresponding to its mass-to-charge can be removed from the scan. This notch allows for an excitation free window around a desired ion. The converse of this method can also be applied to eject ions of a specific mass-to-charge and is known as an rf burst. By scanning only a small frequency range, the resonant ions will be ejected leaving the other populations in the analyzer cell.

A second excitation method utilizes correlated harmonic excitation fields (CHEF) [59]. A modification of the rf chirp, the CHEF algorithm allows for correlation of the excitation field with the cyclotron frequency of a given ion to be selected. In doing so, off-resonance excitation is minimized by deliberate selection of the duration for the frequency step to coincide with nodes in the power spectrum for the selected ion. The resulting waveform, seen in Figure A.12, results in an ion experiencing an integer number of off-resonance excitation/relaxation periods prior to the end of the rf chirp.

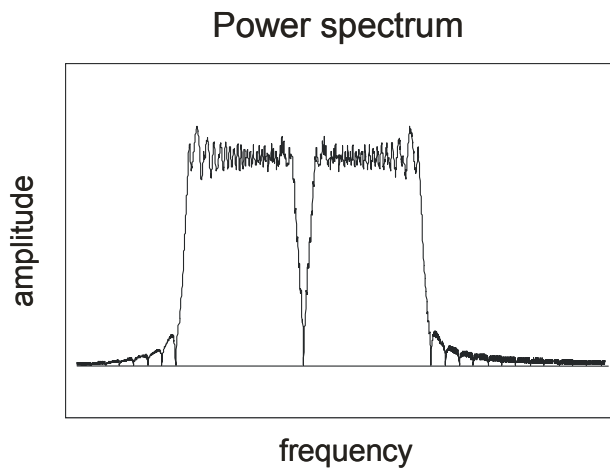


**FIGURE A.12** Modification of an rf chirp waveform to generate a CHEF isolation.

In order to develop a more ideal excitation waveform, the desired time domain excitation properties are specified in the frequency domain. This technique is known as a stored waveform inverse Fourier transform (SWIFT) [60]. An inverse Fourier Transform is applied to the frequency spectrum producing an excitation signal of uniform power across a specified range and minimal excitation of adjacent ions due to a nearly instantaneous decrease in power outside of the excitation window observed in Figure A.13. The SWIFT algorithm can be further tailored to allow for excitation and ejection by decreasing the power applied to an ion within the ejection frequency range resulting in an increase in cyclotron orbit instead of ejection. Recent applications of this technique have been shown to enable sub-ppm mass accuracy in complex mixtures [61, 62].

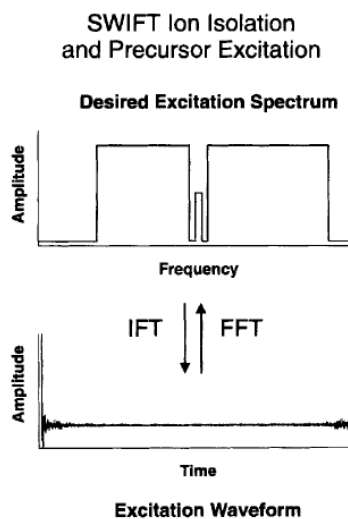


**FIGURE A.13** A SWIFT waveform generated for both excitation and isolation. To achieve the desired output, the waveform is constructed in the frequency domain and inverse Fourier transformed to produce the input. (*From Amster 1996 [24]*)

## PERFORMANCE

Although the FT-ICR mass analyzer possesses 10-100 times the resolving power of any other mass analyzer, there are still factors that can lead to a decrease in resolution. Two key factors have been mentioned previously during the discussion on heterodyne detection. The duration of the acquired transient and sampling rate of the transient have a direct effect on the peak resolution after the Fourier transform. A reduction in either will lead to undesirable peak broadening in the mass spectrum and a decrease in resolution. In-homogeneity of the magnetic field can also lead to reduced resolution in FT-ICR MS [63]. The primary effect of this in-homogeneity is the appearance of side-bands adjacent to the true isotopic peaks in the spectrum, shown in Figure A.14, due to increased z-axis oscillation or trapping motion. Proper shimming of the magnet upon installation minimizes this problem initially.

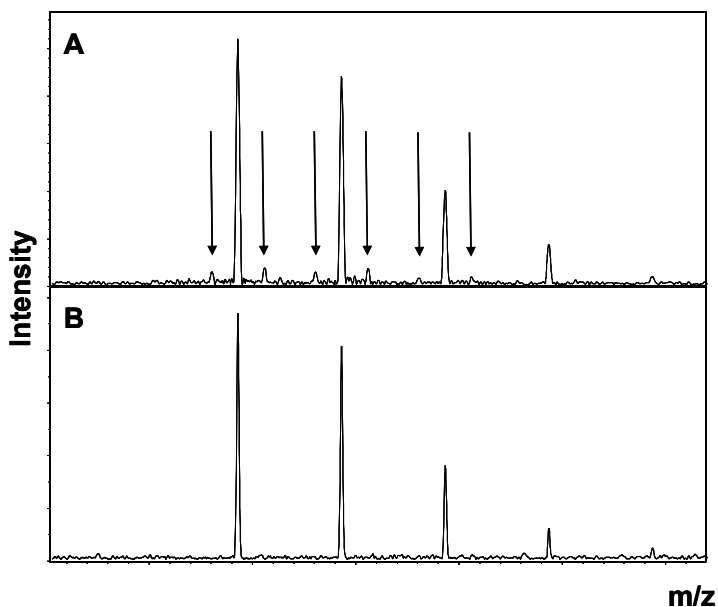


**FIGURE A.14** (A) A mass spectrum showing peak sidebands due to increased z-axis oscillations and (B) the same spectrum with sidebands eliminated.

Although it is generally not feasible to routinely increase the strength of the static magnetic field due to monetary constraints, there are multiple benefits to performing FT-ICR MS experiments at high fields. Most modern instruments operate with magnetic fields ranging from 4.7 T, 7 T, 9.4 T, to 12 T. Magnets of higher field (14.5 T and 18 T) exist but are not as widespread at this time. Currently, a 21 T superconducting solenoidal magnet is in preparation at the National High Magnetic Field Laboratory [64]. By operating at higher field, performance can either increase linearly or quadratically as shown in Figure A.15 [25].

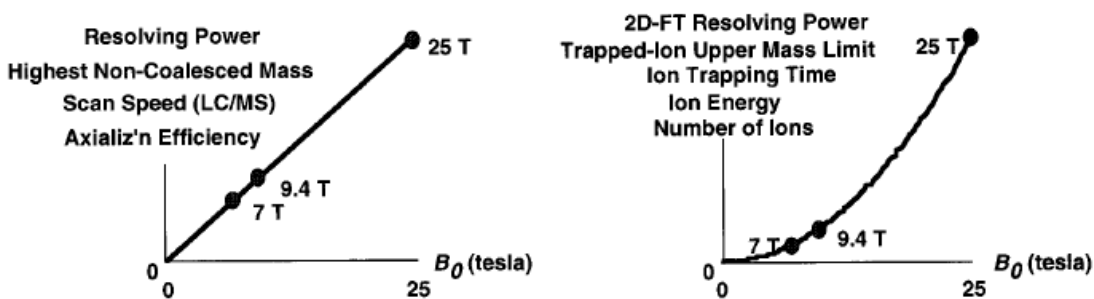


**FIGURE A.15** FTICR-MS figures of merit that are dependent upon magnetic field strength. (*From Marshall 1998 [25]*)

The applied electric potentials can also influence performance in FT-ICR MS. In the idealized case of a perfect Penning trap, the applied potential is perfectly hyperbolic and quadrupolar. When exciting ions to higher cyclotron orbit, the field encountered is entirely homogeneous. The observed cyclotron frequency is therefore independent of where an ion is located within the Penning trap. In most ion traps utilized for FT-ICR, the fields are inhomogeneous but are approximately quadrupolar at the center. By

exciting into different regions of the trap, the ions will experience varying field intensities. This inhomogeneity leads to differences in the measured cyclotron frequency and subsequently introduces mass errors.

Resolution can also be influenced by ions within the analyzer cell. For a high molecular weight, multiply charged ion from an electrospray ion source, there will be a large distribution in isotopes for a given ion. This population will initially be excited to a coherent cyclotron orbit, but will soon begin to lose coherence and spread in orbital position. As the image current of this distribution is monitored, the time-domain transient will only be observed when all of the population is coherently orbiting within the cell. These periods of signal are known as isotopic beats [65]. At all other times, the frequencies will interfere destructively leading to periods of no signal. The motions of the isotopes can be visualized as a superposition of sine waves, shown in Figure A.16, which exhibit periods of constructive and destructive interference. As the number of sinusoids increases in insets A-D, these beats become shorter yet more intense and the interval between beats increases. This pattern is analogous to increasing the number of isotopes for a given ion, with each isotope orbiting at a distinct frequency. In order to obtain isotopic resolution from such a transient, at least 2 beats must be sampled. As the beats increase in spacing, this requirement becomes a challenge due to signal damping.

Space charge effects can also influence the observed peaks in FT-ICR MS. If a large population is trapped within the analyzer, ion-ion repulsion will begin to influence the orbital behavior of the ions. These interactions will drive ions into inhomogeneous regions of the trapping field leading to peak shifts and/or broadening. Another reduction

in resolution arises due to ion population coalescence. Although the two populations will initially orbit at their cyclotron frequency, if the frequencies are comparable, the orbits

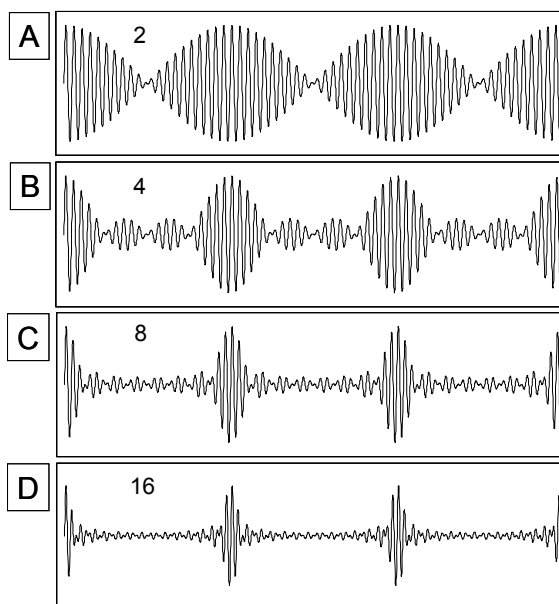


**FIGURE A.16** Simulated beat patterns due to the summation of sinusoids increasing from 2 in A to 16 in D. These patterns are analogous to beats observed in FTICR-MS transients where the interference of the evenly spaced frequencies of an ion's isotopes results in periods of no observable signal, which increase in duration as the number of isotopes increases. (From Wolff and Amster 2009 [66] )

will synchronize. This behavior results in the appearance of a single peak where two should be observed in the resulting mass spectrum. Both space charge effects and ion population coalescence can be minimized in the FT-ICR analyzer cell. By initially

decreasing the ion population entering the cell and decreasing the trapping voltage, the peaks will sharpen and separate as demonstrated in Figure A.17.

As previously described, the FT-ICR analyzer cell is a combination of geometric plates upon which varied electric potentials are applied. A variety of ion trap geometries

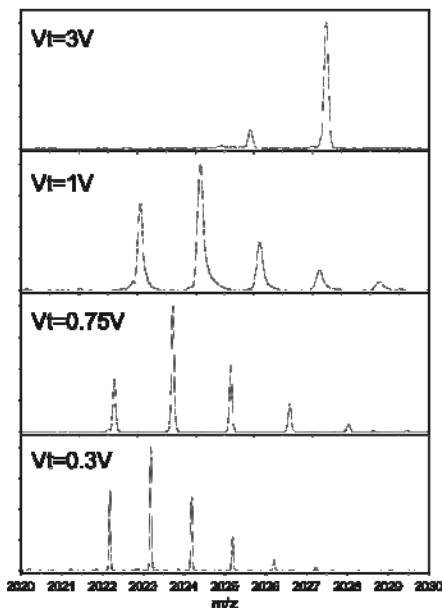


**FIGURE A.17** Peak coalescence due to the applied trapping voltage. As the voltage is increased (bottom to top), peaks gradually broaden and coalesce. (*From Amster 1996* [24])

and their principles have been covered in detail by Guan and Marshall [67]. Regardless of the cell design, these plates fall into three categories:

- 1) Trapping: to confine the ion motion axially along the magnetic field lines
- 2) Excitation: to increase the ion's cyclotron orbit
- 3) Detection: to measure the alternating image current imposed by an ion

Currently, the most widely utilized analyzer cells fall into three general categories, cubic, open-ended cylindrical, and closed-end cylindrical, as displayed in Figure A.18. Within each there are variations, but only the general properties of each will be discussed here.

As described in the section covering ion physics, the initial FT-ICR experiment was implemented with a drift analyzer cell. The main limitation of this design was the time an ion was available for detection within the cell. In order to increase the detection

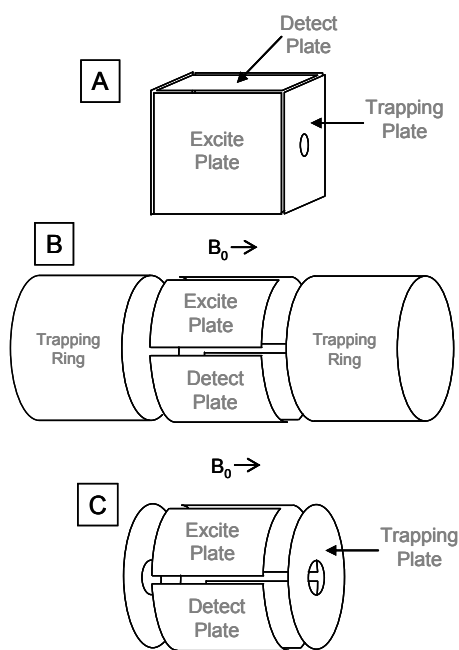


**FIGURE A.18** The three dominant cell designs in FTICR-MS (A) cubic (B) open-ended cylindrical and (C) closed-end cylindrical with the electrodes for trapping, excitation, and detection noted in each. (Adapted from Wolff and Amster 2009 [66])

time, a pair of trapping plates was placed on the ends of the cell to confine ions axially in the magnetic field [33]. This configuration increased the detection time from 1-2 milliseconds to 0.10 seconds, which allowed for acquisition of a longer transient and therefore increased the resolution. Prior to the implementation of trapping plates, ions were continuously generated external to the analyzer and transported to the cell for detection. This trapping mode converted the ICR experiment into a series of pulses, as described earlier. The ability to segment the experiment into pulses temporally removed the ionizing electron beam from detection therefore eliminating space charge effects on the ions in the cell. Finally, the pulsed mode of operation allowed for a single region to be utilized for ionization and detection, reducing the instrumental complexity. Comisarow later modified this initial design from the orthorhombic dimensions of the trapped cell to a cubic dimension [68], allowing for use in the solenoidal magnets.

The rectilinear geometry was later altered to that of a cylinder [69]. This shape is more amenable to the cylindrical bore of a solenoidal superconducting magnet [70]. In McIver's original trapped ion cell design, sidebands resulted from the coupling the cyclotron and trapping motions. By applying symmetrically overlapping d.c. and rf fields in their cylindrical design and decoupling the motions, Lee et al. were able to eliminate the sidebands. The coupling of cyclotron and trapping motion also leads to ion ejection along the z-axis [71-73]. If the applied frequency is larger than the cyclotron frequency during an excitation frequency sweep, the trapping motion will also be excited [74]. The excitation can then lead to ion neutralization by striking the trapping plates if the applied rf amplitude is sufficiently large.

Although closed cells can be manipulated electronically to enhance the applied potentials, the termination of field lines on adjacent perpendicular elements leads to inhomogeneous fields and introduces undesirable components such as a radial portion to the trapping potential and an axial portion to the excitation potential [75]. As recently discussed the axial portion leads to ion ejection along the z-axis while the radial portion introduces the magnetron motion [35] and reduces the observed cyclotron frequency as shown in Eqn. 5. The presence of trapping plates also limits the access to the interior of the cell to perform in-cell or near-cell ionization and reduces gas conductance in the UHV regime of the analyzer, which increases the pump-down time after an collision gas is introduced. To overcome these deficiencies, Beu and Laude introduced the open-ended cell to the FT-ICR MS community [76]. As shown in Figure A.19, the trapping potentials are extended collinear with the excite and detect region of the analyzer.

Although the termination of field lines at the perpendicular plate intersection was eliminated, the problem of axial ejection was not entirely eliminated because the trap was still of finite dimension. This problem was overcome by the capacitive coupling of the excitation plates to the trapping plates [76]. As seen in Figure A.19C, this coupling extends the excitation field beyond the trapping potential and eliminates the axial ejection pathway.

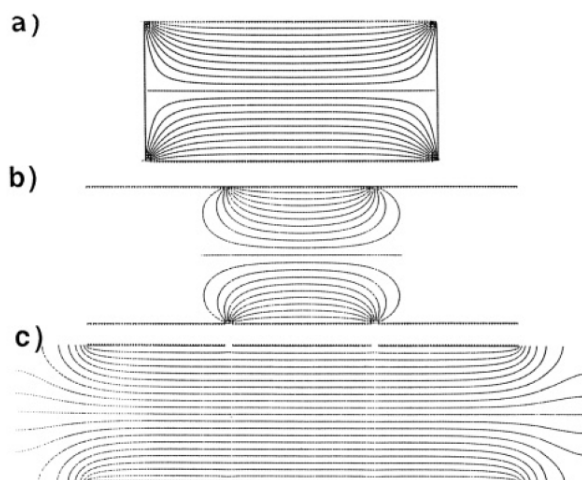


**FIGURE A.19** Isopotential surfaces due to finite dimensions of an analyzer cell in (a) closed end orthorhombic (b) open-ended cell and (c) capacitively-coupled open-ended cell. Shown in (c) the field lines extend beyond the dimensions of the cell, reducing axial ejection. (*From Beu and Laude 1992 [76]*)

The most recent significant development in FT-ICR MS analyzer cell technology is the closed-end cylindrical cell or the ‘Infinity Cell’ [77]. As the name suggests, the Infinity design attempts to emulate the properties of an infinitely long potential, which would have no portion of the excitation field parallel to the z-axis, therefore eliminating the possibility for axial ejection. By designing trapping plates that will produce such a potential, the cell will appear to be infinitely long to an ion trapped within the potential. Although this trap does include end plates that pose a physical barrier to ion injection and reduce conductance, these problems are minor compared to the advantage of a more uniform potential.

## TANDEM MASS SPECTROMETRY

The dominant modern application of the FT-ICR mass analyzer has been in the determination of biomolecule structure, due to the increased mass accuracy and resolution offered by the instrument. Although early FT-ICR MS experiments relied on ionization within the magnetic field, most modern experiments rely on external ionization methods such as electrospray [78] or high-pressure/intermediate pressure MALDI [79, 80]. With these developments, differential pumping was required to couple the high pressure regions of the ion sources to the ultra-high vacuum region of the analyzer and methods were needed to pass ions through the fringe field of the magnet and overcome the magnetic mirror effect [81]. For an ion to enter the field, one of two requirements must be met. It must possess a trajectory that aligns with the central axis of the field as it will not experience a Lorentz force or it must have some minimum kinetic energy to penetrate the field if it is off-axis. To hold ions on-axis, an rf-only multipole [55, 81] or electrostatic ion guide [58, 82, 83] is commonly employed. For off-axis ions, accelerating ion optics such as an Einzel lens can be utilized [56, 57].

Once an ion enters the fringe magnetic field, it must then enter the FT-ICR analyzer cell. The initial drift cells posed no barrier to entry based on the absence of trapping potentials. With the addition of trapping plates, another barrier is presented for an ion to enter the cell. In initial experiments, this potential was static and an ion would need to possess enough kinetic energy to overcome the potential barrier. The trapping potentials were later varied to increase the efficiency of transmission into the cell and trapping [84-86].

To increase the transmission of ions into the cell, it is possible to control the voltage applied to a trapping plate by a technique known as gated trapping [84]. By coordinating a decrease in the applied voltage with an ion pulse, ions of lower kinetic energy can enter the FT-ICR cell. Upon confinement, the voltage can be returned to its original value to regain the potential well for axial trapping. As discussed earlier, the application of a terminal trapping potential generates the trapping motion and a radially repulsive electric field. By applying a low-amplitude rf signal to the trapping plates instead of a static voltage, it is possible to reduce the radial repulsion by generating a potential with a zero-time average [86]. This technique is known as dynamic trapping. In addition to external ion sources, quadrupole mass analyzers and rf only multipoles have been coupled to FT-ICR analyzers to generate hybrid instruments [55], and example of which is shown in Figure A.20.

The FT-ICR analyzer functions sub-optimally once the ion density reaches  $10^6$  ions/cm<sup>3</sup>, based on the cell design and physical volume. The addition of a mass-selective quadrupole external to the cell allows for an ion population of interest to be mass-selected and then transferred to the analyzer, therefore allowing for increased performance by maintaining a population size lower than the space charge limit. This feature is especially useful in the analysis of heterogeneous mixtures in which the space charge limit is exceeded but very few components are above the limit of detection. Shown in Figure A.21, the MS of a mixture of glycosaminoglycan carbohydrates containing oligosaccharides varying in length, charge state, degree of sulfation, and sodium/hydrogen heterogeneity produces a spectrum with poor signal-to-noise. Signal improvement can be achieved by isolating regions of the mass spectrum

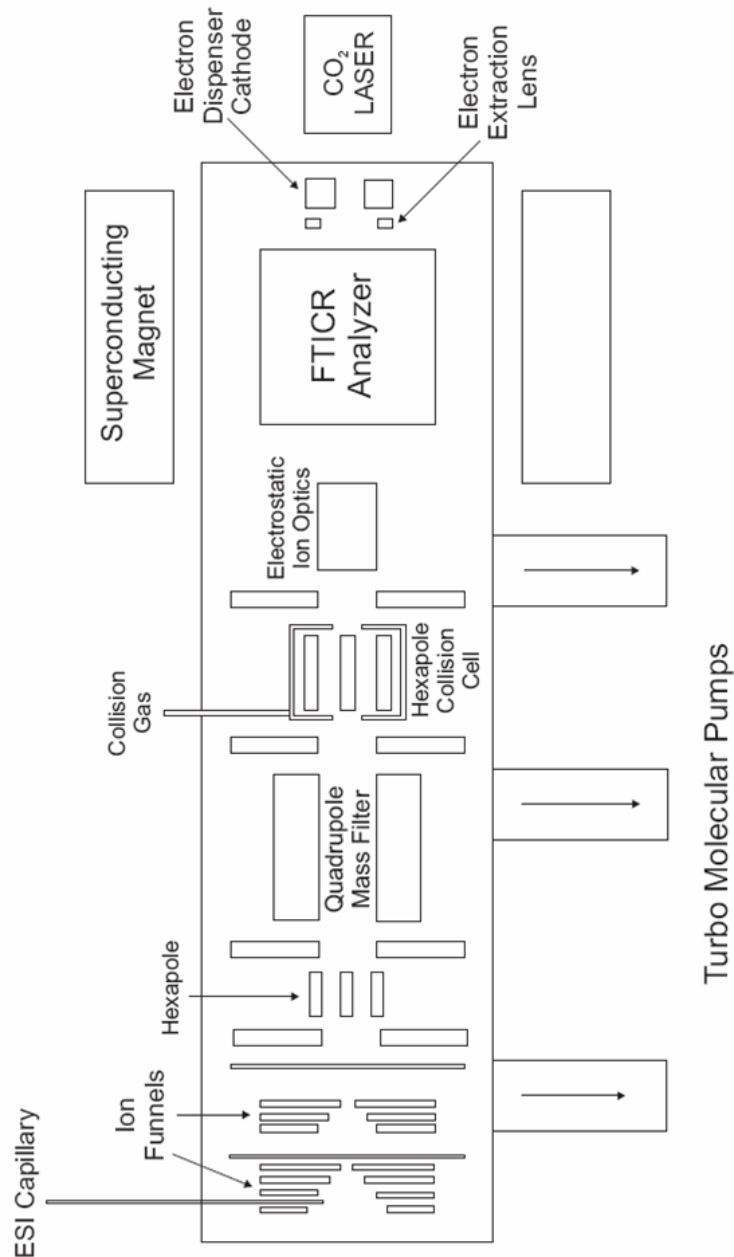


**FIGURE A.20** A schematic diagram of a modern hybrid FT-ICR instrument. Precursor ion isolation is enabled by the addition of a quadrupole mass filter exterior to the magnetic field. Tandem mass spectrometry can be performed outside of the analyzer (beam type CID in the hexapole collision cell) or in the analyzer (SORI-CAD, IRMPD, ECD, EDD).

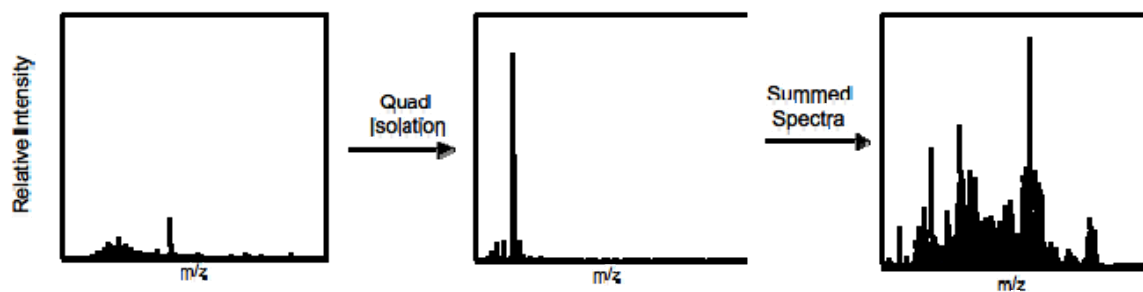


**FIGURE A.21** MS of a heterogeneous mixture of glycosaminoglycan oligosaccharides demonstrating low S/N and the benefit of a mass isolation window for signal improvement.

which maintains an ion number below the space charge limit of the analyzer. Once an ion has been mass selected, multiple packets can also accumulated by storage in an rf-only multipole. This period of accumulation also allows for increased signal-to-noise in the acquired spectrum.

The technological advancement of hybrid instruments now allows for spatially and temporally separated levels of mass spectrometry or  $MS^n$ . The general premise is that an ion of interest, or precursor, is mass selected and fragmented into product ions. It is then possible to select a fragment ion for further fragmentation. This iterative process can be repeated  $n$  times by coupling  $n$  mass analyzers in series, as is the case for an  $MS^2$  experiment on a TOF/TOF instrument where two time-of-flight mass analyzers are connected. By utilizing a single mass analyzer, such as a quadrupole, outside of the FT-ICR mass analyzer an hybrid  $MS^n$  setup is attained. Whereas, most mass analyzers operate spatially, the FT-ICR mass analyzer operates temporally. Ions can be continually

fragmented, a product isolated, and subsequently fragmented in the same space because the events are separated in time.  $MS^n$  can be achieved without the presence of an external quadrupole, but the hybrid combination allows for precursor selection and fragmentation through collisionally induced dissociation (CID) or collisionally activated dissociation (CAD) external to the mass analyzer.

After ionization, a mass filtering quadrupole is employed to select a precursor ion for analysis. This mass selected precursor is then passed into a multipole (hexa- or octa-) where it encounters a neutral collision gas, typically Argon. In the collision cell, ions lose energy and are cooled through low-energy collisions with the introduced gas. Additionally, ions can be accumulated in the multipole to increase the population that is delivered to the FT-ICR analyzer cell. By applying a DC potential to the multipole, more energetic collisions occur between the precursor and the collision gas leading to vibrational activation of the precursor. After some threshold energy has been reached, fragmentation ensues and the resulting products are ejected from the multipole and transferred to the FT-ICR analyzer for detection or subsequent isolation and further fragmentation.

While CID/CAD can be performed outside of the FT-ICR cell, it is also possible to induce fragmentation by collisions within the cell. Typically, the FT-ICR cell is at a sufficiently low pressure to minimize collisions and allow for a sufficient time period for a transient to be acquired. In order to achieve in-cell CAD, a collision gas must first be pulsed into the cell at high enough pressures to introduce collisions. This pressure is normally on the order of  $10^{-5}$  Torr. The ions must then be excited by an applied electric field that can either be on-resonance [40] or off-resonance [87] in relation to its natural

cyclotron frequency. This pulse excites the ion motion and increases the number of collisions between the ion and neutral collision gas. The application of an on-resonance pulse is limited in intensity by the threshold energy to eject an ion from the FT-ICR analyzer cell; therefore, only short duration pulses can be applied before ion ejection occurs. By increasing the applied magnetic field, this problem can be overcome, but that is not the most practical solution. In order to increase the collisional energy of an ion within the cell and eliminate the ejection pathway, it is possible to apply an off-resonance pulse, known as sustained off-resonance irradiation (SORI) [87]. This excitation results in periods of acceleration and deceleration in an ion's cyclotron orbit. It is therefore possible to excite a given ion for an extended period of time without ejecting it from the cell. Eventually, the ion will attain the threshold energy necessary for dissociation through collisions with the introduced gas and fragmentation will ensue.

Another threshold fragmentation method in FT-ICR MS is known as infrared multiple photon dissociation (IRMPD) [88-90]. In the application to FT-ICR MS, IRMPD is conducted within the analyzer cell by positioning a CO<sub>2</sub> laser, typically 10.6 μm in wavelength, on the lee side of the cell. This setup allows for on-axis irradiation of the ion cloud without interfering with the injection of ions into the magnetic field, as shown in Figure A.20. The basis of IRMPD is the introduction of multiple low energy photons into the analyzer cell. After absorption of the appropriate number of photons, the threshold for fragmentation will be reached shown in Figure A.22. [88, 89] Although

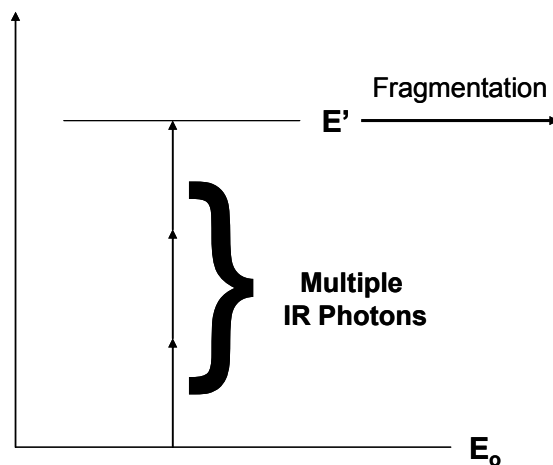


**FIGURE A.22** A depiction of the absorption of multiple IR photons by an ion at an initial energy state ( $E_0$ ) which increases the internal energy to some threshold state ( $E'$ ), leading to fragmentation.

this is the same fundamental mechanism as CID, it has several advantages. For CID conducted within the analyzer cell, there is a required delay to pump out the collision gas before image current detection adding to the acquisition time. Additionally, the efficiency of converting translational energy into internal energy and therefore leading to fragmentation varies based on the size of the ion. For CID in the analyzer, the internal energy gained is also dependent on the applied rf, the duration of the signal, and the collision gas pressure. These parameters are simplified by using IRMPD where the internal energy attained is attenuated by only the laser power and pulse duration.

The most recent development in MS/MS methods are based on the activation of ions with electrons, summarized in Figure A.23. Developed by Zubarev and McLafferty,

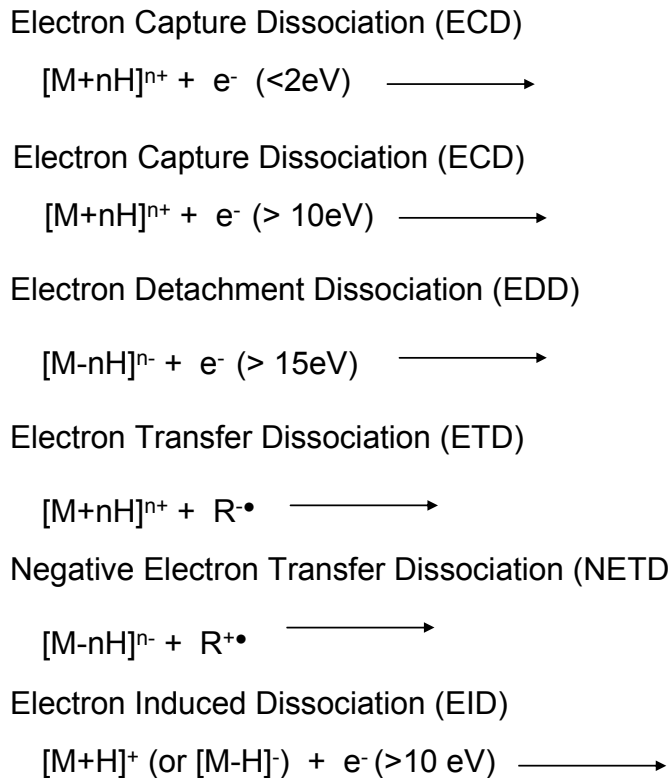


**FIGURE A.23** Electron-based activation techniques available in FT-ICR.

electron capture dissociation (ECD) relies on the injection of low-energy electrons ( $\sim 0.2$  eV) [91] into the analyzer cell from a heated or more recently indirectly heated filament, also seen in Figure A.20. Subsequent capture of an electron leads to a radical-driven fragmentation mechanism. Due to its proposed non-ergodic mechanism, ECD has been applied to a variety of biomolecules to determine the sites of labile modifications and to sequence proteins by top-down methods [92-94]. ECD can also be performed with moderate energy electrons ( $\sim 10$  eV). This variation is called hot ECD or HECD [95].

One of the main advantages of ECD is that it produces complementary fragments to those generated by threshold activation, illustrated in Figure A.24. Typically in CID or

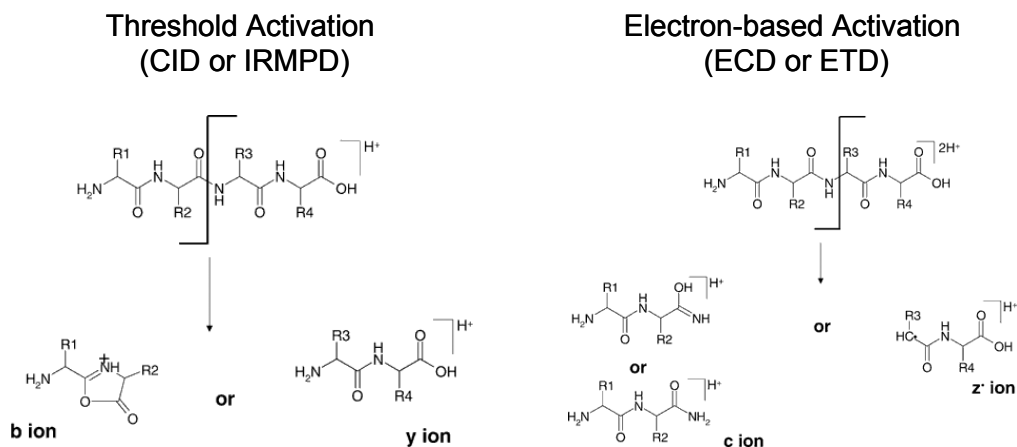


**FIGURE A.24** A comparison of the product ions generated from the threshold activation versus electron based activation of a model peptide. (*Adapted from Cooper 2004 [96]*)

IRMPD of peptides, b and y ions are produced whereas in ECD c and z (or z<sup>•</sup>) ions are generated. This complementary nature can also be seen in Figure A.25, where the three techniques have been applied to a tryptic peptide of bovine serum albumin (BSA).

Shortly after the introduction of ECD, McLafferty also introduced an advanced technique known as activated ion ECD (AI-ECD) [97]. Initial attempts to sequence large proteins (> 42 kDa), were limited by the number of backbone sites available for electron capture due to being concealed by higher order structures. By introducing a collision gas or IR laser pulse, noncovalent interactions are broken due to vibrational excitation, increasing the number of sites available for electron capture.

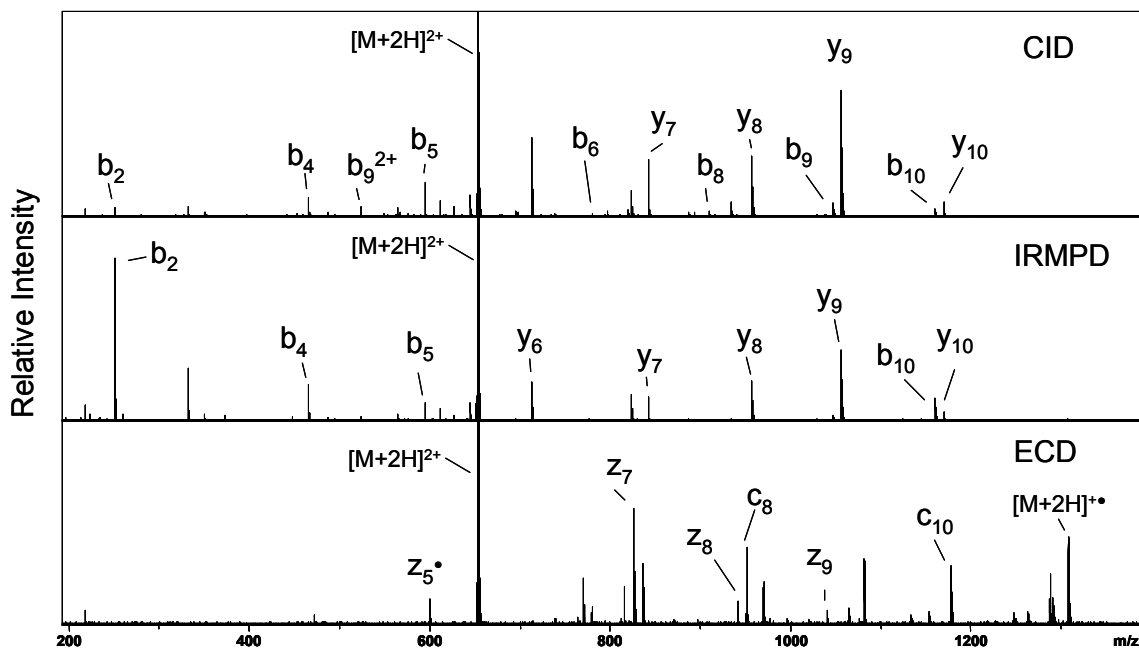


**FIGURE A.25** Tandem mass spectra from a doubly protonated tryptic peptide of bovine serum albumin (BSA) depicting the complementary nature of threshold ion activation (CID and IRMPD) and electron based activation (ECD).

Although ECD is an extremely useful MS/MS technique, it has two minor limitations. The first is the precursor ion must be multiply charged. If a singly charged ion were to capture an electron, the resulting product would be neutral and not observed. The selection of higher charges states ( $>2^+$ ) also increases the likelihood for capture by increasing the cross-section available for ion-electron interaction [98]. The second limitation is that ECD can only be applied to a precursor that is positive in charge. To overcome this deficiency, Zubarev developed an analogous technique known as electron detachment dissociation (EDD) [99] for polyanions. Unlike ECD, EDD employs

electrons that are typically 15-20 eV in energy. As the name implies, an electron is detached generating an odd-electron species and fragmentation results. EDD has been utilized for the analysis of a variety of deprotonated biomolecules including peptides [99], oligonucleotides [100, 101], and carbohydrates [102-104].

Electron-based activation can also be conducted via ion-ion reactions. Electron transfer dissociation (ETD) [105] and negative electron transfer dissociation (NETD) [106, 107] involve the reaction of multiply charge precursor ions with radical reagent ions and have recently been adapted to FT-ICR [108]. Although the majority of ions subjected to electron-based activation are multiply charged, it is possible to activate singly charged ions. This technique is known as electron induced dissociation (EID) [109] or electronic excitation dissociation (EED) [110] and involves the irradiation of the precursor ion with moderate to high energy electrons (> 10 eV).

## **ADVANTAGES/DISADVANTAGES**

The primary advantages of the FT-ICR MS mass analyzer are the well known benefits of high mass accuracy and resolution due to the non-destructive measurement of an ion's image current in the time domain. These key attributes enable the analysis of complex mixtures of biomolecules or hydrocarbons where many the isotopes of many ions may possess the same nominal mass. Aside from the direct benefits of the FT-ICR mass analyzer, there are many indirect advantages such as adaptability to virtually any ion source and implementation of a variety of ion activation methods for tandem mass spectrometry.

Although the FT-ICR analyzer is based on conceptually simple physics of ion cyclotron motion, the instrumental implementation is much more complex and costly. Currently, FT-ICR instruments are the most expensive mass spectrometers available and contain sophisticated control electronics that are typically not serviceable by most end-users. Aside from the initial investment, perpetual costs arise for magnet cryogenics. To maintain the field of a solenoidal superconducting magnet, liquid helium as well as liquid nitrogen are required. Cryogen costs can be minimized in the long term by recovery of boil-off and compression to re-liquefy the helium gas.

## **FUTURE PROSPECTS**

As with most scientific pursuits, continued advancement is supported by technological progress. This paradigm has certainly held true for the FT-ICR mass analyzer as significant advances in electronics have allowed for the acquisition and processing of data sets that would have seemed unattainable only a decade or two ago. The most recent advances relevant to FT-ICR MS are in the area of magnet technology. In the coming years, development of a 21 T solenoidal superconducting magnet at the NIMFL will be complete and the magnet put into service.

The implementation of new analyzer cell designs has seen recent resurgence in an attempt to attain a perfectly quadrupolar potential. The most recently published designs have revisited developments in the fundamental physics community where the electrodes are shimmed to approach quadrupolarity [111]. Advances in the fundamental understanding of FT-ICR phenomena are also an area of continued interest. To achieve routine sub-ppm mass accuracy, it is necessary to thoroughly understand the source of

frequency shifts in FT-ICR such as space charge and image charge interactions. These issues can be studied experimentally in the laboratory, but multi-particle ion trajectory simulations [112-114] have recently been employed to gain insight into these effects by providing a highly controlled environment [115].

## REFERENCES

1. Comisarow, M. B. and Marshall, A. G., Fourier Transform Ion Cyclotron Resonance Spectroscopy. *Chem. Phys. Lett.* **1974**, *25*, 282-283.
2. Mann, M. and Kelleher, N. L., Precision proteomics: The case for high resolution and high mass accuracy. *Proceedings of the National Academy of Sciences* **2008**, *105*, 18132-18138.
3. Zubarev, R. and Mann, M., On the Proper Use of Mass Accuracy in Proteomics. *Molecular & Cellular Proteomics* **2007**, *6*, 377-381.
4. Haas, W.; Faherty, B. K.; Gerber, S. A.; Elias, J. E.; Beausoleil, S. A.; Bakalarski, C. E.; Li, X.; VillÃ©n, J. and Gygi, S. P., Optimization and Use of Peptide Mass Measurement Accuracy in Shotgun Proteomics. *Molecular & Cellular Proteomics* **2006**, *5*, 1326-1337.
5. Marshall, A. G. and Rodgers, R. P., Petroleomics: The Next Grand Challenge for Chemical Analysis. *Acc. Chem. Res.* **2003**, *37*, 53-59.
6. Rodgers, R. P.; Schaub, T. M. and Marshall, A. G., Petroleomics: MS Returns to Its Roots. *Anal. Chem.* **2005**, *77*, 20 A-27 A.
7. Fenn, J. B.; Mann, M.; Meng, C. K.; Wong, S. F. and Whitehouse, C. M., Electrospray ionization for mass spectrometry of large biomolecules. *Science* **1989**, *246*, 64-71.
8. Karas, M. and Hillenkamp, F., Laser Desorption Ionization Of Proteins With Molecular Masses Exceeding 10,000 Daltons. *Anal. Chem.* **1988**, *60*, 2299-2301.

9. Tanaka, K.; Waki, H.; Ido, Y.; Akita, S.; Yoshida, Y.; Yoshida, T. and Matsuo, T., Protein And Polymer Analyses Up To  $m/z$  100,000 By Laser Ionization Time-Of-Flight Mass Spectrometry. *Rapid Commun. Mass Spectrom.* **1988**, *2*, 151-153.
10. Baldeschwieler, J. D., Ion Cyclotron Resonance Spectroscopy. *Science* **1968**, *159*, 263-273.
11. Beauchamp, J. L., Ion Cyclotron Resonance Spectroscopy. *Annu. Rev. Phys. Chem.* **1971**, *22*, 527-561.
12. Loo, J. A.; Quinn, J. P.; Ryu, S. I.; Henry, K. D.; Senko, M. W. and McLafferty, F. W., High-resolution tandem mass spectrometry of large biomolecules. *Proc. Natl. Acad. Sci. U. S. A.* **1992**, *89*, 286-289.
13. Lawrence, E. O. and Edlefsen, N. E., On the Production of High Speed Protons. *Science* **1930**, *72*, 376.
14. Lawrence, E. O. and Livingston, M. S., The Production of High Speed Light Ions Without the Use of High Voltages. *Physical Review* **1932**, *40*, 19.
15. Hipple, J. A.; Sommer, H. and Thomas, H. A., A Precise Method of Determining the Faraday by Magnetic Resonance. *Physical Review* **1949**, *76*, 1877.
16. Sommer, H.; Thomas, H. A. and Hipple, J. A., The Measurement of eM by Cyclotron Resonance. *Physical Review* **1951**, *82*, 697.
17. Wobschall, D., Ion Cyclotron Resonance Spectrometer. *Rev. Sci. Instrum.* **1965**, *36*, 466-475.
18. Anders, L. R.; Beauchamp, J. L.; Dunbar, R. C. and Baldeschwieler, J. D., ION-CYCLOTRON DOUBLE RESONANCE. *J. Chem. Phys.* **1966**, *45*, 1062-&.
19. McLafferty, F. W., Tandem mass spectrometry. *Science* **1981**, *214*, 280-287.

20. Ernst, R. R. and Anderson, W. A., Application of Fourier Transform Spectroscopy to Magnetic Resonance. *Rev. Sci. Instrum.* **1966**, *37*, 93-102.
21. Comisarow, M. B. and Marshall, A. G., Frequency-Sweep Fourier Transform Ion Cyclotron Resonance Spectroscopy. *Chem. Phys. Lett.* **1974**, *26*, 489-490.
22. Comisarow, M. B., Signal modeling for ion cyclotron resonance. *The Journal of Chemical Physics* **1978**, *69*, 4097-4104.
23. Comisarow, **M. B.** and **Marshall, A. G.**, The Early Development of Fourier Transform Ion Cyclotron Resonance (FT-ICR) Spectroscopy. *J. Mass Spec.* **1996**, *31*, 581-585.
24. Amster, I. J., Fourier Transform Mass Spectrometry. *J. Mass Spec.* **1996**, *31*, 1325-1337.
25. Marshall, A. G.; Hendrickson, C. L. and Jackson, G. S., Fourier transform ion cyclotron resonance mass spectrometry: A primer. *Mass Spectrom. Rev.* **1998**, *17*, 1-35.
26. Marshall, A. G., Fourier Transform Ion Cyclotron Resonance Mass Spectrometry. *Acc. Chem. Res.* **1985**, *18*, 316-322.
27. Marshall, A. G. and Verdun, F. R., Fourier Transforms in NMR, Optical, and Mass Spectrometry: A User's Handbook, Elsevier: Amsterdam, 1990.
28. Mitchell, D. W., Theory of trapped ion motion in the non-quadrupolar electrostatic potential of a cubic ion cyclotron resonance cell. *Int. J. Mass Spectrom. Ion Processes* **1995**, *142*, 1-22.
29. Penning, F. M., *Physica (Utrecht)* **1936**, *3*,

30. Brown, L. S. and Gabrielse, G., Geonium theory: Physics of a single electron or ion in a Penning trap. *Reviews of Modern Physics* **1986**, 58, 233.
31. Rempel, D. L.; Ledford, E. B.; Huang, S. K. and Gross, M. L., Parametric Mode Operation Of A Hyperbolic Penning Trap For Fourier Transform Mass Spectrometry. *Anal. Chem.* **1987**, 59, 2527-2532.
32. Shi, S. D. H.; Drader, J. J.; Freitas, M. A.; Hendrickson, C. L. and Marshall, A. G., Comparison and interconversion of the two most common frequency-to-mass calibration functions for Fourier transform ion cyclotron resonance mass spectrometry. *Int. J. Mass Spectrom.* **2000**, 195-196, 591-598.
33. McIver, R. T., A Trapped Ion Analyzer Cell For Ion Cyclotron Resonance Spectroscopy. *Rev. Sci. Instrum.* **1970**, 41, 555-&.
34. Sharp, T. E.; Eyler, J. R. and Li, E., Trapped-ion motion in ion cyclotron resonance spectroscopy. *International Journal or Mass Spectrometry and Ion Physics* **1972**, 9, 421-439.
35. Dunbar, R. C.; Chen, J. H. and Hays, J. D., Magnetron motion of ions in the cubical ICR cell. *Int. J. Mass Spectrom. Ion Processes* **1984**, 57, 39-56.
36. Francl, T. J.; Fukuda, E. K. and McIver, R. T., A diffusion model for nonreactive ion loss in pulsed ion cyclotron resonance experiments. *International Journal or Mass Spectrometry and Ion Physics* **1983**, 50, 151-167.
37. Delong, S. E.; Mitchell, D. W.; Cherniak, D. J. and Harrison, T. M., z-axis oscillation sidebands in FT/ICR mass spectra. *Int. J. Mass Spectrom. Ion Processes* **1989**, 91, 273-282.

38. Alemann, M.; Kellerhals, H. P. and Wanczek, K. P., Sidebands in the ICR spectrum and their application for exact mass determination. *Chem. Phys. Lett.* **1981**, *84*, 547-551.
39. Cody, R. B.; Burnier, R. C. and Freiser, B. S., Collision-Induced Dissociation with Fourier Transform Mass Spectrometry. *Anal. Chem.* **1982**, *54*, 96-101.
40. Cody, R. B. and Freiser, B. S., Collision-Induced Dissociation In A Fourier-Transform Mass-Spectrometer. *Int. J. Mass Spectrom. Ion Processes* **1982**, *41*, 199-204.
41. Francl, T. J.; Sherman, M. G.; Hunter, R. L.; Locke, M. J.; Bowers, W. D. and McIver, R. T., Experimental-Determination of the Effects of Space-Charge on Ion-Cyclotron Resonance Frequencies. *Int. J. Mass Spectrom. Ion Processes* **1983**, *54*, 189-199.
42. Jeffries, J. B.; Barlow, S. E. and Dunn, G. H., Theory of Space-Charge Shift of Ion-Cyclotron Resonance Frequencies. *Int. J. Mass Spectrom. Ion Processes* **1983**, *54*, 169-187.
43. Marshall, A. G. and Hendrickson, C. L., Fourier transform ion cyclotron resonance detection: principles and experimental configurations. *Int. J. Mass Spectrom.* **2002**, *215*, 59-75.
44. Ledford, E. B.; Rempel, D. L. and Gross, M. L., Space charge effects in Fourier transform mass spectrometry. II. Mass calibration. *Anal. Chem.* **1984**, *56*, 2744-2748.
45. Burton, R. D.; Matuszak, K. P.; Watson, C. H. and Eyler, J. R., Exact mass measurements using a 7 tesla fourier transform ion cyclotron resonance mass

- spectrometer in a good laboratory practices-regulated environment. *J. Am. Soc. Mass Spectrom.* **1999**, *10*, 1291-1297.
46. Masselon, C.; Tolmachev, A. V.; Anderson, G. A.; Harkewicz, R. and Smith, R. D., Mass Measurement Errors Caused by "Local" Frequency Perturbations in FTICR Mass Spectrometry. *J. Am. Soc. Mass Spectrom.* **2002**, *13*, 99-106.
47. Schweikhard, L.; Guan, S. and Marshall, A. G., Quadrupolar excitation and collisional cooling for axialization and high pressure trapping of ions in Fourier transform ion cyclotron resonance mass spectrometry. *Int. J. Mass Spectrom. Ion Processes* **1992**, *120*, 71-83.
48. Savard, G.; Becker, S.; Bollen, G.; Kluge, H. J.; Moore, R. B.; Otto, T.; Schweikhard, L.; Stolzenberg, H. and Wiess, U., A new cooling technique for heavy ions in a Penning trap. *Phys. Lett. A* **1991**, *158*, 247-252.
49. Speir, J. P.; Gorman, G. S.; Pitsenberger, C. C.; Turner, C. A.; Wang, P. P. and Amster, I. J., Remeasurement of ions using quadrupolar excitation Fourier transform ion cyclotron resonance spectrometry. *Anal. Chem.* **1993**, *65*, 1746-1752.
50. Hendrickson, C. L.; Drader, J. J. and Laude, J. D. A., Simplified application of quadrupolar excitation in Fourier transform ion cyclotron resonance mass spectrometry. *J. Am. Soc. Mass Spectrom.* **1995**, *6*, 448-452.
51. Dahl, D. A., SIMION for the personal computer in reflection. *Int. J. Mass Spectrom.* **2000**, *200*, 3-25.

52. Karas, M.; Bachmann, D.; Bahr, U. and Hillenkamp, F., Matrix-Assisted Ultraviolet Laser Desorption Of Non-Volatile Compounds. *Int. J. Mass Spectrom. Ion Processes* **1987**, *78*, 53-68.
53. McLafferty, F. W. and Turecek, F., Interpretation of Mass Spectra, 4th; University Science Books: Mill Valley, CA, 1993.
54. Chen, F. F., 2nd; Plenum Press: New York, 1984.
55. McIver, R. T.; Hunter, R. L. and Bowers, W. D., Coupling A Quadrupole Mass-Spectrometer And A Fourier-Transform Mass-Spectrometer. *Int. J. Mass Spectrom. Ion Processes* **1985**, *64*, 67-77.
56. Kofel, P.; Allemann, M.; Kellerhals, H. and Wanczek, K. P., External generation of ions in ICR spectrometry. *Int. J. Mass Spectrom. Ion Processes* **1985**, *65*, 97-103.
57. Alford, J. M.; Williams, P. E.; Trevor, D. J. and Smalley, R. E., Metal cluster ion cyclotron resonance. Combining supersonic metal cluster beam technology with FT-ICR. *Int. J. Mass Spectrom. Ion Processes* **1986**, *72*, 33-51.
58. Limbach, P. A.; Marshall, A. G. and Wang, M., An electrostatic ion guide for efficient transmission of low energy externally formed ions into a Fourier transform ion cyclotron resonance mass spectrometer. *Int. J. Mass Spectrom. Ion Processes* **1993**, *125*, 135-143.
59. de Koning, L. J.; Nibbering, N. M. M.; van Orden, S. L. and Laukien, F. H., Mass selection of ions in a Fourier transform ion cyclotron resonance trap using correlated harmonic excitation fields (CHEF). *Int. J. Mass Spectrom.* **1997**, *165*, 209-219.

60. Marshall, A. G.; Wang, T. C. L. and Ricca, T. L., Tailored Excitation For Fourier-Transform Ion-Cyclotron Resonance Mass-Spectrometry. *J. Am. Chem. Soc.* **1985**, *107*, 7893-7897.
61. Kaiser, N. K.; Savory, J. J.; McKenna, A. M.; Hendrickson, C. L. and Marshall, A. G., Tailored Ion Spatial Distribution in FT-ICR MS for Improved Analysis of Complex Mixtures, *Proceedings of the 58th ASMS Conference on Mass Spectrometry and Allied Topics*, Salt Lake City, UT, 2010.
62. Jing, L.; Li, C.; Wong, R. L.; Kaplan, D. A. and Amster, I. J., Improved Mass Accuracy for Higher Mass Peptides by Using SWIFT Excitation for MALDI-FTICR Mass Spectrometry. *J. Am. Soc. Mass Spectrom.* **2008**, *19*, 76-81.
63. Mitchell, D. W.; Rockwood, A. L. and Smith, R. D., Frequency-Shifts and Modulation Effects Due To Solenoidal Magnetic-Field Inhomogeneities in Ion-Cyclotron Mass-Spectrometry. *Int. J. Mass Spectrom.* **1995**, *141*, 101-116.
64. Marshall, A. G.; Hendrickson, C. L.; Ernmetta, M. R.; Rodgers, R. P.; Blakney, G. T. and Nilsson, C. L., Fourier transform ion cyclotron resonance: state of the art. *Eur. J. Mass Spectrom.* **2007**, *13*, 57-59.
65. Hofstadler, S. A.; Bruce, J. E.; Rockwood, A. L.; Anderson, G. A.; Winger, B. E. and Smith, R. D., Isotopic beat patterns in Fourier transform ion cyclotron resonance mass spectrometry: implications for high resolution mass measurements of large biopolymers. *Int. J. Mass Spectrom. Ion Processes* **1994**, *132*, 109-127.
- 66.

67. Guan, S. H. and Marshall, A. G., Ion Traps For Fourier-Transform Ion-Cyclotron Resonance Mass-Spectrometry - Principles And Design Of Geometric And Electric Configurations. *Int. J. Mass Spectrom. Ion Processes* **1995**, *146*, 261-296.
68. Comisarow, M. B., Cubic trapped-ion cell for ion cyclotron resonance. *International Journal of Mass Spectrometry and Ion Physics* **1981**, *37*, 251-257.
69. Lee, S. H.; Wanczek, K. P. and Hartmann, H., A New Cylindrical Trapped Ion ICR Cell. *Advances in Mass Spectrometry* **1980**, *8B*, 1645-1649.
70. Allemann, M.; Kellerhals, H. and Wanczek, K. P., A new fourier-transform mass spectrometer with a superconducting magnet. *Chem. Phys. Lett.* **1980**, *75*, 328-331.
71. Huang, S. K.; Rempel, D. L. and Gross, M. L., Mass-dependent z-excitation of ions in cubic traps used in FTMS. *Int. J. Mass Spectrom. Ion Processes* **1986**, *72*, 15-31.
72. Rempel, D. L.; Huang, S. K. and Gross, M. L., Relation of signal sensitivity and ion z-motion in cubic cells. Theory and implication for ion kinetic studies. *Int. J. Mass Spectrom. Ion Processes* **1986**, *70*, 163-184.
73. Allemann, M.; Kofel, P.; Kellerhals, H. and Wanczek, K. P., Ejection of low-mass charged particles in high magnetic field ICR spectrometers. *Int. J. Mass Spectrom. Ion Processes* **1987**, *75*, 47-54.
74. Kofel, P.; Allemann, M.; Kellerhals, H. and Wanczek, K. P., Coupling of axial and radial motions in ICR cells during excitation. *Int. J. Mass Spectrom. Ion Processes* **1986**, *74*, 1-12.

75. Beu, S. C. and Laude, D. A., Open Trapped Ion Cell Geometries For Fourier-Transform Ion-Cyclotron Resonance Mass-Spectrometry. *Int. J. Mass Spectrom. Ion Processes* **1992**, *112*, 215-230.
76. Beu, S. C. and Laude, D. A., Elimination Of Axial Ejection During Excitation With A Capacitively Coupled Open Trapped-Ion Cell For Fourier-Transform Ion-Cyclotron Resonance Mass-Spectrometry. *Anal. Chem.* **1992**, *64*, 177-180.
77. Caravatti, P. and Allemann, M., The Infinity Cell - A New Trapped-Ion Cell with Radiofrequency Covered Trapping Electrodes for Fourier-Transform Ion-Cyclotron Resonance Mass-Spectrometry. *Org. Mass Spectrom.* **1991**, *26*, 514-518.
78. Henry, K. D.; Williams, E. R.; Wang, B. H.; McLafferty, F. W.; Shabanowitz, J. and Hunt, D. F., Fourier-Transform Mass Spectrometry of Large Molecules by Electrospray Ionization. *Proc. Natl. Acad. Sci. U. S. A.* **1989**, *86*, 9075-9078.
79. Hettich, R. L. and Buchanan, M. V., Matrix-assisted laser desorption fourier transform mass spectrometry for the structural examination of modified nucleic acid constituents. *Int. J. Mass Spectrom. Ion Processes* **1991**, *111*, 365-380.
80. Hettich, R. L. and Buchanan, M. V., Investigation of UV matrix-assisted laser desorption Fourier transform mass spectrometry for peptides. *J. Am. Soc. Mass Spectrom.* **1991**, *2*, 22-28.
81. McIver, R. T., Trajectory Calculations For Axial Injection Of Ions Into A Magnetic-Field - Overcoming The Magnetic-Mirror Effect With An Rf Quadrupole Lens. *Int. J. Mass Spectrom. Ion Processes* **1990**, *98*, 35-50.

82. Marto, J. A.; Marshall, A. G.; May, M. A. and Limbach, P. A., Ion Trajectories In An Electrostatic Ion Guide For External Ion-Source Fourier-Transform Ion-Cyclotron Resonance Mass-Spectrometry. *J. Am. Soc. Mass Spectrom.* **1995**, *6*, 936-946.
83. Guan, S.; Pasa-Tolic, L.; Marshall, A. G. and Xiang, X., Off-axis injection into an ICR ion trap: a means for efficient capture of a continuous beam of externally generated ions. *Int. J. Mass Spectrom. Ion Processes* **1994**, *139*, 75-86.
84. Dey, M.; Castoro, J. A. and Wilkins, C. L., Determination of Molecular Weight Distributions of Polymers by MALDI-FTMS. *Anal. Chem.* **1995**, *67*, 1575-1579.
85. Hofstadler, S. A.; Wu, Q.; Bruce, J. E.; Chen, R. and Smith, R. D., Enhanced accumulated trapping efficiency using an auxiliary trapping electrode in an external source Fourier transform ion cyclotron resonance mass spectrometer. *Int. J. Mass Spectrom. Ion Processes* **1995**, *142*, 143-150.
86. Gorshkov, M. V.; Guan, S. and Marshall, A. G., Dynamic ion trapping for Fourier-transform ion cyclotron resonance mass spectrometry: Simultaneous positive- and negative-ion detection. *Rapid Commun. Mass Spectrom.* **1992**, *6*, 166-172.
87. Gauthier, J. W.; Trautman, T. R. and Jacobson, D. B., Sustained Off-Resonance Irradiation For Collision-Activated Dissociation Involving Fourier-Transform Mass-Spectrometry - Collision-Activated Dissociation Technique That Emulates Infrared Multiphoton Dissociation. *Anal. Chim. Acta* **1991**, *246*, 211-225.

88. Basov, N. G.; Markin, E. P.; Oraevski, A. N.; Pankratov, A. V. and Shachkov, A. N., Stimulation of Chemical Processes by Infrared Laser Radiation. *JETP Letters* **1971**, *14*, 165-169.
89. Woodin, R. L.; Bomse, D. S. and Beauchamp, J. L., Multiphoton dissociation of molecules with low power continuous wave infrared laser radiation. *J. Am. Chem. Soc.* **1978**, *100*, 3248-3250.
90. Little, D. P.; Speir, J. P.; Senko, M. W.; O'Connor, P. B. and McLafferty, F. W., Infrared Multiphoton Dissociation of Large Multiply Charged Ions for Biomolecule Sequencing. *Anal. Chem.* **1994**, *66*, 2809-2815.
91. Zubarev, R. A.; Kelleher, N. L. and McLafferty, F. W., Electron capture dissociation of multiply charged protein cations. A nonergodic process. *J. Am. Chem. Soc.* **1998**, *120*, 3265-3266.
92. Sze, S. K.; Ge, Y.; Oh, H. and McLafferty, F. W., Top-down mass spectrometry of a 29-kDa protein for characterization of any posttranslational modification to within one residue. *Proceedings of the National Academy of Sciences* **2002**, 251691898.
93. Kelleher, N. L.; Zubarev, R. A.; Bush, K.; Furie, B.; Furie, B. C.; McLafferty, F. W. and Walsh, C. T., Localization of Labile Posttranslational Modifications by Electron Capture Dissociation: The Case of  $\gamma$ -Carboxyglutamic Acid. *Anal. Chem.* **1999**, *71*, 4250-4253.
94. Kelleher, N. L.; Lin, H. Y.; Valaskovic, G. A.; Aaserud, D. J.; Fridriksson, E. K. and McLafferty, F. W., Top Down versus Bottom Up Protein Characterization by

- Tandem High-Resolution Mass Spectrometry. *J. Am. Chem. Soc.* **1999**, *121*, 806-812.
95. Kjeldsen, F.; Haselmann, K. F.; Budnik, B. A.; Jensen, F. and Zubarev, R. A., Dissociative capture of hot (3-13 eV) electrons by polypeptide polycations: an efficient process accompanied by secondary fragmentation. *Chem. Phys. Lett.* **2002**, *356*, 201-206.
96. Helen, J. C.; Kristina, H. and Alan, G. M., The role of electron capture dissociation in biomolecular analysis. *Mass Spectrom. Rev.* **2005**, *24*, 201-222.
97. Horn, D. M.; Ge, Y. and McLafferty, F. W., Activated Ion Electron Capture Dissociation for Mass Spectral Sequencing of Larger (42 kDa) Proteins. *Anal. Chem.* **2000**, *72*, 4778-4784.
98. Kruger, N. A.; Zubarev, R. A.; Horn, D. M. and McLafferty, F. W., Electron capture dissociation of multiply charged peptide cations. *Int. J. Mass Spectrom.* **1999**, *187*, 787-793.
99. Budnik, B. A.; Haselmann, K. F. and Zubarev, R. A., Electron detachment dissociation of peptide di-anions: an electron-hole recombination phenomenon. *Chem. Phys. Lett.* **2001**, *342*, 299-302.
100. Yang, J. and Hakansson, K., Fragmentation of Oligoribonucleotides from Gas-Phase Ion-Electron Reactions. *J. Am. Soc. Mass Spectrom.* **2006**, *17*, 1369-1375.
101. Yang, J.; Mo, J.; Adamson, J. T. and Hakansson, K., Characterization of Oligodeoxynucleotides by Electron Detachment Dissociation Fourier Transform Ion Cyclotron Resonance Mass Spectrometry. *Anal. Chem.* **2005**, *77*, 1876-1882.

102. Wolff, J. J.; Amster, I. J.; Chi, L. and Linhardt, R. J., Electron Detachment Dissociation of Glycosaminoglycan Tetrasaccharides. *J. Am. Soc. Mass Spectrom.* **2007**, *18*, 234-244.
103. Adamson, J. T. and Hakansson, K., Electron Detachment Dissociation of Neutral and Sialylated Oligosaccharides. *J. Am. Soc. Mass Spectrom.* **2007**, *18*, 2162-2172.
104. Wolff, J. J.; Laremore, T. N.; Busch, A. M.; Linhardt, R. J. and Amster, I. J., Electron Detachment Dissociation of Dermatan Sulfate Oligosaccharides. *J. Am. Soc. Mass Spectrom.* **2008**, *19*, 294-304.
105. Syka, J. E. P.; Coon, J. J.; Schroeder, M. J.; Shabanowitz, J. and Hunt, D. F., Peptide and protein sequence analysis by electron transfer dissociation mass spectrometry. *Proc. Natl. Acad. Sci. U. S. A.* **2004**, *101*, 9528-9533.
106. Herron, W. J.; Goeringer, D. E. and McLuckey, S. A., Gas-Phase Electron Transfer Reactions from Multiply-Charged Anions to Rare Gas Cations. *J. Am. Chem. Soc.* **1995**, *117*, 11555-11562.
107. Coon, J. J.; Shabanowitz, J.; Hunt, D. F. and Syka, J. E. P., Electron Transfer Dissociation of Peptide Anions. *J. Am. Soc. Mass Spectrom.* **2005**, *16*, 880-882.
108. Kaplan, D. A.; Hartmer, R.; Speir, J. P.; Stoermer, C.; Gumerov, D.; Easterling, M., L. ; Brekenfeld, A.; Kim, T.; Laukien, F. and Park, M. A., Electron transfer dissociation in the hexapole collision cell of a hybrid quadrupole-hexapole Fourier transform ion cyclotron resonance mass spectrometer. *Rapid Commun. Mass Spectrom.* **2008**, *22*, 271-278.

109. Wolff, J. J.; Laremore, T. N.; Aslam, H.; Linhardt, R. J. and Amster, I. J., Electron-Induced Dissociation of Glycosaminoglycan Tetrasaccharides. *J. Am. Soc. Mass Spectrom.* **2008**, *19*, 1449-1458.
110. Nielsen, M. L.; Budnik, B. A.; Haselmann, K. F.; Olsen, J. V. and Zubarev, R. A., Intramolecular hydrogen atom transfer in hydrogen-deficient polypeptide radical cations. *Chem. Phys. Lett.* **2000**, *330*, 558-562.
111. Gabrielse, G.; Haarsma, L. and Rolston, S. L., Open-endcap Penning traps for high precision experiments. *Int. J. Mass Spectrom. Ion Processes* **1989**, *88*, 319-332.
112. Mitchell, D. W. and Smith, R. D., Two dimensional many particle simulation of trapped ions. *Int. J. Mass Spectrom. Ion Processes* **1997**, *165-166*, 271-297.
113. Mitchell, D. W., Realistic simulation of the ion cyclotron resonance mass spectrometer using a distributed three-dimensional particle-in-cell code. *J. Am. Soc. Mass Spectrom.* **1999**, *10*, 136-152.
114. Eugene, N. N.; Ron, M. A. H.; Alexander, M. P.; Alexander, V. P. and Konstantin, S. C., Realistic modeling of ion cloud motion in a Fourier transform ion cyclotron resonance cell by use of a particle-in-cell approach. *Rapid Commun. Mass Spectrom.* **2007**, *21*, 3527-3546.
115. Leach III, F. E.; Kharchenko, A.; Heeren, R. M. A.; Nikolaev, E. and Amster, I. J., Comparison of Particle-In-Cell Simulations with Experimentally Observed Frequency Shifts Between Ions of the Same Mass-To-Charge in Fourier Transform Ion Cyclotron Resonance Mass Spectrometry. *J. Am. Soc. Mass Spectrom.* **2010**, *21*, 203-208.

## APPENDIX B

### COMPARISON OF PARTICLE-IN-CELL SIMULATIONS WITH EXPERIMENTALLY OBSERVED FREQUENCY SHIFTS BETWEEN IONS OF THE SAME MASS-TO-CHARGE IN FOURIER TRANSFORM ION CYCLOTRON RESONANCE MASS SPECTROMETRY<sup>1</sup>

---

<sup>1</sup> Leach III, F. E.; Kharchenko, A.; Heeren, R. M. A.; Nikolaev, E. and Amster, I. J. **2010**  
*Journal of the American Society for Mass Spectrometry*, 21:203-208. Reproduced  
with permission of publisher.

## ABSTRACT

It has been previously observed that the measured frequency of ions in a Fourier transform mass spectrometry experiment depend upon the number of trapped ions, even for populations consisting exclusively of a single mass-to-charge. Since ions of the same mass-to-charge are thought not to exert a space-charge effect among themselves, the experimental observation of such frequency shifts raises questions about their origin. To determine the source of such experimentally observed frequency shifts, multi-particle ion trajectory simulations have been conducted on monoisotopic populations of  $\text{Cs}^+$  ranging from  $10^2$  ions to  $10^6$  ions. A close match to experimental behavior is observed. By probing the effect of ion number and orbital radius on the shift in the cyclotron frequency, it is shown that for a monoisotopic population of ions, the frequency shift is caused by the interaction of ions with their image-charge. The addition of ions of a second mass-to-charge to the simulation allows the comparison of the magnitude of the frequency shift resulting from space-charge (ion-ion) effects versus ion interactions with their image charge.

## INTRODUCTION

Fourier transform ion cyclotron resonance mass spectrometry (FTICR-MS) [1] provides the highest mass accuracy and highest mass resolution of any currently available mass spectrometer. The cyclotron motion of an ion arises due to a radially constraining magnetic field and the frequency of this motion can be defined as:

$$\omega_c = \frac{qB}{m} \quad (\text{Equation 1})$$

where B is the magnetic field, q is the ion's charge, and m is the ion's mass. Values of cyclotron frequency ( $\omega_c/2\pi$ ) range from tens of kHz to MHz for most ions. In practice, the magnitude of the observed cyclotron frequency is slightly reduced by the radially-repulsive trapping electric field, and to a lesser degree, by the repulsive electric field that exists between ions of like charge, also known as space-charge. The study of deviations from the expected cyclotron frequency has been of continued interest in FTICR-MS [2-9] as the desire to reduce mass errors to the sub-ppm range has increased. These ion population dependent shifts are small in magnitude, corresponding to shifts of several Hz to less than 1 Hz. For example, a shift of 0.1 Hz for an ion of m/z 500 at 7.0 T corresponds to 0.47 ppm in mass measurement error. These differences in measured frequency are due to space charge interactions in the FTICR analyzer cell [10, 11] as well as image-charge interactions [12].

Recently, our laboratory has made an experimental investigation of frequency shifts amongst monoisotopic populations of Cs<sup>+</sup> ions [13] and attributed the source of

these shifts to be due to space charge interaction between like ions. These findings contradict previous theoretical studies of space charge interactions of ions contained within a Penning trap where like ions have been proposed to have no coulombic effect on cyclotron frequency [2, 12]. Although coulombic interactions can be investigated in the laboratory, the experimental approach is limited by the inability to precisely know the number of ions present in the analyzer cell or their spatial distribution. In contrast, computational simulations provide the means to specify the number of ions present in the analyzer, as well as their mass, charge, and spatial distribution. Multi-particle simulations can be used to examine ion motion in FTICR-MS as a function of the above-mentioned parameters and to determine the root causes of frequency shifts for a monoisotopic population of ions.

To gain insight into ion motion in the presence of applied electric and magnetic fields it is possible to utilize a commercially available software package, such as SIMION [14], but this approach is limited to the motion of a tens of ions, whereas typical experimental populations range from  $10^3$  to  $10^6$ , and does not incorporate ion-ion interaction nor ion-image charge interaction. A SIMION model has recently been developed which incorporates ion-image charge detection, but does not include the forces of the coulombic interactions [15]. Particle-particle methods can be applied to account for ion-ion interaction and allow for the calculation of FTICR spectral line shapes as well as frequency shifts [16] but require very large computational resources [17].

The particle-in-cell (PIC) approach provides a computationally tractable method for simulating the ion motion of large populations of ions, with a realistic model for coulombic effects such as ion-ion and ion-image charge interactions [18-22]. Originally

developed by the plasma physics community, particle-in-cell methods were first applied to ion trajectory simulations in FTICR-MS by Mitchell [23, 24] and subsequently Nikolaev *et al.* [25]. Using a PIC algorithm, a model has been developed to simulate prior experimental observations in our laboratory. As shown below, these simulations reveal the source of observed frequency shifts to be due to interactions between ions and their image charge induced in the surrounding electrodes.

## **EXPERIMENTAL METHODS**

Multi-particle ion trajectory simulations were conducted on Linux clusters located at the University of Georgia and the Foundation for Fundamental Research on Matter-Institute for Atomic and Molecular Physics (FOM-AMOLF) using a serial version of the PIC code and parameters summarized in Table B.1. A monoisotopic  $\text{Cs}^+$  ( $m/z$  132.9054,  $z = 1$ ) population was varied in ion number from  $10^2$  to  $10^6$  while constrained radially by a magnetic field of 7.0 T and trapped axially by 1 V. A cubic trapping potential and an idealized quadrupolar trapping potential of a Penning trap were employed using particle-in-cell methods to enable coulombic interactions. The analyzer geometry in all simulations was 5.08 cm x 5.08 cm x 5.08 cm, corresponding to a two-inch cubic cell. A cylindrical geometry is currently being implemented for further studies. During simulations of two distinct  $m/z$  values, a second singly-charged ion of  $m/z$  150.0000 is included in a 1:1 ratio to the Cs ion number. Prior to excitation, the ion cloud is generated as an ellipsoid (major axis 0.2 cm, minor axis 0.05 cm), with the major axis parallel to the magnetic field and a uniform distribution of particles. The initial particle velocity distribution is Maxwellian at 300 K. For each particle, the direction of the

velocity vector is randomized. For excitation in the single  $m/z$  simulations of  $\text{Cs}^+$ , an on-resonance radiofrequency (RF) burst was utilized. Variation in the excite voltage from 2  $V_{p-p}$  to 10  $V_{p-p}$  resulted in an orbital radius ranging from 15% to 85% of the analyzer

**TABLE B.1** Parameters utilized for PIC simulations and prior experimental data.

<b><u>Simulation</u></b>	
Trapping Potential	1.0 V
Magnetic Field	7.0 T
Analyzer geometry	Cubic
Ion Cloud	Ellipsoid
Semi-major axis	0.2 cm
Semi-minor axis	0.05 cm
Trap Dimension	5.08 cm
PIC Grid	32x32x32
Simulated Particles	100 - 1,000,000
Ion $m/z$	132.9054, 150.0
<i>Excitation</i>	
Voltage	2-180 ( $V_{p-p}$ )
Excitation Steps	16383
Duration	90 $\mu\text{s}$
Time Step	0.005 $\mu\text{s}$ / step
<i>Detection</i>	
Detection Steps	2097152
Duration	52 ms
Time step	0.024 $\mu\text{s}$ /step
<b><u>Experimental</u></b>	
Trapping Potential	1.0 V
Magnetic Field	7.0 T
Analyzer geometry	Closed-end Cylindrical
<i>Detection</i>	
Excitation Voltage	100 $V_{p-p}$
Duration	47.5 msec

cell radius. During simulations of ions with two distinct  $m/z$  values, a chirp excitation was utilized with voltages ranging from 60 V<sub>p-p</sub> – 180 V<sub>p-p</sub> producing orbital radii ranging from 15% to 60%. For each computational experiment, a simulated time domain transient was acquired and a frequency domain spectrum was derived using the fast Fourier transform (FFT) incorporated in FOM-AMOLF's AWE software [26]. Visualization of the simulated ion cloud was accomplished with in-house software developed at FOM-AMOLF [27].

## **RESULTS AND DISCUSSION**

Contrary to prior published proposals regarding space-charge interaction between ions of the same mass-to-charge [2, 12], experimental results in our lab have demonstrated frequency shifts among monoisotopic populations of Cs<sup>+</sup> ions [13]. A linear decrease in frequency with increasing ion abundance was observed over most of the range of ion abundance, and attributed to space charge induced frequency shifts between Cs<sup>+</sup> ions. At the lowest ion abundance values that could be measured, an increase in frequency with an increase in ion abundance was observed, suggesting another, yet to be explained phenomenon. At intermediate ion number, the observed frequency reaches a maximum, shown in Figure B.1. Simulations allow this effect to be examined in systematic fashion by varying parameters such as ion number or radius of the cyclotron orbit.

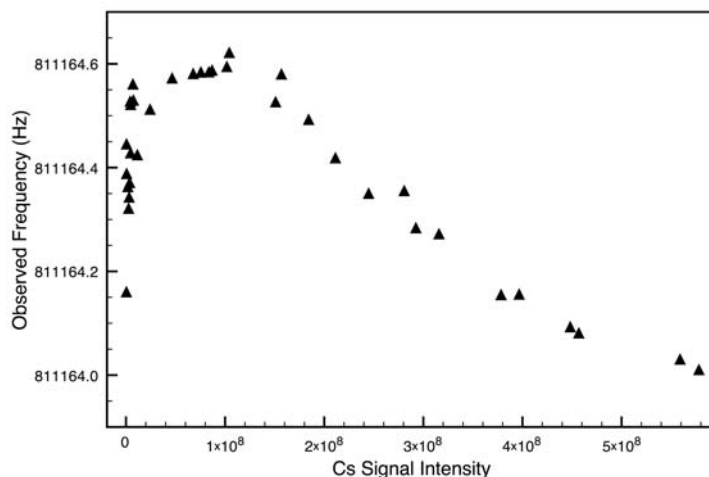


**FIGURE B.1** Experimentally observed frequency shifts observed for a monoisotopic  $\text{Cs}^+$  population, acquired by varying the concentration of a CsI electrospray solution and ion accumulation time in a storage hexapole prior to injection into the FTICR analyzer (replotted from data published in Reference 13.) Simulated frequencies vary from these experimental frequencies by  $\sim 2$  kHz because simulations were conducted at exactly 7.0 T whereas the experimental magnetic field is on the order of 7.02 T.

### *Simulation Model Validation*

Prior to initiating computational experiments to determine the source of the frequency shifts, a model of the experimental configuration was constructed based on the parameters for the initial data acquisition. One difference limits the direct comparison of our simulation results: the previously published experimental results were acquired on a Bruker FTICR-MS equipped with a close-ended cylindrical cell [28]. For the simulations, we are currently limited to the cubic cell geometry, but are able to apply

either a trapping potential for a cubic cell or an idealized quadrupolar potential. The shape of the trapping potential of the close-ended cylindrical cell lies in between these two extremes, therefore simulation results were obtained with both trapping electric field geometries, allowing for a reasonable approximation of our experimental configuration.

Ion trajectory simulations performed with a resonance excitation voltage of 4 Vp-p, shown in Figure B.2, correspond to a final cyclotron radius of approximately 35% of the analyzer cell radius. For both applied trapping potentials, a nearly linear decrease in

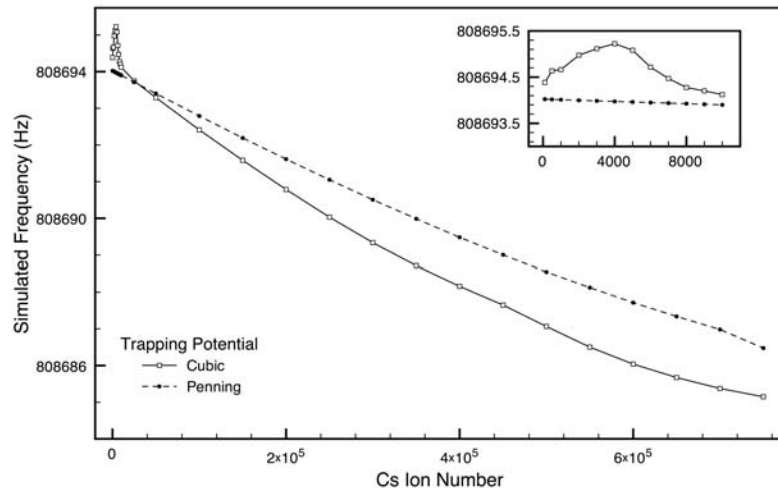


**FIGURE B.2** Simulated frequency shifts for a cubic and quadrupolar trapping potential for  $\text{Cs}^+$  populations ranging from 100 to 750,000 at 35 % cell radius. The inset shows an expansion of the low ion number region of the curve.

calculated cyclotron frequency is observed as the ion number increases. This trend is consistent with the prior experimental results described above. The difference in slope

between the two types of trapping potentials can be attributed to variations between exciting an ion into an inhomogeneous cubic trapping potential versus an ideal quadrupolar potential. At low ion numbers, the simulations using either potential both approach the reduced cyclotron frequency. In the case of the cubic potential, a maximum is observed in the plot of observed frequency versus ion number, and a reduction in frequency occurs for decreasing ion number when the number of ions is less than 4000. This feature may be due to a combination of inhomogeneities in the cubic trapping potential and cloud decoherence at low ion number [25]. Ion trajectory visualizations reveal a loss of coherence in the ion cloud near the maxima for the cubic potential, while the cloud maintains coherence in the quadrupolar potential. As we do not fully understand the source of this anomaly in the cubic trapping potential, a quadrupolar potential was chosen for the remainder of our current simulations. This variation will be a source of further study.

#### *Excitation Radius Dependence – Image Charge Interaction Effects*

Simulations of varying  $\text{Cs}^+$  number were conducted using burst excitation voltages ranging from 2 V<sub>p-p</sub> to 10 V<sub>p-p</sub>, in increments of 2 V. These applied voltages correspond to orbital radii of approximately 15%, 35%, 50%, 65% and 85% of the cell radius. As shown in Figure B.3, increasing the excitation radius of a monoisotopic ion population produces an increase in the slope of the plot of the observed frequency shift

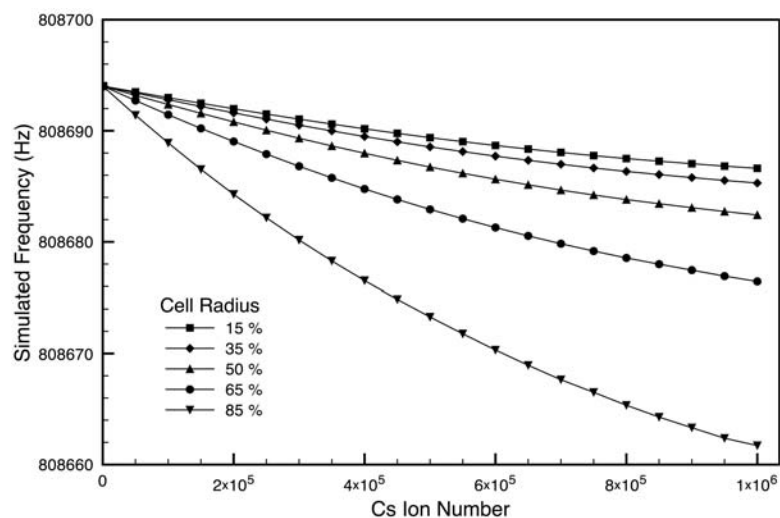


**FIGURE B.3** Simulated frequency shifts for ion orbital radii ranging from 15% to 85% of the cell radius for Cs<sup>+</sup> populations ranging from 100 to 1,000,000 in a quadrupolar trapping potential.

versus ion number. For a given excitation radius, this frequency shift versus ion number is approximately linear.

Previously, Easterling et al. observed not only a linear correlation between observed frequency and ion number in MALDI FTICR-MS [29] for a group of ions of various mass-to-charge values, but also a decrease in frequency shift with increasing excitation voltage. This experimental result was rationalized as a decrease in ion-ion interactions (space-charge) as the radius of excitation increased; at higher radius, the ion density decreases, thus reducing the frequency shift based on space charge effects between ions of different mass-to-charge. In sharp contrast, for ions of a single mass-to-charge value, the frequency shift from the multi-particle simulations is found to increase in slope with increasing excitation voltage. This result can be attributed to an increase in

the interaction between the ions and their image charge as the orbital radius increases, bringing ions closer to the excitation and detection electrodes. In the experimental results with ions of differing  $m/z$  values present, space-charge effects between ions of different mass-to-charge were significantly larger than the ion-image current interaction, and so the dominating effect observed was that of decreasing space charge with increasing orbital radius. The simulations suggest that there is no space-charge effect on observed frequency for ions of the same mass-to-charge, in agreement with the work of Comisarow [2]. Thus, the much smaller effect from ion-image charge interactions can be observed, and this is expected to increase with increasing orbital radius.

Marshall and co-workers have previously made analytical calculations of the image charge interaction of a single ion in orthorhombic/cubic and cylindrical geometries as functions of radial and axial position [6]. The calculated frequency shift for a cubic cell was approximately  $1.0 \times 10^{-5}$  Hz per ion for excitation to 50% of the cell radius (1.0'' cubic cell, 3.0 T magnetic field.) Correcting for the  $1/B$  dependence, this shift becomes  $4.29 \times 10^{-6}$  at 7.0 T. This value is in close agreement with the results of our simulations, where we observe a  $1.5 \times 10^{-5}$  Hz shift per ion in a cubic cell (2.0'' cubic cell at 7.0 T magnetic field) orbiting at 50% of the cell radius. The analytical solution of the line charge model previously utilized by Gorshkov [5] and Mitchell [24] can also serve as a baseline for comparison. The calculated shift for a single ion in a 2.0'' cell at 7.0 T is  $2.6 \times 10^{-6}$  Hz. Tinkle and Barlow have also calculated this shift in a cubic cell [30]. For a single ion at 7.0 T (1.6'' cubic cell), the magnitude of the shift is  $2.7 \times 10^{-6}$  Hz. Allowing for the variations in cell design and ion position for each study, these values are all in good agreement.

There is a slight curvature to the plots in Figure B.3, corresponding to frequency shifts that are slightly smaller than one would predict for linear scaling with ion number. Linear scaling is expected if all of the ions were located at the same point in space. As the number of ions increases, coulombic repulsion results in a larger, more diffuse ion cloud and a more diffuse image charge, leading to a small reduction in the ion-image charge interaction. Such behavior was not predicted by the analytical calculations of Marshall or Barlow, as they focused on the behavior of a single ion.

The dependence of the observed frequency on the orbital radius of an ion, shown in Figure B.4, also shows good agreement with Marshall's calculations for single ions.

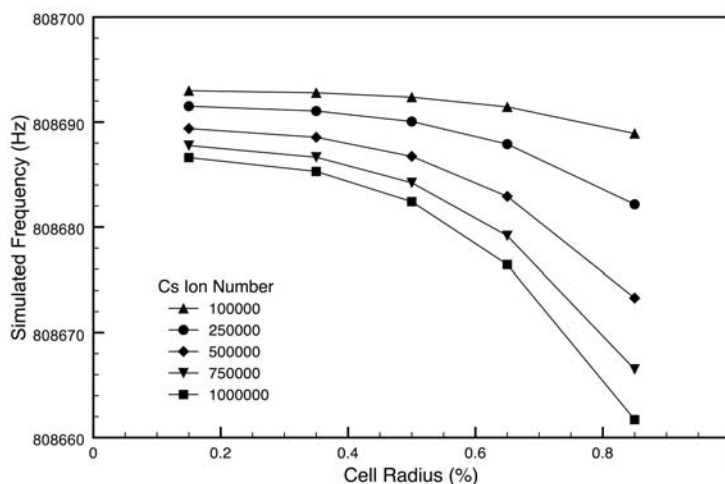


**FIGURE B.4** Simulated frequency shifts as a function of orbital radius for selected Cs<sup>+</sup> numbers in a quadrupolar trapping potential.

The frequency shift increases quadratically as the distance between the ions and the cell plate decreases, as one would expect for the interaction of two point charges. At low ion

number, there is a very small shift ( $< 1.0$  Hz) as the radius is increased, but this shift increases to several Hz with increasing ion number. For an orbital radius of 50% of the cell radius, the frequency shift is 8 Hz for  $10^6$  ions, and 14 Hz at an orbital radius of 65% of the cell radius.

#### *Comparison to Interactions between Ions of Different m/z Values*

To further validate the source of the experimentally observed frequency shifts in  $\text{Cs}^+$ , a series of simulations were conducted in which a second population of singly-charged ions of  $m/z$  150 was introduced in a 1:1 ratio to the  $\text{Cs}^+$  number. Based on the ability of the PIC code to enable coulombic interactions between particles, space charge effects can be recorded in these calculations. The observed frequency of  $\text{Cs}^+$  for three excitation radii is shown in Figure B.5, compared to the observed frequency without the addition of an ion of different mass-to-charge. Over the range of ion numbers, 500 to 250,000, the frequency for  $\text{Cs}^+$  present by itself decreases by only 3 Hz whereas the frequency for  $\text{Cs}^+$  when ions of a second  $m/z$  value are present (same total number of ions) decreases by 21 Hz, for an orbital radius of 35%. The resulting ratio of the slopes is 1:7, in excellent agreement to the experimental value of 1:7.5 [13]. The much steeper slope of the simulated frequencies for two different mass-to-charge values corresponds to the addition of ion-ion space charge effects to the ion-image charge interaction. Also shown in Figure B.5, the previously discussed space charge behavior described by Easterling *et al.* is also replicated by the simulations. As the excitation radius is increased, the slope of the frequency shift decreases,

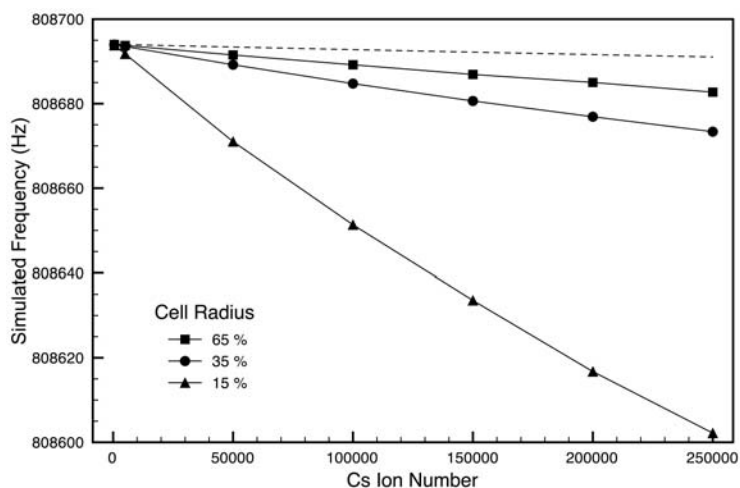


**FIGURE B.5** Simulated frequency shifts in  $\text{Cs}^+$  when a second ion is added to the FTICR-MS analyzer employing a quadrupolar trapping potential. Orbital radii from 15% to 60% of the cell radius are shown. The dashed line represents the frequency shifts present at 35% cell radius for a population of only  $\text{Cs}^+$ , for comparison.

demonstrating that space-charge interactions between ions of differing mass-to-charge decrease as the orbital radius increases. In contrast, ion-image current interactions increase with increasing orbital radius. For cell designs in which the orbital radius can approach the cell radius, the magnitude of the frequency shift from ion-image charge interactions may approach or exceed that from ion-ion interactions.

#### *Considerations for Mass Calibration*

The exact relationship between frequency and mass-to-charge in FT-ICR MS depends upon a number of experimental factors, and various calibration laws have been proposed to attain this value with high accuracy by including terms that account for

space-charge effects either explicitly or implicitly [11, 29, 31-34]. Muddiman and co-workers have examined several calibration equations, and have proposed a statistically-derived equation that includes terms that can be interpreted as being due to both global and local space-charge [31]. Global space-charge is the general reduction in observed frequency that occurs as a function of the total summed ion abundance, while local space charge is a smaller term that takes into account a reduced interaction between ions of the same mass-to-charge [7, 34]. Based on the work presented here, it would appear that the latter term in the Muddiman calibration law accounts for ion-image charge interactions. For mass spectra in which the intensity distribution of detected ions is relatively constant over the mass range, the effect of ion-image charge interactions would be negligibly small compared to conventional space-charge interactions. On the other hand, in MS/MS experiments where the precursor intensity is much greater in intensity than the product ions, for example, electron capture dissociation [35] or electron detachment dissociation [36], the image charge induced frequency shift will be significant for the precursor ion, but insignificant for the product ions. For this reason, the precursor ion should not be used for internal calibration or lock-mass calibration unless the calibration equation accounts explicitly for ion-image charge interactions.

## **CONCLUSIONS**

The application of particle-in-cell ion trajectory calculations provides the means to gain insight into the fundamentals of ion behavior in FT-ICR MS. Prior experimental results for both like and unlike ions have been explained based on the observed frequency shifts as experimental parameters are varied during simulations, and analytical

calculations of image charge induced frequency shifts for single ions have been validated for ion populations of a size that is typical for real experiments. Space charge induced shifts can be minimized by exciting to increased cell radius, but image charge based frequency shifts will increase and provide mass errors in FT-ICR MS that should be taken into consideration for mass calibration. The close correspondence of the PIC simulation results with prior experiment and theory provides validation for this approach to accurately modeling the interactions of large populations of ions in FT-ICR MS [24, 25].

## **ACKNOWLEDGEMENTS**

F. E. Leach III and I. J. Amster gratefully acknowledge financial support for travel to the Netherlands from PIRE: A U.S. - Dutch Mass Spectrometry Consortium for Advanced Modeling and Biological Structure and Imaging Applications sponsored by the National Science Foundation Office of International Science and Engineering (OISE-730072). F.E. Leach III also acknowledges Marco Konijnenburg (FOM-AMOLF) for assistance with modifications to the AWE software. E. Nikolaev and A. Kharchenko acknowledge Gleb Vladimirov (Institute for Energy Problems of Chemical Physics) for his contributions to the development of the PIC code.

## REFERENCES

1. Comisarow, M. B. and Marshall, A. G., Fourier-Transform Ion-Cyclotron Resonance Spectroscopy. *Chem. Phys. Lett.* **1974**, *25*, 282-283.
2. Chen, S. P. and Comisarow, M. B., Simple Physical Models for Coulomb-Induced Frequency Shifts and Coulomb-Induced Inhomogeneous Broadening for Like and Unlike Ions in Fourier Transform Ion Cyclotron Resonance Mass Spectrometry. *Rapid Commun. Mass Spectrom.* **1991**, *5*, 450-455.
3. Chen, S. P. and Comisarow, M. B., Modelling Coulomb Effects in Fourier-Transform Ion Cyclotron Resonance Mass Spectrometry by Charged Disks and Charged Cylinders. *Rapid Commun. Mass Spectrom.* **1992**, *6*, 1-3.
4. Mitchell, D. W. and Smith, R. D., Cyclotron Motion of 2 Coulombically Interacting Ion Clouds with Implications to Fourier-Transform Ion-Cyclotron Resonance Mass-Spectrometry. *Physical Review E* **1995**, *52*, 4366-4386.
5. Gorshkov, M. V.; Marshall, A. G. and Nikolaev, E. N., Analysis and Elimination of Systematic Errors Originating from Coulomb Mutual Interaction and Image Charge in Fourier Transform Ion Cyclotron Resonance Precise Mass Difference Measurements. *J. Am. Soc. Mass Spectrom.* **1993**, *4*, 855-868.
6. Xiang, X.; Grosshans, P. B. and Marshall, A. G., Image Charge-Induced Ion Cyclotron Orbital Frequency Shift for Orthorhombic and Cylindrical FT-ICR Ion Traps. *Int. J. Mass Spectrom. Ion Processes* **1993**, *125*, 33-43.
7. Masselon, C.; Tolmachev, A. V.; Anderson, G. A.; Harkewicz, R. and Smith, R. D., Mass Measurement Errors Caused by "Local" Frequency Perturbations in FTICR Mass Spectrometry. *J. Am. Soc. Mass Spectrom.* **2002**, *13*, 99-106.

8. Aizikov, K. and O'Connor, P. B., Use of the Filter Diagonalization Method in the Study of Space Charge Related Frequency Modulation in Fourier Transform Ion Cyclotron Resonance Mass Spectrometry. *J. Am. Soc. Mass Spectrom.* **2006**, *17*, 836-843.
9. Aizikov, K.; Mathur, R. and O'Connor, P. B., The Spontaneous Loss of Coherence Catastrophe in Fourier Transform Ion Cyclotron Resonance Mass Spectrometry. *J. Am. Soc. Mass Spectrom.* **2009**, *20*, 247-256.
10. Jeffries, J. B.; Barlow, S. E. and Dunn, G. H., Theory of Space-Charge Shift of Ion-Cyclotron Resonance Frequencies. *Int. J. Mass Spectrom. Ion Processes* **1983**, *54*, 169-187.
11. Francl, T. J.; Sherman, M. G.; Hunter, R. L.; Locke, M. J.; Bowers, W. D. and McIver, R. T., Experimental-Determination of the Effects of Space-Charge on Ion-Cyclotron Resonance Frequencies. *Int. J. Mass Spectrom. Ion Processes* **1983**, *54*, 189-199.
12. Wineland, D. and Dehmelt, H., Line Shifts and Widths of Axial, Cyclotron and G-2 Resonances in Tailored, Stored Electron (Ion) Cloud. *International Journal or Mass Spectrometry and Ion Physics* **1975**, *16*, 338-342.
13. Wong, R. L. and Amster, I. J., Experimental Evidence for Space-Charge Effects Between Ions of the Same Mass-to-Charge in Fourier-Transform Ion Cyclotron Resonance Mass Spectrometry. *Int. J. Mass Spectrom.* **2007**, *265*, 99-105.
14. Dahl, D. A., SIMION for the Personal Computer in Reflection. *Int. J. Mass Spectrom.* **2000**, *200*, 3-25.

15. Hendrickson, C. L.; Beu, S. C.; Blakney, G. T. and Marshall, A. G., SIMION Modeling of Ion Image Charge Detection in Fourier Transform Ion Cyclotron Resonance Mass Spectrometry. *Int. J. Mass Spectrom. In Press, Corrected Proof*,
16. Nikolaev, E. N.; Miluchihin, N. V. and Inoue, M., Evolution of an Ion Cloud in a Fourier Transform Ion Cyclotron Resonance Mass Spectrometer During Signal Detection: Its Influence on Spectral Line Shape and Position. *Int. J. Mass Spectrom. Ion Processes* **1995**, *148*, 145-157.
17. Miluchihin, N. V.; Miura, K. and Inoue, M., Application of a Parallel Computer to Simulation of Ion Trajectories in an Ion Cyclotron Resonance Spectrometer. *Rapid Commun. Mass Spectrom.* **1993**, *7*, 966-970.
18. Hockney, R. W. and Eastwood, J. W., Computer Simulations Using Particles, Adam Hilger: New York, 1988.
19. Birdsall, C. K., Particle-In-Cell Charged-Particle Simulations, Plus Monte-Carlo Collisions With Neutral Atoms, PIC-MCC. *Ieee Transactions on Plasma Science* **1991**, *19*, 65-85.
20. Peratt, A. L., Advances in Numerical Modeling of Astrophysical and Space Plasmas. *Astrophys. Space Sci.* **1996**, *242*, 93-163.
21. Dawson, J. M., Particle Simulation of Plasmas. *Reviews of Modern Physics* **1983**, *55*, 403.
22. Birdsall, C. K. and Langdon, A. B., Plasma Physics via Computer Simulation, McGraw-Hill: New York, 1985.
23. Mitchell, D. W. and Smith, R. D., Two Dimensional Many Particle Simulation of Trapped Ions. *Int. J. Mass Spectrom.* **1997**, *165*, 271-297.

24. Mitchell, D. W., Realistic Simulation of the Ion Cyclotron Resonance Mass Spectrometer Using A Distributed Three-Dimensional Particle-In-Cell Code. *J. Am. Soc. Mass Spectrom.* **1999**, *10*, 136-152.
25. Nikolaev, E. N.; Heeren, R. M. A.; Popov, A. M.; Pozdnev, A. V. and Chingin, K. S., Realistic Modeling of Ion Cloud Motion in a Fourier Transform Ion Cyclotron Resonance Cell by Use of a Particle-In-Cell Approach. *Rapid Commun. Mass Spectrom.* **2007**, *21*, 3527-3546.
26. Mize, T. H.; Taban, I.; Duursma, M.; Seynen, M.; Konijnenburg, M.; Vijftigschild, A.; Doornik, C. V.; Rooij, G. V. and Heeren, R. M. A., A Modular Data and Control System to Improve Sensitivity, Selectivity, Speed of Analysis, Ease of Use, and Transient Duration in an External Source FTICR-MS. *Int. J. Mass Spectrom.* **2004**, *235*, 243-253.
27. Burakiewicz, W. and van Liere, R., Analyzing Complex FTMS Simulations: A Case Study in High-Level Visualization of Ion Motions. *IEEE Trans. Vis. Comput. Graphics* **2006**, *12*, 1037-1043.
28. Caravatti, P. and Allemann, M., The Infinity Cell - A New Trapped-Ion Cell with Radiofrequency Covered Trapping Electrodes for Fourier-Transform Ion-Cyclotron Resonance Mass-Spectrometry. *Org. Mass Spectrom.* **1991**, *26*, 514-518.
29. Easterling, M. L.; Mize, T. H. and Amster, I. J., Routine Part-per-Million Mass Accuracy for High-Mass Ions: Space-Charge Effects in MALDI FT-ICR. *Anal. Chem.* **1999**, *71*, 624-632.

30. Tinkle, M. D. and Barlow, S. E., Image Charge Forces Inside Conducting Boundaries. *J. Appl. Phys.* **2001**, *90*, 1612-1624.
31. Muddiman, D. C. and Oberg, A. L., Statistical Evaluation of Internal and External Mass Calibration Laws Utilized in Fourier Transform Ion Cyclotron Resonance Mass Spectrometry. *Anal. Chem.* **2005**, *77*, 2406-2414.
32. Ledford, E. B.; Rempel, D. L. and Gross, M. L., Space Charge Effects in Fourier Transform Mass Spectrometry. II. Mass calibration. *Anal. Chem.* **1984**, *56*, 2744-2748.
33. Li-Kang, Z.; Don, R.; Birendra, N. P. and Michael, L. G., Accurate Mass Measurements by Fourier Transform Mass Spectrometry. *Mass Spectrom. Rev.* **2005**, *24*, 286-309.
34. Burton, R. D.; Matuszak, K. P.; Watson, C. H. and Eyler, J. R., Exact Mass Measurements Using a 7 Tesla Fourier Transform Ion Cyclotron Resonance Mass Spectrometer in a Good Laboratory Practices-Regulated Environment. *J. Am. Soc. Mass Spectrom.* **1999**, *10*, 1291-1297.
35. Zubarev, R. A.; Kelleher, N. L. and McLafferty, F. W., Electron Capture Dissociation of Multiply Charged Protein Cations. A Nonergodic Process. *J. Am. Chem. Soc.* **1998**, *120*, 3265-3266.
36. Wolff, J. J.; Amster, I. J.; Chi, L. and Linhardt, R. J., Electron Detachment Dissociation of Glycosaminoglycan Tetrasaccharides. *J. Am. Soc. Mass Spectrom.* **2007**, *18*, 234-244.

## APPENDIX C

### ANALYSIS OF PHASE DEPENDENT FREQUENCY SHIFTS IN PARTICLE-IN-CELL SIMULATED FOURIER TRANSFORM MASS SPECTROMETRY TIME DOMAIN TRANSIENTS USING THE FILTER DIAGONALIZATION METHOD<sup>1</sup>

---

<sup>1</sup> Leach III, F. E.; Kharchenko, A.; Valdimirov, G.; Aizikov, K.; O'Connor, P.B., Nikolaev, E., Heeren, R.M.A.; and I.J. Amster. To be submitted to *Journal of the American Society for Mass Spectrometry*.

## **ABSTRACT**

Space charge effects are present in any mass spectrometer at a point when ions are stored. In Fourier transform mass spectrometry (FTMS), periods of space charge interaction occur as ion packets are pulsed through the instrument and during image current detection as the ions are confined with the volume of the analyzer cell. These effects are problematic in that they perturb the natural cyclotron or axial frequency of an ion, but calibration laws and experimental techniques have been developed to minimize the perturbation and provide an accurate mass measurement. To closely examine space charge effects during the detection period, particle-in-cell ion trajectory simulations have been conducted. The period of coulombic interaction when the orbital phases of distinct ions coincide is short, and the fast Fourier transform (FFT) fails to provide high resolution on such time scales. To determine simulated frequencies, harmonic inversion is performed by the filter diagonalization method (FDM). Models are developed based upon the molecular ion of a single peptide as well as a simple tryptic digest.

## INTRODUCTION

Fourier transform ion cyclotron resonance mass spectrometry (FT-ICR MS) [1] provides the highest mass accuracy and highest mass resolution of any currently available mass spectrometer. The cyclotron motion of an ion arises due to a radially constraining magnetic field and the frequency of this motion can be defined as:

$$\omega_c = \frac{qB}{m} \quad (\text{Equation 1})$$

where B is the magnetic field, q is the ion's charge, and m is the ion's mass. Values of cyclotron frequency ( $\omega_c/2\pi$ ) range from tens of kHz to MHz for most ions. The study of deviations from the expected cyclotron frequency has been of continued interest in FT-ICR MS [2-9] as the desire to reduce mass errors to the sub-ppm range has increased.

In practice, the magnitude of the observed cyclotron frequency is slightly reduced by the radially-repulsive trapping electric field, and to a lesser degree, by the repulsive electric field that exists between ions of like charge, also known as space-charge [10, 11]. This space-charge effect can be approximated by the following expression:

$$\Delta\omega_{sc} = 2\pi \frac{q\rho G_i}{\epsilon_0 B} \quad (\text{Equation 2})$$

where q is the elementary unit of charge,  $\rho$  is the charge density,  $G_i$  is a geometrical description of the charge distribution,  $\epsilon_0$  is the free permittivity of space, and  $B$  is the applied magnetic field. Examination of these terms reveals that the effect is directly proportional to charge and ion density and inversely proportional to applied magnetic field. Space charge frequency shifts can be reduced experimentally by control of ion

number and excitation conditions [12, 13], which reduce ion density, and post-experiment by mass calibration [11, 14-19].

The fast nature of the space charge interaction requires a harmonic inversion technique that can operate on short time domain signals, as demonstrated in the work of Aizikov and O'Connor [8, 9], wherein the filter diagonalization method (FDM) [20] was utilized to dissect FT-ICR transients to reveal modulations in the orbital frequencies of ions during an experimental acquisition. The fast Fourier transform (FFT) [21] has limited value when applied to truncated time domain signals due to limited spectral resolution. Alternative inversion techniques such as the short-time Fourier transform [22] or linear prediction [23] can also be utilized but have their own limitations. FDM provides an attractive method due to high spectral resolution and moderate computational demands.

To examine the nature of dynamic phase-dependent space charge events during FTMS experiments in a controlled manner, particle-in-cell (PIC) ion trajectory calculations have been employed [24-26]. PIC results have been shown to accurately model experimental results [27] and currently serve as a valuable tool to gain insight into fundamental aspects of ion behavior. A model has been developed to systematically examine the space charge induced frequency shifts due to isotopes of a molecular ion. Extension of this model to selected peptides of a tryptic digest approach conditions of a typical MS experiment. Space charge effects are present in any ion-trapping instrument and extension of FDM analysis to simulated orbitrap time domain signals are also presented.

## EXPERIMENTAL METHODS

Multi-particle ion trajectory simulations were conducted on Linux clusters located at the Foundation for Fundamental Research on Matter- Institute for Atomic and Molecular Physics (FOM-AMOLF) using a serial version of the PIC code and parameters summarized in Table C.1. Ion populations were constrained radially by a magnetic field of 7.0 T and trapped axially by 1 V. A cubic trapping potential and an idealized quadrupolar trapping potential of a Penning trap were employed using particle-in-cell methods to enable coulombic interactions on a finite grid 32 x 32 x 32 in dimension. The analyzer geometry in all simulations was 5.08 cm x 5.08 cm x 5.08 cm, corresponding to a two-inch cubic cell. Analyzer cells of arbitrary geometry will be implemented for further studies. Prior to excitation, the ion cloud is generated as an ellipsoid (major axis 0.2 cm, minor axis 0.05 cm), with the major axis parallel to the magnetic field and a uniform distribution of particles. The initial particle velocity distribution is Maxwellian at 300 K. For each particle, the direction of the velocity vector is randomized. Prior to image current detection, a chirp excitation (90 Vp-p) was utilized to produce an orbital radius of approximately 35 %. The orbitrap geometry employed for PIC simulations was mathematically derived from the analytical expression of the potential with relevant element radii listed in Table C.1. Ions were initially accelerating by 1300 V towards the central spindle, which was held at 3500 V.

For each computational experiment, a simulated time domain transient was generated and a frequency domain spectrum was derived using the fast Fourier transform (FFT) incorporated in FOM-AMOLF's AWE software [28]. The filter diagonalization method (FDM) was also imported in AWE. Frequency chasing experiments were

performed using a segment of 15k-25k data points and incremented 10k data points to provide overlap and reduce boundary effects. Visualization of the simulated ion cloud was accomplished with in-house software (Particle Vis) developed at FOM-AMOLF.

**TABLE C.1** Parameters utilized for PIC simulations.

<b><u>FT-ICR Simulation</u></b>	
Trapping Potential	1.0 V
Magnetic Field	7.0 T
Analyzer geometry	Cubic
Ion Cloud	Ellipsoid
Semi-major axis	0.2 cm
Semi-minor axis	0.05 cm
Trap Dimension	5.08 cm
PIC Grid	32x32x32
Simulated Particles	30,000 – 52,000
Ion m/z	
<i>Excitation</i>	
Voltage	90 (Vp-p)
Excitation Steps	16383
Duration	90 $\mu$ s
Time Step	0.005 $\mu$ s / step
<i>Detection</i>	
Detection Steps	1045876
Duration	97.5 ms
Time step	0.093 $\mu$ s /step
<b><u>Orbitrap</u></b>	
PIC Grid	32x32x64
Initial Ion Acceleration	1300 V
Characteristic Radius	22 mm
Shell Electrode Radius	15 mm
Spindle Electrode Radius	6 mm
Spindle Potential	3500 V
Detection Time Step	0.131 $\mu$ s / step
Detection Duration	26.2 msec

## RESULTS AND DISCUSSION

In the simple case of single ion detection in FT-ICR MS, the time signal is a sinusoid generated as the particle passes across the surface of the detection electrodes. In the case of two ions of distinct  $m/z$ , two sinusoids, with frequencies proportional to each ion's  $m/z$  are present, with the phase between the periodic motions due to the cyclotron frequency difference. As the phase approaches  $0^\circ$ , the ions are located on the same side of the analyzer cell and a maximum amplitude is observed in the time domain signal. When the phase approaches  $180^\circ$ , the two ions are located on opposite sides of the analyzer cell, and a node occurs due to destructive interference in the image current signal. This well-known behavior is the basis of isotopic beats in FTMS [29]. This illustrative example is difficult to generate experimentally due to the occurrence of a variety of isotopes, yet straightforward to generate via computer simulation.

To establish a model for the study of space charge interactions, simulations were conducted based on the isotopes of substance P. This ion was selected as a model based on prior work by Aizikov and O'Connor [8], but could have been arbitrarily selected. The monoisotopic ion is denoted as 'A' with additional peaks differing by one heavy isotope as 'A+1' and 'A+2'. At an applied magnetic field of 7.0 T, the cyclotron frequency difference between 'A' and 'A+1' or 'A+1' and 'A+2' are both approximately 60 Hz (16.7 ms) with the difference between 'A' and 'A+2' as 120 Hz (8.3 ms).

### *Simulation of 'A' only*

PIC simulation of only the A or monoisotopic ion results in the time domain signal shown in Figure C.1. A sinusoid of constant amplitude is generated, but is not

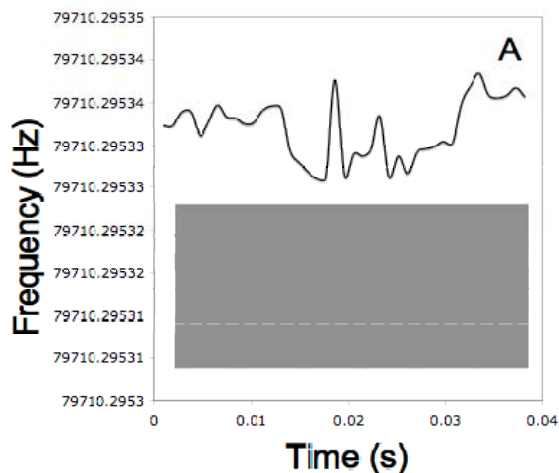


**FIGURE C.1** Simulated FT-ICR time domain signal for the monoisotopic ion (A peak) of substance P and corresponding FDM frequency analysis. No beat pattern or frequency shifts are observed due to the lack of adjacent ions due to isotopes.

entirely apparent due to the short period of oscillation. Due to the lack of additional isotopes, a beat pattern is not observed. FDM analysis of the signal results in a frequency that is stable to within 10 ppb. In the absence of space-charge interactions, an ion's cyclotron frequency is extremely stable and systematic examination of the addition of these interactions could provide more precise methods for accounting for induced perturbations to the cyclotron mode. The presented data was simulated with a perfectly quadrupolar trapping potential and produced variation of only 60  $\mu$ Hz. When compared to a simulation employing the trapping potential of a cubic cell, frequency variation ranged approximately 30 mHz, nearly three orders of magnitude larger. This result further validates that the incorporation of a more ideal trapping potential, through

compensation or novel cell design, reduces the variation in measured frequency and results in a more accurate mass measurement.

*Simulation of 'A' and 'A+1'*

Introduction of an ion corresponding to the 'A+1' peak differing only by the mass of one  $^{13}\text{C}$  incorporation is shown to introduce the anticipated isotopic beat in Figure C.2.

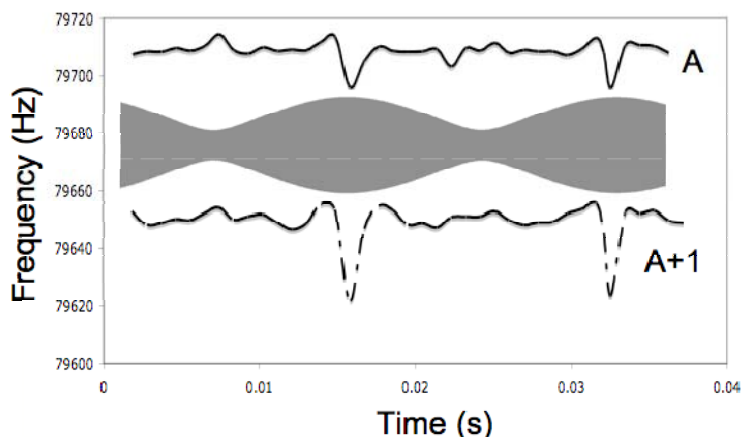


**FIGURE C.2** Simulated FT-ICR time domain signal for the monoisotopic ion (A) and A+1 of substance P and corresponding FDM frequency analysis. A beat pattern with period of 16.7 ms is observed due to  $\sim 59$  Hz difference between cyclotron frequencies.

The calculated cyclotron frequency difference between these two ions is approximately 60 Hz and corresponds to the beat period of 17.3 ms in the time domain. As the ions come into phase with one another, an amplitude maximum is observed in the transient, whereas a node is observed when ions are on opposite sides of the analyzer due to

deconstructive interference. Considering the location of each ion, the maximum space charge interaction is anticipated to occur during a beat as the charge density reaches a maximum.

FDM analysis of the simulated transient produces two frequencies, also shown in Figure C.2, the higher frequency due to the A peak and lower frequency due to the A+1. Each frequency displays variability of several Hz, but a periodic reduction of approximately 15 Hz is shown for the A peak and 30 Hz for the A+1. When the frequency analysis and time domain signal are aligned, the maximum frequency shift is shown to occur at the beat maximum.

#### *Simulation of 'A' and 'A+2'*

Elimination of the 'A+1' ion and incorporation of an ion two amu higher than the monoisotopic ion generates the time domain signal shown in Figure C.3. Due to the difference in cyclotron frequency doubling, the isotopic beat now occurs twice as often in the time domain. As depicted in the corresponding frequency chase, the periodic frequency shift now occurs twice as often when compared to the previous data for the A and A+1 peaks and remains aligned with the transient maximum. Frequency reductions of 15 Hz and 20 Hz are observed, respectively, for the A and A+2 peaks. Examination of further combinatorial possibilities due to isotopes is possible, but not necessary, as the method has shown validity when compared to theory and prior experimental result.

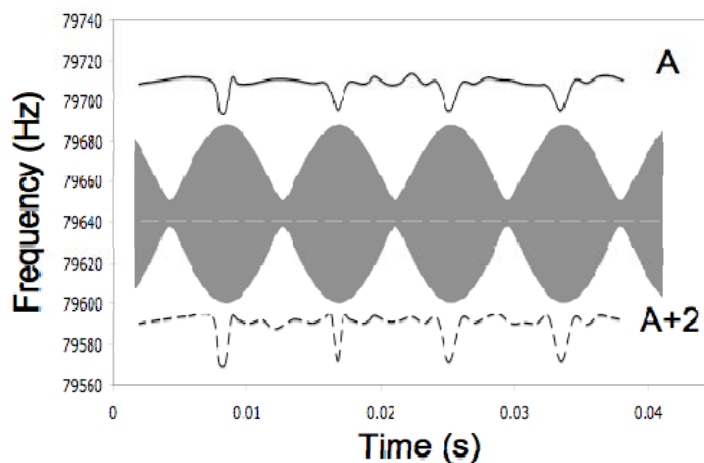


**FIGURE C.3** Simulated FT-ICR time domain signal for the monoisotopic ion (A) and A+2 of substance P and corresponding FDM frequency analysis. A beat pattern with period of 8.3 ms is observed due to  $\sim 120$  Hz difference between cyclotron frequencies.

#### *Simulation of a Protein Tryptic Digest*

Simulations of the isotopes for a single charge state provide method validation and fundamental insight, but are of limited value. To extend this analysis to typical experimental conditions, simulations were conducted based on a more complex mixture of ions. The ion assemblage was based on the components of a MALDI FT-ICR MS spectrum acquired from a tryptic digest of BSA. Nine peptides and their corresponding isotopes were selected as an example, shown in Figure C.4.

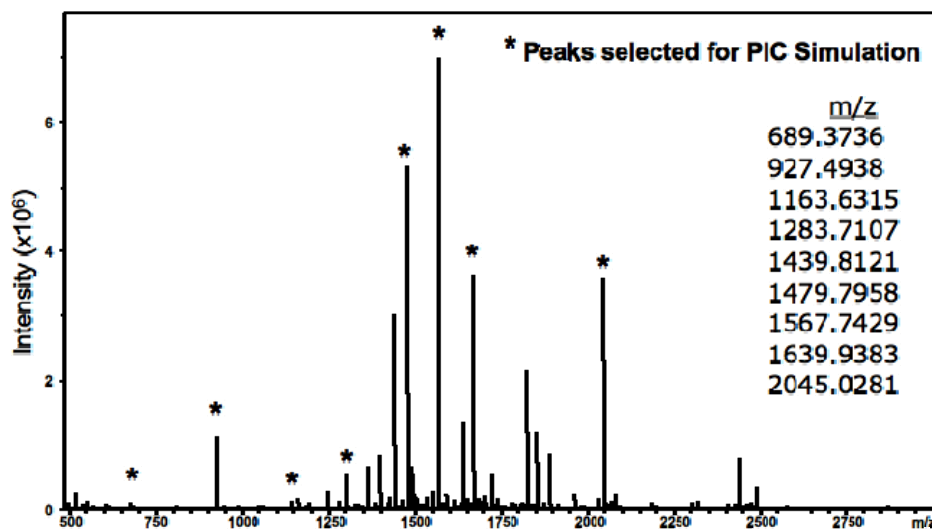


**FIGURE C.4.** Experimental MALDI spectrum and corresponding monoisotopic peaks selected for PIC simulation.

In Figure C.5, the FDM analysis of the frequency corresponding to the monoisotopic ion (1567 m/z) for the most intense peptide is shown. A periodic reduction in frequency is shown to occur on an interval of 23 ms. The period corresponds to the frequency difference between the monoisotopic ion and its ‘A+1’ ion, which is approximately 44 Hz. This result is consistent with simplified simulation results for substance P discussed earlier as well as what is known experimentally in the literature. For comparison, the FFT of the time domain signal is shown. The FFT result is the apparent time average of the instantaneous variations in frequency during the experiment. A detailed examination of frequency shifts for other components of complex mixtures will be the subject of a future manuscript.

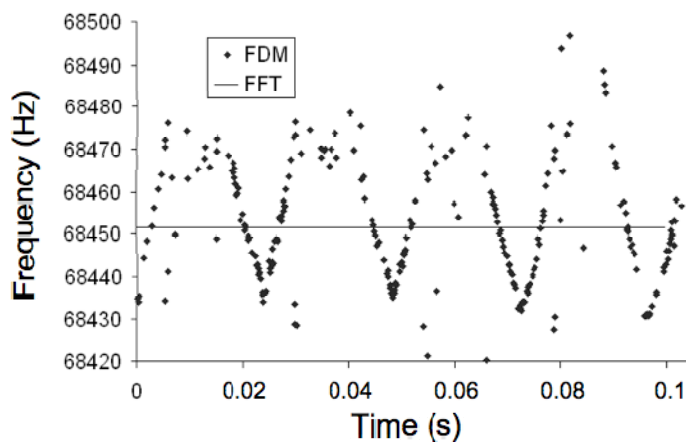


**FIGURE C.5** FDM analysis of the frequency shifts in the simulated cyclotron frequency for most intense monoisotopic ion in a peptide mixture. For comparison, the FT frequency is shown.

### *Simulation of Ion Motion in an Orbitrap*

Space charge effects have not been examined in depth for orbital FTMS but recent work has provided a mass calibration to account for these interactions [30]. The occurrence of isotope beating is not limited to FT-ICR, and is known to occur in orbital FTMS instruments such as the Orbitrap [31]. The question arises as to whether similar frequency shifts are present during an Orbitrap experiment. Unfortunately, public access is not provided to directly analyze real world time domain signals from the instrument, but we have been able to conduct ion trajectory calculations to simulate such an experiment.

Although isotope beating occurs in both types of FTMS instruments, the nature of the effect differs for the Orbitrap. After injection into the analyzer, ion clouds form tori which oscillate axially along the central electrode. As the analyzer is segmented to allow

for image current detection, maximum amplitude of the time domain signal occurs when ions are on the same side of the analyzer whereas a node occurs when ions are on opposite sides. This behavior is displayed in Figure C.6, where the sinusoids generated by monitoring the position of the two ions is displayed as a sum. Calculation of the beat

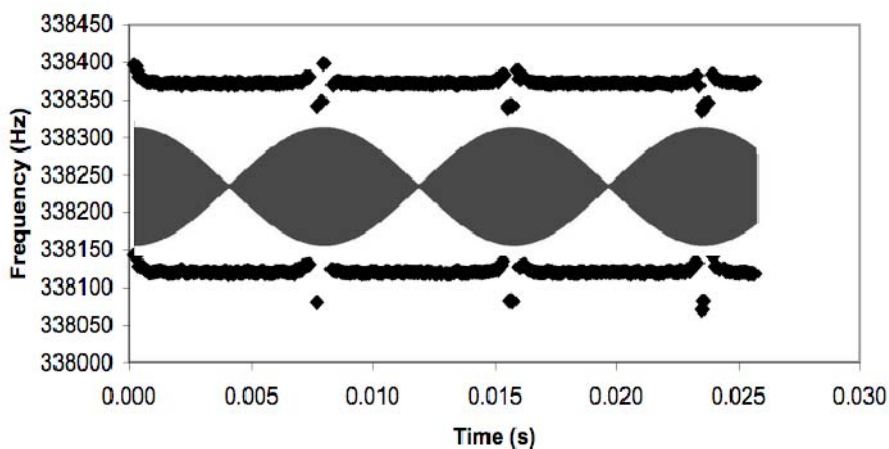


**FIGURE C.6** Simulated orbitrap time domain signal generated by summing the Z-axial positions of the A and A+2 ions of substance P and corresponding FDM derived frequencies.

period based on theory [31] is approximately 7 ms for isotopes differing by 2 amu and is consistent with our simulation. Corresponding FDM analysis of the image current signal reveals a periodic reduction in axial frequency of  $\sim 30$  Hz for the A ion and  $\sim 40$  Hz for the A+2 ion and corresponds to the beat. The case of isotopes differing by only 1 amu has also been examined and is consistent with these results, differing only in the beat period. In the presented example, the frequency perturbation is approximately double

that of ICR. Due to differences in analyzer geometry and image current detection, the results are not directly comparable aside from both originating from the physical basis of increased space charge interaction when ion densities are high and interaction distance reduced.

## **CONCLUSIONS**

Space charge induced frequency shifts in FTMS instruments arise due to ion confinement required for image current detection. This effect can be localized or global in nature, but is greatest in the examination of a molecular ion and its isotopes due to closely spaced frequencies and therefore short interaction distances. Manipulation of ion population size and calibration can account for space charge, but the effects on an ion's frequency are difficult to completely characterize analytically due to the large number of interactions in a typical experiment. PIC simulation of a molecular ion's isotopes and a simple mixture of ions from a tryptic digest have provided simple models to examine these frequency perturbations through harmonic inversion of the time domain signal by filter diagonalization. Although FDM allows for examination of these fast interactions, the FFT is still a robust harmonic inversion method, which effectively averages the phase dependent frequency shifts due to space charge.

## **ACKNOWLEDGEMENTS**

F. E. Leach III and I. J. Amster gratefully acknowledge financial support for travel to the Netherlands from PIRE: A U.S. - Dutch Mass Spectrometry Consortium for Advanced Modeling and Biological Structure and Imaging Applications sponsored by the National Science Foundation Office of International Science and Engineering (OISE-730072). F.E. Leach III also acknowledges Marco Konijnenburg (FOM-AMOLF) for assistance with modifications to the AWE software. E. Nikolaev and A. Kharchenko acknowledge Gleb Vladimirov (Institute for Energy Problems of Chemical Physics) for his contributions to the development of the PIC code.

## REFERENCES

1. Comisarow, M. B. and Marshall, A. G., Fourier Transform Ion Cyclotron Resonance Spectroscopy. *Chemical Physics Letters* **1974**, 25, 282-283.
2. Chen, S. P. and Comisarow, M. B., Simple Physical Models for Coulomb-Induced Frequency Shifts and Coulomb-Induced Inhomogeneous Broadening for Like and Unlike Ions in Fourier Transform Ion Cyclotron Resonance Mass Spectrometry. *Rapid Commun. Mass Spectrom.* **1991**, 5, 450-455.
3. Chen, S. P. and Comisarow, M. B., Modelling Coulomb Effects in Fourier-Transform Ion Cyclotron Resonance Mass Spectrometry by Charged Disks and Charged Cylinders. *Rapid Commun. Mass Spectrom.* **1992**, 6, 1-3.
4. Mitchell, D. W. and Smith, R. D., Cyclotron Motion of 2 Coulombically Interacting Ion Clouds with Implications to Fourier-Transform Ion-Cyclotron Resonance Mass-Spectrometry. *Physical Review E* **1995**, 52, 4366-4386.
5. Gorshkov, M. V.; Marshall, A. G. and Nikolaev, E. N., Analysis and Elimination of Systematic Errors Originating from Coulomb Mutual Interaction and Image Charge in Fourier Transform Ion Cyclotron Resonance Precise Mass Difference Measurements. *J. Am. Soc. Mass Spectrom.* **1993**, 4, 855-868.
6. Xiang, X.; Grosshans, P. B. and Marshall, A. G., Image Charge-Induced Ion Cyclotron Orbital Frequency Shift for Orthorhombic and Cylindrical FT-ICR Ion Traps. *Int. J. Mass Spectrom. Ion Processes* **1993**, 125, 33-43.
7. Masselon, C.; Tolmachev, A. V.; Anderson, G. A.; Harkewicz, R. and Smith, R. D., Mass Measurement Errors Caused by "Local" Frequency Perturbations in FTICR Mass Spectrometry. *J. Am. Soc. Mass Spectrom.* **2002**, 13, 99-106.

8. Aizikov, K. and O'Connor, P. B., Use of the Filter Diagonalization Method in the Study of Space Charge Related Frequency Modulation in Fourier Transform Ion Cyclotron Resonance Mass Spectrometry. *J. Am. Soc. Mass Spectrom.* **2006**, *17*, 836-843.
9. Aizikov, K.; Mathur, R. and O'Connor, P. B., The Spontaneous Loss of Coherence Catastrophe in Fourier Transform Ion Cyclotron Resonance Mass Spectrometry. *J. Am. Soc. Mass Spectrom.* **2009**, *20*, 247-256.
10. Jeffries, J. B.; Barlow, S. E. and Dunn, G. H., Theory of Space-Charge Shift of Ion-Cyclotron Resonance Frequencies. *Int. J. Mass Spectrom. Ion Processes* **1983**, *54*, 169-187.
11. Francl, T. J.; Sherman, M. G.; Hunter, R. L.; Locke, M. J.; Bowers, W. D. and McIver, R. T., Experimental-Determination of the Effects of Space-Charge on Ion-Cyclotron Resonance Frequencies. *Int. J. Mass Spectrom. Ion Processes* **1983**, *54*, 189-199.
12. Jing, L.; Li, C.; Wong, R. L.; Kaplan, D. A. and Amster, I. J., Improved Mass Accuracy for Higher Mass Peptides by Using SWIFT Excitation for MALDI-FTICR Mass Spectrometry. *J. Am. Soc. Mass Spectrom.* **2008**, *19*, 76-81.
13. Kaiser, N. K.; Savory, J. J.; McKenna, A. M.; Hendrickson, C. L. and Marshall, A. G., Tailored Ion Spatial Distribution in FT-ICR MS for Improved Analysis of Complex Mixtures, *Proceedings of the 58th ASMS Conference on Mass Spectrometry and Allied Topics*, Salt Lake City, UT, 2010.

14. Easterling, M. L.; Mize, T. H. and Amster, I. J., Routine Part-per-Million Mass Accuracy for High-Mass Ions: Space-Charge Effects in MALDI FT-ICR. *Anal. Chem.* **1999**, *71*, 624-632.
15. Taylor, P. K. and Amster, I. J., Space charge effects on mass accuracy for multiply charged ions in ESI-FTICR. *Int. J. Mass Spectrom.* **2003**, *222*, 351-361.
16. Ledford, E. B.; Rempel, D. L. and Gross, M. L., Space charge effects in Fourier transform mass spectrometry. II. Mass calibration. *Anal. Chem.* **1984**, *56*, 2744-2748.
17. Muddiman, D. C. and Oberg, A. L., Statistical Evaluation of Internal and External Mass Calibration Laws Utilized in Fourier Transform Ion Cyclotron Resonance Mass Spectrometry. *Anal. Chem.* **2005**, *77*, 2406-2414.
18. Li-Kang, Z.; Don, R.; Birendra, N. P. and Michael, L. G., Accurate Mass Measurements by Fourier Transform Mass Spectrometry. *Mass Spectrom. Rev.* **2005**, *24*, 286-309.
19. Burton, R. D.; Matuszak, K. P.; Watson, C. H. and Eyler, J. R., Exact mass measurements using a 7 tesla fourier transform ion cyclotron resonance mass spectrometer in a good laboratory practices-regulated environment. *J. Am. Soc. Mass Spectrom.* **1999**, *10*, 1291-1297.
20. Wall, M., R. and Neuhauser, D., Extraction, through filter-diagonalization, of general quantum eigenvalues or classical normal mode frequencies from a small number of residues or a short-time segment of a signal. I. Theory and application to a quantum-dynamics model. *The Journal of Chemical Physics* **1995**, *102*, 8011-8022.

21. Press, W. H.; Teukolsky, S. A.; Vetterling, W. T. and Flannery, B. P., Numerical Recipes in C, 2nd; Cambridge University Press: Ithaca, NY, 1992.
22. Allen, J. B. and Rabiner, L. R., A unified approach to short-time Fourier analysis and synthesis. *Proceedings of the IEEE* **1977**, *65*, 1558-1564.
23. Guan, S. and Marshall, A. G., Linear Prediction Cholesky Decomposition vs Fourier Transform Spectral Analysis for Ion Cyclotron Resonance Mass Spectrometry. *Anal. Chem.* **1997**, *69*, 1156-1162.
24. Mitchell, D. W. and Smith, R. D., Two Dimensional Many Particle Simulation of Trapped Ions. *Int. J. Mass Spectrom.* **1997**, *165*, 271-297.
25. Mitchell, D. W., Realistic Simulation of the Ion Cyclotron Resonance Mass Spectrometer Using A Distributed Three-Dimensional Particle-In-Cell Code. *J. Am. Soc. Mass Spectrom.* **1999**, *10*, 136-152.
26. Nikolaev, E. N.; Heeren, R. M. A.; Popov, A. M.; Pozdnev, A. V. and Ching, K. S., Realistic Modeling of Ion Cloud Motion in a Fourier Transform Ion Cyclotron Resonance Cell by Use of a Particle-In-Cell Approach. *Rapid Commun. Mass Spectrom.* **2007**, *21*, 3527-3546.
27. Leach III, F. E.; Kharchenko, A.; Heeren, R. M. A.; Nikolaev, E. and Amster, I. J., Comparison of Particle-In-Cell Simulations with Experimentally Observed Frequency Shifts Between Ions of the Same Mass-To-Charge in Fourier Transform Ion Cyclotron Resonance Mass Spectrometry. *Journal of the American Society for Mass Spectrometry* **2010**, *21*, 203-208.
28. Mize, T. H.; Taban, I.; Duursma, M.; Seynen, M.; Konijnenburg, M.; Vijftigschild, A.; Doornik, C. V.; Rooij, G. V. and Heeren, R. M. A., A Modular

- Data and Control System to Improve Sensitivity, Selectivity, Speed of Analysis, Ease of Use, and Transient Duration in an External Source FTICR-MS. *Int. J. Mass Spectrom.* **2004**, 235, 243-253.
29. Hofstadler, S. A.; Bruce, J. E.; Rockwood, A. L.; Anderson, G. A.; Winger, B. E. and Smith, R. D., Isotopic beat patterns in Fourier transform ion cyclotron resonance mass spectrometry: implications for high resolution mass measurements of large biopolymers. *Int. J. Mass Spectrom. Ion Processes* **1994**, 132, 109-127.
30. Gorshkov, M. V.; Good, D. M.; Lyutvinskiy, Y.; Yang, H. and Zubarev, R. A., Calibration Function for the Orbitrap FTMS Accounting for the Space Charge Effect. *J. Am. Soc. Mass Spectrom.* 21, 1846-1851.
31. Makarov, A. and Denisov, E., Dynamics of Ions of Intact Proteins in the Orbitrap Mass Analyzer. *J. Am. Soc. Mass Spectrom.* **2009**, 20, 1486-1495.

**APPENDIX D**

**SUPPLEMENTAL DATA**

TABLE D.1 Product ion assignments for Figure 7.4.

<b>m/z</b>	<b>ID</b>	<b>Charge</b>	<b>Na Counter Ions</b>
157.0142	B1-SO3	1-	0
168.4892	Y1	2-	0
204.6473	Y2	3-	1
236.9711	B1	1-	0
238.4947	B2-SO3	2-	0
240.0183	Z1-SO3	1-	0
254.9816	C1	1-	0
277.9699	B3	3-	1
278.4731	B2	2-	0
283.9735	C3	3-	1
284.9892	Y3-SO3	3-	0
287.4784	C2=Z2	2-	0
289.4641	B2	2-	1
291.3008	C3	3-	2
296.4837	Y2	2-	0
298.4694	M	4-	2
298.6591	0,2A4-2SO3	3-	2
298.9618	2,4X2	3-	2
301.9646	B2+Z3	1-	0
307.4746	Y2	2-	1
309.4603	C2=Z2	2-	2
311.0078	3,5A2-SO3	1-	0
312.9653	Z3	3-	2
318.4656	Y2	2-	2
319.9752	Z1	1-	0
321.4721	1,5X2	2-	1
322.4811	3,5A2	2-	0
323.9465	B2+Z3	1-	1
325.3113	0,2A4-SO3	3-	2
332.9723	0,2X3-SO3	3-	2
333.4721	3,5A2	2-	1
335.516	C3-2SO3	2-	0
337.9857	Y1	1-	0
341.9571	Z1	1-	1
346.507	C3-2SO3	2-	1
347.9701	B2+1,5X3	1-	0
351.9636	0,2A4	3-	2
357.0133	0,2A2	1-	0
359.6246	0,2X3	3-	2
359.9677	Y1	1-	1
365.9806	1,5X1	1-	0
366.4892	B3-SO3	2-	0
370.444	0,2X3+B3	2-	2
371.6426	M-SO3	3-	2
375.4994	C3-SO3	2-	0
377.4801	B3-SO3	2-	1

379.0038	Z3-SO3	2-	1
382.9598	1,5A4	3-	2
386.4854	C3-SO3	2-	1
387.9626	1,5X1	1-	1
388.4711	B3-SO3	2-	2
389.9947	Z3-SO3	2-	2
390.9647	3,5A2	1-	0
397.4764	C3-SO3	2-	2
398.0399	B2-SO3	1-	0
398.2949	M	3-	2
407.4907	2,4A4-SO3	2-	1
412.9466	3,5A2	1-	1
415.4728	C3	2-	0
416.0504	C2-2SO3=Z2- 2SO3	1-	0
418.4817	2,4A4-SO3	2-	2
418.9822	Z3-SO3	2-	1
426.4638	C3	2-	1
426.9643	2,4X2	2-	0
428.4495	B3	2-	2
429.9731	Z3-SO3	2-	2
436.9701	0,2A2	1-	0
437.4548	C3	2-	2
438.9784	Y3-SO3	2-	2
442.9572	2,5A2	1-	1
447.4691	2,4A4	2-	1
448.4922	0,2A4-2SO3	2-	2
452.9759	1,5X3-SO3	2-	2
458.4601	2,4A4	2-	2
458.9521	0,2A2	1-	1
469.9516	Z3	2-	2
477.9967	B2-SO3	1-	0
478.9568	Y3-SO3	2-	2
480.934	0,2A2	1-	2
488.4706	0,2A4-SO3	2-	2
494.9865	1,5A4-SO3	2-	2
496.0072	C2-SO3=Z2-SO3	2-	0
499.9786	B2-SO3	1-	1
505.4463	3,5A4	2-	2
516.9814	M-2SO3	2-**	2
517.9892	C2-SO3=Z2-SO3	1-	1
521.9606	B2-SO3	1-	2
528.449	0,2A4	2-	2
533.9276	0,3X1	1-	2
534.9649	1,5A4-SO3	2-	2
535.9998	Y2-SO3	1-	1
539.9711	C2-SO3=Z2-SO3	1-	2
547.9545	M-H2SO4	2-**	2
556.9598	M-SO3	2-**	2
557.9817	Y2-SO3	1-	2
563.9947	1,5X2-SO3	1-	1

579.9354	B2	1-	1
587.9947	3,5A3-SO3	1-	1
597.946	C2=Z2	1-	1
601.9174	B2	1-	2
615.9566	Y2	1-	1
619.928	C2=Z2	1-	2
637.9385	Y2	1-	2
643.9515	1,5X2	1-	1
665.9334	1,5X2	1-	2
667.9515	3,5A3	1-	1
676.0107	B3-2SO3	1-	1
755.9675	B3-SO3	1-	1
777.9495	B3-SO3	1-	2
795.96	C3-SO3	1-	2
857.9063	B3	1-	2
875.9169	C3	1-	2